JMIR Biomedical Engineering

Engineering for health technologies, medical devices, and innovative medical treatments and procedures
Volume 6 (2021), Issue 2 ISSN 2561-3278 Editor in Chief: Syed A. A. Rizvi, MD, PhD, MBA, MPH, BSN

Contents

Short Paper

Review

Plasmonic and Hybrid Whispering Gallery Mode–Based Biosensors: Literature Review

Maurizio Manzo[1], PhD; Omar Cavazos[1], MSc; Zhenhua Huang[2], PhD; Liping Cai[2], PhD

[1]Photonics Micro-Devices Fabrication Lab, Department of Mechanical Engineering, University of North Texas, Denton, TX, United States

[2]Department of Mechanical Engineering, University of North Texas, Denton, TX, United States

Corresponding Author:
Maurizio Manzo, PhD
Photonics Micro-Devices Fabrication Lab
Department of Mechanical Engineering
University of North Texas
3940 N Elm St, F115
Denton, TX, 76207
United States
Phone: 1 940 369 8266
Email: maurizio.manzo@unt.edu

Abstract

Background: The term “plasmonic” describes the relationship between electromagnetic fields and metallic nanostructures. Plasmon-based sensors have been used innovatively to accomplish different biomedical tasks, including detection of cancer. Plasmonic sensors also have been used in biochip applications and biosensors and have the potential to be implemented as implantable point-of-care devices. Many devices and methods discussed in the literature are based on surface plasmon resonance (SPR) and localized SPR (LSPR). However, the mathematical background can be overwhelming for researchers at times.

Objective: This review article discusses the theory of SPR, simplifying the underlying physics and bypassing many equations of SPR and LSPR. Moreover, we introduce and discuss the hybrid whispering gallery mode (WGM) sensing theory and its applications.

Methods: A literature search in ScienceDirect was performed using keywords such as “surface plasmon resonance,” “localized plasmon resonance,” and “whispering gallery mode/plasmonic.” The search results retrieved many articles, among which we selected only those that presented a simple explanation of the SPR phenomena with prominent biomedical examples.

Results: SPR, LSPR, tilted fiber Bragg grating, and hybrid WGM phenomena were explained and examples on biosensing applications were provided.

Conclusions: This minireview presents an overview of biosensor applications in the field of biomedicine and is intended for researchers interested in starting to work in this field. The review presents the fundamental notions of plasmonic sensors and hybrid WGM sensors, thereby allowing one to get familiar with the terminology and underlying complex formulations of linear and nonlinear optics.

(JMIR Biomed Eng 2021;6(2):e17781) doi:10.2196/17781

KEYWORDS

plasmonic; whispering gallery mode, microlasers, biomedical; sensors

Introduction

The term “plasmonic” describes the relationship between electromagnetic fields and metallic nanostructures [1]. Plasmonic sensors have attracted great interest from researchers and engineers alike. Surface plasmon resonances (SPRs) are electromagnetic waves that are produced when a metal nanostructure (ie, spherical or cylindrical) interacts with a dielectric material [2,3]. The interesting optical characteristics of surface plasmons have made many important contributions to the field of medicine [4]. For example, highly sensitive plasmonic sensors have been developed to detect many kinds of cancers [5], and based on the SPR concept, a plasmonic interferometer array–based sensor was developed for detecting cancers [6].

This paper discusses the physical principles in brief and introduces several methods employing plasmonic systems such as SPR and localized plasmon resonance. SPR methods have attracted great interest in biomedical applications. This technique entails observing small changes in the refractive index of the combination of dielectric materials and metal [7]. In addition, plasmonic nanoparticles and nanostructures have been used in biosensing applications. These structures are typically made of noble metals such as gold and silver [8,9]. The cytotoxicity of these metals based on their concentrations are under investigation and studies have shown potential biomedical applications for these metals at certain concentrations [10,11]. These nanostructures are used in photoacoustic imaging and phototherapy. For example, gold nanorods with varied light absorption peaks have been used in imaging and theranostics [12]. Plasmonic sensors also have been used in biochip applications and biosensors [13-15]. Other techniques such as localized plasmon resonance have also been utilized in various biomedical applications [16]. In summary, plasmon-based sensing methods are indispensable tools for sensing in the field of biomedicine. Moreover, these devices have the potential to be implemented as implantable point-of-care devices [17-19].

Methods

We performed a literature search on ScienceDirect for studies on plasmonic and hybrid whispering gallery mode (WGM) sensors and retrieved more than 3400 articles (both research and review articles) published in the field of medicine and dentistry. According to their characteristics, sensors were grouped into 4 categories, namely, SPR, localized SPR (LSPR), tilted fiber Bragg grating (TFBG), and hybrid WGM sensors.

The search for articles related to SPR and LSPR was straightforward. The search results retrieved many articles, among which we selected only those that presented a simple explanation of the aforesaid phenomenon with prominent biomedical examples. Within these 2 fields, a third field was categorized (TFBG) due to the prominent presence of biosensor-based devices that utilize the TFBG principle.

The keyword “whispering gallery mode” was associated with the term “plasmon” and only retrieved 3 papers in the pharmacology, toxicology, and pharmaceutical fields. Therefore, for the latest category (ie, hybrid WGM sensors), the search was expanded to the engineering field and eventually 35 reports were identified. More papers were found in other fields such as physics, astronomy, material science, and chemistry.

Results

Many papers, for example [20-33], describe the physical principle of SPR, and provide the definitions and discuss exemplary applications to illustrate how changing the refractive index can be used for sensing through the plasmonic effect and how the light is generally coupled to the biosensor. A total of 6 papers [23-27,29] illustrated that optical fibers can be used in conjunction with SPR for sensing applications. Also, 13 papers were selected to discuss SPR-based metal nanostructures [2,20-22,34-42].

LSPR is discussed based on 11 papers [36-39,43-49]. As before, the physical principle and 2 representative examples are provided to understand the main differences between LSPR and the previous methods.

Although TFBG could be associated with the SPR-based optical fiber sensing method, many different papers have been found on this topic, and therefore, a separate category (ie, tilted fiber Bragg grating) was created. Several papers are used to illustrate the physical principle and applications.

Lastly, 20 papers were used to introduce the WGM and the hybrid WGM sensing [34,35,40-42,50-63]. This type of sensing methodology was not directly related to the medical literature, but biomedical applications were proposed and the future implementation of this method is likely to become the gold standard in some areas. This review paper presents and discusses the sensing techniques, including SPR, LSPR, TFBG, and hybrid WGM, as well as their applications using representative examples in the biomedical fields.

Discussion

Surface Plasmon Resonance

The term “plasmonic” describes the relationship between metallic structures and dielectrics in an electric field. The oscillations of electrons between a metal sample and a dielectric field are referred to as SPR. The attenuated total reflection (ATR) configuration is one of the prism coupling–based SPR methods [20-22]. In ATR, a metal sheet is placed on top of a light coupling substrate, such as glass (Figure 1). The light source is then directed into a prism and a detector gathers the resonances. Therefore, the resonance is displaced as a sharp dip in the output spectrum due to the absorption of the surface plasmon wave [20]. In a previous study [20], the ATR configuration was used to monitor the refractive index of the human skin as shown in Figure 1. Besides, this same configuration has been used for monitoring humidity, where the effect of the temperature on the sensor was analyzed. The sensor consisted of a chalcogenide substrate layer, gold layer, and buffer layer [22].

Optical fiber sensing with SPR has been used to detect different kinds of biological targets such as antibodies. The phenomenon of SPR occurs on the surface of the optical fiber [23]. Optical fiber SPR methods have advantages over traditional prism methods such as the ATR technique, which can be explained as follows: optical sensors use remote sensing and optical fibers have a reasonably lower cost and a more compact size. In addition, these types of sensors provide label-free sensing with high sensitivity [24]. In some cases, finite-element methods were used to analyze the design of the optical fiber sensors [25,26].

Figure 1. Proposed SPR sensor probe setup for the determination of refractive index of human skin tissues. IB: incoming light beam; SB: sensed light beam. Reproduced, with permission, from Elsevier [20].

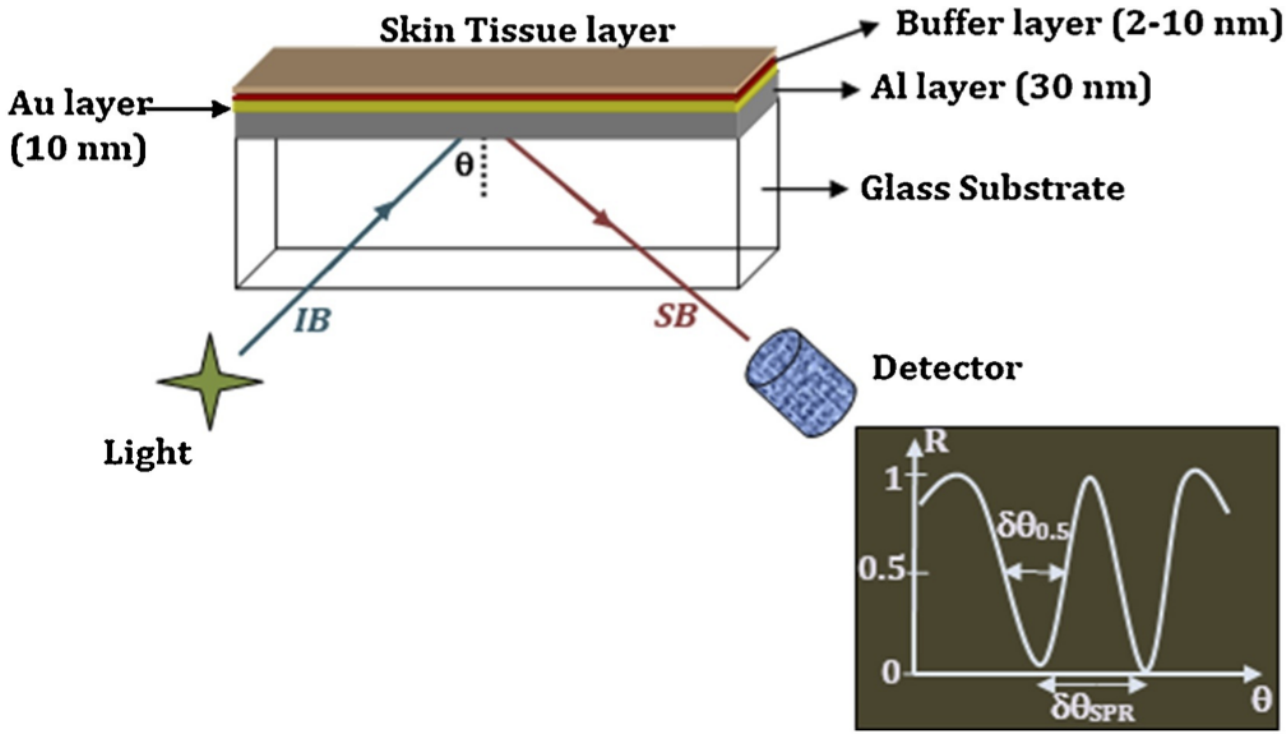

Another class of optical fiber based on SPR uses photonic crystal fibers, which have been used as alternatives to traditional optical fibers. A notable advantage of these fibers is that they have more controllable birefringence and therefore a better control on light propagation and confinement directions [27]. Photonic crystals are dielectric materials that have a periodicity (repeated optical structure) in two or three dimensions. They are usually fabricated by etching, which can form a photonic bandgap, allowing to configure the light for different uses. The bandgap depends on the structural content of the crystal, such as refractive index and periodicity. The peak frequency shown in the transmission spectrum depends on the shape and size of the lattice defects [28].

Another method for SPR is the use of metallic nanostructures. Gold and silver nanostructures have been extensively used in past years, because they can be characterized by their size and shape [29]. Silver nanorods are suitable for biomolecular detection [30]. In addition, the iron oxide–gold nanoparticles can experience both plasmonic and magnetic phenomena, which allows for their use in different biomedical applications. One advantage of this type of particle is that it can be moved due to its magnetic property and still demonstrate plasmonic behavior. This can tremendously facilitate the analysis of biological targets [31]. In another study, a piece of portable SPR instrument was developed using nanoparticles, which was able to detect testosterone [32]. Another type of SPR sensor is the plasmonic waveguide. Plasmonic waveguide designs tend to be suitable for chipping applications. This is mainly because of their compactness and the use of SPRs [33].

Localized Surface Plasmon Resonance

Localized SPR (LSPR) is the amplitude of oscillation of free electrons that occurs at a certain frequency, which can be used to detect biomolecules such as proteins in real time. In one study, a gold nanoplasmonic sensor was used to detect cancer markers in clinical samples. The sensor could also detect proteins such as biotin (Figure 2). Besides, it has the potential to detect DNA [43]. LSPR is mainly related to nanostructure/nanoparticles such as nanorods. In addition, LSPR does not require coupling, for example, with prims and is easy to operate. Therefore, this method is widely used in the scientific field [44]. The type of nanostructure used has an impact on the strength of LSPR. For example, nanostars can be used for tuning the sensors and promoting a strong LSPR signal. However, structures such as nanorods and nanospheres have widely been investigated for various imaging applications [45].

Figure 2. Detection of protein-protein binding event on the gold nanostructure through LSPR peak shift. Licensed under Creative Commons Attribution 4.0 by the authors [43]. LSPR: localized surface plasmon resonance.

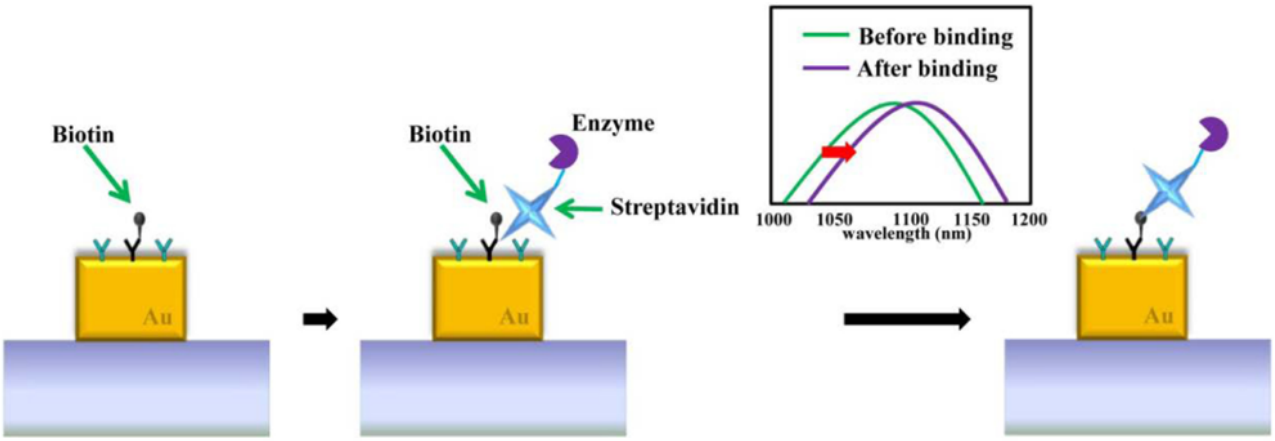

Gold nanorods have been used as plasmonic sensors for detecting mercury. The deposition of mercury on the nanorods was observed by monitoring the LSPR shifts using darkfield microscopy [46]. Tao et al [47] used a gold and silver alloy nanoplasmonic device to detect mercury concentrations. LSPR has also been used to develop silk plasmonic absorber sensors [36]. In this case, silk protein is used as an insulator in the insulator–metal resonator configuration. Besides, the silk plasmonic absorber sensor was applied as a glucose sensor, which demonstrated a high sensitivity of 1200 nm/RIU (refractive index unit) and high relative intensity change [36]. Metal nanoparticles have also been used for copper detection in samples, mainly because LSPR is influenced by the morphology and size of particles. Ding et al [37] used gold nanoparticles to detect specific copper ions. Besides, LSPR sensors have been integrated into optical fiber devices. Tu et al [38] used hollow gold nanocages for LSPR optical fiber sensors. The sensor had a sensitivity of around 1933 nm/RIU. Furthermore, the sensitivity can be adjusted by changing the aspect ratio of the gold nanocages. Yousuf et al [39] developed a metal–insulator–metal configuration, which consisted of an elliptical nanorod, rectangular nanoslabs, and a metallic grating. Unser et al [48] developed a selective collagen gold nanoparticle–based sensor, which works based on the plasmonic coupling of the nanoparticles and the collagen fibrils. A redshift (toward the right side of the spectrum) in the LSPR frequency indicates the detection of glucose. Overall, the conjugates were able to detect glucose and heparin (Figure 3).

Figure 3. The 2 sensing schemes addressed in this work using collagen-nanoparticle conjugates. (A) The native collagen is added before the gold nanoparticles (AuNPs); (B) the collagen after it has been coated in AuNPs forming a collagen-nanoparticle scaffold; (C) in order to carry out biosensing measurements of glucose, the collagen nanoparticle scaffold is crosslinked by glucose after it has been incubated at 35°C and the covalent product glucosepane has formed; (D) lastly, the binding interactions between the collagen-nanoparticle scaffold and the heparin-coated 80-nm gold nanoparticles are used to detect heparin. Licensed under Creative Commons Attribution 4.0 by the authors [48].

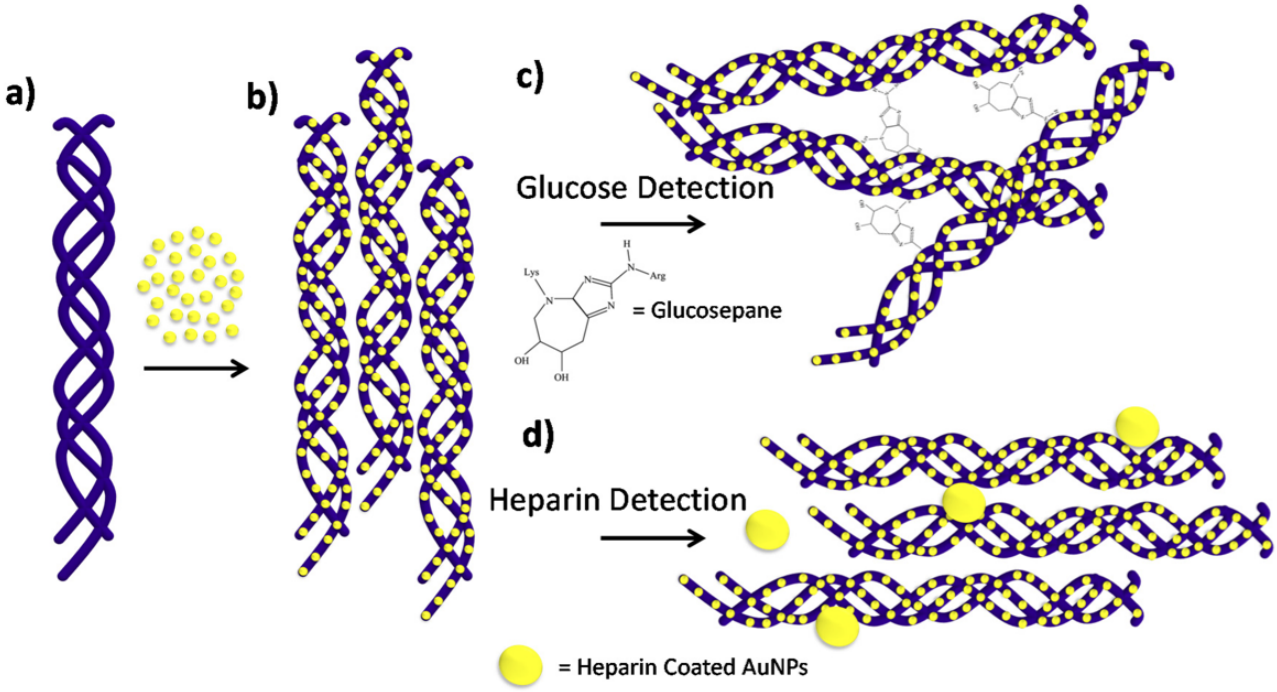

Tilted Fiber Bragg Grating

In the configuration of TFBG, the refractive index modulation planes are in a tilted position, which helps to measure very small changes. These small changes can be fully analyzed by observing the refractive index of the fiber. The tilted grating disrupts the fiber's symmetry, which causes some core-guided lights to be coupled that allows the cladding mode resonances to be observed. These resonances are observed as a comb of sharp dips. It has been noted that these methods can greatly increase quality factors (ie, Q values of up to 10^4) [64].

Therefore, this type of sensing method can be widely used for biomedical applications in constricted spaces. Fiber optic–based sensors allow easy sensor installation. In one study, TFBG was used to detect the variation in protein in the urine of rats [65]. Results were obtained using a coated TFBG embedded inside a microfluidic channel. The experiment was able to distinguish different kinds of urine. Results demonstrated a clear relationship between protein outflow and changes in the refractive index of the urine. This approach showed improvements in the detection of proteins at low concentrations [65]. The TFBG SPR sensor has been used for the detection of glycoprotein. Zhang et al [66] coated 10° TFBG with a 50-nm gold film to stimulate SPR on a sensor surface as shown in Figure 4. The sensor was able to distinguish between nonglycoproteins and glycoproteins. The TFBG-based sensor was also used to detect S-adenosyl-l-homocysteine (AdoHcy), with concentrations of up to 1 nM detected [67].

Figure 4. (A) Schematic of the tilted fiber Bragg grating (TFBG)-based surface plasmon resonance (SPR) (TFBG-SPR) sensor. (B) Transmission spectra of the sensor under P and S polarization. (C) Experimental setup. Licensed under Creative Commons Attribution 4.0 by the authors [66].

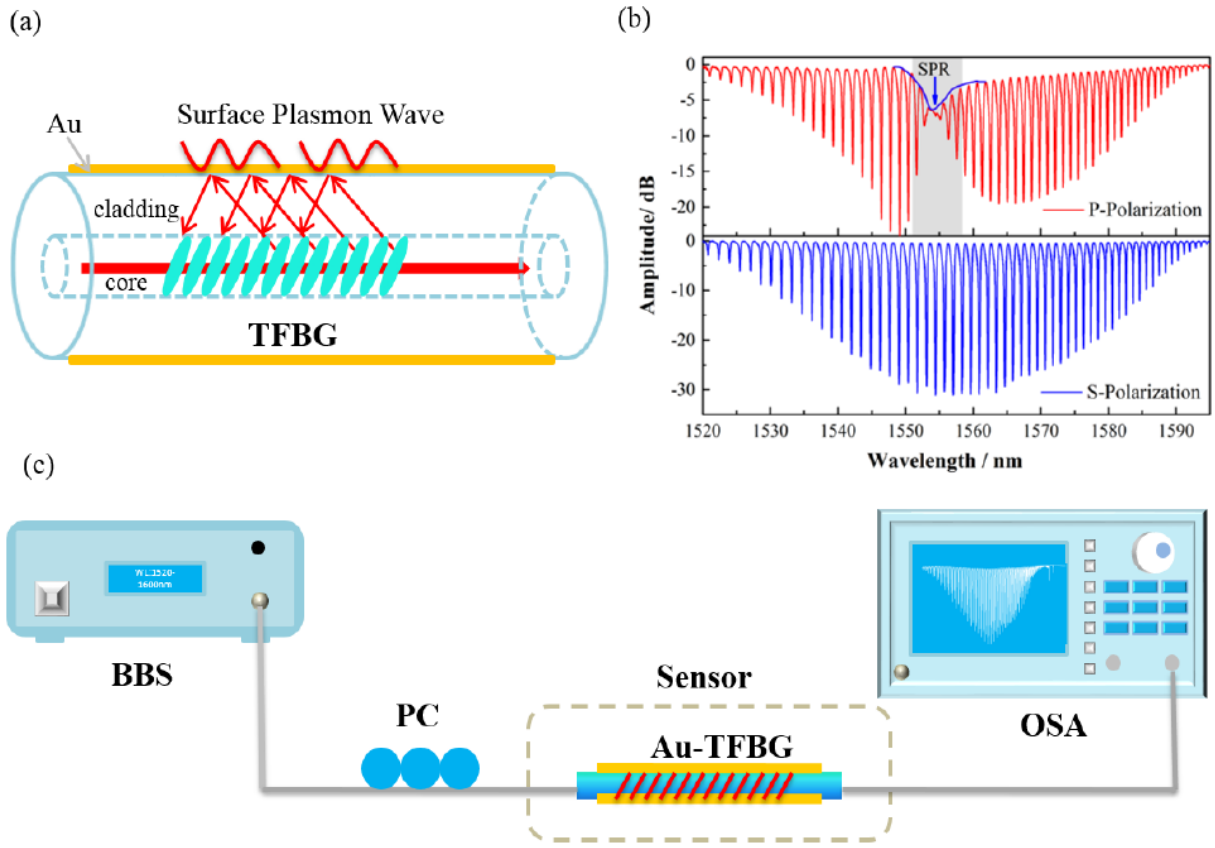

Hybrid Whispering Gallery Mode Sensors

WGM resonators have been used for different applications, especially for high-sensitivity and resolution sensors [40,50-55]. The WGM microstructure can be made in various types of shapes such as spheres, cylinders, and toroid [40,50-55]. The WGMs of the resonator can be observed by coupling light to the resonator. These electromagnetic waves circulate near the internal edge of the resonator [54]. Therefore, the resonances are generated by the total internal reflection of the confined light and when the optical path of the light is a multiple integer of the wavelength [55]. The WGM shift caused by an excitation method can be used to determine the change in the measured quantities [40,56]. The WGMs can be tuned by excitation sources such as uniaxial stress and electric field. The theory is that the WGMs propagate across the pole of the spheres. Then, the deformation along the ends of the sphere and index of refraction change modify the position of WGM resonances [56,57]. WGM resonators have been developed using fused silica. Fused silica resonators have a quality factor (Q) of 10^9 [58]. Silica resonators have been used, but have low sensitivity because they exhibit high Young modulus and therefore high resistance to any deformation. Different materials such as polydimethylsiloxanes have been used to address the issue of low sensitivity [59]. The WGM resonances can be observed using different techniques. For example, a study used a charge-coupled device camera and a spectrometer to observe

the resonances, and therefore when doping WGM resonators with a laser dye material, the hybrid functions as tiny lasers that emit light under proper excitation conditions [40,50-55,67]. The light emitted from the resonator could then be coupled into the spectrometer using an optical lens setup [40]. Another study discussed a novel fiber-taper coupling system that couples light into microresonators. It has been observed that tapered optical fibers promote high coupling efficiency to the resonators. The experiment was completed with a silica microresonator coupled to a tapered optical fiber [34]. In a similar study, a silica microsphere resonator was critically coupled to a fiber taper. The fiber taper is useful because it allows for simple focusing and alignment of the input beam but uses the resonator as a passive element, which limits the application due to the presence of optical cablings [35,50].

Hybrid WGM methods have been analyzed in recent studies by coupling a WGM resonator to metal nanoparticles [40-42]. One study observed the effects of adding a gold nanoparticle to the equator of a microparticle. The motivation for this hybrid resonator was the need to rapidly detect pathogens. It works based on the principle of creating a plasmonic effect near the equator of the sensor, which enhances the already high-sensing capabilities of WGM-based sensors [41]. Other studies have used triangular gold nanoprisms coupled with WGM sensors. In one case, a gold triangular nanoprism was placed inside a microtoroid WGM resonator. It was shown that the tips of the nanoprism had regions of great plasmonic enhancement. This type of plasmonic enhancement permits the detection of larger protein molecules with high precision as shown in Figure 5 [42].

Figure 5. Geometrical scheme of whispering gallery mode (WGM) microtoroid with a gold triangular nanoprism bound to its surface. Reproduced from Nadgaran H, Afkhami Garaei M. Enhancement of a whispering gallery mode microtoroid resonator by plasmonic triangular gold nanoprism for label-free biosensor applications. Journal of Applied Physics 2015 Jul 28;118(4):043101. [doi:10.1063/1.4927266], with the permission of AIP Publishing [42].

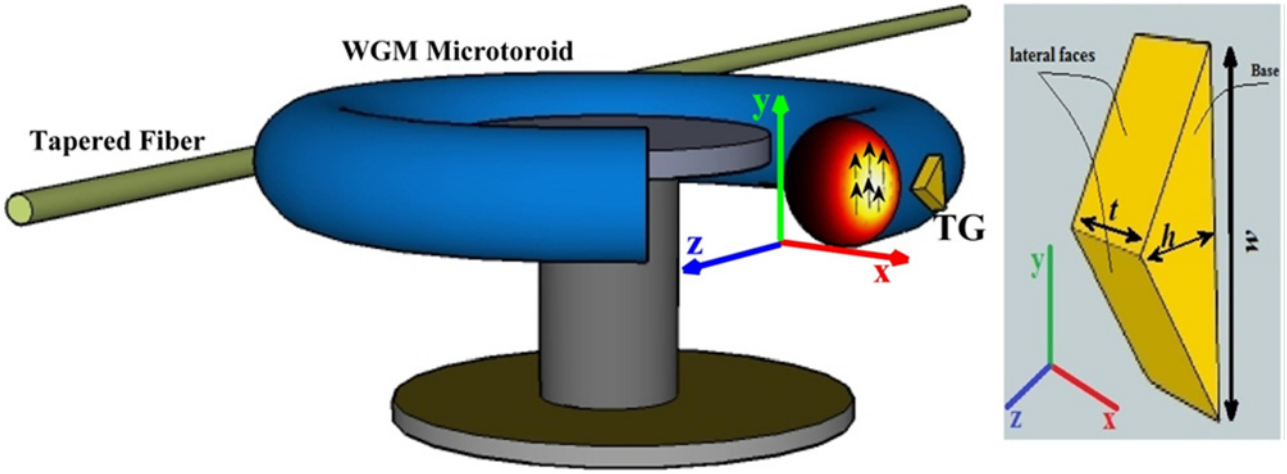

In other studies, polymeric WGM–based spherical resonators have been doped with metal nanoparticles to lower the energy required to activate the sensor [40]. In this case, the plasmonic effect enhanced light emission and lowered the energy threshold required for the structure to lase with higher temporal duration and more stable amplitude of the optical resonances, enabling multiplexed capabilities [40].

Electrically controlled graphene has also been applied to improve the performance of a hybrid silver–silica microdisk resonator. Most notably, the Q factor (energy stored and energy loss ratio) was improved and had a sensitivity higher than 1000 nm/RIU. Therefore, the hybrid sensor has a huge potential for use as a refractometer [60]. In recent years, there has been a growing interest in utilizing hybridization whispering gallery microstructures with the plasmonic effect. The motivation for this hybrid concept is that the single plasmonic sensing generates low Q factors (higher losses), whereas the presence of a resonant structure overcomes this limitation, thereby increasing the sensitivity of these hybrid sensors [61]. One example of the application of hybrid WGM biosensors is in the determination of proteins. More specifically, it was used to quantify the amount of bovine serum albumin that is absorbed by the gold nanoparticles [62], making the hybrid sensor a perfect candidate for combining plasmonic and high-sensitivity resonant microstructures. In addition, Huckabay et al [63] used WGM resonators to analyze a biomarker for ovarian cancer (CA-125) in a buffer.

Some Other Relevant Examples of SPR/TFBG Applications in the Biomedical Field

SPR is one of the prominent methods used for biomedical applications. Sharma [68] used a sensor based on SPR to detect the concentration of hemoglobin in human blood. Hemoglobin detection is an important medical procedure that has an impact on several clinical methods. Overall, this method of analyzing blood using SPR will lead to its use in blood analysis. Luo et al [69] used a plasmonic method employing gold nanoparticles, improving detection of tumor-targeted cells during X-ray radiotherapy (Figure 6).

Figure 6. Schematic illustration of targeted prostate cancer radiotherapy using prostate-specific membrane antigen (PSMA)-targeted gold nanoparticles (AuNPs) of various sizes. With permission from the Royal Society of Chemistry, 2019 [69].

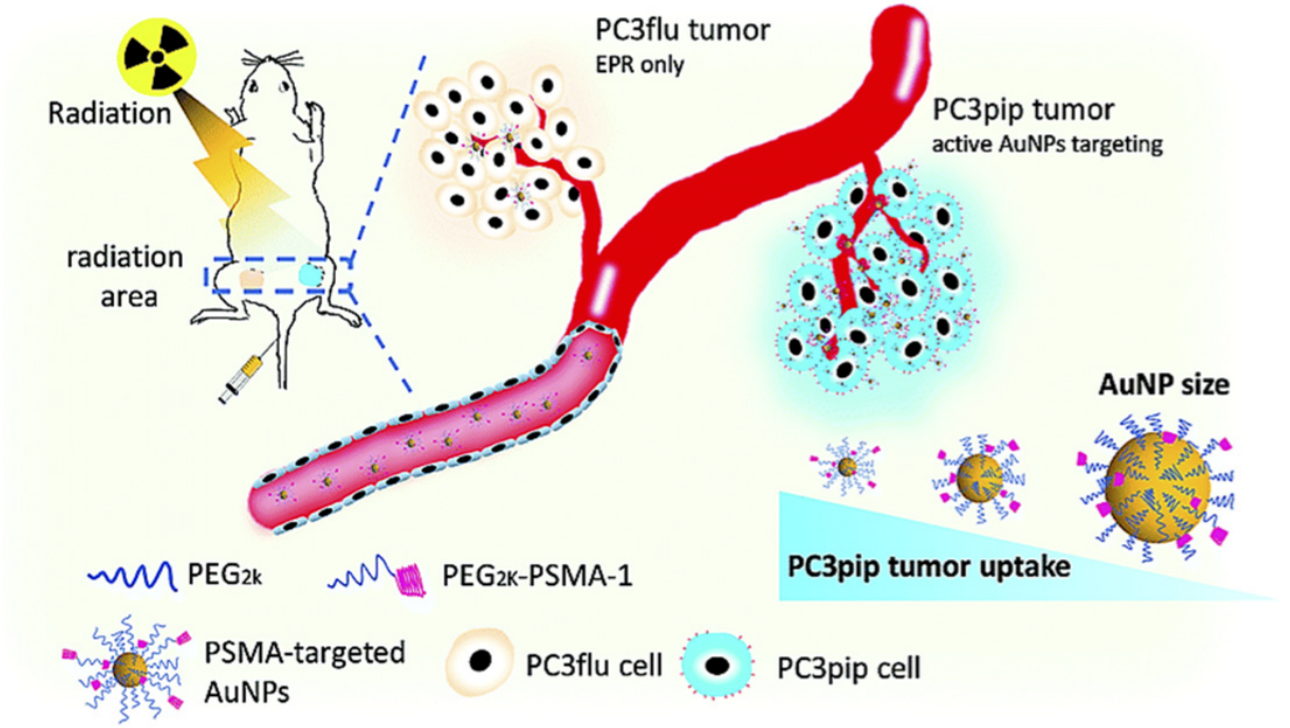

Others have used gold nanorods to detect breast cancer biomarkers [5,70]. In addition to gold and silver, a few new plasmonic sensors based on different metals, such as magnesium, have been developed recently [71]. TFBG-based sensors have also been used to detect small biomarkers to diagnose lung cancers. The sensor was able to monitor the amplitude shift of sensitive spectrum modes of the TFBG SPR [72]. Furthermore, an immunosensor was used to detect biomarkers for risk stratification and prognosis of heart failure [73]. The detection of drugs and metabolites in patients currently remains a challenge and requires novel tools and methodologies. One study developed a diagnostic system based on silver nanoshells to detect metabolites in biofluids and identify whether patients had postoperative brain infection using embedded gold nanoparticles [74]. By contrast, ELISAs have been used to detect disease biomarkers at ultra-low concentrations. One study used this technique to detect HIV-2 capsid antigen p24 and prostate-specific antigen. This type of cost-effective technique can assist developing countries that require better methods to detect HIV infections. Therefore, it was noted that the plasmonic ELISA is a versatile method of detection for application in biomedical fields [19,75]. Silver nanocubes have also been applied for detecting lung cancer biomarkers, such as microRNAs. microRNAs, which are known to act as tumor suppressors, can be used for biomedical diagnosis. Zhang et al [49] developed a plasmonic nanoprobe technique to rapidly detect miR-21 biomarkers. miR-21 was used as a biomarker for diagnosing lung cancer early. The technique was based on the LSRP spectral shift that was caused by a change in the refractive index. Plasmon-based sensors are very versatile and in the near future it will be possible to see robust and cheap point-of-care devices for various daily monitoring and diagnosis of different medical conditions [19].

Conclusions and Future Prospects

In this brief review paper, different plasmonic sensing methods and biosensing applications were discussed. Overall, biosensing is an attractive research area and novel sensing methods are being developed rapidly. Biosensing is a very powerful technique and will have a substantial impact on the biomedical community. This review summarized current methods and results that have influenced applications based on plasmonic biosensors. It was observed that the SPR is a notable principle for biosensing. This method is used for different applications such as for detection of sweat loss, biomarkers, and even hemoglobin concentration in human blood. Plasmon-based biosensors are versatile and will continue to be investigated and developed with technological advancements in the future to improve selectivity and robustness.

Conflicts of Interest

None declared.

References

1. Virk M, Xiong K, Svedendahl M, Käll M, Dahlin AB. A thermal plasmonic sensor platform: resistive heating of nanohole arrays. Nano Lett 2014 Jun 11;14(6):3544-3549. [doi: 10.1021/nl5011542] [Medline: 24807397]
2. Ma Y, Farrell G, Semenova Y, Wu Q. Analysis and applications of nanocavity structures used as tunable filters and sensors. Infrared Physics & Technology 2012 Sep;55(5):389-394. [doi: 10.1016/j.infrared.2012.07.005]
3. Nouri-Novin S, Sadatgol M, Zarrabi FB, Bazgir M. A hollow rectangular plasmonic absorber for nano biosensing applications. Optik 2019 Jan;176:14-23. [doi: 10.1016/j.ijleo.2018.09.065]
4. Tong L, Wei H, Zhang S, Xu H. Recent advances in plasmonic sensors. Sensors (Basel) 2014 May 05;14(5):7959-7973 [FREE Full text] [doi: 10.3390/s140507959] [Medline: 24803189]
5. Sugumaran S, Jamlos M, Ahmad M, Bellan C, Schreurs D. Nanostructured materials with plasmonic nanobiosensors for early cancer detection: A past and future prospect. Biosens Bioelectron 2018 Feb 15;100:361-373. [doi: 10.1016/j.bios.2017.08.044] [Medline: 28946108]
6. Zeng X, Yang Y, Zhang N, Ji D, Gu X, Jornet JM, et al. Plasmonic Interferometer Array Biochip as a New Mobile Medical Device for Cancer Detection. IEEE J. Select. Topics Quantum Electron 2019 Jan;25(1):1-7. [doi: 10.1109/jstqe.2018.2865418]
7. Zhao F, Zeng J, Shih W. Nanoporous Gold Nanocomposites as a Versatile Platform for Plasmonic Engineering and Sensing. Sensors (Basel) 2017 Jun 28;17(7):1519 [FREE Full text] [doi: 10.3390/s17071519] [Medline: 28657586]
8. Xavier J, Vincent S, Meder F, Vollmer F. Advances in optoplasmonic sensors-combining optical nano/microcavities and photonic crystals with plasmonic nanostructures and nanoparticles. Nanophotonics 2018;7(1):1-38 [FREE Full text] [doi: 10.1515/nanoph-2017-0064]
9. Liu N, Mesch M, Weiss T, Hentschel M, Giessen H. Infrared perfect absorber and its application as plasmonic sensor. Nano Lett 2010 Jul 14;10(7):2342-2348. [doi: 10.1021/nl9041033] [Medline: 20560590]
10. Carnovale C, Bryant G, Shukla R, Bansal V. Identifying Trends in Gold Nanoparticle Toxicity and Uptake: Size, Shape, Capping Ligand, and Biological Corona. ACS Omega 2019 Jan 04;4(1):242-256. [doi: 10.1021/acsomega.8b03227]
11. Ferdous Z, Nemmar A. Health Impact of Silver Nanoparticles: A Review of the Biodistribution and Toxicity Following Various Routes of Exposure. Int J Mol Sci 2020 Mar 30;21(7):2375 [FREE Full text] [doi: 10.3390/ijms21072375] [Medline: 32235542]
12. Lee D, Jeong SH, Kang E. Nanodiamond/gold nanorod nanocomposites with tunable light-absorptive and local plasmonic properties. Journal of Industrial and Engineering Chemistry 2018 Sep;65:205-212. [doi: 10.1016/j.jiec.2018.04.030]
13. Tokel O, Yildiz UH, Inci F, Durmus NG, Ekiz OO, Turker B, et al. Portable microfluidic integrated plasmonic platform for pathogen detection. Sci Rep 2015 Mar 24;5(1):9152 [FREE Full text] [doi: 10.1038/srep09152] [Medline: 25801042]
14. Cetin A, Coskun A, Galarreta B, Huang M, Herman D, Ozcan A, et al. Handheld high-throughput plasmonic biosensor using computational on-chip imaging. Light Sci Appl 2014 Jan 3;3(1):e122-e122. [doi: 10.1038/lsa.2014.3]
15. Hong L, Li H, Yang H, Sengupta K. Fully Integrated Fluorescence Biosensors On-Chip Employing Multi-Functional Nanoplasmonic Optical Structures in CMOS. IEEE J. Solid-State Circuits 2017 Sep;52(9):2388-2406. [doi: 10.1109/jssc.2017.2712612]
16. Katzer C, Grosse V, Schmidl F, Michalowski P, Schmidl G, Mueller R, et al. YBa2Cu3O7−δ matrix-induced in situ growth of plasmonic Au nanoparticles for biological sensor devices. J Nanopart Res 2012 Nov 10;14(12):1285. [doi: 10.1007/s11051-012-1285-7]
17. Anker JN, Hall WP, Lyandres O, Shah NC, Zhao J, Van Duyne RP. Biosensing with plasmonic nanosensors. Nat Mater 2008 Jun;7(6):442-453. [doi: 10.1038/nmat2162] [Medline: 18497851]
18. Rodrigues D, Barbosa AI, Rebelo R, Kwon IK, Reis RL, Correlo VM. Skin-Integrated Wearable Systems and Implantable Biosensors: A Comprehensive Review. Biosensors (Basel) 2020 Jul 21;10(7):79 [FREE Full text] [doi: 10.3390/bios10070079] [Medline: 32708103]
19. Tokel O, Inci F, Demirci U. Advances in plasmonic technologies for point of care applications. Chem Rev 2014 Jun 11;114(11):5728-5752 [FREE Full text] [doi: 10.1021/cr4000623] [Medline: 24745365]
20. Sharma A, Mohr G. Plasmonic optical sensor for determination of refractive index of human skin tissues. Sensors and Actuators B: Chemical 2016 Apr;226:312-317. [doi: 10.1016/j.snb.2015.11.119]
21. Rifat A, Ahmed R, Yetisen A, Butt H, Sabouri A, Mahdiraji G, et al. Photonic crystal fiber based plasmonic sensors. Sensors and Actuators B: Chemical 2017 May;243:311-325. [doi: 10.1016/j.snb.2016.11.113]
22. Sharma A, Gupta A. Design of a plasmonic optical sensor probe for humidity-monitoring. Sensors and Actuators B: Chemical 2013 Nov;188:867-871. [doi: 10.1016/j.snb.2013.08.002]
23. Shevchenko Y, Camci-Unal G, Cuttica DF, Dokmeci MR, Albert J, Khademhosseini A. Surface plasmon resonance fiber sensor for real-time and label-free monitoring of cellular behavior. Biosens Bioelectron 2014 Jun 15;56:359-367 [FREE Full text] [doi: 10.1016/j.bios.2014.01.018] [Medline: 24549115]
24. Sharma AK, Pandey AK, Kaur B. A Review of advancements (2007–2017) in plasmonics-based optical fiber sensors. Optical Fiber Technology 2018 Jul;43:20-34. [doi: 10.1016/j.yofte.2018.03.008]
25. Popescu VA, Puscas NN, Perrone G. Simulation of the Sensing Performance of a Plasmonic Biosensor Based on Birefringent Solid-Core Microstructured Optical Fiber. Plasmonics 2016 Aug 8;12(3):905-911. [doi: 10.1007/s11468-016-0342-y]
26. Popescu VA. Application of a Plasmonic Biosensor for Detection of Human Blood Groups. Plasmonics 2016 Nov 22;12(6):1733-1739. [doi: 10.1007/s11468-016-0440-x]

27. Momota MR, Hasan MR. Hollow-core silver coated photonic crystal fiber plasmonic sensor. Optical Materials 2018 Feb;76:287-294. [doi: 10.1016/j.optmat.2017.12.049]
28. Derbali J, AbdelMalek F, Obayya SSA, Bouchriha H, Letizia R. Design of a compact photonic crystal sensor. Opt Quant Electron 2010 Dec 24;42(8):463-472. [doi: 10.1007/s11082-010-9429-4]
29. Lim WQ, Gao Z. Plasmonic nanoparticles in biomedicine. Nano Today 2016 Apr;11(2):168-188. [doi: 10.1016/j.nantod.2016.02.002]
30. Xu H, Kan C, Wei J, Ni Y, Miao C, Wang C, et al. Synthesis and Plasmonic Property of Ag Nanorods. Plasmonics 2016 Jun 2;11(6):1645-1652. [doi: 10.1007/s11468-016-0257-7]
31. Lim J, Majetich S. Composite magnetic–plasmonic nanoparticles for biomedicine: Manipulation and imaging. Nano Today 2013 Feb;8(1):98-113. [doi: 10.1016/j.nantod.2012.12.010]
32. Yockell-Lelièvre H, Bukar N, McKeating KS, Arnaud M, Cosin P, Guo Y, et al. Plasmonic sensors for the competitive detection of testosterone. Analyst 2015 Aug 07;140(15):5105-5111. [doi: 10.1039/c5an00694e] [Medline: 26034786]
33. Kamada S, Okamoto T, El-Zohary SE, Mori A, Haraguchi M. Design optimization and resonance modes of a plasmonic sensor based on a rectangular resonator. Optics Communications 2018 Nov;427:220-225. [doi: 10.1016/j.optcom.2018.06.076]
34. Spillane SM, Kippenberg TJ, Painter OJ, Vahala KJ. Ideality in a Fiber-Taper-Coupled Microresonator System for Application to Cavity Quantum Electrodynamics. Phys. Rev. Lett 2003 Jul 22;91(4):043902. [doi: 10.1103/physrevlett.91.043902]
35. Cai M, Painter O, Vahala KJ. Observation of Critical Coupling in a Fiber Taper to a Silica-Microsphere Whispering-Gallery Mode System. Phys. Rev. Lett 2000 Jul 3;85(1):74-77. [doi: 10.1103/physrevlett.85.74]
36. Lee M, Jeon H, Kim S. A highly tunable and fully biocompatible silk nanoplasmonic optical sensor. Nano Lett 2015 May 13;15(5):3358-3363. [doi: 10.1021/acs.nanolett.5b00680] [Medline: 25821994]
37. Ding L, Gao Y, Di J. A sensitive plasmonic copper(II) sensor based on gold nanoparticles deposited on ITO glass substrate. Biosens Bioelectron 2016 Sep 15;83:9-14. [doi: 10.1016/j.bios.2016.04.002] [Medline: 27093484]
38. Tu M, Sun T, Grattan K. LSPR optical fibre sensors based on hollow gold nanostructures. Sensors and Actuators B: Chemical 2014 Feb;191:37-44. [doi: 10.1016/j.snb.2013.09.094]
39. Yousuf SMEH, Sakib MA, Islam MZ. A High-Performance Plasmonic Nanosensor Based on an Elliptical Nanorod in an MIM Configuration. IEEE Sensors J 2018 Aug 1;18(15):6145-6153. [doi: 10.1109/jsen.2018.2847760]
40. Manzo M, Schwend R. A Novel Microlaser-Based Plasmonic-Polymer Hybrid Resonator for Multiplexed Biosensing Applications. ASME Journal of Medical Diagnostics 2019 May;2(2):021006. [doi: 10.1115/1.4042377]
41. Shopova SI, Rajmangal R, Holler S, Arnold S. Plasmonic enhancement of a whispering-gallery-mode biosensor for single nanoparticle detection. Appl. Phys. Lett 2011 Jun 13;98(24):243104. [doi: 10.1063/1.3599584]
42. Nadgaran H, Afkhami Garaei M. Enhancement of a whispering gallery mode microtoroid resonator by plasmonic triangular gold nanoprism for label-free biosensor applications. Journal of Applied Physics 2015 Jul 28;118(4):043101. [doi: 10.1063/1.4927266]
43. Chung T, Lee S, Song E, Chun H, Lee B. Plasmonic nanostructures for nano-scale bio-sensing. Sensors (Basel) 2011;11(11):10907-10929 [FREE Full text] [doi: 10.3390/s111110907] [Medline: 22346679]
44. Liu Y, Park Y, Lee SE. Thermo-responsive mechano-optical plasmonic nano-antenna. Appl. Phys. Lett 2016 Jul 04;109(1):013109. [doi: 10.1063/1.4954907]
45. Yuan H, Register JK, Wang H, Fales AM, Liu Y, Vo-Dinh T. Plasmonic nanoprobes for intracellular sensing and imaging. Anal Bioanal Chem 2013 Jul 11;405(19):6165-6180. [doi: 10.1007/s00216-013-6975-1] [Medline: 23665636]
46. Schopf C, Martín A, Iacopino D. Plasmonic detection of mercury via amalgam formation on surface-immobilized single Au nanorods. Sci Technol Adv Mater 2017 Jan 09;18(1):60-67 [FREE Full text] [doi: 10.1080/14686996.2016.1258293] [Medline: 28179959]
47. Tao H, Lin Y, Yan J, Di J. A plasmonic mercury sensor based on silver–gold alloy nanoparticles electrodeposited on indium tin oxide glass. Electrochemistry Communications 2014 Mar;40:75-79. [doi: 10.1016/j.elecom.2014.01.002]
48. Unser S, Holcomb S, Cary R, Sagle L. Collagen-Gold Nanoparticle Conjugates for Versatile Biosensing. Sensors (Basel) 2017 Feb 15;17(2):378 [FREE Full text] [doi: 10.3390/s17020378] [Medline: 28212282]
49. Zhang L, Zhang Y, Hu Y, Fan Q, Yang W, Li A, et al. Refractive index dependent real-time plasmonic nanoprobes on a single silver nanocube for ultrasensitive detection of the lung cancer-associated miRNAs. Chem Commun (Camb) 2015;51(2):294-297. [doi: 10.1039/c4cc06663d] [Medline: 25407574]
50. Manzo M, Ioppolo T. Untethered photonic sensor for wall pressure measurement. Opt. Lett 2015 May 06;40(10):2257. [doi: 10.1364/ol.40.002257]
51. Manzo M. Untethered wall pressure and temperature sensor based on dye doped micro-scale resonator (Southern Methodist University). Ann Arbor, MI: ProQuest Dissertations Publishing; 2015.
52. Ioppolo T, Manzo M. Dome-shaped whispering gallery mode laser for remote wall temperature sensing. Appl. Opt 2014 Jul 31;53(22):5065. [doi: 10.1364/ao.53.005065]
53. Manzo M, Cavazos O. Neurotransducers Based Voltage Sensitive Dye-Doped Microlasers. Washington, DC: OSA Publication; 2019 Presented at: Biophotonics Congress: Optics in the Life Sciences Congress 2019 (BODA,BRAIN,NTM,OMA,OMP); 15–17 April 2019; Tucson, AZ. [doi: 10.1364/BODA.2019.JT4A.14]

54. Manzo M, Cavazos O, Ramirez-Cedillo E, Siller H. Embedded Spherical Microlasers for In-vivo Diagnostic Biomechanical Performances. ASME Journal of Medical Diagnostics 2020 Nov;3(4):044504. [doi: 10.1115/1.4048466]
55. Vollmer F, Braun D, Libchaber A, Khoshsima M, Teraoka I, Arnold S. Protein detection by optical shift of a resonant microcavity. Appl. Phys. Lett 2002 May 27;80(21):4057-4059. [doi: 10.1063/1.1482797]
56. Manzo M, Ioppolo T, Ayaz UK, Lapenna V, Ötügen MV. A photonic wall pressure sensor for fluid mechanics applications. Rev Sci Instrum 2012 Oct;83(10):105003. [doi: 10.1063/1.4757569] [Medline: 23126796]
57. Wagner HP, Schmitzer H, Lutti J, Borri P, Langbein W. Effects of uniaxial pressure on polar whispering gallery modes in microspheres. Journal of Applied Physics 2013 Jun 28;113(24):243101. [doi: 10.1063/1.4811447]
58. Hanumegowda NM, Stica CJ, Patel BC, White I, Fan X. Refractometric sensors based on microsphere resonators. Appl. Phys. Lett 2005 Nov 14;87(20):201107. [doi: 10.1063/1.2132076]
59. Li B, Wang Q, Xiao Y, Jiang X, Li Y, Xiao L, et al. On chip, high-sensitivity thermal sensor based on high-Q polydimethylsiloxane-coated microresonator. Appl. Phys. Lett 2010 Jun 21;96(25):251109. [doi: 10.1063/1.3457444]
60. Fan H, Xia C, Fan L, Wang L, Shen M. Graphene-supported plasmonic whispering-gallery mode in a metal-coated microcavity for sensing application with ultrahigh sensitivity. Optics Communications 2018 Mar;410:668-673. [doi: 10.1016/j.optcom.2017.11.018]
61. Foreman MR, Vollmer F. Theory of resonance shifts of whispering gallery modes by arbitrary plasmonic nanoparticles. New J. Phys 2013 Aug 02;15(8):083006. [doi: 10.1088/1367-2630/15/8/083006]
62. Santiago-Cordoba MA, Boriskina SV, Vollmer F, Demirel MC. Nanoparticle-based protein detection by optical shift of a resonant microcavity. Appl. Phys. Lett 2011 Aug 15;99(7):073701. [doi: 10.1063/1.3599706]
63. Huckabay HA, Wildgen SM, Dunn RC. Label-free detection of ovarian cancer biomarkers using whispering gallery mode imaging. Biosens Bioelectron 2013 Jul 15;45:223-229. [doi: 10.1016/j.bios.2013.01.072] [Medline: 23500368]
64. Chen X, Nan Y, Ma X, Liu H, Liu W, Shi L, et al. Detection of Small Biomolecule Interactions Using a Plasmonic Tilted Fiber Grating Sensor. J. Lightwave Technol 2019 Jun 1;37(11):2792-2799. [doi: 10.1109/jlt.2018.2870337]
65. Guo T, Liu F, Liang X, Qiu X, Huang Y, Xie C, et al. Highly sensitive detection of urinary protein variations using tilted fiber grating sensors with plasmonic nanocoatings. Biosens Bioelectron 2016 Apr 15;78:221-228 [FREE Full text] [doi: 10.1016/j.bios.2015.11.047] [Medline: 26618641]
66. Zhang Y, Wang F, Qian S, Liu Z, Wang Q, Gu Y, et al. A Novel Fiber Optic Surface Plasmon Resonance Biosensors with Special Boronic Acid Derivative to Detect Glycoprotein. Sensors (Basel) 2017 Oct 01;17(10):2259 [FREE Full text] [doi: 10.3390/s17102259] [Medline: 28974028]
67. Dong C, He L, Xiao Y, Gaddam VR, Ozdemir SK, Han Z, et al. Fabrication of high-Q polydimethylsiloxane optical microspheres for thermal sensing. Appl. Phys. Lett 2009 Jun 08;94(23):231119. [doi: 10.1063/1.3152791]
68. Sharma A. Plasmonic biosensor for detection of hemoglobin concentration in human blood: Design considerations. Journal of Applied Physics 2013 Jul 28;114(4):044701. [doi: 10.1063/1.4816272]
69. Luo D, Wang X, Zeng S, Ramamurthy G, Burda C, Basilion J. Prostate-specific membrane antigen targeted gold nanoparticles for prostate cancer radiotherapy: does size matter for targeted particles? Chem. Sci 2019 Sep 11;10(35):8119-8128. [doi: 10.1039/C9SC02290B]
70. Chen S, Zhao Q, Zhang L, Wang L, Zeng Y, Huang H. Combined detection of breast cancer biomarkers based on plasmonic sensor of gold nanorods. Sensors and Actuators B: Chemical 2015 Dec;221:1391-1397. [doi: 10.1016/j.snb.2015.08.023]
71. Li R, Xie S, Zhang L, Li L, Kong D, Wang Q, et al. Soft and transient magnesium plasmonics for environmental and biomedical sensing. Nano Res 2018 Mar 21;11(8):4390-4400. [doi: 10.1007/s12274-018-2028-6]
72. Ribaut C, Voisin V, Malachovská V, Dubois V, Mégret P, Wattiez R, et al. Small biomolecule immunosensing with plasmonic optical fiber grating sensor. Biosens Bioelectron 2016 Mar 15;77:315-322. [doi: 10.1016/j.bios.2015.09.019] [Medline: 26432194]
73. Luo B, Wu S, Zhang Z, Zou W, Shi S, Zhao M, et al. Human heart failure biomarker immunosensor based on excessively tilted fiber gratings. Biomed. Opt. Express 2016 Dec 05;8(1):57. [doi: 10.1364/boe.8.000057]
74. Kuruvinashetti K, Kashani AS, Badilescu S, Beaudet D, Piekny A, Packirisamy M. Intracellular Localized Surface Plasmonic Sensing for Subcellular Diagnosis. Plasmonics 2017 Dec 18;13(5):1639-1648. [doi: 10.1007/s11468-017-0673-3]
75. de la Rica R, Stevens MM. Plasmonic ELISA for the ultrasensitive detection of disease biomarkers with the naked eye. Nat Nanotechnol 2012 Dec 28;7(12):821-824. [doi: 10.1038/nnano.2012.186] [Medline: 23103935]

Abbreviations

AdoHcy: S-adenosyl-l-homocysteine
ATR: attenuated total reflection
LSPR: localized surface plasmon resonance
SPR: surface plasmon resonance
TFBG: tilted fiber Bragg grating
WGM: whispering gallery mode

Edited by G Eysenbach; submitted 13.01.20; peer-reviewed by A Civit, A Aminbeidokhti; comments to author 10.03.20; revised version received 01.10.20; accepted 11.03.21; published 12.04.21.

Please cite as:
Manzo M, Cavazos O, Huang Z, Cai L
Plasmonic and Hybrid Whispering Gallery Mode–Based Biosensors: Literature Review
JMIR Biomed Eng 2021;6(2):e17781
URL: https://biomedeng.jmir.org/2021/2/e17781
doi:10.2196/17781
PMID:

Viewpoint

Using Medical Device Standards for Design and Risk Management of Immersive Virtual Reality for At-Home Therapy and Remote Patient Monitoring

Joseph Peter Salisbury[1], PhD

Playhab R&D, Cognivive, Inc., Davis, CA, United States

Corresponding Author:
Joseph Peter Salisbury, PhD
Playhab R&D
Cognivive, Inc.
2003 Baywood Ln
Davis, CA, 95618
United States
Phone: 1 530 361 6006
Email: joey@cognivive.com

Abstract

Numerous virtual reality (VR) systems have received regulatory clearance as therapeutic medical devices for in-clinic and at-home use. These systems enable remote patient monitoring of clinician-prescribed rehabilitation exercises, although most of these systems are nonimmersive. With the expanding availability of affordable and easy-to-use head-mounted display (HMD)-based VR, there is growing interest in immersive VR therapies. However, HMD-based VR presents unique risks. Following standards for medical device development, the objective of this paper is to demonstrate a risk management process for a generic immersive VR system for remote patient monitoring of at-home therapy. Regulations, standards, and guidance documents applicable to therapeutic VR design are reviewed to provide necessary background. Generic requirements for an immersive VR system for home use and remote patient monitoring are identified using predicate analysis and specified for both patients and clinicians using user stories. To analyze risk, failure modes and effects analysis, adapted for medical device risk management, is performed on the generic user stories and a set of risk control measures is proposed. Many therapeutic applications of VR would be regulated as a medical device if they were to be commercially marketed. Understanding relevant standards for design and risk management early in the development process can help expedite the availability of innovative VR therapies that are safe and effective.

(JMIR Biomed Eng 2021;6(2):e26942) doi:10.2196/26942

KEYWORDS

virtual reality; telerehabilitation; remote patient monitoring; medical device design; safety; medical device regulation; risk assessment; failure modes and effects analysis

Introduction

Virtual Reality as a Medical Device

Therapeutic virtual reality (VR) offers tremendous potential to provide innovative treatments in a broad range of clinical areas, including mental health disorders [1] (eg, traumatic stress [2,3], anxiety disorders [4], depression [5], schizophrenia [6], eating disorders [7]), pain management [8,9], motor and cognitive rehabilitation of neurodegenerative disorders [10,11], traumatic brain injury [12], stroke [13,14], and cognitive disorders [15,16].

While a wide variety of approaches have been referred to as VR in the literature, VR is popularly understood to include the use of a wearable head-mounted display (HMD) that creates a sense of being immersed in a virtual environment. HMD-based immersive VR has only recently begun to approach the same level of affordability as nonimmersive VR. The sense of presence that immersive VR offers has considerable potential to differentiate the impact of VR in clinical contexts, including telerehabilitation, moving forward [17-19]. Critically, immersive VR offers the potential for greater ecological validity in therapy, allowing the brain to respond to stimuli similar to how it does in the real world [20-24].

As VR interventions are developed and evaluated by clinicians and patients—particularly in an at-home environment—it is essential to evaluate the regulatory requirements that may restrict the translation of such technologies to routine clinical practice. For VR interventions that will be classified as a medical device,

it is strongly recommended that requirements be identified early in the design and development phase to prevent costly reworkings of the system, software, and associated documentation [25-27].

While VR interventions include both a hardware and software component, many proposed VR interventions (particularly those for at-home use) leverage off-the-shelf (OTS) VR technology. In the most recent wave of technology, this includes the standalone VR headsets with 6-degrees of freedom (6-DOF) tracking, including the Vive Focus Plus, Oculus Quest, and Pico Neo. While designed primarily for nonmedical purposes, this does not restrict their use as a component of a medical device. A consumer VR headset is transformed into a medical device by virtue of the intended use of the software it is running. While additional, built-for-purpose hardware components may be introduced into a therapeutic VR system (eg, custom sensors, adaptive controllers), the software component is necessary and essential for transforming OTS VR devices into a medical device, and thus, can be considered as part of the larger category of software as a medical device (SaMD) [28].

While the design, development, testing, and postmarket surveillance of therapeutic VR include many of the same considerations, HMD-based VR presents unique challenges in comparison to the broader category of SaMD. In addition to the potentially hazardous situations introduced by wearing an occlusive headset that can induce side effects ranging from simulator sickness [29,30] to seizure, fully immersive VR introduces novel challenges for interface design among a population that will typically have little-to-no experience with the technology [31-33]. Thus, it is becoming useful to discuss the requirements of VR as a medical device (VRaMD) in their own right.

Medical Device Quality Requirements

To understand what regulatory requirements may be for a given VR intervention, it is important to first consider whether the intended use is indeed classified as a "medical device" in a particular jurisdiction. The Global Harmonization Task Force published a guidance document toward an internationally recognized definition of a medical device [34]. In the United States, a medical device is defined in section 201(h) of the Food, Drug, and Cosmetic Act [35].

The US Food and Drug Administration (FDA) has published guidance [36] that outlines certain software functions that may meet the definition of a medical device, but as they pose a lower risk to the public, the FDA intends to exercise enforcement discretion. That is, the FDA will not enforce medical device regulatory requirements on this software. Included in the type of software is one that "use video and video games to motivate patients to do their physical therapy exercises at home." With that said, this guidance document also states that software becomes a regulated medical device by performing patient-specific analysis and providing patient-specific diagnosis or treatment recommendations. Furthermore, there are specific regulatory classifications in the United States that classify "interactive rehabilitation exercise devices" as Class II medical devices, providing a clear regulatory path for a VRaMD intended to provide rehabilitation. Ultimately, manufacturers interested in commercialization in the United States are encouraged to contact the FDA to determine what, if any, regulatory requirements may apply.

Assuming the intended use of a VRaMD is determined to be a regulated medical device in a particular jurisdiction, it is important to understand regulatory requirements early in the device and development process. When developing a novel medical device, those without a background in medical device engineering may assume the burden to demonstrate the safety and effectiveness of a medical device is the domain of clinical investigators. However, it is important to note that the universal expectation of regulatory bodies is that safety and effectiveness be built into the system in early design and development stages. In the United States, Title 21 of the Code of Federal Regulations (CFR) [37] provides specific regulations that define the minimum current good manufacturing practice (cGMP) requirements for drugs, biologics, and medical devices. The cGMP regulations, also known as the quality system regulation (QSR), are based on the "quality-by-design" principle, which calls for quality to be built into the product, as testing alone cannot be relied on to ensure product quality [38].

cGMP regulations require establishment of a quality management system (QMS). The QMS impacts an organization's daily activities at every level, including product planning, design, development, testing, and change management. Software professionals coming from a nonregulated software development industry may find it difficult to adapt to the planning and documentation requirements imposed by quality requirements [39,40]. Quality requirements for medical device software development may seem to conflict with agile software development methodologies and impose a large amount of overhead when developing medical device software [41]. Still, it is critical that software professionals confront the challenge of medical device quality requirements head on not only to be compliant with regulations, but also to ensure medical device software is safe and effective for its intended purpose. For medical device software, there are clear expectations for how to document the entire software development life cycle, from establishing user needs through to verification, validation, postmarket surveillance, and change management.

Quality requirements for medical devices include the integration of risk management across the product life cycle. As a component of risk management, a systematic risk assessment for a device must be performed with risk controls implemented and verified to mitigate unacceptable device hazards. Implementing risk management as part of the requirements analysis and design process of an SaMD can aid in improving designs early in the development process. This can prevent the need for reworking solutions and changing project scope late in the development process when changes can be more costly. In the case of home-use VRaMD, risk analysis can reveal new system requirements that can help improve system usability and adoption while mitigating risks to patients.

Objectives of This Paper

This paper reviews regulations, standards, guidance documents, and technical reports that can be relevant for the design and development of a VRaMD. To demonstrate the application of

these standards in the design and development process, the requirements for a generic home-use VRaMD system for at-home therapy are specified. A risk assessment is performed on the requirements to derive a set of risk control measures. Methods for verifying these risk control measures are discussed. The objectives of this paper are to:

1. Provide an overview of medical device standards that are applicable to the development of VRaMD intended for home use and remote patient monitoring.
2. Analyze the requirements of a generic home-use VRaMD and demonstrate how risk management can be used to identify and evaluate hazards, determine appropriate risk control measures, and limit potentially hazardous situations.

Design Standards Applicable to VRaMD

General Quality Management System Requirements

Medical device regulations are the legally defined requirements within a jurisdiction for how medical device manufacturers must operate. Requirements for a particular medical device can be determined by classifying the device within the risk-based classification system of a particular jurisdiction. One of the most fundamental requirements of a medical device organization is implementation of a QMS [42]. A QMS is a formal system that documents policies, procedures, and responsibility to manage product or process quality. QMS requirements are specified by regulatory bodies to ensure medical devices will be safe and perform as intended. It is important to note that while QMS regulations and standards outline a range of specific requirements, they are typically broadly defined to allow a variety of ways an organization can achieve their goals. Thus, the scope and complexity of an organization's QMS can vary widely depending on the device type, organization size and structure, and the nature of specific regulatory requirements.

While the requirement that a QMS be certified varies depending on regulatory jurisdiction and device type, to achieve broad recognition many manufacturers follow ISO 13485:2016 [43]. ISO 13485 specifies requirements for a QMS that can be used by an organization involved in one or more stages of the life cycle of a medical device. These stages can include design, development, and production of a medical device, as well as storage, distribution, installation, technical support, servicing, decommission, and disposal. In the United States, adherence to ISO 13485 is not required, although the US QSR is generally aligned with this standard.

An important aspect of the QMS relevant for VRaMD development is the concept of design controls. Design controls are a set of policies and practices intended to ensure consistent translation of input requirements into a product that meets those requirements. Both ISO 13485 and FDA QSR set out a series of requirements for design controls. Design control is an iterative process following a structured methodology to ensure the device under development will be safe, effective, and meet end-user needs. The design control process is often illustrated with the V-model [44]. Design control requirements specify a general framework where various deliverables are generated and approved at each stage of the design and development process through to device verification and validation activities. These deliverables are necessary for auditing the QMS and meeting regulatory needs, requiring a robust system of procedures for maintaining documentation and approvals.

While the expectations of the QMS design controls are well-defined, there remains considerable room for how an organization decides to carry out these objectives. As part of QMS requirements, it is expected that an organization establishes detailed design and development plans for each product. These plans should specify how the development process is carried out, including assignment of responsibilities to adequately trained personnel and how these procedures are aligned with regulatory requirements and appropriate standards.

Risk Management for Medical Devices

As part of fulfilling regulatory requirements, organizations must perform risk management activities. For example, under the 2017 European Union Medical Device Regulation (EU MDR) [45], manufacturers must have a documented risk management plan, identify and analyze the known and foreseeable hazards for each device, estimate and evaluate the associated risks, and eliminate or control those risks. Risk analysis is required as part of the US FDA's design control requirements (21 CFR 820.30) [46] and is a component of FDA premarket submissions. ISO 14971:2019 [47], recognized worldwide by regulatory bodies, is widely acknowledged as the principal standard for this purpose. As part of ISO 14971, an organization develops a risk management plan, which includes how device risk assessments should be conducted.

ISO 14971 describes the requirements of a risk management process for medical device development, including 6 key stages: risk analysis, risk evaluation, risk control, evaluation of overall residual risk acceptability, risk management report, and production and postproduction information. Like quality management requirements, the details of how these processes are carried out in practice are left to the manufacturer. To implement ISO 14971, a company must first establish and document how they will conduct a risk management process that includes the required components in the standard. To accomplish risk analysis, Annex G of ISO 14971 provides guidance on some techniques, including preliminary hazard analysis, fault tree analysis, and failure modes and effects analysis (FMEA).

FMEA enables any effect or consequence of individual components to be systematically identified and is more appropriate as the design matures [48]. FMEA can be applied during the design process to understand the impact of potential defects and incorporate changes relatively early when they are less expensive to make. Thus, safety is improved and performance is enhanced by minimizing the probability and severity of hazardous situations.

It is important to note that, although FMEA is a recognized risk assessment tool specified in ISO 14971, completing FMEA according to the FMEA standard IEC 60812:2018 [49] does not fulfill all the requirements of ISO 14971. For example, FMEA focuses on defects, whereas the focus of ISO 14971 is on harm. In ISO 14971, both normal and abnormal circumstances must

be considered, as opposed to a focus on failure situations in FMEA. That is, even when the device is functioning as intended, hazardous situations may still occur, which must be identified. For example, the device may function as intended, but a specific subset of patients may experience side effects. Patients may also misinterpret instructions or feedback provided by the system. Of course, hazardous situations that arise from system malfunction, such as damage or misuse of the system leading to degraded system performance, must also be considered.

Furthermore, FMEA can allow for low-priority defects to persist, whereas risks in a medical device should be reduced or eliminated as far as reasonably possible before a medical device can be marketed. Both ISO 14971 and FMEA require the risk parameters of occurrence and severity to be addressed, where occurrence is the probability of occurrence of harm and severity is the extent of its impact or consequences. However, FMEA also considers the probability of detecting the harm before it occurs, which is not part of ISO 14971. Harm may still happen even if it is detected, and harms not easily detectable may unnecessarily raise risk levels. Thus, this parameter is excluded. Once the differences between FMEA and ISO 14971 are understood, it is possible to adapt FMEA to meet the requirements of ISO 14971 (Figure 1).

To conduct the risk management process, the first step is to identify the hazards, hazardous situations, and associated harms of a device. Hazard identification can be performed by reviewing the medical device characteristics, such as intended use, technologies used in the device, how the device is intended to function in clinical procedures, what could occur if the device is misused, and what could occur if information from the device is misinterpreted.

Once hazards are identified, for each hazardous situation, risk estimation is performed whereby the probability of occurrence and severity of that harm is estimated. It is the responsibility of the manufacturer to establish an appropriate quantitative or qualitative method for categorizing probability of occurrence of harm and severity of harm. Tables 1 and 2 provide example ways of categorizing severity of harm and probability of harm occurrence. Note that these tables are intentionally kept simple for illustration purposes and could include greater (or fewer) categories, as appropriate.

Figure 1. Overview of ISO 14971 risk management process requirements and how FMEA can be adapted. Redrawn and adapted from resources developed by Gantus and Semoegy (unpublished data). FMEA: failure mode and effects analysis; ISO: International Organization for Standardization; RPN: risk priority number.

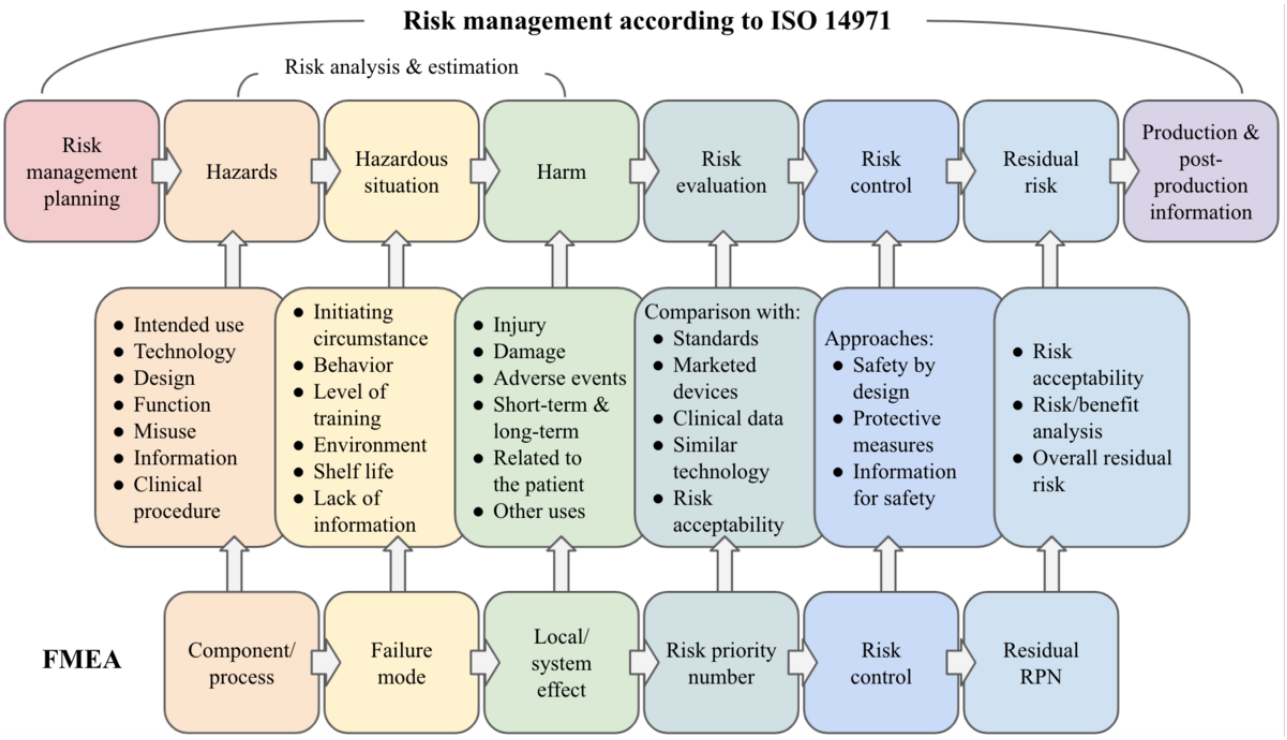

Table 1. Example severity table.

Rank	Description	Criteria
5	Critical	Loss of limb or life-threatening injury.
4	Major	Severe, long-term injury; potential disability.
3	Serious	Short-term injury or impairment requiring additional medical intervention to correct.
2	Minor	Slight inconvenience with little to no effect on product performance; minor injury not requiring medical intervention.
1	Negligible	No significant risk of injury to patient.

Table 2. Example probability of occurrence table.

Rank	Description	Criteria
5	Frequent	1 in 100
4	Probable	1 in 1000
3	Occasional	1 in 10,000
2	Remote	1 in 100,000
1	Improbable	1 in 1,000,000

Acceptable methods for estimating risks are provided in ISO 14971 and include published standards, scientific technical data, field data from similar devices, usability tests, clinical evidence, and expert opinion. It is often not practical to assign numerical estimations for the likelihood of an occurrence of a particular harm. Thus, following qualitative descriptors can provide a reasonable method for estimating the probability of occurrence in the absence of precise data.

The "Rank" column is included in Tables 1 and 2 so that, following the FMEA approach, a risk priority number (RPN) can be generated for risk evaluation. In Figure 2, a risk evaluation matrix is generated by multiplying the probability of occurrence ranks with the severity of harm ranks. The risk evaluation matrix is divided into 3 risk regions to define acceptable risks (green), borderline risks (yellow), and unacceptable risks (red). Again, the illustrated risk regions are provided merely as an example, and a manufacturer can establish their own way of delineating acceptable and unacceptable risks, as may be appropriate for their device.

Hazards that are evaluated to have an unacceptable risk level require risk control measures. Borderline risks may also require risk control measures upon further investigation. While not required, risk control measures may also be desirable for acceptable risks as these may still improve the safety and performance of the device and lead to better end-user satisfaction. RPNs provide a way to prioritize the allocation of limited resources within a particular risk region.

Risk control measures defined in ISO 14971 include inherent safety by design, protective measures in the medical device itself or in the manufacturing process, and information for safety. Implementation and effectiveness of risk control measures must be verified and validated by the manufacturer. To evaluate the effectiveness of risk control measures, it is often necessary to conduct usability tests. For example, if information for safety is utilized, it is important that information is perceivable, understandable, and supports correct use of the device by the intended user group in the context of its intended use environment. IEC 62366-1 [50] is an international standard that can be used with ISO 14971 to conduct these evaluations. The US FDA has also developed their own guidance document [51].

After risk control measures are applied, any residual risk is required to be evaluated. Residual risk that is judged not to be acceptable requires further risk control measures. In the event residual risk is not acceptable and further risk control is not practicable, the manufacturer may conduct a risk–benefit analysis by gathering and reviewing data and literature to determine if the medical benefits of the intended use outweigh the residual risk. Information for safety may be used by the manufacturer to disclose risks that may outweigh the benefits of the device.

Figure 2. Risk evaluation matrix with risk priority numbers (RPNs) generated when multiplying the severity of harm rank (Table 1) with the corresponding probability of occurrence rank (Table 2). The risk evaluation matrix is divided into 3 risk regions, with acceptable risks in green, unacceptable risks in red, and borderline risks in yellow.

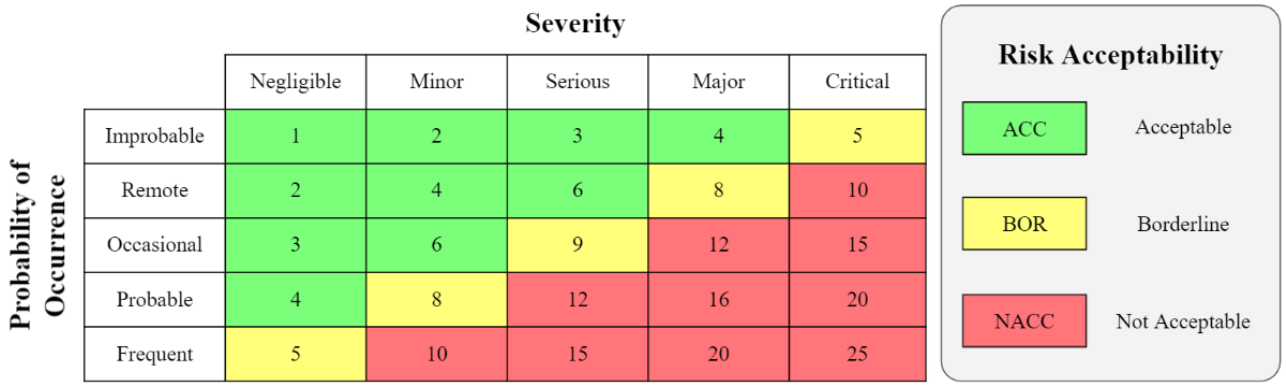

Software Life Cycle Processes

The majority of software problems are traceable to design and development errors, making software design control critical [52]. In both the United States and EU, all software components must be under design control or purchasing control, including design validation that includes software validation and risk analysis [53]. The EU adopted a new essential requirement regarding software in 2007, Essential Requirement 12.1.a [54], addressing the software life cycle. In EU MDR, safety and performance requirements (SPRs) replace the essential requirements and SPR 17 places greater emphasis on the entire product life cycle, as well as introducing specific requirements for mobile computing platforms and information security.

Likewise, the US FDA has guidance on general validation principles applicable to medical device software [55].

IEC 62304 [56] provides specific guidance on the processes to be performed for the development of medical device software, including risk management activities. IEC 62304 is an EU harmonized standard and is recognized by the FDA as an approved consensus standard and thus can be used as a benchmark to comply with both markets' regulatory requirements. This standard provides a life cycle process framework, with activities and tasks necessary for safe medical development. A central theme of IEC 62304 is the need to establish and maintain traceability between system requirements, software requirements, software testing, and risk control measures implemented in software [57]. Established user needs provide the foundation from which all software requirements are derived and must be maintained throughout the product life cycle. It is important to note that while the V-model is often used to illustrate these requirements, a "waterfall" approach is not necessary. IEC 62304 clarifies incremental strategies (eg, Agile), which acknowledge user needs may not be fully defined or may evolve throughout the product life cycle, can still meet the requirements specified in the standard.

Ultimately, it is the responsibility of the manufacturer to define how user needs and system requirements are captured, refined, and tested during product development. Numerous resources are available to help with this process and provide a way for manufacturers to demonstrate traceability and generate reports necessary for regulatory compliance while benefiting from the value of Agile practices. For example, the Association for the Advancement of Medical Instrumentation (AAMI) has published a technical information report (TIR)—AAMI TIR45:2012 [58]—to help provide guidance on how best to align Agile and medical device regulatory perspectives to develop safe and effective medical device software. AAMI TIR45 covers key topics such as documentation, evolutionary design and architecture, traceability, verification and validation, management changes, and "done" criteria. While adopting the practices recommended in AAMI TIR45 is not strictly required, and there are certainly other sensible ways to adapt Agile methodologies for medical device development, the US FDA recognizes AAMI TIR45 as a consensus standard. This recognition provides assurance that Agile practices can be successfully adapted to meet regulatory compliance requirements.

An important feature of AAMI TIR45 is that it provides a framework for reconciling the user story approach [59] for incrementally specifying product requirements with the design input/design output framework used in medical device development. A user story is a short, simple description of a feature told from the perspective of the person who desires the new capability (ie, an end user of the system or other stakeholder). User stories are typically written following the template: *As a <type of user>, I want <some goal> so that <some reason>*. To elaborate on a story, an accompanying set of acceptance criteria can be specified. User stories can also be broken down into more specific user stories when necessary and appropriate. As AAMI TIR45 explains, the goal of a user story is to be persistent and lightweight, capturing just enough essence of a requirement to allow for future discussions to uncover or elaborate more when needed.

Summary of VRaMD Design and Development Considerations

To summarize:

1. Depending on the regulatory jurisdiction and classification, VRaMD design and development may need to be captured in a QMS following design control requirements. This may include use of ISO 13485 or local regulations (eg, US FDA QSR).
2. For software development specifically, IEC 62304 provides a standard framework. AAMI TIR45 can used as guidance for adopting Agile practices, if desired.
3. Risk management according to ISO 14971 should be performed during the design process. FMEA is one risk analysis tool that can be adapted to ISO 14971. Effectiveness of risk control measures can be evaluated in usability tests following IEC 62366.

To demonstrate these concepts, a VRaMD for home use and remote patient monitoring is specified using a set of generic user stories. Applying FMEA, hazards associated with each user story are identified and risk is evaluated based on estimations of probability of occurrence and severity of harm. Risk control measures are proposed, and the residual risk is determined to demonstrate how a safe and effective VRaMD may be designed.

Risk Management for a Generic VRaMD

Requirements Analysis

To specify the requirements for an at-home VR rehabilitation system, it is helpful to review similar devices that are already legally marketed. In the United States, this is a common regulatory strategy. Demonstrating substantial equivalence to a legally marketed device, referred to as a predicate device, enables many devices to be cleared under the premarket notification [510(k)] submission process. In the US FDA medical device classification scheme, devices are classified as Class I, II, or III based on risk level, with Class I devices presenting the lowest risk, and Class III devices presenting the highest risk. Within each FDA class, device types are classified within regulations, which include special control requirements for Class II devices. The intended use and technological characteristics of a system obtaining 510(k) clearance are often made publicly available as a "510(k) Summary" (21 CFR 807.92).

Over the past decade, numerous devices that included at-home physical rehabilitation using video game technology received 510(k) clearance. This began with Jintronix (Jintronix Inc.) [60-62] and went on to include the Recovr Rehabilitation System (Recovr, Inc.) [63], Vera (Reflexion Health, Inc.) [64], the Yugo System (BioGaming Ltd.), the Virtual Occupational Therapy Application (Barron Associates, Inc., marketed as SaeboVR by Saebo, Inc.) [65-67], Uincare Home (UINCARE Corp.) [68], and MindMotion Go (MindMaze SA) [69]. These devices are regulated as Class II devices in the United States. None of these

systems utilize HMD-based VR, but rather the Microsoft Kinect motion tracking system. Still, each system includes the intended use of supporting physical rehabilitation of adults at-home by providing therapy guidance for patients and remotely accessible performance metrics for medical professionals.

By examining 510(k) Summaries for these devices, it can be seen they generally include 3 separate applications: a patient-facing application, a clinician-facing application, and a cloud-based server for providing data storage and managing communication between the 2 applications. The patient-facing application (henceforth, patient application) prompts and monitors patients in the performance of a therapy prescribed by their clinicians, reports performance data to the clinician for analysis, and provides an interface for patients to communicate with their clinician. The clinician facing-application (henceforth, clinician application) allows a clinician to define and update a patient's personal data, a patient's therapy prescription, monitor a patient's performance of that therapy, and permit a clinician to communicate with a patient. Thus, the common components of a VR telerehabilitation system have been established. Taking these descriptions into account, the core functionality for an immersive VR therapy system can be specified by replacing the Kinect with a standalone HMD-based VR system with 6-DOF tracking (Figure 3). A generic set of user stories for the patient application can be constructed from the descriptions of these systems (Table 3). Likewise, a generic set of user stories for the clinician application can also be constructed (Table 4). These generic user stories have provided a basis for designing additional therapy systems, including one using HMD-based VR [70,71].

Figure 3. Overview of generic VR as a medical device system for home-use and telerehabilitation. HMD: head-mounted display; VR: virtual reality.

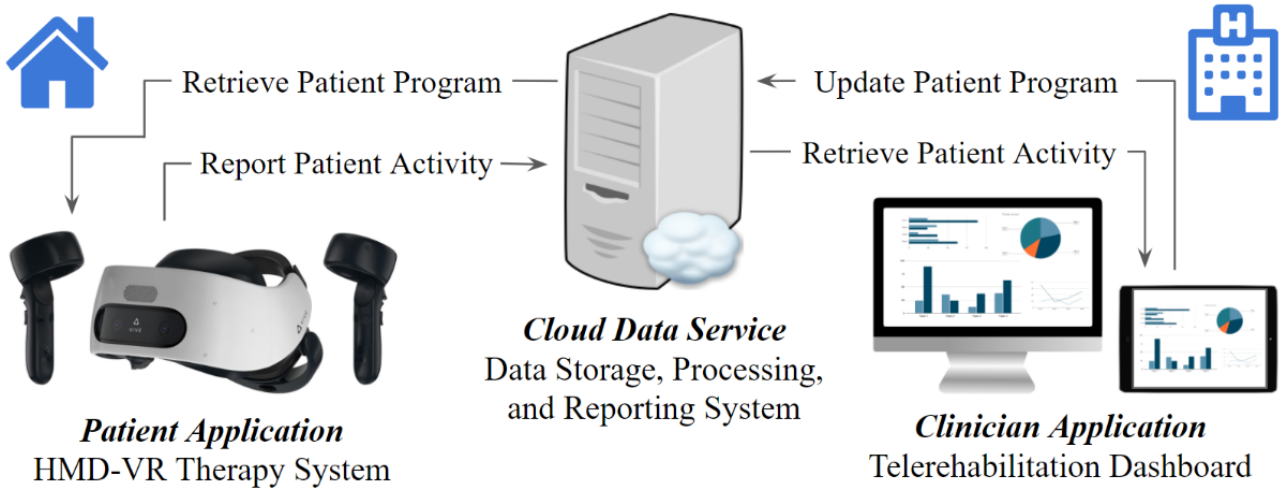

Table 3. Overview of virtual reality system requirements—patient stories.

ID	Summary	As a patient I want...	so that...
P1	Trusted exercise	to trust that exercises I perform have clinical utility	I know the time I spend using the system is worthwhile and will benefit my health.
P2	Ease of use	to feel confident I will be able to use the system at-home with minimal assistance	I can effectively benefit from the system and recover independently.
P3	Portability	to be able to perform therapy at home	I do not have to rely on transportation and scheduling and can recover on my own.
P4	Clinician supervision	my clinical health care provider to have access to my therapy data	communication regarding my at-home therapy is streamlined.
P5	Instructions	to have clear instructions on how to perform exercises	I am reminded how to properly complete these actions.
P6	Feedback	to have feedback as I am performing exercises	I know if I am performing exercises effectively.
P7	Motivation	exercises to feel more like a video game than homework	I am motivated to adhere to prescribed exercises.
P8	Performance summary	to see the results of my exercise performance	I know if I am performing exercises effectively based on established targets.
P9	Track progress	see my progress over time	I am intrinsically motivated to advance my recovery.
P10	Reminders	to be reminded to do exercises	I do not forget and take longer to recover.

Table 4. A generic set of clinician requirements for a virtual reality as a medical device system designed for home use and remote patient monitoring.

ID	Summary	As a clinician I want...	so that...
C1	Clinical validity	to know how system routines correspond to clinically valid therapies	I know how to apply my current understanding of therapy to the system's functionality.
C2	Instructions	to be able to learn the system quickly and completely	I am confident I understand how to utilize the system and integrate it into my practice without too much difficulty.
C3	Ease of use	to be able to quickly train patients and caregivers on the system	I feel confident they will be able to utilize the system at home.
C4	Manage patients	an online dashboard to manage my patients	I can add patients to the system.
C5	Personalization	to be able to give each patient their own profile	I can customize individual patients and track their progress over time.
C6	Customization	to be able to specify exercises for patients	I can target areas where patients need improvement.
C7	Assessment	to be able to assess patient ability	I can determine a baseline challenge level that can be used to monitor progress.
C8	Reminders	to remind patients to complete therapy	patients can be re-engaged if they are not active.
C9	Adherence tracking	to know when patients complete therapy	I know if patients are adhering to recommended frequency.
C10	Exercise tracking	to know how much patients complete therapy	I know if patients how much patients accomplish and whether they are being adequately challenged.
C11	Movement tracking	to know how patients perform treatment	I know how patient's exercise and if they are using clinically valid movements.
C12	Progress tracking	to know how well patients perform exercises	I know a patient's ability at a given time.
C13	Symptom tracking	to know how patient symptoms change (eg, improve)	I know if the patient can progress in a therapy.
C14	Remote feedback	a way to provide feedback to patients	I can communicate with patients, if necessary.
C15	Exportability	a way to export patient performance records (eg, through a printable report)	I can share clinically interpretable data with other members of the patient's clinical care team and with payers.
C16	Cybersecurity	my patients' records to be secure and protected	I can manage protected health information responsibly.

Risk Analysis and Evaluation

For each user story, the adapted FMEA process can be used to identify hazards (ie, potential sources of harm) of that feature (Multimedia Appendix 1). Hazards can lead to hazardous situations which may then cause harm. As part of the risk analysis, the probability of occurrence of harm is estimated based on a combination of the likelihood of both the hazard and the hazardous situation. Then, the severity of the harm produced by each hazardous situation is considered. For example, the display screens used in HMD-based VR can be considered a consistent hazard, which may lead to a variety of different hazardous situations. When identifying hazardous situations, it is important to consider both normal and abnormal use of the device. Likewise, hazards can still cause harm without a device failure. Even when using HMD-based VR as intended, there is potential for side effects including eye strain, claustrophobia, overstimulation, anxiety, and seizures. On one extreme, eye strain may be considered a common side effect of using HMD-based VR. However, the severity of resulting short-lasting headaches may be considered low. Alternatively, patients with photosensitivity may experience seizures. While the probability of this occurrence is much lower, if the patient is using the system independently at home, this seizure could fatal, and thus, critically severe.

In addition to the hazardous situations related to HMD-VR specifically, Multimedia Appendix 1 lists many hazards that would be common to non-HMD-VR at-home therapies. For example, data failing to properly synchronize between the clinician and patient applications can lead to the patient not receiving proper treatment. Hazardous situations also arise whenever either user group is unable to properly interpret instructions or data provided to them. This is most severe when it leads to the patient not being able to benefit from treatment. Thus, it can be seen how critical usability engineering can be to ensure proper medical device function. Figure 4 summarizes the identified risks associated with the system.

Figure 4. Risk analysis summary for a head-mounted display-based virtual reality (HMD-VR) medical device for home use and telerehabilitation.

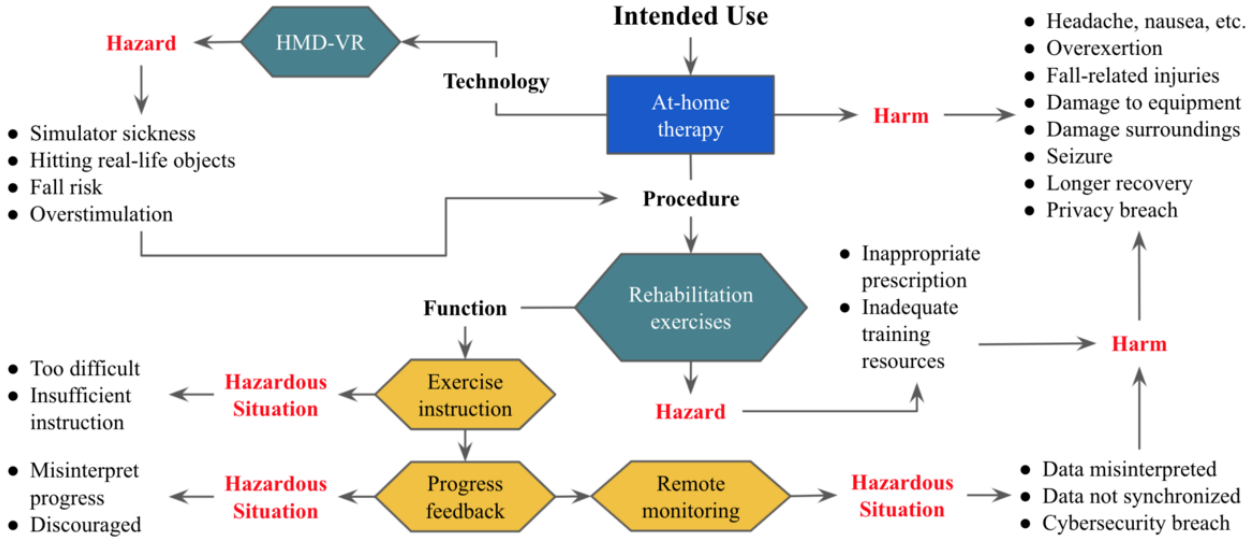

Risk Control Measures and Residual Risk Evaluation

ISO 14971 defines “safety” as freedom from unacceptable risk. Based on the risk assessment and acceptability criteria defined earlier, several unacceptable risks were identified that require risk control measures. A variety of borderline risks were also identified, which would require further investigation to determine whether risk control measures are necessary. While the remaining hazards were deemed to have an acceptable risk level, these potential failure points highlight opportunities to improve the system design and create greater patient and clinician satisfaction with the system. Thus, in Multimedia Appendix 2, risk control measures have been proposed for all hazards.

After completing the residual risk evaluation, almost all risks have been brought within the acceptable region. The only remaining borderline risk is associated with the potential for seizures in patients with photosensitivity. While the likelihood of a patient with these issues can be reduced by prescreening patients for a history of seizures, the harm associated with this situation is still considered severe. Overall, an HMD-based VRaMD can be designed to be safe for at-home use and remote patient monitoring when risk control measures are applied. Figure 5 summarizes the risk control measures that are recommended.

When examining the potential sources of unacceptable risks, important areas to consider early in the design and development of a VRaMD can be identified. For example, one source of unacceptable risk is related to insufficient clinician training resources, which can lead to a clinician not understanding the proper intended use of the system and prescribing it to inappropriate patients; clinicians not understanding how to properly configure the system to meet patient needs; and clinicians not understanding how to train patients on the system. To control for this risk, usability testing with clinicians should verify the system’s intended use is understandable and meets clinician needs. For clinicians to be able to utilize the system, they must both understand how to develop individualized patient treatment plans and interpret patient data generated by the system. Furthermore, there should be adequate resources available for clinicians to be able to train patients on the system, if necessary. Likewise, usability testing with patients should verify patient application exercise instructions are adequate to elicit target therapeutic actions. Resources specific to VRaMD usability evaluations should be considered [72]. System feedback provided to patients should also be interpretable by patients and, ideally, provide motivation so patients do not become discouraged by their results for whatever reason.

Hazardous situations can also occur when data between the patient and clinician applications can not properly synchronize due to internet connectivity issues. Depending on the severity of harm, it may be necessary for an internet connection to be provided as part of the system to ensure data can synchronize. This could also alleviate risk caused by patients not being able to connect the device to their home network. However, if a stable internet connection is available, it may be sufficient to provide adequate instruction and have a remote provider verify the patient has completed the necessary set up.

Finally, cybersecurity and patient privacy issues must be addressed. Indeed, protections for these concerns are critical for adoption of a connected health technology [73,74].

Figure 5. Summary of risk control measures to improve safety and end-user satisfaction.

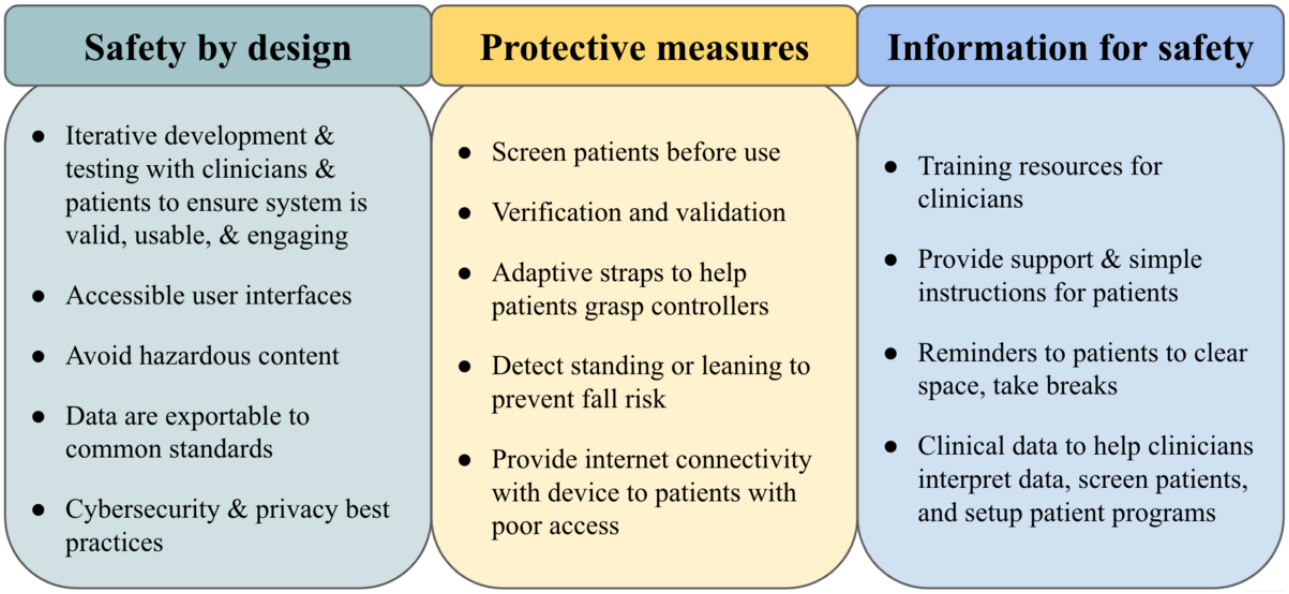

Cybersecurity and Patient Privacy Protections

Regulatory bodies generally require cybersecurity considerations as an aspect of the device design and risk management process. MDCG 2019-16 [75] provides guidance on how to fulfill essential requirements regarding cybersecurity specified in Annex I of EU MDR. Likewise, the US FDA provides guidance regarding cybersecurity information to be included in FDA premarket submissions [76], as well as guidance for postmarket management of cybersecurity vulnerabilities [77]. While it is generally up to the manufacturer to determine what cybersecurity controls are necessary for their device, applying recognized standards can help demonstrate implemented capabilities are appropriate and effective.

A variety of standards for addressing medical device cybersecurity are available to help manufacturers ensure they are following industry best practices. Selecting which standards to adopt can depend on the specific technologies and interfaces used by a product (see [78] for further discussion). One starting point is ANSI/AAMI/IEC TIR80001-2-2:2012 [79], which presents an informative set of high-level security capabilities that are intended to facilitate more effective communication of security requirements with stakeholders. The Manufacturer Disclosure Statement for Medical Device Security (MDS2) form [80] is aligned with the security capabilities described in TIR80001-2-2 and provides manufacturers a format for reporting the data assets handled by a medical device, as well as the approach taken to secure it. The MDS2 form thus provides a way for manufacturers to disclose to health care organizations (eg, hospitals) information necessary for them to conduct their own cybersecurity risk analyses [81].

Once necessary security capabilities are identified through risk management and understanding stakeholder needs, AAMI/IEC TIR80001-2-8:2016 can be used to determine specific design requirements from a set of common security standards. This allows a design team to select appropriate standards, as well as provide evidence that each of the applicable security capabilities have been met [78].

When evaluating necessary cybersecurity capabilities (eg, data access controls) and associated procedures (eg, notification of patient's data rights, notifications of detected data breaches to appropriate stakeholders), medical device manufacturers must understand and comply with the local legal requirements (eg, General Data Protection Regulation [GDPR], Health Insurance Portability and Accountability Act [HIPAA]). Regarding data rights and governance, manufacturers may employ end user license agreements, terms of service, and privacy policies to establish and convey company and user data rights for monitoring, evaluation, and distribution of collected data [73]. Additional precautions may be necessary for certain patient populations, such as children (eg, the Children's Online Privacy Protection Act).

Discussion

Summary of Recommendations

HMD-based VRaMDs, depending upon their intended use, will likely be subject to the same regulatory requirements as other medical devices. Quality requirements such as design controls may be unfamiliar to product designers and software professionals coming from unregulated fields. While design control requirements may appear to suggest a "waterfall" approach is necessary, it is not incompatible with Agile practices, which can be used once properly adapted. Incorporating regulatory requirements early in the design process is not only necessary but also helps eliminate costly reworkings later in development. Incorporating a risk management process will help systematically expose ways to make the product safer and improve end-user satisfaction. A comprehensive usability engineering plan is necessary to verify risk control measures are effective.

Using non-HMD-based VR systems already legally marketed in the United States for at-home therapy, a generic set of user stories for both patients and clinicians was specified here. While HMD-based VR introduces unique hazards to at-home therapy, the associated risks can be mitigated with appropriate control

measures, demonstrating that HMD-based VR can be designed to be safe for home use and remote patient monitoring.

For clinicians, it is important they understand the proper intended use of the system. This will enable them to prescribe the system to appropriate patients, understand how to configure the system to meet a particular patient's needs, and be able to interpret system performance metrics as intended to progress a patient through treatment. This can be accomplished through robust user interface design and providing clinicians with the necessary training resources. The effectiveness of these measures should be verified in usability testing. Finally, the accuracy of OTS movement tracking sensors should be verified to be within clinically relevant ranges if 3D motion data are used in assessing patient performance. Studies have already evaluated the accuracy of the Oculus Touch controllers [82] and HTC VIVE motion tracking sensors [83] for clinical use in motor rehabilitation.

Patients must understand risks associated with HMD-VR so that they may avoid hazardous situations at home. General risks may be avoided by properly clearing the environment of obstacles, avoiding standing with the headset on, taking breaks to rest, and stopping use of the device if they experience negative effects. When instructing patients to perform therapeutic actions, it is important they have the necessary guidance and feedback to determine if they are performing the therapy as intended. When providing patients with progress data, it is important these data are easily interpretable. Ideally, performance feedback data should not discourage the patient from continuing treatment. To determine if system safety information is effective, usability testing in patients' homes is necessary. An iterative human-centered design approach with clinicians and patients can help guide design concepts toward success early in development [84,85]. Assuming transmission of data between clinicians and patients is necessary for effective treatment, measures should be taken to verify the device is connected to the internet upon arrival at the patient's home.

Finally, appropriate patient privacy and cybersecurity protections are essential. Standards can be utilized to determine necessary security measures and how to implement them effectively. Stakeholder needs, including relevant data privacy regulations, will contribute to the assessment of necessary cybersecurity capabilities. The MDS2 form provides one method for communicating with health care providers data handled by the system and how they are protected. End users should be provided with a privacy notice that describes how data are collected, used, and retained, the types of data that the product obtains, the length of data retention, and how and by whom information is used.

Limitations

This paper describes a generic VRaMD system, using devices with a similar intended use as a basis. System functionality was specified at only the highest level to provide a reasonable scope for examination and discussion in the paper. Given a more specific intended use, more detailed requirements will be specified that may introduce new hazards to the system. The probability of occurrence and severity of device harms were roughly estimated for practical purposes.

A standalone HMD-based VR system with 6-DOF tracking was used as the core technology. Use of other VR systems may introduce different hazards. For example, a non-standalone system with external sensors (eg, Oculus Rift) may require additional set up and monitoring of sensor placement. More expensive head-mounted augmented and mixed reality systems (eg, Microsoft HoloLens, Magic Leap) were also not considered, although augmented and mixed reality–based medical devices are in development and may resolve certain hazards and limitations associated with occlusive VRaMD [86,87].

Overall, the intention of this paper was to provide an overview of an ISO 14971-compliant risk management process. To accomplish this, it was necessary to review related medical device regulations, standards, and guidance documents. While these requirements and recommendations are applicable to a variety of SaMD, specific devices and regulatory jurisdictions may require additional considerations. This paper was also not intended to be an exhaustive review of applicable standards. For example, the IEC 60601-1 [88] series of standards for electrical medical devices was not discussed. This was done to keep the focus of the paper on software and implementation of IEC 62304. However, IEC 60601-1 may be necessary for demonstrating the safety and electromagnetic compatibility of system hardware. More general (ie, nonmedical device specific) standards may also be useful for the design process, such as ISO 9241-210:2019 [89]. The IEEE Virtual Reality and Augmented Reality Working Group is developing standards for VR design that could be useful to apply to improve the safety, usability, and standardization of VRaMD [90]. Ultimately, a VRaMD manufacturer should communicate with the appropriate regulatory bodies when developing a new product intended for commercialization. The review provided here is intended to help orient those new to medical device development and provide a broad overview of regulatory requirements applicable to a variety of jurisdictions.

Comparison With Prior Work

Recent advances in the widespread availability of VR and its potential in therapy have led to growing interest in the development of industry best practices for translating this potential to a reality. For example, the Virtual Reality Clinical Outcomes Research Experts (VR-CORE) committee has published a framework for iterative clinical trial design for validating VR therapies [91]. Numerous papers have also shared the design process for various HMD-based VR interventions [92-99]. The focus of this paper was less about the design of a particular system, and more about demonstrating a risk management process to develop a VRaMD safe for home use and remote patient monitoring.

Numerous reports have examined challenges and best practices for introducing medical device regulatory requirements, such as design controls and risk management, into contemporary software development practices such as Agile [39,40,100-110]. Here, Agile techniques were introduced primarily as a method for specifying the requirements of the system through user stories. Additional concepts were introduced as necessary to demonstrate the risk management process. It is expected that VR developers working on VRaMD will be coming from

nonregulated fields (eg, video games, entertainment), and thus it is important to provide some necessary background. While the transition to medical device development can be challenging, this paper describes how Agile practices can be utilized to develop a safe and effective VRaMD. More recently, the HMD-based REAL Immersive system obtained 510(k) clearance for in-clinic use, providing further evidence that immersive VRaMD can successfully meet regulatory requirements.

Conclusions

HMD-based VR offers tremendous potential for novel at-home treatments. However, for these treatments to be successfully translated into clinical practice, VRaMD will need to be designed following the necessary regulatory requirements. While regulatory requirements can appear challenging, VRaMD designers should find it beneficial to gain an understanding of what is required so they may adapt their design process early in development. While medical device design controls present a need for comprehensive documentation of device design, incorporating risk management early in this process should help further refine system requirements. Following these recommendations will help make VRaMDs safe and effective, as well as improve patient and clinician satisfaction with these novel digital therapeutics.

Acknowledgments

This work was supported in part by the US National Institutes of Health (R43AG05287).

Conflicts of Interest

JPS is an employee of Cognivive, Inc., which markets CogniviveVR, an HMD-based immersive VR rehabilitation system for home use.

Multimedia Appendix 1
Risk analysis and risk evaluation of patient and clinician user stories.
[XLSX File (Microsoft Excel File), 46 KB - biomedeng_v6i2e26942_app1.xlsx]

Multimedia Appendix 2
Failure modes and effects analysis including risk control measures and residual risk analysis.
[XLSX File (Microsoft Excel File), 60 KB - biomedeng_v6i2e26942_app2.xlsx]

References

1. Jerdan SW, Grindle M, van Woerden HC, Kamel Boulos MN. Head-Mounted Virtual Reality and Mental Health: Critical Review of Current Research. JMIR Serious Games 2018 Jul 06;6(3):e14 [FREE Full text] [doi: 10.2196/games.9226] [Medline: 29980500]
2. Knaust T, Felnhofer A, Kothgassner OD, Höllmer H, Gorzka R, Schulz H. Virtual Trauma Interventions for the Treatment of Post-traumatic Stress Disorders: A Scoping Review. Front Psychol 2020;11:562506 [FREE Full text] [doi: 10.3389/fpsyg.2020.562506] [Medline: 33281664]
3. Singh S, Nathan-Roberts D. Virtual Reality Exposure Therapy and Military Personnel with Post-Traumatic Stress Disorder: A Systematic Review. 2019 Nov 20 Presented at: Proceedings of the Human Factors and Ergonomics Society Annual Meeting; 2019; Los Angeles, CA p. 1378-1383. [doi: 10.1177/1071181319631178]
4. Oing T, Prescott J. Implementations of Virtual Reality for Anxiety-Related Disorders: Systematic Review. JMIR Serious Games 2018 Nov 07;6(4):e10965. [doi: 10.2196/10965] [Medline: 30404770]
5. Lindner P, Hamilton W, Miloff A, Carlbring P. How to Treat Depression With Low-Intensity Virtual Reality Interventions: Perspectives on Translating Cognitive Behavioral Techniques Into the Virtual Reality Modality and How to Make Anti-Depressive Use of Virtual Reality-Unique Experiences. Front Psychiatry 2019;10:792 [FREE Full text] [doi: 10.3389/fpsyt.2019.00792] [Medline: 31736809]
6. Bisso E, Signorelli MS, Milazzo M, Maglia M, Polosa R, Aguglia E, et al. Immersive Virtual Reality Applications in Schizophrenia Spectrum Therapy: A Systematic Review. Int J Environ Res Public Health 2020 Aug 22;17(17):6111 [FREE Full text] [doi: 10.3390/ijerph17176111] [Medline: 32842579]
7. Clus D, Larsen ME, Lemey C, Berrouiguet S. The Use of Virtual Reality in Patients with Eating Disorders: Systematic Review. J Med Internet Res 2018 Dec 27;20(4):e157 [FREE Full text] [doi: 10.2196/jmir.7898] [Medline: 29703715]
8. Pourmand A, Davis S, Marchak A, Whiteside T, Sikka N. Virtual Reality as a Clinical Tool for Pain Management. Curr Pain Headache Rep 2018 Jun 15;22(8):53. [doi: 10.1007/s11916-018-0708-2] [Medline: 29904806]
9. Smith V, Warty RR, Sursas JA, Payne O, Nair A, Krishnan S, et al. The Effectiveness of Virtual Reality in Managing Acute Pain and Anxiety for Medical Inpatients: Systematic Review. J Med Internet Res 2020 Nov 02;22(11):e17980 [FREE Full text] [doi: 10.2196/17980] [Medline: 33136055]

10. Maggio MG, Russo M, Cuzzola MF, Destro M, La Rosa G, Molonia F, et al. Virtual reality in multiple sclerosis rehabilitation: A review on cognitive and motor outcomes. J Clin Neurosci 2019 Jul;65:106-111. [doi: 10.1016/j.jocn.2019.03.017] [Medline: 30898488]
11. Triegaardt J, Han TS, Sada C, Sharma S, Sharma P. The role of virtual reality on outcomes in rehabilitation of Parkinson's disease: meta-analysis and systematic review in 1031 participants. Neurol Sci 2020 Mar;41(3):529-536 [FREE Full text] [doi: 10.1007/s10072-019-04144-3] [Medline: 31808000]
12. Maggio MG, De Luca R, Molonia F, Porcari B, Destro M, Casella C, et al. Cognitive rehabilitation in patients with traumatic brain injury: A narrative review on the emerging use of virtual reality. J Clin Neurosci 2019 Mar;61:1-4. [doi: 10.1016/j.jocn.2018.12.020] [Medline: 30616874]
13. Wiley E, Khattab S, Tang A. Examining the effect of virtual reality therapy on cognition post-stroke: a systematic review and meta-analysis. Disabil Rehabil Assist Technol 2020 May 02:1-11. [doi: 10.1080/17483107.2020.1755376] [Medline: 32363955]
14. Mekbib DB, Han J, Zhang L, Fang S, Jiang H, Zhu J, et al. Virtual reality therapy for upper limb rehabilitation in patients with stroke: a meta-analysis of randomized clinical trials. Brain Inj 2020 Mar 20;34(4):456-465. [doi: 10.1080/02699052.2020.1725126] [Medline: 32064964]
15. Clay F, Howett D, FitzGerald J, Fletcher P, Chan D, Price A. Use of Immersive Virtual Reality in the Assessment and Treatment of Alzheimer's Disease: A Systematic Review. J Alzheimers Dis 2020;75(1):23-43 [FREE Full text] [doi: 10.3233/JAD-191218] [Medline: 32280091]
16. D'Cunha NM, Nguyen D, Naumovski N, McKune AJ, Kellett J, Georgousopoulou EN, et al. A Mini-Review of Virtual Reality-Based Interventions to Promote Well-Being for People Living with Dementia and Mild Cognitive Impairment. Gerontology 2019;65(4):430-440 [FREE Full text] [doi: 10.1159/000500040] [Medline: 31108489]
17. Garrett B, Taverner T, Gromala D, Tao G, Cordingley E, Sun C. Virtual Reality Clinical Research: Promises and Challenges. JMIR Serious Games 2018 Oct 17;6(4):e10839 [FREE Full text] [doi: 10.2196/10839] [Medline: 30333096]
18. Smits M, Staal JB, van Goor H. Could Virtual Reality play a role in the rehabilitation after COVID-19 infection? BMJ Open Sport Exerc Med 2020;6(1):e000943 [FREE Full text] [doi: 10.1136/bmjsem-2020-000943] [Medline: 33178449]
19. Kim W, Cho S, Ku J, Kim Y, Lee K, Hwang H, et al. Clinical Application of Virtual Reality for Upper Limb Motor Rehabilitation in Stroke: Review of Technologies and Clinical Evidence. J Clin Med 2020 Oct 21;9(10):3369 [FREE Full text] [doi: 10.3390/jcm9103369] [Medline: 33096678]
20. Clemenson GD, Stark CEL. Virtual Environmental Enrichment through Video Games Improves Hippocampal-Associated Memory. J Neurosci 2015 Dec 09;35(49):16116-16125 [FREE Full text] [doi: 10.1523/JNEUROSCI.2580-15.2015] [Medline: 26658864]
21. Choi JW, Kim BH, Huh S, Jo S. Observing Actions Through Immersive Virtual Reality Enhances Motor Imagery Training. IEEE Trans Neural Syst Rehabil Eng 2020 Jul;28(7):1614-1622. [doi: 10.1109/TNSRE.2020.2998123] [Medline: 32634098]
22. Kothgassner OD, Felnhofer A. Does virtual reality help to cut the Gordian knot between ecological validity and experimental control? Annals of the International Communication Association 2020 Jul 12;44(3):210-218. [doi: 10.1080/23808985.2020.1792790]
23. Horan B, Heckenberg R, Maruff P, Wright B. Development of a new virtual reality test of cognition: assessing the test-retest reliability, convergent and ecological validity of CONVIRT. BMC Psychol 2020 Jun 12;8(1):61 [FREE Full text] [doi: 10.1186/s40359-020-00429-x] [Medline: 32532362]
24. Parsons TD. Virtual Reality for Enhanced Ecological Validity and Experimental Control in the Clinical, Affective and Social Neurosciences. Front Hum Neurosci 2015;9:660 [FREE Full text] [doi: 10.3389/fnhum.2015.00660] [Medline: 26696869]
25. Hrgarek N. Certification and regulatory challenges in medical device software development. 2012 Presented at: 2012 4th International Workshop on Software Engineering in Health Care (SEHC); June 4-5, 2012; Zurich, Switzerland. [doi: 10.1109/sehc.2012.6227011]
26. Gilman BL, Brewer JE, Kroll MW. Medical device design process. Annu Int Conf IEEE Eng Med Biol Soc 2009;2009:5609-5612. [doi: 10.1109/IEMBS.2009.5333644] [Medline: 19964397]
27. Kinsel D. Design control requirements for medical device development. World J Pediatr Congenit Heart Surg 2012 Jan 01;3(1):77-81. [doi: 10.1177/2150135111422720] [Medline: 23804688]
28. International Medical Device Regulators Forum. Software as a Medical Device (SaMD): Key Definitions. 2013. URL: http://www.imdrf.org/docs/imdrf/final/technical/imdrf-tech-131209-samd-key-definitions-140901.pdf [accessed 2021-02-22]
29. Sharples S, Cobb S, Moody A, Wilson JR. Virtual reality induced symptoms and effects (VRISE): Comparison of head mounted display (HMD), desktop and projection display systems. Displays 2008 Mar;29(2):58-69. [doi: 10.1016/j.displa.2007.09.005]
30. Serge SR, Moss JD. Simulator Sickness and the Oculus Rift: a First Look. In: Proceedings of the Human Factors and Ergonomics Society Annual Meeting. 2016 Dec 20 Presented at: Proceedings of the Human Factors and Ergonomics Society Annual Meeting; 2015; Los Angeles, CA p. 761-765. [doi: 10.1177/1541931215591236]

31. McGill M, Boland D, Murray-Smith R, Brewster S. A Dose of Reality: Overcoming Usability Challenges in VR Head-Mounted Displays. New York, NY: ACM Press; 2015 Presented at: CHI '15: CHI Conference on Human Factors in Computing Systems; April 2015; Seoul, Republic of Korea. [doi: 10.1145/2702613.2732491]
32. Baker S, Waycott J, Robertson E, Carrasco R, Neves BB, Hampson R, et al. Evaluating the use of interactive virtual reality technology with older adults living in residential aged care. Information Processing & Management 2020 May;57(3):102105. [doi: 10.1016/j.ipm.2019.102105]
33. Tuena C, Pedroli E, Trimarchi PD, Gallucci A, Chiappini M, Goulene K, et al. Usability Issues of Clinical and Research Applications of Virtual Reality in Older People: A Systematic Review. Front Hum Neurosci 2020;14:93 [FREE Full text] [doi: 10.3389/fnhum.2020.00093] [Medline: 32322194]
34. Global Harmonization Task Force. Report No.: GHTF/SG1/N071:2012. Definition of the Terms "Medical Device" and "In Vitro Diagnostic (IVD) Medical Device". URL: http://www.imdrf.org/docs/ghtf/final/sg1/technical-docs/ghtf-sg1-n071-2012-definition-of-terms-120516.pdf [accessed 2021-02-22]
35. Definitions; generally - 21 U.S. Code § 321(h). 2019. URL: https://www.govinfo.gov/content/pkg/USCODE-2019-title21/pdf/USCODE-2019-title21-chap9-subchapII-sec321.pdf [accessed 2021-05-29]
36. US Food and Drug Administration. Policy for device software functions and mobile medical applications. 2019. URL: https://www.fda.gov/media/80958/download [accessed 2021-02-22]
37. Quality System Regulation, 21 C.F.R. § 820. 2020. URL: https://www.govinfo.gov/content/pkg/CFR-2020-title21-vol8/pdf/CFR-2020-title21-vol8.pdf [accessed 2021-05-29]
38. US Food and Drug Administration. Guidance for industry: Quality systems approach to pharmaceutical cGMP regulations. 2006. URL: https://www.fda.gov/media/71023/download [accessed 2021-02-22]
39. McHugh M, McCaffery F, Casey V, Pikkarainen M. Integrating Agile Practices with a Medical Device SDLC. European Systems and Software Process Improvement and Innovation Conference (EuroSPI, Vienna, Austria, 21-25 May). 2012. URL: https://core.ac.uk/download/pdf/35316287.pdf [accessed 2021-05-20]
40. Spence J. There has to be a better way! software development. New York, NY: IEEE; 2005 Presented at: Agile Development Conference (ADC'05); Denver, CO; July 24-29, 2005 p. 272. [doi: 10.1109/adc.2005.47]
41. McHugh M, Cawley O, McCaffcry F, Richardson I, Wang X. An agile v-model for medical device software development to overcome the challenges with plan-driven software development lifecycles. 2013 Presented at: 5th International Workshop on Software Engineering in Health Care (SEHC); 2013; San Francisco, California. [doi: 10.1109/sehc.2013.6602471]
42. Luczak J. Establishing a small company's medical device quality system. The TQM Journal 2012 Jun 08;24(4):363-373. [doi: 10.1108/17542731211247382]
43. ISO 13485:2016 Medical devices — Quality management systems — Requirements for regulatory purposes. International Organization for Standardization. URL: https://www.iso.org/standard/59752.html [accessed 2021-02-22]
44. Forsberg K, Mooz H. The Relationship of System Engineering to the Project Cycle. In: INCOSE International Symposium. 1991 Oct Presented at: INCOSE International Symposium; 1991; Chattanooga, TN p. 57-65. [doi: 10.1002/j.2334-5837.1991.tb01484.x]
45. European Commission. Regulation (EU) 2017/745 of the European Parliament and of the Council. 2017. URL: https://eur-lex.europa.eu/legal-content/EN/TXT/?uri=uriserv:OJ.L_.2017.117.01.0001.01.ENG [accessed 2021-05-29]
46. Design Controls, 21 C.F.R. § 820.30. 2020. URL: https://www.govinfo.gov/content/pkg/CFR-2020-title21-vol8/pdf/CFR-2020-title21-vol8.pdf [accessed 2021-05-29]
47. ISO 14971:2019 Medical devices — Application of risk management to medical devices. International Organization for Standardization. URL: https://www.iso.org/standard/72704.html [accessed 2021-02-22]
48. Stadler J, Seidl N. Software failure modes and effects analysis. 2013 Jan Presented at: Proceedings Annual Reliability and Maintainability Symposium (RAMS); 2013; Orlando, Florida, USA. [doi: 10.1109/rams.2013.6517710]
49. IEC 60812:2018 — Failure modes and effects analysis (FMEA and FMECA). International Electrotechnical Commission. URL: https://webstore.iec.ch/publication/26359 [accessed 2021-02-22]
50. IEC 62366-1:2015 Medical devices — Part 1: Application of usability engineering to medical devices. International Electrotechnical Commission. URL: https://www.iso.org/standard/63179.html [accessed 2021-02-22]
51. Applying human factors and usability engineering to medical devices. US Food and Drug Administration. 2016. URL: https://www.fda.gov/media/80481/download [accessed 2021-02-22]
52. Wallace DR, Kuhn DR. Failure modes in medical device software: an analysis of 15 years of recall data. Int. J. Rel. Qual. Saf. Eng 2011 Nov 21;08(04):351-371. [doi: 10.1142/s021853930100058x]
53. Hall G, editor. Fundamentals of Medical Device Regulations, Third Edition. Rockville, MD: Regulatory Affairs Professionals Society (RAPS); 2020.
54. European Commission. Directive 2007/47/EC of the European Parliament and of the Council. 2007. URL: http://eur-lex.europa.eu/legal-content/EN/TXT/?uri=CELEX:32007L0047 [accessed 2021-05-29]
55. General Principles of Software Validation. US Food and Drug Administration. 2002. URL: https://www.fda.gov/regulatory-information/search-fda-guidance-documents/general-principles-software-validation [accessed 2021-02-22]
56. IEC 62304:2006 Medical device software — Software life cycle processes. International Electrotechnical Commission. URL: https://www.iso.org/standard/38421.html [accessed 2021-02-22]

57. Regan G, Mc Caffery F, Mc Daid K, Flood D. Medical device standards' requirements for traceability during the software development lifecycle and implementation of a traceability assessment model. Computer Standards & Interfaces 2013 Nov;36(1):3-9. [doi: 10.1016/j.csi.2013.07.012]
58. AAMI TIR45(R2018) - Guidance on the use of AGILE practices in the development of medical device software. Association for the Advancement of Medical Instrumentation. URL: https://webstore.ansi.org/Standards/AAMI/AAMITIR452012R2018 [accessed 2021-02-22]
59. Cohn M. User stories applied: For agile software development. Crawfordsville, Indiana: Addison-Wesley Professional; 2004.
60. Martel D, Lauzé M, Agnoux A, Fruteau de Laclos L, Daoust R, Émond M, et al. Comparing the effects of a home-based exercise program using a gerontechnology to a community-based group exercise program on functional capacities in older adults after a minor injury. Exp Gerontol 2018 Jul 15;108:41-47. [doi: 10.1016/j.exger.2018.03.016] [Medline: 29577975]
61. Valiani V, Lauzé M, Martel D, Pahor M, Manini TM, Anton S, et al. A New Adaptive Home-based Exercise Technology among Older Adults Living in Nursing Home: A Pilot Study on Feasibility, Acceptability and Physical Performance. J Nutr Health Aging 2017;21(7):819-824 [FREE Full text] [doi: 10.1007/s12603-016-0820-0] [Medline: 28717812]
62. Lauzé M, Martel DD, Aubertin-Leheudre M. Feasibility and Effects of a Physical Activity Program Using Gerontechnology in Assisted Living Communities for Older Adults. J Am Med Dir Assoc 2017 Dec 01;18(12):1069-1075. [doi: 10.1016/j.jamda.2017.06.030] [Medline: 28818422]
63. Hart E, Hayes A, Hodges L, Jett K, Finetto C, Hutchison S, et al. Feasibility of and Adherence to a Home-Based Video Game Rehabilitation Protocol. Am J Occup Ther 2020 Aug 01;74(4_Supplement_1):7411520504p1. [doi: 10.5014/ajot.2020.74s1-po9724]
64. Prvu Bettger J, Green CL, Holmes DN, Chokshi A, Mather RC, Hoch BT, et al. Effects of Virtual Exercise Rehabilitation In-Home Therapy Compared with Traditional Care After Total Knee Arthroplasty: VERITAS, a Randomized Controlled Trial. J Bone Joint Surg Am 2020 Jan 15;102(2):101-109. [doi: 10.2106/JBJS.19.00695] [Medline: 31743238]
65. Adams RJ, Lichter MD, Krepkovich ET, Ellington A, White M, Diamond PT. Assessing upper extremity motor function in practice of virtual activities of daily living. IEEE Trans Neural Syst Rehabil Eng 2015 Mar;23(2):287-296 [FREE Full text] [doi: 10.1109/TNSRE.2014.2360149] [Medline: 25265612]
66. Ellington A, Adams R, White M, Diamond P. Behavioral intention to use a virtual instrumental activities of daily living system among people with stroke. Am J Occup Ther 2015;69(3):6903290030p1-6903290030p8 [FREE Full text] [doi: 10.5014/ajot.2015.014373] [Medline: 25871604]
67. Adams RJ, Lichter MD, Ellington A, White M, Armstead K, Patrie JT, et al. Virtual Activities of Daily Living for Recovery of Upper Extremity Motor Function. IEEE Trans Neural Syst Rehabil Eng 2018 Jan;26(1):252-260. [doi: 10.1109/TNSRE.2017.2771272] [Medline: 29324411]
68. Lee H, Chang W, Lee J, Hwang J. Therapeutic potential of the home-based exercise program with the augmented reality system on balance in stroke patients: A preliminary report. Annals of Physical and Rehabilitation Medicine 2018 Jul;61:e36. [doi: 10.1016/j.rehab.2018.05.079]
69. Storz C, Schulte-Göcking H, Woiczinski M, Azqueta-Gavaldon M, Azad SC, Kraft E. [Exergames for patients with complex regional pain syndrome : A feasibility study]. Schmerz 2020 Apr 24;34(2):166-171. [doi: 10.1007/s00482-019-00436-x] [Medline: 32095887]
70. Salisbury J, Liu R, Minahan L, Shin H, Karnati S, Duffy S. Patient Engagement Platform for Remote Monitoring of Vestibular Rehabilitation with Applications in Concussion Management and Elderly Fall Prevention. 2018 Presented at: IEEE International Conference on Healthcare Informatics (ICHI); 2018; New York City, NY. [doi: 10.1109/ichi.2018.00082]
71. Salisbury J, Aronson T, Simon T. At-Home Self-Administration of an Immersive Virtual Reality Therapeutic Game for Post-Stroke Upper Limb Rehabilitation. In: Extended Abstracts of the 2020 Annual Symposium on Computer-Human Interaction in Play. 2020 Nov Presented at: 2020 Annual Symposium on Computer-Human Interaction in Play; November 2020; Virtual Event (Canada). [doi: 10.1145/3383668.3419935]
72. Zhang T, Booth R, Jean-Louis R, Chan R, Yeung A, Gratzer D, et al. A Primer on Usability Assessment Approaches for Health-Related Applications of Virtual Reality. JMIR Serious Games 2020 Oct 28;8(4):e18153 [FREE Full text] [doi: 10.2196/18153] [Medline: 33112243]
73. Patel NA, Butte AJ. Characteristics and challenges of the clinical pipeline of digital therapeutics. NPJ Digit Med 2020 Dec 11;3(1):159 [FREE Full text] [doi: 10.1038/s41746-020-00370-8] [Medline: 33311567]
74. Christodoulakis C, Asgarian A. Barriers to adoption of information technology in healthcare. 2017 Nov Presented at: Proceedings of the 27th Annual International Conference on Computer Science and Software Engineering; 2017; Markham, ON, Canada p. 66-75.
75. Medical Device Coordination Group. MDCG 2019-16 Guidance on Cybersecurity for Medical Devices. 2019. URL: https://ec.europa.eu/docsroom/documents/41863 [accessed 2021-05-29]
76. Content of Premarket Submissions for Management of Cybersecurity in Medical Devices. US Food and Drug Administration. 2014. URL: https://www.fda.gov/media/86174/download [accessed 2021-02-22]
77. Postmarket Management of Cybersecurity in Medical Devices. US Food and Drug Administration. 2016. URL: https://www.fda.gov/media/95862/download [accessed 2021-02-22]

78. Jump M, Finnegan A. Using Standards to Establish Foundational Security Requirements for Medical Devices. Biomed Instrum Technol 2017 Sep 02;51(s6):33-37. [doi: 10.2345/0899-8205-51.s6.33] [Medline: 29161099]
79. Association for the Advancement of Medical Instrumentation. AAMI TIR80001-2-2:2012 – Application of risk management for IT-networks incorporating medical devices – Part 2-2: Guidance for the disclosure and communication of medical device security needs, risks and controls. URL: https://store.aami.org/s/store#/store/browse/detail/a152E000006j62XQAQ [accessed 2021-05-29]
80. Manufacturer Disclosure Statement for Medical Device Security. National Electrical Manufacturers Association. 2015. URL: https://www.nema.org/Standards/view/Manufacturer-Disclosure-Statement-for-Medical-Device-Security [accessed 2021-02-22]
81. Wu F, Eagles S. Cybersecurity for Medical Device Manufacturers: Ensuring Safety and Functionality. Biomed Instrum Technol 2016;50(1):23-33. [doi: 10.2345/0899-8205-50.1.23] [Medline: 26829136]
82. Shum LC, Valdés BA, Van der Loos HM. Determining the Accuracy of Oculus Touch Controllers for Motor Rehabilitation Applications Using Quantifiable Upper Limb Kinematics: Validation Study. JMIR Biomed Eng 2019 Jun 06;4(1):e12291. [doi: 10.2196/12291]
83. Hemphill S, Nguyen A, Rodriguez ST, Menendez M, Wang E, Lawrence K, et al. Mobilization and calibration of the HTC VIVE for virtual reality physical therapy. Digit Health 2020;6:2055207620950929 [FREE Full text] [doi: 10.1177/2055207620950929] [Medline: 32963801]
84. Harte R, Quinlan LR, Glynn L, Rodríguez-Molinero A, Baker PM, Scharf T, et al. Human-Centered Design Study: Enhancing the Usability of a Mobile Phone App in an Integrated Falls Risk Detection System for Use by Older Adult Users. JMIR Mhealth Uhealth 2017 May 30;5(5):e71 [FREE Full text] [doi: 10.2196/mhealth.7046] [Medline: 28559227]
85. Harte R, Glynn L, Rodríguez-Molinero A, Baker PM, Scharf T, Quinlan LR, et al. A Human-Centered Design Methodology to Enhance the Usability, Human Factors, and User Experience of Connected Health Systems: A Three-Phase Methodology. JMIR Hum Factors 2017 Mar 16;4(1):e8 [FREE Full text] [doi: 10.2196/humanfactors.5443] [Medline: 28302594]
86. Held JPO, Yu K, Pyles C, Veerbeek JM, Bork F, Heining S, et al. Augmented Reality-Based Rehabilitation of Gait Impairments: Case Report. JMIR Mhealth Uhealth 2020 May 26;8(5):e17804 [FREE Full text] [doi: 10.2196/17804] [Medline: 32452815]
87. Salisbury JP, Keshav NU, Sossong AD, Sahin NT. Concussion Assessment With Smartglasses: Validation Study of Balance Measurement Toward a Lightweight, Multimodal, Field-Ready Platform. JMIR Mhealth Uhealth 2018 Jan 23;6(1):e15 [FREE Full text] [doi: 10.2196/mhealth.8478] [Medline: 29362210]
88. International Electrotechnical Commission. IEC 60601-1 - Medical electrical equipment - Part 1: General requirements for basic safety and essential performance. URL: https://webstore.iec.ch/publication/2606 [accessed 2021-05-29]
89. ISO 9241-210:2019 Ergonomics of Human-System Interaction — Part 210: Human-Centred Design for Interactive Systems. 2019. URL: https://www.iso.org/standard/77520.html [accessed 2021-02-22]
90. Yuan Y. Paving the Road for Virtual and Augmented Reality [Standards]. IEEE Consumer Electron. Mag 2018 Jan;7(1):117-128. [doi: 10.1109/mce.2017.2755338]
91. Birckhead B, Khalil C, Liu X, Conovitz S, Rizzo A, Danovitch I, et al. Recommendations for Methodology of Virtual Reality Clinical Trials in Health Care by an International Working Group: Iterative Study. JMIR Ment Health 2019 Jan 31;6(1):e11973 [FREE Full text] [doi: 10.2196/11973] [Medline: 30702436]
92. AlMousa M, Al-Khalifa HS, AlSobayel H. Requirements Elicitation and Prototyping of a Fully Immersive Virtual Reality Gaming System for Upper Limb Stroke Rehabilitation in Saudi Arabia. Mobile Information Systems 2017;2017:1-12. [doi: 10.1155/2017/7507940]
93. Tong X, Gromala D, Amin A, Choo A. The Design of an Immersive Mobile Virtual Reality Serious Game in Cardboard Head-Mounted Display for Pain Management. In: Pervasive Computing Paradigms for Mental Health. Cham, Switzerland: Springer International Publishing; 2016 Presented at: 5th International Conference, MindCare 2015; September 24-25, 2015; Milan, Italy p. 284-293. [doi: 10.1007/978-3-319-32270-4_29]
94. Eisapour M, Cao S, Domenicucci L, Boger J. Participatory Design of a Virtual Reality Exercise for People with Mild Cognitive Impairment. In: Extended Abstracts of the 2018 CHI Conference on Human Factors in Computing Systems. New York, NY: ACM Press; 2018 Presented at: 2018 CHI Conference on Human Factors in Computing Systems; April 21–26, 2018; Montréal, QC, Canada p. 1-9. [doi: 10.1145/3170427.3174362]
95. Eisapour M, Cao S, Domenicucci L, Boger J. Virtual Reality Exergames for People Living with Dementia Based on Exercise Therapy Best Practices. 2018 Sep 27 Presented at: Proceedings of the Human Factors and Ergonomics Society Annual Meeting; 2018; Los Angeles, CA p. 528-532. [doi: 10.1177/1541931218621120]
96. Shen J, Xiang H, Luna J, Grishchenko A, Patterson J, Strouse RV, et al. Virtual Reality-Based Executive Function Rehabilitation System for Children With Traumatic Brain Injury: Design and Usability Study. JMIR Serious Games 2020 Aug 25;8(3):e16947 [FREE Full text] [doi: 10.2196/16947] [Medline: 32447275]
97. Elor A, Teodorescu M, Kurniawan S. Project Star Catcher. ACM Trans. Access. Comput 2018 Nov 22;11(4):1-25. [doi: 10.1145/3265755]
98. Dias P, Silva R, Amorim P, Lains J, Roque E, Pereira ISF, et al. Using Virtual Reality to Increase Motivation in Poststroke Rehabilitation. IEEE Comput Graph Appl 2019;39(1):64-70. [doi: 10.1109/MCG.2018.2875630] [Medline: 30869599]

99. Ou Y, Wang Y, Chang H, Yen S, Zheng Y, Lee B. Development of virtual reality rehabilitation games for children with attention-deficit hyperactivity disorder. J Ambient Intell Human Comput 2020 Apr 10;11(11):5713-5720. [doi: 10.1007/s12652-020-01945-9]
100. Rottier P, Rodrigues V. Agile development in a medical device company. New York, NY: IEEE; 2008 Aug Presented at: Agile 2008 Conference; August 4-8, 2008; Toronto, ON, Canada p. 218-223. [doi: 10.1109/agile.2008.52]
101. McHugh M, McCaffery F, Coady G. An Agile Implementation within a Medical Device Software Organisation. Cham, Switzerland: Springer International Publishing; 2014 Nov Presented at: International Conference on Software Process Improvement and Capability Determination; November 4-6, 2014; Vilnius, Lithuania p. 190-201. [doi: 10.1007/978-3-319-13036-1_17]
102. Gordon WJ, Stern AD. Challenges and opportunities in software-driven medical devices. Nat Biomed Eng 2019 Jul;3(7):493-497. [doi: 10.1038/s41551-019-0426-z] [Medline: 31278389]
103. Kostić M. Challenges of Agile Practices Implementation in the Medical Device Software Development Methodologies. European Project Management Journal 2017;7(2):36-44 [FREE Full text]
104. Laukkarinen T, Kuusinen K, Mikkonen T. Regulated software meets DevOps. Information and Software Technology 2018 May;97:176-178. [doi: 10.1016/j.infsof.2018.01.011]
105. Laukkarinen T, Kuusinen K, Mikkonen T. DevOps in regulated software development: case medical devices. New York, NY: IEEE; 2017 Presented at: 2017 IEEE/ACM 39th International Conference on Software Engineering: New Ideas and Emerging Technologies Results Track (ICSE-NIER); May 20-28, 2017; Buenos Aires, Argentina p. 15-18. [doi: 10.1109/icse-nier.2017.20]
106. Lie M, Sánchez-Gordón M, Colomo-Palacios R. DevOps in an ISO 13485 regulated environment: A multivocal literature review. In: Proceedings of the 14th ACM/IEEE International Symposium on Empirical Software Engineering Measurement (ESEM). New York, NY: ACM; 2020 Presented at: 14th ACM/IEEE International Symposium on Empirical Software Engineering Measurement (ESEM); October 2020; Bari, Italy p. 1-11. [doi: 10.1145/3382494.3410679]
107. Keutzer L, Simonsson US. Medical Device Apps: An Introduction to Regulatory Affairs for Developers. JMIR Mhealth Uhealth 2020 Jun 26;8(6):e17567 [FREE Full text] [doi: 10.2196/17567] [Medline: 32589154]
108. Lang M. Heart Rate Monitoring Apps: Information for Engineers and Researchers About the New European Medical Devices Regulation 2017/745. JMIR Biomed Eng 2017 Aug 18;2(1):e2 [FREE Full text] [doi: 10.2196/biomedeng.8179]
109. Lewis TL, Wyatt JC. mHealth and mobile medical Apps: a framework to assess risk and promote safer use. J Med Internet Res 2014 Sep 15;16(9):e210 [FREE Full text] [doi: 10.2196/jmir.3133] [Medline: 25223398]
110. Vincent CJ, Niezen G, O'Kane AA, Stawarz K. Can standards and regulations keep up with health technology? JMIR Mhealth Uhealth 2015 Jun 03;3(2):e64 [FREE Full text] [doi: 10.2196/mhealth.3918] [Medline: 26041730]

Abbreviations

AAMI: Association for the Advancement of Medical Instrumentation
CFR: Code of Federal Regulations
cGMP: current good manufacturing practice
DOF: degrees of freedom
EU: European Union
FDA: Food and Drug Administration
FMEA: failure modes and effects analysis
HMD: head-mounted display
IEC: International Electrotechnical Commission
ISO: International Organization for Standardization
MDCG: Medical Device Coordination Group
MDR: Medical Device Regulation
MDS2: Manufacturer Disclosure Statement for Medical Device Security
OTS: off-the-shelf
QMS: quality management system
QSR: quality system regulation
SaMD: software as a medical device
SPR: safety and performance requirements
TIR: technical information report
VR: virtual reality
VRaMD: virtual reality as a medical device

Edited by G Eysenbach; submitted 04.01.21; peer-reviewed by C Jones, B Kim, S van der Veen; comments to author 25.01.21; revised version received 22.02.21; accepted 17.04.21; published 03.06.21.

Please cite as:
Salisbury JP
Using Medical Device Standards for Design and Risk Management of Immersive Virtual Reality for At-Home Therapy and Remote Patient Monitoring
JMIR Biomed Eng 2021;6(2):e26942
URL: https://biomedeng.jmir.org/2021/2/e26942
doi:10.2196/26942
PMID:

Original Paper

Virtual Reality–Guided Meditation for Chronic Pain in Patients With Cancer: Exploratory Analysis of Electroencephalograph Activity

Henry Fu[1], BScE, MASc; Bernie Garrett[2], DPhil; Gordon Tao[3], MSc; Elliott Cordingley[2], BSc; Zahra Ofoghi[4], PhD; Tarnia Taverner[2], DPhil; Crystal Sun[2], MPH; Teresa Cheung[1,5,6], PhD

[1]School of Engineering Science, Simon Fraser University, Burnaby, BC, Canada

[2]School of Nursing, University of British Columbia, Vancouver, BC, Canada

[3]School of Rehabilitation Sciences, University of British Columbia, Vancouver, BC, Canada

[4]School of Interactive Arts and Technology, Simon Fraser University, Surrey, BC, Canada

[5]Surrey Memorial Hospital, Fraser Health Authority, Surrey, BC, Canada

[6]Behavioural and Cognitive Neuroscience Institute, Simon Fraser University, Burnaby, BC, Canada

Corresponding Author:
Bernie Garrett, DPhil
School of Nursing
University of British Columbia
T201-2211 Wesbrook Mall
Vancouver, BC, V6T 2B5
Canada
Phone: 1 604 822 7443
Email: bernie.garrett@nursing.ubc.ca

Abstract

Background: Mindfulness-based stress reduction has demonstrated some efficacy for chronic pain management. More recently, virtual reality (VR)–guided meditation has been used to assist mindfulness-based stress reduction. Although studies have also found electroencephalograph (EEG) changes in the brain during mindfulness meditation practices, such changes have not been demonstrated during VR-guided meditation.

Objective: This exploratory study is designed to explore the potential for recording and analyzing EEG during VR experiences in terms of the power of EEG waveforms, topographic mapping, and coherence. We examine how these measures changed during a VR-guided meditation experience in participants with cancer-related chronic pain.

Methods: A total of 10 adult patients with chronic cancer pain underwent a VR-guided meditation experience while EEG signals were recorded during the session using a BioSemi ActiveTwo system (64 channels, standard 10-20 configuration). The EEG recording session consisted of an 8-minute resting condition (pre), a 30-minute sequence of 3 VR-guided meditation conditions (med), and a final rest condition (post). Power spectral density (PSD) was compared between each condition using a cluster-based permutation test and across conditions using multivariate analysis of variance. A topographic analysis, including coherence exploration, was performed. In addition, an exploratory repeated measures correlation was used to examine possible associations between pain scores and EEG signal power.

Results: The predominant pattern was for increased β and γ bandwidth power in the meditation condition (P<.025), compared with both the baseline and postexperience conditions. Increased power in the δ bandwidth was evident, although not statistically significant. The pre versus post comparison also showed changes in the θ and α bands (P=.02) located around the frontal, central, and parietal cortices. Across conditions, multivariate analysis of variance tests identified 4 clusters with significant (P<.05) PSD differences in the δ, θ, β, and γ bands located around the frontal, central, and parietal cortices. Topographically, 5 peak channels were identified: AF7, FP2, FC1, CP5, and P5, and verified the changes in power in the different brain regions. Coherence changes were observed primarily between the frontal, parietal, and occipital regions in the θ, α, and γ bands (P<.0025). No significant associations were observed between pain scores and EEG PSD.

Conclusions: This study demonstrates the feasibility of EEG recording in exploring neurophysiological changes in brain activity during VR-guided meditation and its effect on pain reduction. These findings suggest that distinct altered neurophysiological

brain signals are detectable during VR-guided meditation. However, these changes were not necessarily associated with pain. These exploratory findings may guide further studies to investigate the highlighted regions and EEG bands with respect to VR-guided meditation.

Trial Registration: ClinicalTrials.gov NCT00102401; http://clinicaltrials.gov/ct2/show/NCT00102401

(JMIR Biomed Eng 2021;6(2):e26332) doi:10.2196/26332

KEYWORDS

virtual reality; guided meditation; neurophysiology; electroencephalograph; EEG

Introduction

Background

Chronic pain (CP) is a common condition occurring in 1 in 5 Canadians [1], and it has limited effective treatment approaches. Mindfulness-based stress reduction (MBSR) has shown some evidence of efficacy in this area [2,3] and has also been used to treat other clinical conditions, such as migraine, depression, addiction, and substance misuse [2,4].

Mindfulness meditation encompasses a range of mental exercises that share a common focus on regulating attention and awareness to improve well-being [2-4]. It is described as the quality of being completely engaged in the present moment, free from distractions and judgments, and being aware of bodily sensations, thoughts, and feelings without getting caught up by them, and it is used as a therapeutic technique in MBSR [5,6]. These practices involve mental training that allows practitioners to develop their minds in specific ways to help them deal with stress and anxiety [7,8]. Although the clinical benefits remain somewhat controversial, it is generally viewed as a beneficial practice for mental well-being, stress reduction, and pain management [9-11].

A recent trend in MBSR practice has been the use of immersive virtual reality (VR) to help participants focus on meditative exercise [12-16]. However, to date, neurological studies have not been performed with VR-guided meditation practices. Therefore, this exploratory study sought to identify any identifiable neurological effects of VR-guided meditation practices using electroencephalographs (EEGs).

Neurological Mindfulness Studies

Subjective reports of the benefits of mindfulness meditation have prompted investigations into the potential corresponding neurophysiological states. Exploration of fluctuations in brain wave voltage amplitude (power) topography and coherence (associated areas of activity) using EEG variations in neural activity assessed with functional magnetic resonance imaging and cortical evoked responses to visual and auditory stimuli that reflect the impact of meditation on attention [4,17-26]. However, findings remain speculative. EEG studies have previously reported modulation in α, θ, and γ band frequencies, generally with increased power and coherence during mediation [4,7,17,27]. Some studies theoretically conjectured how meditative states relate to EEG bandwidths. For example, Travis and Shear [28] suggested that focused attention (sustained attention is focused on a given object) increases γ band power, open monitoring (nonreactive monitoring of an ongoing experience) increases θ, and an automatic-self-transcending stage (transcending the procedures of the meditation) increases α [28]. Nevertheless, a consensus on what we currently know about how EEG forms correlate with meditation or how this may map onto stages of mental development or specific cognitive skills is yet to be reached [7,8].

The α frequency band lies between 8 and 12 Hz and is predominantly located in the occipital cortex. α waves are present in deep relaxation and sleep, usually when the eyes are closed. θ waves are characterized by oscillations in the 4-8 Hz band found in both cortical and subcortical structures. Increases in θ have been described during a variety of learning and recognition tasks, light sleep (including the rapid-eye-movement dream state), and deep meditation. θ and α power changes have been reported to increase in a number of meditation studies [4,17,19,29-31]. Moreover, γ is a higher frequency range generally regarded as between 30 and 50 Hz, although the range reported has varied substantially between 20 and 200 Hz across different studies [30]. This initial research suggests that γ is associated with a number of sensory and cognitive high-level information processing functions, such as semantic insights, learning, and neural plasticity. Peak γ frequencies around 40 Hz in bilateral hemispheres have only been observed in highly practiced meditators [7,30]. In addition, a posterior increase in γ activity may be related to enhanced perceptual clarity reported in some open monitoring (focusing on awareness itself) meditative processes [7,17,30].

VR-Assisted Mindfulness

VR is rapidly developing as a new form of media and uses computer-generated audio-visual displays and hand controller user interfaces to produce a sense of immersion in a digital 3D environment. Instead of watching an image on a typical computer or video display, VR technologies provide an increased sense of presence by engaging the senses (sight, sound, and touch) in real-time stereoscopic audio-visual media where users can move around and explore the environment as if they were there.

VR in Pain Management

One of the most common health care applications of VR is its use in pain management. Several studies have explored the value of MBSR in CP management, although the reported effect sizes for this technique have been typically mild to moderate, and regular adherence with meditative practice is problematic [3,32,33]. It has been suggested that combining mindfulness meditation within a VR intervention may help support acceptance and adherence to practice while having a synergistic effect on pain reduction through immersive VR distraction

[34-36]. This remains an active area of research, as adjunctive VR strategies have been used successfully in the treatment of acute pain [37-41] and more recently have also been explored with CP [12,35,42,43]. The theoretical rationale behind why VR may enhance mindfulness skills is that VR provides the user with cognitive displacement by actively engaging in a coping activity that provides a profound sense of through presence in another world. Cognitive distraction is a common strategy in pain control and relies on creating competition for cognitive resources, that is, attention to a novel spatial orientation, and engaging within it reduces the perception of pain [32,33,44]. Therefore, immersive VR interventions using stereoscopic head-mounted displays (HMDs) have been proposed as powerful tools for providing visual, audio, cognitive, and emotional engagement [45-47]. In MBSR, VR experiences are typically accomplished using computer-simulated environments, stereoscopic headsets, and motion tracking to support a more immersive meditative experience. This was the approach taken in this study, and an EEG analysis was selected as a practical technique to assess neurophysiological activity while experiencing VR.

Objectives

Overall, this inductive exploratory study sought to assess how EEG power of waveforms, their topographic mapping, and coherence measures altered in 3 main states during a VR-guided meditation experience in patients with cancer-related CP: at baseline (pre), during VR-guided meditation (med), and after VR-guided meditation (post). Moreover, we explored whether their pain level was associated with waveform power measures. We were particularly interested in the power, topography, and coherence of α, γ, and θ wave activity, and possible synchrony with VR activity, as other researchers have reported changes in these 3 waveforms with MBSR activities. Therefore, we were interested in determining whether prior findings were consistent with those observed during a VR experience. Specifically, the questions we sought to address in this study were as follows:

1. Were there any observable or significant changes between pre and during VR-guided meditation experiences and between pre and post VR-guided meditation experiences with the power, topographic changes, or EEG coherence in specific waveforms?
2. Was there any evidence that changes in the pain experienced by participants during a VR-guided meditation activity were associated with observable EEG changes?

Methods

Approach

An exploratory, single-subject design study was undertaken to compare EEG activity and pain levels before, during, and after VR-based meditation practice. This study was reviewed and approved by the University of British Columbia Clinical Research Ethics Board.

Recruitment

A convenience sample of 10 participants was used and recruited from those in an existing randomized controlled trial (RCT; ClinicalTrials.gov: NCT 02995434) where patients with cancer were using VR as an adjunctive therapy to help manage their CP (Textbox 1). These participants were completing or had completed cancer treatment and experienced a range of cancer-related pain, including neuropathy, fibromyalgia, postsurgical pain, or an exacerbation of pre-existing pain.

Textbox 1. Randomized controlled trial eligibility criteria.

Eligibility Criteria

- Aged ≥16 years, with a past or current diagnosis of cancer
- Prior or ongoing cancer treatment
- A chronic pain diagnosis (ongoing daily pain for ≥3 months, with a Neuropathic Pain Rating Scale of ≥4)
- Able to understand English (read and write)
- Normal stereoscopic vision
- Able to move their head up, down, left, and right and able to wear a virtual reality head-mounted display
- Sufficient fine motor control in one hand to use a game controller
- Have space at home for a computer and monitor

Participants were purposively recruited, focusing on recruiting those from the RCT cohort who had previously responded well to a VR-based meditation experience, with a self-reported reduction of a Visual Analog Scale for Pain ≥1. They were invited to participate in a single 2-hour VR-guided meditation experience, with EEG recorded in their home or at the university, and were offered a Can $100 (US $83) honorarium and expenses for taking part. As an exploratory study designed to establish methods and feasibility using a limited convenience sample, with an unknown effect size, the power to inform the sample size was not calculated a priori. This is acceptable for this type of inductive study [48].

Equipment

EEG signals were recorded during the session using a BioSemi ActiveTwo system (BioSemi) with 64 channels in a standard 10-20 configuration. This system uses a head cap system with pin active silver chloride electrodes. The EEG ground (labeled DRL [Driven Right Leg]) on the Biosemi system was placed between POz and PO4, and the EEG reference (labeled CMS [Command Mode Sense]) was placed between POz and PO3.

The antialiasing filter was a fixed first-order analog filter with −3 dB at 3.6 kHz, and the low-pass filter was a fifth-order cascaded integrator-comb digital filter with −3 dB at one-fifth the sample rate. A powerline notch filter was not applied because the system used active electrodes, a battery power supply, and optic fiber, greatly reducing noise from the powerline. Each channel consisted of a 24-bit analog-to-digital converter. Recordings were made at 1024 Hz (although one was recorded at 2048 Hz) using ActiView software (Biosemi Instrumentation).

An HTC Vive VR system (HTC) with a Deluxe Audio Strap fitted over the top of the EEG cap was used. This system features a 2160×1200 resolution, 90 Hz refresh rate, and 110° field of view. Positional tracking from 2 infrared cameras enabled 5-degrees-of-freedom motion tracking of the headset and hand controllers. Integrated stereo headphones supported 3D audio immersions. During the initial pilot testing, this system was found to work effectively. Minor noise was evident in the EEG from the VR system on rare occasions, but we were able to remove most of this noise by careful repositioning of the equipment.

For meditation practice, a commercially available Guided Meditation VR application (Cubicle Ninjas) was used. As each meditation was only 10 minutes in this app, we selected a single sequence of 3 unique meditations, Zen 2-4, to form a 30-minute block of meditation. In the guided meditation experience, users were situated in the *Lost Woods* virtual environment with the *Calm* music selected. They were able to explore a calm, forest 3D environment with running water features with soft chirping bird and gentle wind sounds. Using a controller, participants could move to different positions in the forest to explore or find a particular viewpoint they liked and found most conducive to their meditation. A narrative provided audio guidance on the meditative practice. This environment was selected to maximize the similarity with the participants' prior VR experiences in the RCT.

Both EEG recording and the VR system were run on a Dell G7 17 7790 gaming laptop (Intel Core i7-8750H, 16 GB DDR4, RTX 2060) placed in front of the participant. During recording, the laptop screen was arranged to display the ActiView software and a mirror window of the Guided Meditation VR application experience, showing the participant's perspective in the VR HMD. In addition, a Windows 10 (Microsoft) camera app was used to record the video. This arrangement was recorded using Snagit (Techsmith) screen capture software to accommodate the time synchronization of EEG and recordings of participants' physical movements (Figure 1).

Figure 1. Electroencephalograph recording during a virtual reality experience.

Procedures

Participants were seated in front of the laptop, and the laptop webcam was framed to capture the participants' head, arms, and upper body. Before putting on the EEG head cap, participants were familiarized with the VR app, its controls, and how to navigate and select meditations. The Cz, inion, and left and right preauricular locations were marked using standard EEG landmarking methods. These locations were used to align the EEG head cap on the participant. The electrode paste was then applied, and the electrode contacts were adjusted until the electrode offsets were less than 50 µV. The VR HMD was then placed in position over the EEG head cap, and the experience commenced.

The overall structure of data collection used an 8-minute resting condition, followed by the 30-minute sequence of meditations and followed by another 8-minute rest condition (Figure 2). The 8-minute period was considered a balance between being shorter to reduce strain and being longer for more data; this period has been used in EEG studies in a variety of fields for baselines [49-51].

Figure 2. (A) Diagram of equipment setup. (B) Timeline of recording, including rest and meditation conditions. (C) Diagram of desktop view. EEG: electroencephalograph; NRS: numerical rating scale.

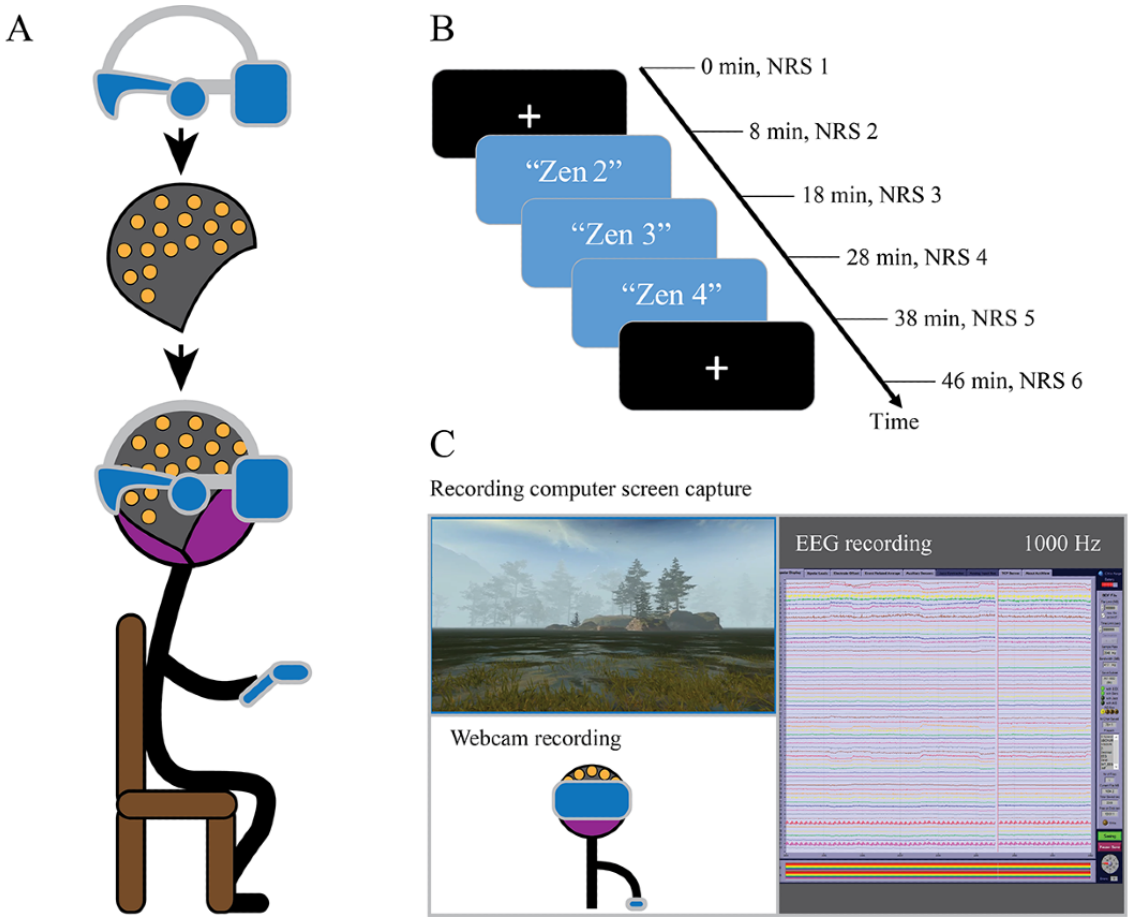

During the rest conditions, the participants were asked to rest quietly and observe a small white crosshair displayed on a black background in the VR HMD. Participants were instructed to keep their eyes open while blinking naturally, to keep their eyes on the crosshair, and to stay still while not thinking about anything. During the meditation practice, participants were instructed to engage with the guided meditation and look around or move around the virtual environment as they liked, to find an enjoyable perspective. Each guided meditation experience lasted 10 minutes, and participants were instructed to begin the next one immediately after the intervening rest condition. Pain was assessed before and after the first rest condition, after each 10-minute guided meditation, and after the second rest condition. Participants were asked to verbally rate their pain from 0 to 10 on the simple numerical rating scale (NRS) [52].

Analysis

Data Preprocessing

The recording sessions of the resting condition, the 3 guided meditation conditions, and the final resting condition were referred to as the *Pre*, *Med1*, *Med2*, *Med3*, and *Post*, respectively, for the analysis. These 5 conditions were extracted based on the time stamps acquired from the EEG video recordings.

Figure 3 illustrates the EEG data preprocessing steps. The raw EEG data in the Biosemi format were imported and preprocessed using FieldTrip software (Donders Institute for Brain, Cognition and Behaviour) [53]. As the bandwidth of interest was less than 50 Hz, the data were downsampled to 512 Hz to reduce computing time in later processes. To prepare for downsampling, an antialiasing sixth-order low-pass Butterworth two-pass filter

set to 70 Hz was first applied to the data. The primary 64 EEG channels were then re-referenced to the averaged left and right mastoid electrodes (T7 and T8). This re-referencing process effectively eliminated the noise introduced from the original reference electrodes. After this process, the reference electrodes T7 and T8 were eliminated from the data, and only 62 channels were retained.

Figure 3. Electroencephalograph data preprocessing chart. EEG: electroencephalograph; ICA: independent component analysis.

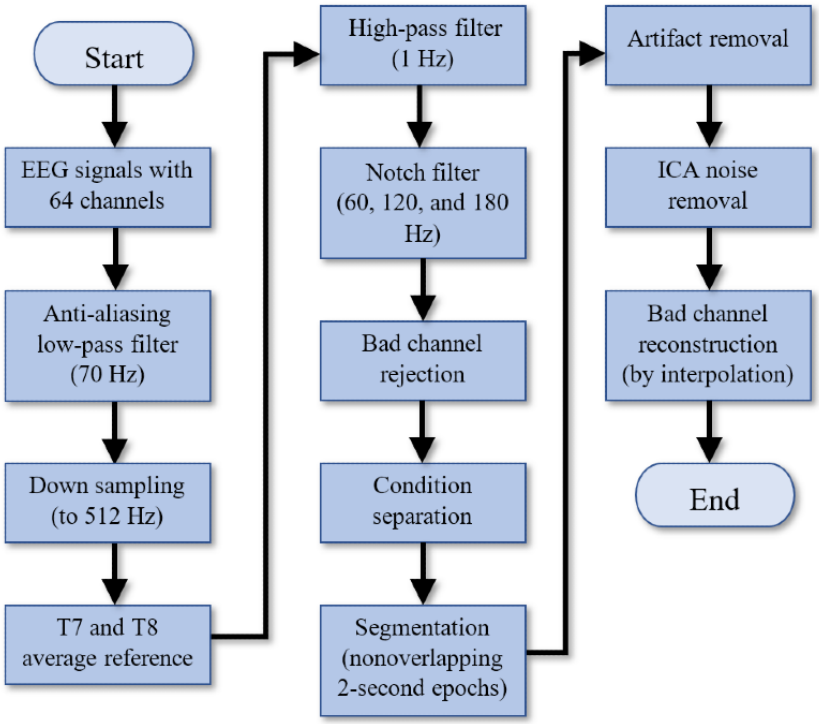

In addition, a sixth-order high-pass Butterworth two-pass filter with a cut-off at 1 Hz was used to remove slow drifts and to prepare the data for independent component analysis (ICA) [54]. The data were further notch-filtered to remove any powerline noise and harmonics, with cut-offs set at 60, 120, and 180 Hz. Bad channels were identified during the EEG recording process using an EEG data browser and rejected.

These data for each condition were further segmented into nonoverlapping epochs of 2 seconds in length to enable signal averaging in the frequency domains [55]. A data cleaning process was then performed using the FieldTrip automatic artifact removal feature, which is based on a Z-transformation and the setting of a threshold to reject bad epochs. This artifact removal result was found to be unsatisfactory, so a manual cleaning process was then performed. Segments with participant movement observed in the videos were identified, and any residual bad segments and channels were rejected. These steps effectively eliminated the artifacts caused by head and body movements.

Any remaining artifacts caused by eye blinks, eye movements, and external noise were eliminated from the data using ICA. These manual artifact removal and ICA processes were repeated 3 times during the cleaning process to ensure that all movement-based artifacts had been captured. Finally, bad channels were repaired [56] using the established practice of spline interpolation of the neighborhood channels on the bad channels [57].

Power Spectral Density Analysis

The power spectral density (PSD) [58] was computed for the conditions using a fast Fourier transform method [59]. Hanning taper smoothing was applied to reduce spectral leakage owing to the discontinuity of the signal at the start and end points of the epochs. To improve the signal-to-noise ratio, the average PSD of the epochs was used. The PSD was further normalized by dividing the average power across all the frequency bins in each channel. The frequency range in the analysis was set to 2-50 Hz, which effectively covers the waveforms commonly used in EEG analysis. The PSD results of the premeditation experiences, during meditation experiences, and postmeditation experiences were then plotted and shown as pre, med, and post conditions, respectively. For med, the average PSD of the meditation conditions was computed using the average of the 3 meditation conditions (Med1, Med2, and Med3). For a graphical overview, a band power box and whisker plot were created. The plot revealed the signal power over the typical EEG frequency bands: 2-4 Hz (δ), 4-8 Hz (θ), 8-12 Hz (α), 12-30 Hz (β), and 30-50 Hz (γ) [60]. The lower boundary of 2 Hz was set to avoid any distortion introduced by the high-pass filter at 1 Hz. The upper boundary of 50 Hz was selected to avoid the heavy power-level drop due to the use of a 60 Hz notch filter. In addition, 50 Hz was considered a reasonable cut-off between the high and low γ ranges.

Topographic and Coherence Analysis

To explore the spatial properties of the signals on each EEG channel, a topographic mapping of the PSD was plotted

according to the traditional frequency ranges. The PSD was plotted using a heat map visualization technique to display the magnitude of the PSD with a 2D color representation. An interpolation based on the MATLAB 4 grid data method was used to smooth the topography, where a surface was fitted to the scattered data points using a biharmonic spline interpolation [61]. This PSD plot was used to graphically illustrate the spatial properties associated with the pre, med, and post experiences.

A coherence analysis [62] was performed to visualize the functional connectivity between the electrodes as an indication of the brain areas that may be functionally integrated. Coherence of the pre, med, and post conditions were plotted for the frequency bands. A value between 0 and 1 was displayed for each channel pair. A value of 1 indicates full synchronization between the channel pair, and a value of 0 reveals that the channel pair does not work in the synchronized condition. The significance of the coherence difference between the conditions was computed using the two-tailed Student *t* test and then plotted.

Pain

Pain experience was measured using the NRS. Pain scores were collected from the patients as an initial baseline at the start, and after each condition, to explore any correlation between pain levels and any PSD changes identified during the meditative experience.

Statistical Analysis

For the PSD and coherence analysis, the null hypothesis set for inferential statistical analysis was that the probability distribution of the condition-specific averages for PSD and coherence would be identical for all conditions.

As a cluster-based permutation test [63] can be used to effectively resolve multiple comparisons in EEG signal statistical analysis, this test was used in this study to examine the overall PSD differences between the pre-med, med-post, and pre-post conditions by identifying the clusters of electrodes with significant changes. The tests were conducted using the Monte Carlo method, with 128 permutations, two tails, and α=.025 (negative and positive tails together equal .05). In addition, for comparison of all 3 conditions together, a multivariate analysis of variance (MANOVA) was used, with 2048 permutations, one tail, and α level set to .05.

The effect size was calculated after the cluster-based permutation test. First, a bounded rectangular area spanning each cluster was identified. This rectangular area was bounded by the frequency window of the cluster and all the channels in that cluster. The PSD in this area was then averaged. The maximum Cohen *d* effect size was then computed using FieldTrip for each of the conditions. The effect size was not computed for the MANOVA because it requires the specification of 2 mean groups for comparison. Generally, a Cohen *d* effect size around 0.2 is considered small and around 0.8 and higher is considered large to very large [64,65]. Finally, peak channel tests were performed to verify the PSD changes, and post hoc power analyses using G*Power [66] were performed to indicate statistical power based on the effect sizes observed in the sample.

For the coherence analysis, the Student *t* test was used to examine significant coherence differences between the conditions. Parameters were set to two-tailed, paired samples, and α=.05, with a 10% false discovery rate (FDR) adjustment set [67].

To explore the associations between pain scores and PSD, repeated measures correlation [68] was conducted. Some peak PSD channels identified with a high significance of PSD change from the cluster topoplot were input for each condition as the repeated independent variable, and the NRS pain score was input as the dependent variable.

Results

Overview

A total of 10 participants were recruited (Table 1). As we went through the data cleaning process, the data from 1 participant (S05) were found to be excessively noisy, and on video review, 2 other participants (S08 and S09) were found not to be following the procedures. Hence, their results were excluded, and a sample size of 7 was used in the final analysis.

Table 1. Participant demographics.

Subject	Age (years)	Sex	Cancer history
S01	59	Female	Abdominal tumors
S02	66	Male	Non-Hodgkin lymphoma
S03	37	Male	Non-Hodgkin lymphoma
S04	58	Female	Breast cancer
S06	47	Female	Chondrosarcoma
S07	50	Female	Colon cancer
S10	64	Male	Prostate cancer

PSD Analysis

Figure 4 illustrates the average of the power spectrum of the 3 conditions to provide a general overview of the power spectrum in the data, whereas Figure 5 shows the box and whisker plot of band power of the pre, med, and post conditions in the 5 traditional frequency ranges. From these figures, the differences in power in the frequency bands between the conditions were identified. The post condition power level had the lowest median and mean values in the δ range. The med condition changed

from the lowest median and mean values in θ and α to the highest median and mean values in β and γ.

Figure 4. Grand average power spectrum.

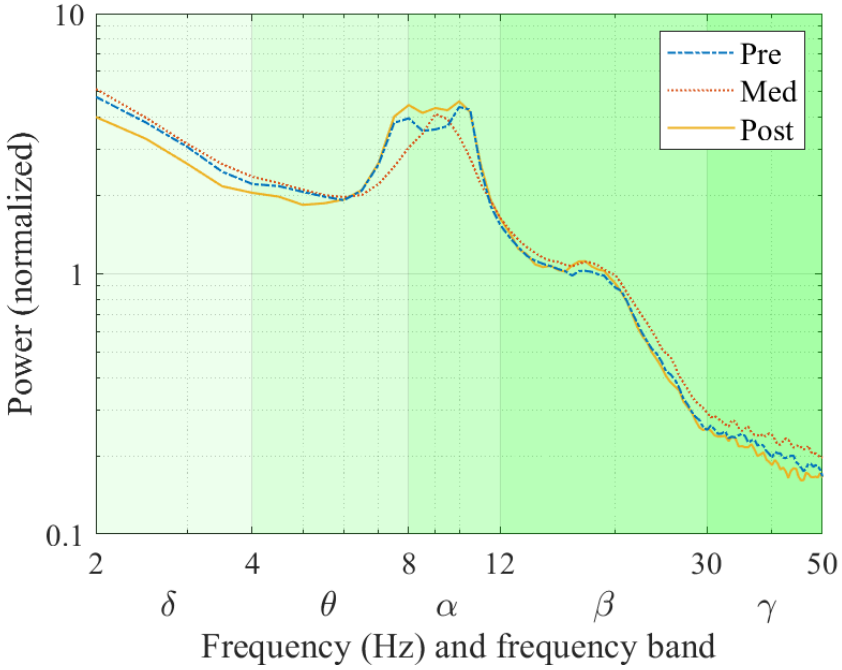

Figure 5. Power level changes between the pre, med, and post conditions in different frequency ranges. Box plot shows the median and range of power level of the participants. Line plot shows the changes in mean power.

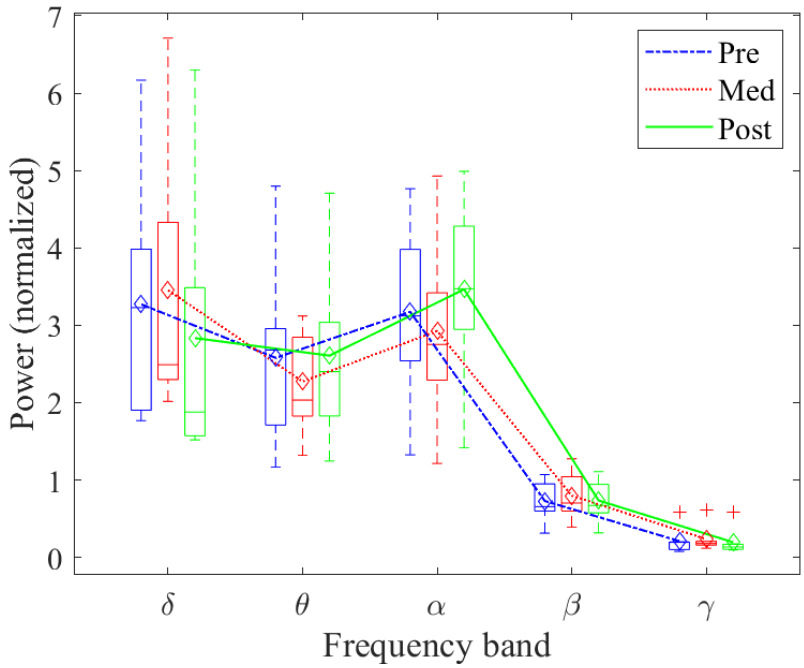

The topographic distribution of the PSD is shown in Figure 6. Differences in pre, med, and post conditions are shown spatially in all bands and in different brain regions. Changes in the power levels during meditation were observed in all frequency bands. In δ, an increase in power level in the central occipital region was observed, and a drop of power in the frontal-central region was observed in the post condition. In θ, there was a drop in the power level in the frontal cortex. In α, a decrease in power level in the central parietal region was noted. In the β band, an increase in power level was found in the bilateral central and prefrontal regions during meditation. In γ, an increase in power level was noted in the left frontal (LF) and right frontal (RF) regions, and a slight increase in the central parietal region was observed.

Figure 6. Topography of power spectrum shown in different frequency ranges. Different color scales are used for the frequency ranges to reveal the details in the central areas.

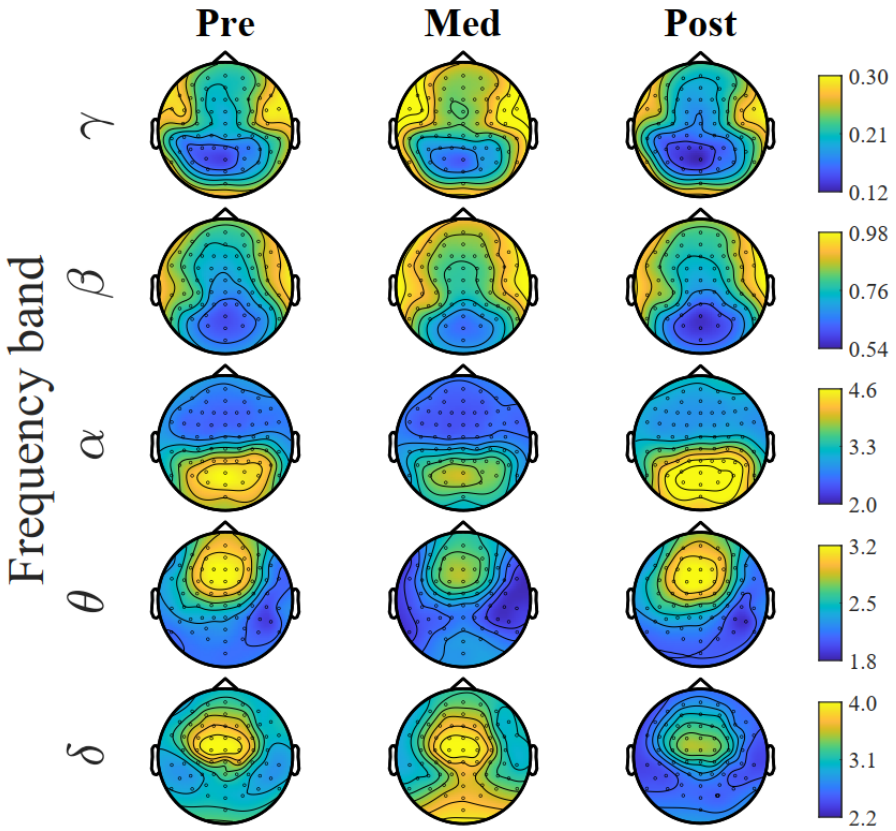

Figure 7 shows the topoplot of the two-tailed cluster-based permutation test results. The conditions were compared in the test, including two-tailed pre versus med, med versus post, and pre versus post and a one-tailed MANOVA for all 3 conditions together. The clusters of electrodes with significant differences found in PSD changes were marked with a circle marker at the electrodes. The color bars indicate the *t* values computed from the test. For the pre versus med comparison, a cluster with a significance of *P*=.02 was found in the range of 24.5-31 Hz (high β and low γ) in the frontal cortex. For the med versus post comparison, significance was found in the β and γ ranges. A cluster with a significance of *P*=.001 was found in the range of 37-50 Hz (γ), and the cluster covered most brain regions; a cluster with a *P* value of .008 was found in the range of 23-36 Hz (high β and low γ) in the frontal and central cortices. For the pre versus post condition comparison, a cluster with *P*=.02 was obtained in the frontal, central, and parietal regions in the range of 8-9.5 Hz (high θ and low α). The MANOVA cluster-based permutation test for all the pre, med, and post conditions returned 4 clusters with *P*≤.05, where the test was one-tailed. The first cluster found has *P*=.002 in the range of 37.5-50 Hz (γ) in the frontal, central, and parietal cortices. The second cluster with *P*=.03 was found in the range of 31-36 Hz (low γ) in the frontal and central cortices. The third cluster with *P*=.03 was found in the range of 2-5 Hz (δ and low θ) in the frontal, central, and parietal cortices. The last cluster with *P*=.04 was found in the range of 24-30 Hz (high β) in the frontal and central cortices. Table 2 shows the test results for all the clusters of significance. The very large effect size indicated that the permutation tests were effective in rejecting the null hypothesis.

Figure 7. Power spectrum analysis using the cluster-based permutation test. Clusters of electrodes found with significant changes in power are marked with a circle marker at the electrodes. The color bars show the permutation test t-value level. MANOVA: multivariate analysis of variance.

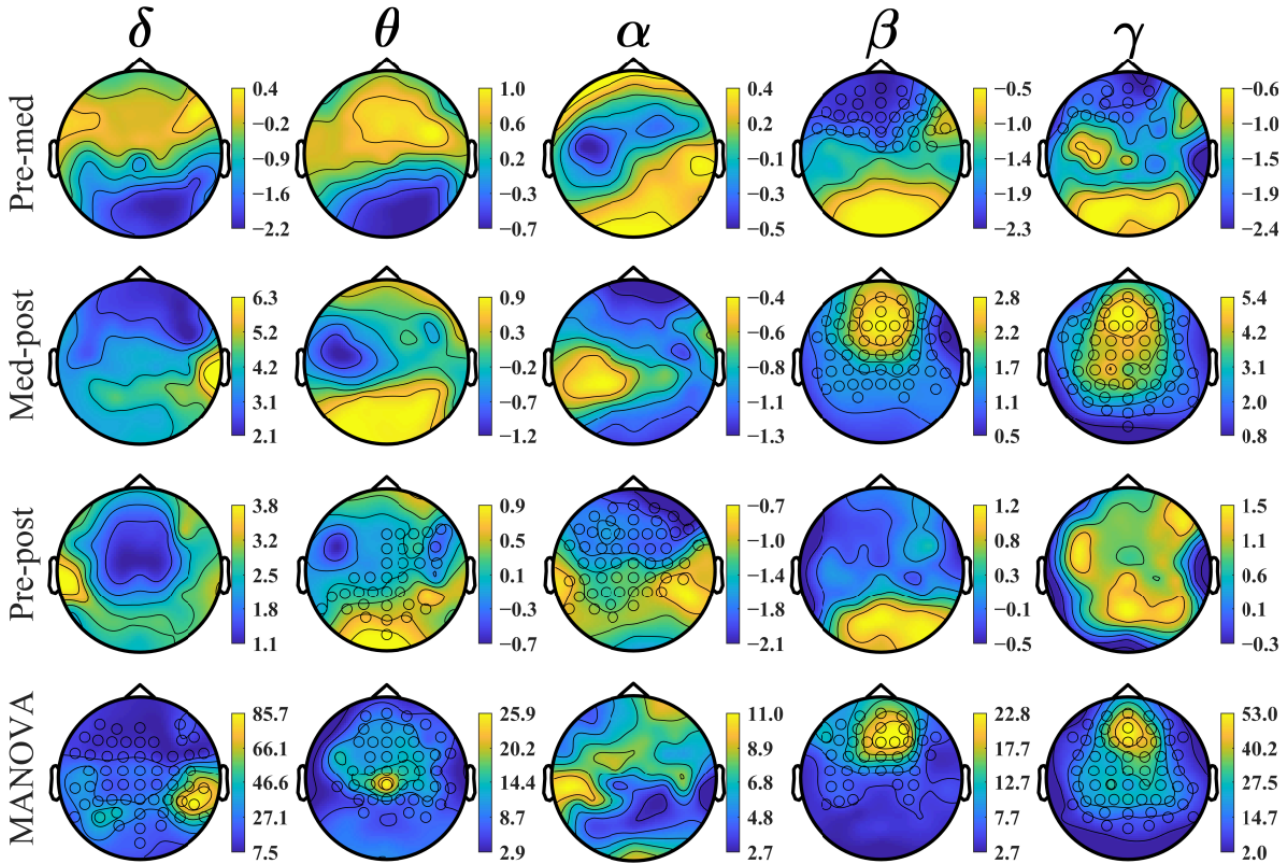

Table 2. Cluster-based permutation test results. All clusters with P≤.025 are shown for the first 3 tests, and clusters with P≤.05 are shown for the multivariate analysis of variance test.

Comparison and cluster	*P* value	Effect size
Pre-med		
1	.02	1.252
Med-post		
1	.001	3.190
2	.008	1.318
Pre-post		
1	.02	1.504
MANOVA[a]		
1	.002	—[b]
2	.03	—
3	.03	—
4	.04	—

[a]MANOVA: multivariate analysis of variance.

[b]Not calculated as it required to specify which 2 conditions to compare.

By inspecting the topoplots (Figures 6 and 7), 5 peak channels with noticeable changes in the power levels between the conditions were selected for additional analysis and for better understanding the observed power level changes. The peak channels selected were AF7 and Fp2 in the prefrontal region, FC1 in the frontal region, CP5 in the left central (LC) region, and P5 in the left parietal (LP) region. Two-tailed, paired-sample *t* tests were performed to examine the overall PSD changes in

different conditions. These tests were conducted on the pre and med, med and post, and pre and post conditions. The resulting *P* values were reported with an FDR adjusted to 10%. The *t* test results were plotted graphically for ease of interpretation. For each of the peak channels, a combined plot of the results of the 3 conditions was used.

Figure 8 shows the *P* values obtained in a graphical form for the comparison of the 3 conditions. The upper shaded areas represent $P \leq .025$. The shaded areas above the dashed line represent the adjusted significance with $P \leq .0025$.

Figure 8. Graphical depiction of *P* values of changes in power spectral density between conditions for the selected channels. Shading indicates significance found at the .025 level, and shading above the dashed line indicates the adjusted significance at the .0025 level (with the false discovery rate set to 10%).

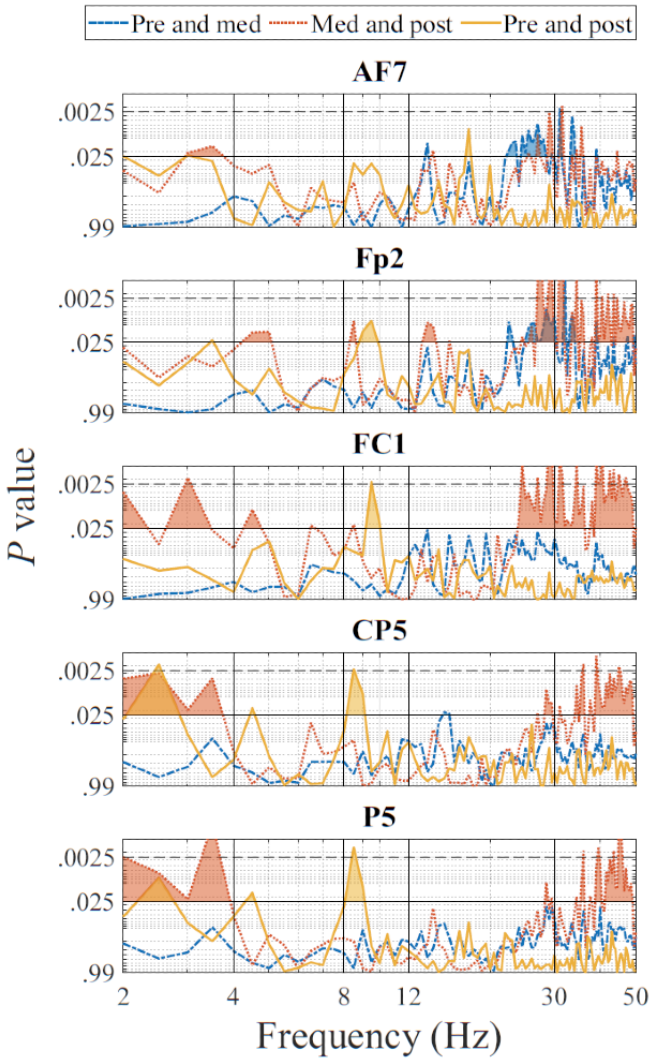

A statistical power analysis was also performed to verify the probability of detecting a true effect in the *t* tests. Table 3 shows the maximum effect size value and the respective frequency point found for each channel and for each comparison. Table 4 shows the statistical power based on the effect sizes listed in Table 3. It is shown that the *t* test results have a high power ≥0.7302 even when using the adjusted α value of .005.

Table 3. The maximum channel effect size and the frequency at which it was located.

Channel (N=7)	Pre-med		Med-post		Pre-post	
	Max effect size	Frequency (Hz)	Max effect size	Frequency (Hz)	Max effect size	Frequency (Hz)
AF7	*1.9542*[a]	*31*	*1.9946*	*31.5*	1.5613	17.5
Fp2	*2.3861*	*32*	*3.7903*	*31.5*	1.4682	9.5
FC1	1.1037	13.5	*2.9888*	*29*	*1.9221*	*9.5*
CP5	1.1651	15	*2.1765*	*39*	*1.9937*	*2.5*
P5	1.0514	40	*2.6077*	*3.5*	*2.0736*	*8.5*

[a]Italicized values indicate where $P \leq .0025$ was found for that frequency value.

Table 4. Power analysis for the effect size found.

Channel	Pre-med, α=.005	Med-post, α=.005	Pre-post, α=.005
AF7	*0.7472*[a]	*0.7676*	0.5073
Fp2	*0.9125*	*0.9998*	0.4450
FC1	0.2225	*0.9890*	*0.7302*
CP5	0.2556	*0.8470*	*0.7672*
P5	0.1962	*0.9558*	*0.8047*

[a]Italicized values indicate where $P \leq .0025$ was achieved.

Topographic and Coherence Analysis

Figure 9 demonstrates the coherence detected in the α band during meditation.

The functional connectivity level is represented by a red to blue color scale. The red color with a value close to 1 indicates that a channel pair is highly synchronized in the signal transfer. The blue color with a value close to 0 indicates that the channel pair is working independently.

Figure 10 shows the significant difference in coherence for the comparison of the med and post conditions in the α band. Channel pairs with $P \leq .025$ are highlighted in green. Those with $P \leq .0025$ (FDR adjusted) are highlighted in yellow. For clarity, the EEG channels were divided into regions according to their respective locations in the brain, namely, LF, LC, LP, left occipital, central parietal and occipital, RF, right central, right parietal and right occipital. Table 5 summarizes the results of a series of plots, as shown in Figure 10, for all the bands and all 3 comparisons. The table shows the significant coherence changes with $P \leq .0025$ between the brain regions, where 1 denotes the pre and med comparison, 2 denotes the med and post comparison, and 3 denotes the pre and post comparison. The frequency band of the region pair at which a significance was found is shown with the Greek letter of the band. The number inside parentheses indicates the number of significant channel pairs in the frequency band.

Figure 9. Coherence between the electroencephalograph channels during the virtual reality–guided meditation and in the α frequency range.

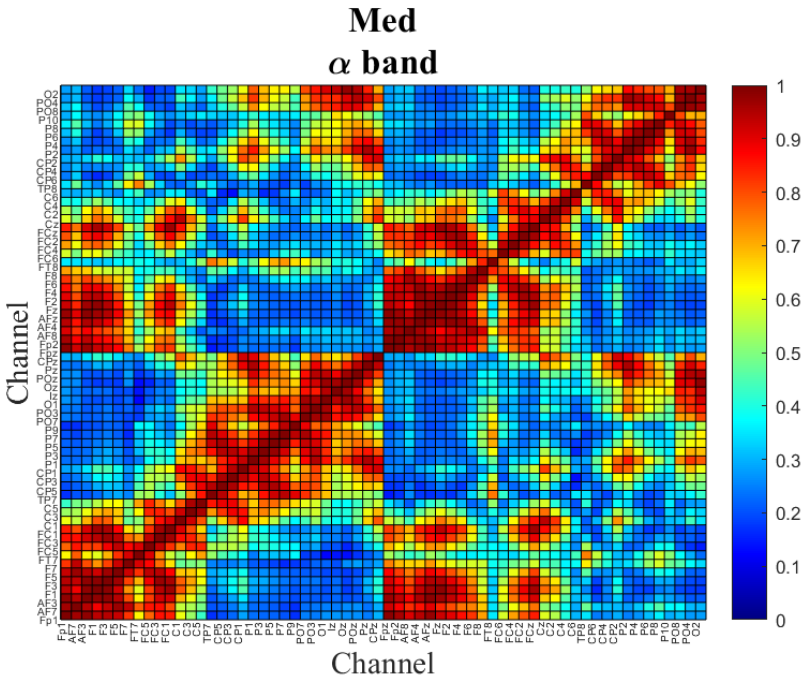

Figure 10. Channel pairs with significant coherence difference between the meditation and post meditation conditions in the α band. t test was used in the analysis, and channel pairs with a P≤.025 are highlighted in green, and channel pairs with a P≤.0025 (with the false discovery rate set to 10%) are highlighted in yellow. CPO: central parietal and occipital; LC: left central; LF: left frontal; LO: left occipital; LP: left parietal; RC: right central; RF: right frontal; RO: right occipital; RP: right parietal.

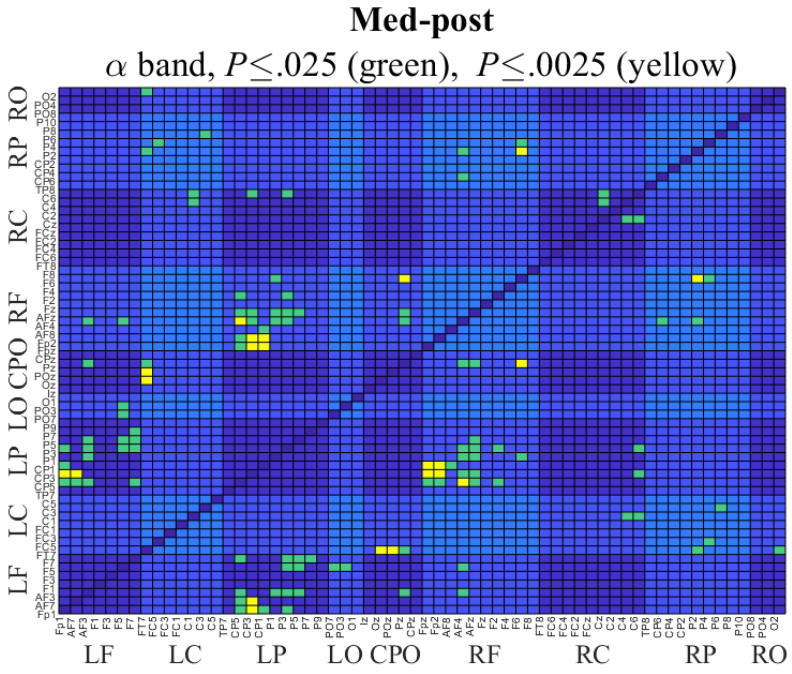

Table 5. False discovery rate–adjusted significant coherence changes found in the region pairs for the 3 comparisons: 1: pre versus med, 2: med versus post, and 3: pre versus post.

Region	LF[a]	LC[b]	LP[c]	LO[d]	CPO[e]	RF[f]	RC[g]	RP[h]	RO[i]
RO	3: δ[j]	3: θ	—[k]	—	—	—	—	—	✓[l]
RP	—	—	2: δ(2)[m]	2: δ	2: δ	2: α; 3: β	1: θ	✓	—
RC	—	—	—	—	—	1: β	3: α (✓)	—	—
RF	—	—	1: γ(2); 2: θ(2), α(5); 3: δ(2)	—	2: α	✓	—	—	—
CPO	3: δ α	1: α; 2: α(2)	—	—	✓	—	—	—	—
LO	—	—	—	✓	—	—	—	—	—
LP	2: θ, α(2), β	—	✓	—	—	—	—	—	—
LC	—	✓	—	—	—	—	—	—	—
LF	✓	—	—	—	—	—	—	—	—

[a]LF: left frontal.

[b]LC: left central.

[c]LP: left parietal.

[d]LO: left occipital.

[e]CPO: central parietal and occipital.

[f]RF: right frontal.

[g]RC: right central.

[h]RP: right parietal.

[i]RO: right occipital.

[j]Greek letter indicates the frequency band of the region pair with significant change.

[k]The empty cells in the upper left of the check mark diagonal show no significant channel pair was found. The cells in the lower right of the check mark diagonal are not used, as they are just mirrored duplicates of the cells in the upper left of the check mark diagonal.

[l]The checkmark indicates a region connects to the same region in the region pair.

[m]Number within parentheses indicates the number of channel pairs with significant changes in that frequency band. If there is only 1 channel pair, the number is not shown.

As shown in Table 5, significant changes were mostly found between the frontal and parietal regions, namely, RF-LP (11 channel pairs) and LF-LP (4 channel pairs). In addition, the most active regions were LP (related to 17 channel pairs), RF (15 channel pairs), LF (7 channel pairs), right parietal (7 channel pairs), and central parietal and occipital (7 channel pairs). For the 3 comparisons overall, significant changes were mostly found between the frontal and parietal and occipital regions, particularly in the θ, α, and β bands in the med-post comparison. For the pre-med comparison, the frontal-parietal region-pair coherence changes were observed in the γ band. For the pre-post comparison, the frontal-parietal and occipital region-pair coherence changes were observed in the δ, α, and β bands. Table 6 shows the effect sizes of the 2 regions of interest, namely, RF-LP and LF-LP. Some large to very large effect sizes (≥0.8) were found in the δ, θ, α, and γ bands.

Table 6. Effect sizes of the 2 region pairs of interest: right frontal-left parietal and left frontal-left parietal.

Band	Region-pair RF-LP[a] average, effect size			Region-pair LF-LP[b] average, effect size		
	Pre-med	Med-post	Pre-post	Pre-med	Med-post	Pre-post
δ	0.2873	0.7545	*0.8511*[c]	0.1636	0.4461	0.2862
θ	0.5568	0.7738	0.1496	0.7464	*0.8234*	0.1610
α	0.5855	*1.3032*	*0.8593*	0.7742	*1.7736*	*1.0655*
β	0.4643	0.6142	0.2211	0.2759	0.5135	0.1294
γ	0.3482	*1.0220*	0.2218	0.3032	0.5880	0.1633

[a]RF-LP: right frontal-left parietal.

[b]LF-LP: left frontal-left parietal.

[c]Italicized values indicate large and very large effect sizes.

Table 7 shows the NRS pain scores collected immediately after the pre, Med1, Med2, Med3, and post conditions. A repeated

measures correlation analysis was performed on some selected peak channels and clusters. In the test, no significant relationship between the collected pain scores and PSD was found.

Table 7. Numerical rating scale scores collected after each condition.

Participant	NRS[a] score				
	Pre	Med1	Med2	Med3	Post
S01	4	2	2	2	1
S02	4	3	0	0	1
S03	7	4	7	5	3
S04	6	5	4	4	3
S06	5	6	5	4	5
S07	3	5	4	2.5	4
S10	3	3	2	2	2

[a]NRS: numerical rating scale.

Discussion

Principal Findings

Overview

In answer to the primary research question, there were significant changes in EEG power and coherence among three conditions (pre, VR-guided meditation, and post). Therefore, the null hypothesis of no difference was rejected.

The visual inspection of the global normalized power spectrum analyses revealed various changes in all bandwidths. The predominant pattern was for increased δ, β, and γ bandwidth power in the meditation condition, compared with both the pre and post conditions. In the θ and α bandwidths, the changes in power were more varied within the 3 conditions.

Pre Medication Versus VR-Guided Meditation

Visual inspection of the topographic distribution showed 2 main patterns comparing meditation with the prior resting condition. The first was an increase in power of δ (mainly in the central and occipital areas), β (mainly in the bilateral prefrontal areas), and γ (mainly in the frontal and bilateral prefrontal areas) during VR-guided meditation.

The second pattern that emerged from the visual topography map was decreased low-frequency range power of the θ (mainly in frontal areas) and α (mainly in occipital and parietal areas) bandwidths in the med condition compared with the pre condition. However, these visually observed changes were not significant in the permutation test.

Among the significant changes identified, the permutation test showed that a cluster of increased signals occurring across the high β and low γ range (24.5-31 Hz) in frontal areas was significantly different in the pre condition than in the med condition. In addition, comparison of single selective channels between conditions showed a significant difference in this bandwidth in the frontal areas recorded from AF7 and FP2.

β waves generally replace α waves when participants open their eyes, and in the motor cortex, β waves are associated with muscle motor activity [58,60]. They are normally most prominent in the frontal and central head regions and attenuate posteriorly. This may have been the case for the increase observed here. β activity is also commonly associated with drowsiness, stage nonrapid eye movement 1 sleep, and subsequently decreases in deeper sleep, and β activity is not affected by eye opening [60]. Interestingly, sedative medications are also known to increase the amplitude and quantity of β activity [69]. This finding suggests that an increase in the power of the β range might potentially be useful as a neurophysiological correlate of VR-guided meditation. Nevertheless, findings regarding changes in the β band with meditation have been inconsistent. Several studies have reported no significant changes associated with meditation in the β range [4,31]. However, an increase in β and θ band power was reported in one study after a longer period of 6 weeks of meditation compared with baseline [70]. It is possible that the changes in β power in the meditation condition compared with the premeditation condition here may be more specific to the use of VR-guided meditation and the visual activity involved, but further work is required to explore this.

In contrast, the activity of the γ band has been reported to be associated with activation of the default mode network. The default mode network is most frequently detected during the resting conditions and reflects the neural activity of different brain areas, such as the cingulate cortex, hippocampus, medial frontal lobes, inferior parietal lobes, and temporal lobes. It is thought to be involved in self-consciousness; self-processing; and introspective functions, including emotional awareness and processing [71-74]. An increase in γ band activity in the frontal and prefrontal areas during VR-guided meditation could reflect the activation of such introspective experiences through meditation. The increase in γ power may also have been due to the activation of attentional networks and visual processing of the meditative VR environment [75].

It is also noteworthy that others have reported an increase in γ band power related to meditation [17,75,76]. For example, one study reported an increase in the γ band (25-45 Hz) during meditation compared with the resting state in the temporal and

parieto-occipital areas in mindfulness meditation practitioners [76]. Another study reported that the proficiency level of the meditator is associated with the increased level of the γ band (60-110 Hz) in the parieto-occipital region in meditative states relative to the mind-wandering state in experienced meditators compared with healthy controls. Although it is noteworthy, in this study, no significant difference was found between the states of meditation and mind wandering [75].

VR-Guided Meditation Versus Post Meditation

In contrast to the pattern of increase in high β and low γ activity in the meditation condition compared with the prior rest condition, here, we observed a pattern of reduced β and γ power in the post condition compared with the meditation condition in the topographic maps. This was followed by permutation test results in terms of 2 significant clusters of differences in the β cluster (23-36 Hz) and γ cluster (37-50 Hz) in the post versus med condition. These findings suggest a potential regression back to the baseline state activity and further suggest that changes in high β and low γ activity are associated with a VR meditative state. Analysis of single selective channels also supported widespread significant differences in the power of β and γ bandwidths in the frontal, central, and parietal channels (FP2, FC1, CP5, and P5).

As γ band oscillation has also been reported to be associated with attention toward pain and hypervigilance [77,78], the significant reduction in γ band activity following the VR meditation experience could potentially show that less attentional capacity is directed toward pain after using a meditative VR environment. However, this is conjectural and requires further verification.

Pre Meditation Versus Post VR-Guided Meditation

The comparison of the pre and post conditions could provide an indication of a VR-guided meditation effect in our study. These changes were mainly observed in the α frequency range in terms of an increase in α power in the frontal and central areas in the post condition compared with the pre condition. This was accompanied by a significant cluster-based permutation analysis finding over a cluster of channels in the frontal and central areas (8-9.5 Hz) and significant differences in α power in channels such as Fp2, FC1, CP5, and P5. An increase in the θ band in the central areas and a decrease in the θ band in the posterior occipital areas were also observed in the power spectrum analysis; however, these changes were not found to be significant in single-channel analysis. The posterior dominant α rhythm is characteristically present in normal conscious EEG recordings in the occipital region. It is a defining feature of the normal background rhythm of the adult EEG, best observed with the eyes closed and during mental relaxation and is attenuated by eye opening and mental effort. θ waveforms are characteristically observed more in drowsiness and in the early stages of sleep, such as light sleep (the nonrapid eye movement 1 and nonrapid eye movement 2 sleep phases) [60]. Increases in α-θ bandwidths have previously been reported to be associated with mindfulness meditation, and the α-θ border (7-8 Hz) has also been suggested as an optimal range for indicating visualization activity [4,79,80].

A final observation worthy of note is that there was a reduction in the δ range power in the post condition compared with the pre condition, which was significantly different in the LC and parietal channels (CP5 and P5). Moreover, although changes in the δ range were not significant in the pairwise pre-post comparison, a cluster of channels was identified to be significant in MANOVA. δ is seen more in deep, dreamless sleep, and meditation activities where awareness is more detached [4,60]. Such a general pattern of reduction in δ power in the post condition compared with the pre condition could possibly be related to the effect of VR-guided meditation on brain activity and would need further work to explore if this is a significant trend.

Coherence

The significant coherence changes suggested that variations in brain connectivity occurred between the different test conditions. Coherence was found predominantly between the frontal and parietal and occipital cortices and in different wave bands, namely, in γ for the pre and med conditions; in θ, α, and β for the med and post conditions; and in δ, α, and β for the pre and post conditions. The γ coherence changes between the pre and med conditions were likely associated with activity during the VR-guided meditation. Between the med and post conditions, it shifted to slower frequencies, possibly suggesting a postmeditation effect. The pre-post comparison showed coherence in the δ, α, and β ranges. The reasons for this are unclear and could be related to the individual responses of the participants after the VR-guided meditation.

Pain and EEG Signals

In terms of the secondary focus of the study to explore pain changes correlated with EEG variations, we found no significant association between pain reduction and changes in electrophysiological signal. This could be due to the limited sample size of this exploratory study. More electrophysiological studies on a larger sample population could potentially identify EEG correlates associated with pain reduction after VR-guided meditation.

Limitations

As an exploratory study, the sample numbers were small and not necessarily representative of the wider population of patients with CP, which limited the power to identify differences. Therefore, there is a need for neurophysiological studies with larger samples to validate these results and to better explore this phenomenon. In addition, this was a single cohort study with no comparison group, although resting states before and after meditation were used as a no-mindfulness within-subjects control. Finally, the study focused on short-term neurophysiological alterations in the electrophysiology of the brain, and the long-term effects of meditative VR environments are still unknown, which will require longitudinal studies.

Conclusions

These findings suggest that distinct altered neurophysiological brain signals are detectable during VR-guided meditation, predominantly in terms of an increase in the power of the β and γ bands. Changes in the α and θ bands were also identified, predominantly as a pattern in VR-guided meditation compared

with the resting baseline, possibly reflecting the specific impact of visual activity during VR-guided meditation. Some changes in coherence were also observed between the frontal and parietal and occipital cortices during VR-guided meditation. No significant association between NRS pain scores and changes in EEG signals was observed. Although this is an exploratory study, the results of this work clearly demonstrate the feasibility of EEG recording and subsequent data processing and analysis during VR experiences in patients using modern VR HMDs. To our knowledge, this is the first exploration of EEG alterations in the brain's electrophysiological signals associated with VR-guided meditation in patients with CP and should provide some valuable initial data to inform future work in this field.

Acknowledgments

The authors would like to acknowledge that the EEG system used in this study was purchased by Dr Urs Ribary using the Canadian Foundation of Innovation funding. The authors would also like to thank Dr Diane Gromala, Director of the Pain Studies Lab, School of Interactive Arts and Technology, Simon Fraser University, for supporting this study, and all participants for their time and effort in taking part in the study. This work was supported by the Lotte and John Hecht Memorial Foundation (grant 4110).

Conflicts of Interest

None declared.

References

1. Chronic pain in Canada: laying a foundation for action. Government of Canada. 2019. URL: https://physiotherapy.ca/sites/default/files/canadian_pain_task_force_june_2019_report_en.pdf [accessed 2021-05-16]
2. Kabat-Zinn J. Mindfulness-based interventions in context: past, present, and future. Clin Psychol Sci Pract 2003;10(2):144-156. [doi: 10.1093/clipsy.bpg016]
3. Rosenzweig S, Greeson JM, Reibel DK, Green JS, Jasser SA, Beasley D. Mindfulness-based stress reduction for chronic pain conditions: variation in treatment outcomes and role of home meditation practice. J Psychosom Res 2010 Jan;68(1):29-36. [doi: 10.1016/j.jpsychores.2009.03.010] [Medline: 20004298]
4. Lomas T, Ivtzan I, Fu CH. A systematic review of the neurophysiology of mindfulness on EEG oscillations. Neurosci Biobehav Rev 2015 Oct;57:401-410. [doi: 10.1016/j.neubiorev.2015.09.018] [Medline: 26441373]
5. Hanson R, Mendius R. Buddha's Brain: The Practical Neuroscience of Happiness, Love & Wisdom. Oakland, California, United States: New Harbringer Publications; 2009:1-272.
6. Nyklíček I, Dijksman SC, Lenders PJ, Fonteijn WA, Koolen JJ. A brief mindfulness based intervention for increase in emotional well-being and quality of life in percutaneous coronary intervention (PCI) patients: the MindfulHeart randomized controlled trial. J Behav Med 2014 Feb 23;37(1):135-144. [doi: 10.1007/s10865-012-9475-4] [Medline: 23180285]
7. Lee DJ, Kulubya E, Goldin P, Goodarzi A, Girgis F. Review of the neural oscillations underlying meditation. Front Neurosci 2018;12:178 [FREE Full text] [doi: 10.3389/fnins.2018.00178] [Medline: 29662434]
8. Schoenberg PL, Vago DR. Mapping meditative states and stages with electrophysiology: concepts, classifications, and methods. Curr Opin Psychol 2019 Aug;28:211-217. [doi: 10.1016/j.copsyc.2019.01.007] [Medline: 30785068]
9. Farias M, Wikholm C. Has the science of mindfulness lost its mind? BJPsych Bull 2016 Dec;40(6):329-332 [FREE Full text] [doi: 10.1192/pb.bp.116.053686] [Medline: 28377813]
10. Keng S, Smoski MJ, Robins CJ. Effects of mindfulness on psychological health: a review of empirical studies. Clin Psychol Rev 2011 Aug;31(6):1041-1056 [FREE Full text] [doi: 10.1016/j.cpr.2011.04.006] [Medline: 21802619]
11. Seay A, Gromala D, Hodges L, Shaw C. The meditation chamber: a debriefing. In: Proceedings of the The 29th International Conference on Computer Graphics and Interactive Techniques. 2002 Presented at: SIGGRAPH02: The 29th International Conference on Computer Graphics and Interactive Techniques; July, 2002; San Antonio Texas p. 263. [doi: 10.1145/1242073.1242276]
12. Botella C, Garcia-Palacios A, Vizcaíno Y, Herrero R, Baños RM, Belmonte MA. Virtual reality in the treatment of fibromyalgia: a pilot study. Cyberpsychol Behav Soc Netw 2013 Mar;16(3):215-223. [doi: 10.1089/cyber.2012.1572] [Medline: 23496678]
13. Erlacher D, Chapin H. Lucid dreaming: Neural virtual reality as a mechanism for performance enhancement: Commentary on "The neurobiology of consciousness: Lucid dreaming wakes up" by J. Allan Hobson. Int J Dream Res 2010;3(1):7-10 [FREE Full text] [doi: 10.1201/b17676-3]
14. Gromala D, Tong X, Choo A, Karamnejad M, Shaw C. The virtual meditative walk: virtual reality therapy for chronic pain management. In: Proceedings of the 33rd Annual ACM Conference on Human Factors in Computing Systems. 2015 Presented at: CHI '15: CHI Conference on Human Factors in Computing Systems; April, 2015; Seoul Republic of Korea p. 521-524. [doi: 10.1145/2702123.2702344]
15. Navarro-Haro MV, Modrego-Alarcón M, Hoffman HG, López-Montoyo A, Navarro-Gil M, Montero-Marin J, et al. Evaluation of a mindfulness-based intervention with and without virtual reality dialectical behavior therapy mindfulness

skills training for the treatment of generalized anxiety disorder in primary care: a pilot study. Front Psychol 2019 Jan 28;10:55 [FREE Full text] [doi: 10.3389/fpsyg.2019.00055] [Medline: 30745888]
16. Venuturupalli RS, Chu T, Vicari M, Kumar A, Fortune N, Spielberg B. Virtual reality-based biofeedback and guided meditation in rheumatology: a pilot study. ACR Open Rheumatol 2019 Dec 11;1(10):667-675 [FREE Full text] [doi: 10.1002/acr2.11092] [Medline: 31872189]
17. Cahn BR, Polich J. Meditation states and traits: EEG, ERP, and neuroimaging studies. Psychol Bull 2006 Mar;132(2):180-211. [doi: 10.1037/0033-2909.132.2.180] [Medline: 16536641]
18. Davidson RJ, Lutz A. Buddha's brain: neuroplasticity and meditation. IEEE Signal Process Mag 2008 Jan 01;25(1):172-176 [FREE Full text] [doi: 10.1109/msp.2008.4431873] [Medline: 20871742]
19. Ivanovski B, Malhi GS. The psychological and neurophysiological concomitants of mindfulness forms of meditation. Acta Neuropsychiatr 2007 Apr 24;19(2):76-91. [doi: 10.1111/j.1601-5215.2007.00175.x] [Medline: 26952819]
20. Panjwani U, Selvamurthy W, Singh S, Gupta H, Mukhopadhyay S, Thakur L. Effect of Sahaja Yoga meditation on Auditory Evoked Potentials (AEP) and Visual Contrast Sensitivity (VCS) in epileptics. Appl Psychophysiol Biofeedback 2000;25(1):1-12. [doi: 10.1023/A:1009523904786]
21. Heeger DJ, Ress D. What does fMRI tell us about neuronal activity? Nat Rev Neurosci 2002 Feb;3(2):142-151. [doi: 10.1038/nrn730] [Medline: 11836522]
22. Chiesa A, Serretti A. A systematic review of neurobiological and clinical features of mindfulness meditations. Psychol Med 2010 Aug;40(8):1239-1252. [doi: 10.1017/S0033291709991747] [Medline: 19941676]
23. Magalhaes AA, Oliveira L, Pereira MG, Menezes CB. Does meditation alter brain responses to negative stimuli? A systematic review. Front Hum Neurosci 2018;12:448 [FREE Full text] [doi: 10.3389/fnhum.2018.00448] [Medline: 30483083]
24. Mishra SK, Khosa S, Singh S, Moheb N, Trikamji B. Changes in functional magnetic resonance imaging with meditation: a pilot study. Ayu 2017;38(3-4):108-112 [FREE Full text] [doi: 10.4103/ayu.AYU_34_17] [Medline: 30254388]
25. Froeliger BE, Garland EL, Modlin LA, McClernon FJ. Neurocognitive correlates of the effects of yoga meditation practice on emotion and cognition: a pilot study. Front Integr Neurosci 2012;6:48 [FREE Full text] [doi: 10.3389/fnint.2012.00048] [Medline: 22855674]
26. Goldin P, Ziv M, Jazaieri H, Hahn K, Gross JJ. MBSR vs aerobic exercise in social anxiety: fMRI of emotion regulation of negative self-beliefs. Soc Cogn Affect Neurosci 2013 Jan;8(1):65-72 [FREE Full text] [doi: 10.1093/scan/nss054] [Medline: 22586252]
27. Delmonte MM. Electrocortical activity and related phenomena associated with meditation practice: a literature review. Int J Neurosci 1984 Nov 07;24(3-4):217-231. [doi: 10.3109/00207458409089810] [Medline: 6392127]
28. Travis F, Shear J. Focused attention, open monitoring and automatic self-transcending: categories to organize meditations from Vedic, Buddhist and Chinese traditions. Conscious Cogn 2010 Dec;19(4):1110-1118. [doi: 10.1016/j.concog.2010.01.007] [Medline: 20167507]
29. Dunn B, Hartigan J, Mikulas W. Concentration and mindfulness meditations: unique forms of consciousness? Appl Psychophysiol Biofeedback 1999;24(3):147-165. [doi: 10.1023/A:1023498629385]
30. Fell J, Axmacher N, Haupt S. From alpha to gamma: electrophysiological correlates of meditation-related states of consciousness. Med Hypotheses 2010 Aug;75(2):218-224. [doi: 10.1016/j.mehy.2010.02.025] [Medline: 20227193]
31. Lagopoulos J, Xu J, Rasmussen I, Vik A, Malhi GS, Eliassen CF, et al. Increased theta and alpha EEG activity during nondirective meditation. J Altern Complement Med 2009 Nov;15(11):1187-1192. [doi: 10.1089/acm.2009.0113] [Medline: 19922249]
32. Eccleston C. Chronic pain and distraction: an experimental investigation into the role of sustained and shifting attention in the processing of chronic persistent pain. Behav Res Ther 1995 May;33(4):391-405. [doi: 10.1016/0005-7967(94)00057-q]
33. Johnson MH. How does distraction work in the management of pain? Curr Pain Headache Rep 2005 Apr;9(2):90-95. [doi: 10.1007/s11916-005-0044-1] [Medline: 15745617]
34. Garrett B, Taverner T, Gromala D, Tao G, Cordingley E, Sun C. Virtual reality clinical research: promises and challenges. JMIR Serious Games 2018 Oct 17;6(4):e10839 [FREE Full text] [doi: 10.2196/10839] [Medline: 30333096]
35. Jin W, Choo A, Gromala D, Shaw C, Squire P. A virtual reality game for chronic pain management: a randomized, controlled clinical study. In: Westwood JD, Westwood SW, Fellander-Tsai L, Fidopiastis CM, Liu A, editors. Medicine Meets Virtual Reality 22: NextMed / MMVR22. Amsterdam, Netherlands: IOS Press; 2016:154-160.
36. Shaw C, Gromala D, Seay A. The meditation chamber: enacting autonomic senses. In: Proceedings of the 4th International Conference on Enactive Interfaces. 2007 Presented at: ENACTIVE/07 4th International Conference on Enactive Interfaces; November 19-22, 2007; Grenoble, France p. 1-4 URL: https://www.sfu.ca/~shaw/papers/Enactive07MedChamber.pdf
37. Garrett B, Taverner T, Masinde W, Gromala D, Shaw C, Negraeff M. A rapid evidence assessment of immersive virtual reality as an adjunct therapy in acute pain management in clinical practice. Clin J Pain 2014 Dec;30(12):1089-1098. [doi: 10.1097/AJP.0000000000000064] [Medline: 24535053]
38. Maani CV, Hoffman HG, Morrow M, Maiers A, Gaylord K, McGhee LL, et al. Virtual reality pain control during burn wound debridement of combat-related burn injuries using robot-like arm mounted VR goggles. J Trauma 2011 Jul;71(1 Suppl):125-130 [FREE Full text] [doi: 10.1097/TA.0b013e31822192e2] [Medline: 21795888]

39. Scapin S, Echevarría-Guanilo ME, Fuculo Jr PR, Gonçalves N, Rocha PK, Coimbra R. Virtual Reality in the treatment of burn patients: a systematic review. Burns 2018 Sep;44(6):1403-1416. [doi: 10.1016/j.burns.2017.11.002] [Medline: 29395400]
40. Schmitt YS, Hoffman HG, Blough DK, Patterson DR, Jensen MP, Soltani M, et al. A randomized, controlled trial of immersive virtual reality analgesia, during physical therapy for pediatric burns. Burns 2011 Feb;37(1):61-68 [FREE Full text] [doi: 10.1016/j.burns.2010.07.007] [Medline: 20692769]
41. Wolitzky K, Fivush R, Zimand E, Hodges L, Rothbaum BO. Effectiveness of virtual reality distraction during a painful medical procedure in pediatric oncology patients. Psychol Health 2005 Dec;20(6):817-824. [doi: 10.1080/14768320500143339]
42. Garrett B, Taverner T, McDade P. Virtual reality as an adjunct home therapy in chronic pain management: an exploratory study. JMIR Med Inform 2017 May 11;5(2):e11 [FREE Full text] [doi: 10.2196/medinform.7271] [Medline: 28495661]
43. Li S, Kay S, Hardicker N. Virtual reality: Towards a novel treatment environment for ankylosing spondylitis. In: Bos L, Blobel B, editors. Medical and Care Compunetics 4. Amsterdam, Netherlands: IOS Press; 2007:190-196.
44. Moore DJ, Keogh E, Eccleston C. The interruptive effect of pain on attention. Q J Exp Psychol (Hove) 2012 Jan;65(3):565-586. [doi: 10.1080/17470218.2011.626865] [Medline: 22136653]
45. Dascal J, Reid M, IsHak WW, Spiegel B, Recacho J, Rosen B, et al. Virtual reality and medical inpatients: a systematic review of randomized, controlled trials. Innov Clin Neurosci 2017;14(1-2):14-21 [FREE Full text] [Medline: 28386517]
46. Li A, Montaño Z, Chen VJ, Gold JI. Virtual reality and pain management: current trends and future directions. Pain Manag 2011 Mar;1(2):147-157 [FREE Full text] [doi: 10.2217/pmt.10.15] [Medline: 21779307]
47. Malloy KM, Milling LS. The effectiveness of virtual reality distraction for pain reduction: a systematic review. Clin Psychol Rev 2010 Dec;30(8):1011-1018. [doi: 10.1016/j.cpr.2010.07.001] [Medline: 20691523]
48. Johanson GA, Brooks GP. Initial scale development: sample size for pilot studies. Educ Psychol Meas 2009 Dec 18;70(3):394-400. [doi: 10.1177/0013164409355692]
49. Boonstra TW, Nikolin S, Meisener A, Martin DM, Loo CK. Change in mean frequency of resting-state electroencephalography after transcranial direct current stimulation. Front Hum Neurosci 2016;10:270 [FREE Full text] [doi: 10.3389/fnhum.2016.00270] [Medline: 27375462]
50. Konicar L, Radev S, Silvoni S, Bolinger E, Veit R, Strehl U, et al. Balancing the brain of offenders with psychopathy? Resting state EEG and electrodermal activity after a pilot study of brain self-regulation training. PLoS One 2021;16(1):e0242830 [FREE Full text] [doi: 10.1371/journal.pone.0242830] [Medline: 33411746]
51. Sikka P, Revonsuo A, Noreika V, Valli K. EEG frontal alpha asymmetry and dream affect: alpha oscillations over the right frontal cortex during REM sleep and presleep wakefulness predict anger in REM sleep dreams. J Neurosci 2019 Jun 12;39(24):4775-4784 [FREE Full text] [doi: 10.1523/JNEUROSCI.2884-18.2019] [Medline: 30988168]
52. Williamson A, Hoggart B. Pain: a review of three commonly used pain rating scales. J Clin Nurs 2005 Aug;14(7):798-804. [doi: 10.1111/j.1365-2702.2005.01121.x] [Medline: 16000093]
53. Oostenveld R, Fries P, Maris E, Schoffelen J. FieldTrip: Open source software for advanced analysis of MEG, EEG, and invasive electrophysiological data. Comput Intell Neurosci 2011;2011:156869 [FREE Full text] [doi: 10.1155/2011/156869] [Medline: 21253357]
54. Makeig S, Jung T, Bell A, Sejnowski T. Independent component analysis of electroencephalographic data. In: Proceedings of the 8th International Conference on Neural Information Processing Systems. 1995 Presented at: 8th International Conference on Neural Information Processing Systems; November 27-30, 1995; Denver, CO, USA p. 145-151. [doi: 10.5555/2998828.2998849]
55. Levy W. Effect of epoch length on power spectrum analysis of the EEG. Anesthesiology 1987 Apr;66(4):489-495 [FREE Full text] [doi: 10.1097/00000542-198704000-00007] [Medline: 3565814]
56. Bigdely-Shamlo N, Mullen T, Kothe C, Su K, Robbins KA. The PREP pipeline: standardized preprocessing for large-scale EEG analysis. Front Neuroinform 2015;9:16 [FREE Full text] [doi: 10.3389/fninf.2015.00016] [Medline: 26150785]
57. Perrin F, Pernier J, Bertrand O, Echallier J. Spherical splines for scalp potential and current density mapping. Electroencephalogr Clin Neurophysiol 1989 Feb;72(2):184-187. [doi: 10.1016/0013-4694(89)90180-6]
58. Johnson L, Lubin A, Naitoh P, Nute C, Austin M. Spectral analysis of the EEG of dominant and non-dominant alpha subjects during waking and sleeping. Electroencephalogr Clin Neurophysiol 1969 Apr;26(4):361-370. [doi: 10.1016/0013-4694(69)90086-8]
59. Cooley JW, Tukey JW. An algorithm for the machine calculation of complex Fourier series. Math Comp 1965 May 01;19(90):297. [doi: 10.1090/s0025-5718-1965-0178586-1]
60. Nayak CS, Anilkumar AC. EEG Normal Waveforms. Treasure Island, FL, U.S: StatPearls Publishing; 2020.
61. Sandwell DT. Biharmonic spline interpolation of GEOS-3 and SEASAT altimeter data. Geophys Res Lett 2012 Dec 07;14(2):139-142. [doi: 10.1029/gl014i002p00139]
62. Classen J, Gerloff C, Honda M, Hallett M. Integrative visuomotor behavior is associated with interregionally coherent oscillations in the human brain. J Neurophysiol 1998 Mar 01;79(3):1567-1573 [FREE Full text] [doi: 10.1152/jn.1998.79.3.1567] [Medline: 9497432]

63. Maris E, Oostenveld R. Nonparametric statistical testing of EEG- and MEG-data. J Neurosci Methods 2007 Aug 15;164(1):177-190. [doi: 10.1016/j.jneumeth.2007.03.024] [Medline: 17517438]
64. Cohen J. Statistical Power Analysis for the Behavioural Sciences. New York: Routledge; 1988:1-567.
65. Sawilowsky SS. New effect size rules of thumb. J Mod App Stat Meth 2009 Nov 01;8(2):597-599. [doi: 10.22237/jmasm/1257035100]
66. Faul F, Erdfelder E, Lang A, Buchner A. G*Power 3: a flexible statistical power analysis program for the social, behavioral, and biomedical sciences. Behav Res Method 2007 May;39(2):175-191. [doi: 10.3758/BF03193146]
67. Benjamini Y, Hochberg Y. Controlling the false discovery rate: a practical and powerful approach to multiple testing. J R Stat Soc Ser B 2018 Dec 05;57(1):289-300. [doi: 10.1111/j.2517-6161.1995.tb02031.x]
68. Bakdash JZ, Marusich LR. Repeated measures correlation. Front Psychol 2017 Apr 7;8:456 [FREE Full text] [doi: 10.3389/fpsyg.2017.00456] [Medline: 28439244]
69. Louis E, Frey L. Electroencephalography (EEG): An Introductory Text and Atlas of Normal and Abnormal Findings in Adults, Children, and Infants. Chicago: American Epilepsy Society; 2016.
70. Ahani A, Wahbeh H, Nezamfar H, Miller M, Erdogmus D, Oken B. Quantitative change of EEG and respiration signals during mindfulness meditation. J Neuroeng Rehabil 2014 May 14;11(1):87 [FREE Full text] [doi: 10.1186/1743-0003-11-87] [Medline: 24939519]
71. Imperatori C, Della Marca G, Brunetti R, Carbone GA, Massullo C, Valenti EM, et al. Default Mode Network alterations in alexithymia: an EEG power spectra and connectivity study. Sci Rep 2016 Nov 15;6:36653 [FREE Full text] [doi: 10.1038/srep36653] [Medline: 27845326]
72. Garrison KA, Zeffiro TA, Scheinost D, Constable RT, Brewer JA. Meditation leads to reduced default mode network activity beyond an active task. Cogn Affect Behav Neurosci 2015 Sep;15(3):712-720 [FREE Full text] [doi: 10.3758/s13415-015-0358-3] [Medline: 25904238]
73. Buckner R, Andrews-Hanna J, Schacter D. The brain's default network: anatomy, function, and relevance to disease. Ann N Y Acad Sci 2008 Mar;1124:1-38. [doi: 10.1196/annals.1440.011] [Medline: 18400922]
74. Greicius MD, Krasnow B, Reiss AL, Menon V. Functional connectivity in the resting brain: a network analysis of the default mode hypothesis. Proc Natl Acad Sci U S A 2003 Jan 07;100(1):253-258 [FREE Full text] [doi: 10.1073/pnas.0135058100] [Medline: 12506194]
75. Braboszcz C, Cahn BR, Levy J, Fernandez M, Delorme A. Increased gamma brainwave amplitude compared to control in three different meditation traditions. PLoS One 2017;12(1):e0170647 [FREE Full text] [doi: 10.1371/journal.pone.0170647] [Medline: 28118405]
76. Berkovich-Ohana A, Glicksohn J, Goldstein A. Mindfulness-induced changes in gamma band activity - implications for the default mode network, self-reference and attention. Clin Neurophysiol 2012 Apr;123(4):700-710. [doi: 10.1016/j.clinph.2011.07.048] [Medline: 21940201]
77. Tiemann L, Schulz E, Winkelmann A, Ronel J, Henningsen P, Ploner M. Behavioral and neuronal investigations of hypervigilance in patients with fibromyalgia syndrome. PLoS One 2012;7(4):e35068 [FREE Full text] [doi: 10.1371/journal.pone.0035068] [Medline: 22509383]
78. Tiemann L, Schulz E, Gross J, Ploner M. Gamma oscillations as a neuronal correlate of the attentional effects of pain. Pain 2010 Aug;150(2):302-308. [doi: 10.1016/j.pain.2010.05.014] [Medline: 20558000]
79. Belkofer CM, Van Hecke AV, Konopka LM. Effects of drawing on alpha activity: a quantitative EEG Study with implications for art therapy. Art Ther 2014 Jun 13;31(2):61-68. [doi: 10.1080/07421656.2014.903821]
80. Faber PL, Lehmann D, Gianotti LR, Milz P, Pascual-Marqui RD, Held M, et al. Zazen meditation and no-task resting EEG compared with LORETA intracortical source localization. Cogn Process 2015 Feb 5;16(1):87-96. [doi: 10.1007/s10339-014-0637-x] [Medline: 25284209]

Abbreviations

CP: chronic pain
CMS: Command Mode Sense
DRL: Driven Right Leg
EEG: electroencephalograph
FDR: false discovery rate
HMD: head-mounted display
ICA: independent component analysis
LC: left central
LF: left frontal
LP: left parietal
MBSR: mindfulness-based stress reduction
MANOVA: multivariate analysis of variance
NRS: numerical rating scale

PSD: power spectral density
RCT: randomized controlled trial
RF: right frontal
VR: virtual reality

Edited by G Eysenbach; submitted 07.12.20; peer-reviewed by C Fowler, G Lewis, E Kutafina, A Mastropietro; comments to author 03.02.21; revised version received 23.04.21; accepted 29.04.21; published 24.06.21.

Please cite as:
Fu H, Garrett B, Tao G, Cordingley E, Ofoghi Z, Taverner T, Sun C, Cheung T
Virtual Reality–Guided Meditation for Chronic Pain in Patients With Cancer: Exploratory Analysis of Electroencephalograph Activity
JMIR Biomed Eng 2021;6(2):e26332
URL: https://biomedeng.jmir.org/2021/2/e26332/
doi:10.2196/26332
PMID:

Original Paper

Smartphone-Based Passive Sensing for Behavioral and Physical Monitoring in Free-Life Conditions: Technical Usability Study

Simone Tonti[1*], MSc; Brunella Marzolini[1], MSc; Maria Bulgheroni[1*], MSc

Ab.Acus srl, Milano, Italy

[*]these authors contributed equally

Corresponding Author:
Maria Bulgheroni, MSc
Ab.Acus srl
Via Francesco Caracciolo 77
Milano, 20155
Italy
Phone: 39 02 89693979
Email: mariabulgheroni@ab-acus.com

Abstract

Background: Smartphone use is widely spreading in society. Their embedded functions and sensors may play an important role in therapy monitoring and planning. However, the use of smartphones for intrapersonal behavioral and physical monitoring is not yet fully supported by adequate studies addressing technical reliability and acceptance.

Objective: The objective of this paper is to identify and discuss technical issues that may impact on the wide use of smartphones as clinical monitoring tools. The focus is on the quality of the data and transparency of the acquisition process.

Methods: QuantifyMyPerson is a platform for continuous monitoring of smartphone use and embedded sensors data. The platform consists of an app for data acquisition, a backend cloud server for data storage and processing, and a web-based dashboard for data management and visualization. The data processing aims to extract meaningful features for the description of daily life such as phone status, calls, app use, GPS, and accelerometer data. A total of health subjects installed the app on their smartphones, running it for 7 months. The acquired data were analyzed to assess impact on smartphone performance (ie, battery consumption and anomalies in functioning) and data integrity. Relevance of the selected features in describing changes in daily life was assessed through the computation of a k-nearest neighbors global anomaly score to detect days that differ from others.

Results: The effectiveness of smartphone-based monitoring depends on the acceptability and interoperability of the system as user retention and data integrity are key aspects. Acceptability was confirmed by the full transparency of the app and the absence of any conflicts with daily smartphone use. The only perceived issue was the battery consumption even though the trend of battery drain with and without the app running was comparable. Regarding interoperability, the app was successfully installed and run on several Android brands. The study shows that some smartphone manufacturers implement power-saving policies not allowing continuous sensor data acquisition and impacting integrity. Data integrity was 96% on smartphones whose power-saving policies do not impact the embedded sensor management and 84% overall.

Conclusions: The main technological barriers to continuous behavioral and physical monitoring (ie, battery consumption and power-saving policies of manufacturers) may be overcome. Battery consumption increase is mainly due to GPS triangulation and may be limited, while data missing because of power-saving policies are related only to periods of nonuse of the phone since the embedded sensors are reactivated by any smartphone event. Overall, smartphone-based passive sensing is fully feasible and scalable despite the Android market fragmentation.

(JMIR Biomed Eng 2021;6(2):e15417) doi:10.2196/15417

KEYWORDS

telemonitoring; data integrity; technical validation; cloud computing; ubiquitous computing; behavioral analysis; mHealth

Introduction

Background

In 2020, smartphone users are approximately 3.5 billion people (ie, about the 45% of the world population). Smartphones are a widely spread resource that health care providers might extensively use to improve the quality and timeliness of service to the citizen at acceptable costs.

Potentialities of smartphones in health care are being widely explored [1]. A PubMed search of "smartphone" or "mobile phone" and "monitoring" for articles published between January 1, 2000, and September 30, 2020, found 5246 articles with 74.04% (3884/5246) published after January 1, 2015, demonstrating a continuous increase of interest in the last few years.

Furthermore, the growing number of available apps in the Google and Apple stores covers an increasingly large spectrum of services able to support most citizens' daily activities. However, the effective diffusion of smartphone in the clinical practice is slowed down by social, organizational, and technical barriers [2]. Clinical practice requires the capability of continuously following up individuals along their care paths (longitudinal monitoring) assessing variations in time due to disease progression or intervention results. For this purpose, an underlying monitoring app must be robust and reliable and able to run on a wide base of smartphones in a totally unobtrusive and transparent way [3,4]. This approach addresses the ubiquitous computing paradigm that, through technologically transparent tools, enables the integration of small connected and inexpensive devices in the daily life of people. Transparency and density of the technological framework lead to higher levels of acceptability and reliability thanks to the reduced intrusiveness and, at the same time, the improved capillarity of the technology.

Meanwhile, the collected data must adhere to robust and device-independent quality standards to ensure measurement repeatability to generate clear clinical outcomes [5], while smartphone vendor policies contribute to increasing fragmentation due to strategic choices. Continuous monitoring apps and in particular passive sensing smartphone-based platforms must cope with constraints and limitations related to manufacturer choices and policies that need to be carefully assessed and cleared before large-scale deployment in health care with prevention and follow-up objectives.

On the other side, the level of engagement of the end user needs to be improved. Today, the longer the follow-up period, the higher the chances are for dropout [6]. Attrition rates from 30% to 70% are often reported [7-9]. Technological issues can dramatically impact the use in a daily routine.

Reliability and robustness are the most important drivers to ensure proper diffusion within the clinical practice; however, studies characterizing the smartphone-based platforms from this point of view are lacking. Many studies address the clinical relevance of the acquired data (see Prior Work section), but very few analyze the impact of technical issues on the scalability of the solutions in the daily routine and their performance in a heterogenous technical environment where hardware characteristics and proprietary policies have a strong impact on the quality of delivered data and calculated indexes.

Prior Work

Mental health–related studies have widely investigated the use of smartphone-based sensing platforms to cope with the need of unobtrusive and continuous data collection while reducing biases in patient behavior. Dogan et al [10] provide a comprehensive review of the current status of the technological impact on affective disorder management. Several studies about the correlation between affective disorders and smartphone use are investigated, and technical problems, in particular issues related to different operating systems, are reported as the most common reasons for discontinuation. The use of smartphone-embedded sensors for health monitoring systems is analyzed by Majumder et al [11] who identify, as a main driver for successful penetration of these technologies, the availability of affordable apps compatible with the main mobile operating systems and devices from different manufacturers. Similarly, the need for apps with reduced battery drain and standardized performances regardless of the device brand is reported by Baig et al [12] and Yu et al [13], while Boonstra et al [14] define performance, interoperability, and battery consumption as the most impacting issues. Differing operating systems are reported as the leading cause of data loss. The data collection rate is still only 55% of the scheduled acquisition time for Android smartphones, indicating the need for additional development work to provide more stable and reliable tools. Finally, Hossain and Poellabauer [15] present the challenges encountered in building the CIMON (Crew Interactive MObile CompanioN) system, a continuous smartphone sensing app. This system is specifically designed for the iOS system, and the main issues reported are energy consumption, storage, and operational continuity. Nevertheless, because of Apple's strict policy development limitations and terms, the variability in terms of technical policies between iOS devices is not even comparable with the Android market, which is required to deal with a broader pool of brands and proprietary management policies.

The need for robust and reliable passive sensing systems that exploit the smartphone as data collector is gaining relevance in the clinical debate, and recent studies [16] show a good correlation between behavioral data collected through smartphones and mental health–related scores [17-19] and also show how features calculated from smartphone data may capture a wider set of behavior descriptors not assessed by standard scores [20]. Other studies report strong correlations between smartphone-related nonmedical parameters, changes in lifestyle, and variations in mood [21]. In particular, frequency [22] and duration [23] of calls have been correlated to the onset of depressive symptoms.

Goal of This Study

In this paper, we identify the main issues a smartphone-based monitoring app must resolve to be a suitable tool for longitudinal measurement of personal behavior on a diverse and continuously changing technological panorama.

A testing platform, QuantifyMyPerson (QMP), has been used for this study as it is a proprietary smartphone-based app that allows direct access to the collected raw data. QMP uses the embedded sensors of the smartphone itself and smartphone use information to provide 24/7 monitoring of the user's life in terms of both physical and cognitive activities. The system architecture allows remote storage and processing of acquired data to be made available to the operator through a web-based dashboard. By design, QMP does not provide any feedback to the user and does not introduce any burden other than carrying the phone to avoid influencing the user's behavior while unobtrusively capturing their life habits.

The aim of this study is to pinpoint the main technological issues encountered within an operating context and identify the most relevant aspects to be considered when a monitoring platform is deployed. The findings of this study will inform technical choices to reach scalable, usable, and reliable solutions that can reach large pools of users.

Despite the fact that the acquisition of data through passive sensing systems happens in the most transparent way, the collected information belongs to the user's private sphere and there are privacy issues. Privacy and ethical issues are relevant perceived barriers in the spread of mobile health (mHealth) solutions and smartphone-based data collectors [24,25]. According to a recent review [26], broad consent and pseudonymization are frequently used approaches to manage these kinds of issues. A robust ethical framework is not yet clearly defined, and future evolutions should consider technical development, clinical benefits, and ethical issues together to shape an effective implementation of passive sensing in health care. Technical findings and outcomes of this study aim also to contribute to the definition of this framework promoting the use of passive data in an ethically safe and sound fashion.

Methods

Data Acquisition System

QMP is a composite system managing background acquisition of 24/7 data related to the social use of the smartphone (through call logs, app use, and device use) and to the user's activity habits (through GPS and accelerometer analysis).

The platform consists of a mobile app based on the Android OS, a cloud backend (backend as a service model), and a web-based dashboard (Figure 1). Data acquisition runs in the background during daily use of the smartphone by means of a passive motion sensor data acquisition approach. Through data processing algorithms, selected features are extracted to describe users' life and behavior changes. The dashboard allows for management of the registry of users and visualization of the acquired data in graphical and numerical forms.

Figure 1. QuantifyMyPerson architecture consists of the user's smartphone, a cloud backend for data storing and processing, and a web-based dashboard for data visualization.

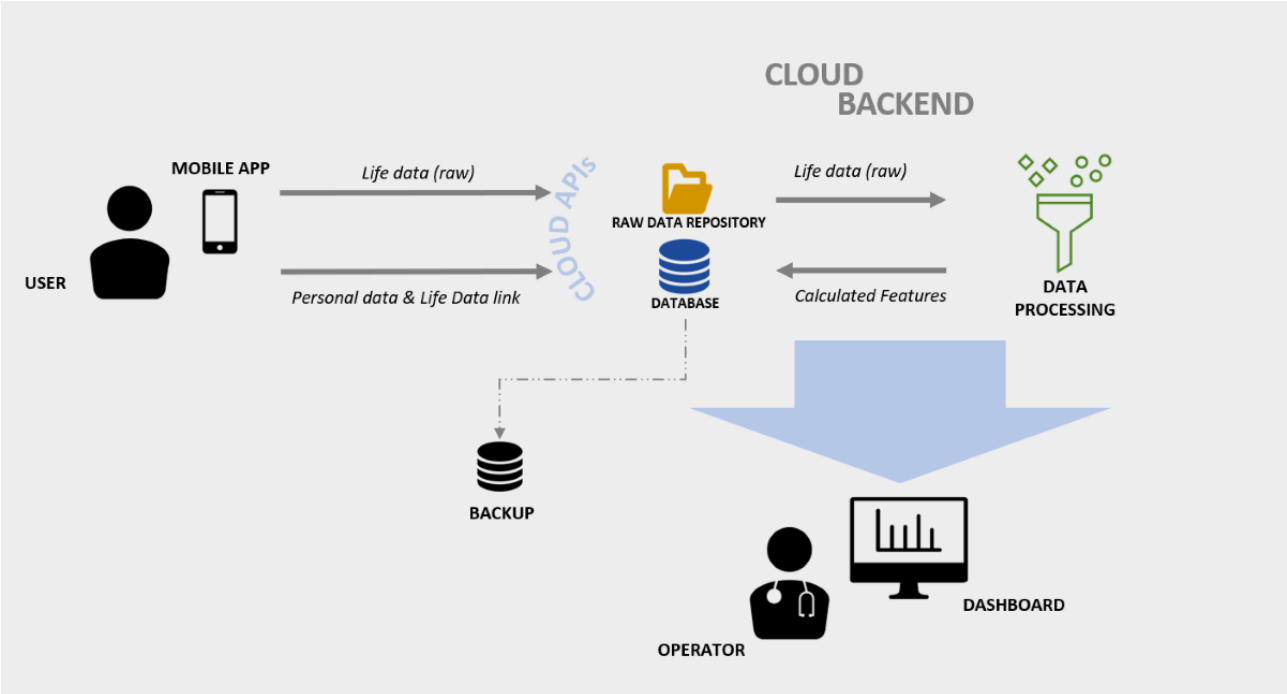

The monitoring app stores data locally on the smartphone and transmits them as Wi-Fi network connectivity becomes available. This strategy allows data collection in a variety of wireless connectivity scenarios with the confidence that intermittent network access does not affect the nature, quality, or quantity of the collected data.

Acquired data are temporarily saved in a remote storage area and processed daily to extract descriptive features. The computed features are saved on an in-cloud database accessed through a web-based dashboard. The dashboard, as a management tool, makes available various means for the management of the patient database while acquired features may be displayed through different graph typologies on freely selectable time windows. The use flow is described in Figure 2.

Figure 2. QuantifyMyPerson data flow from app installation to data visualization.

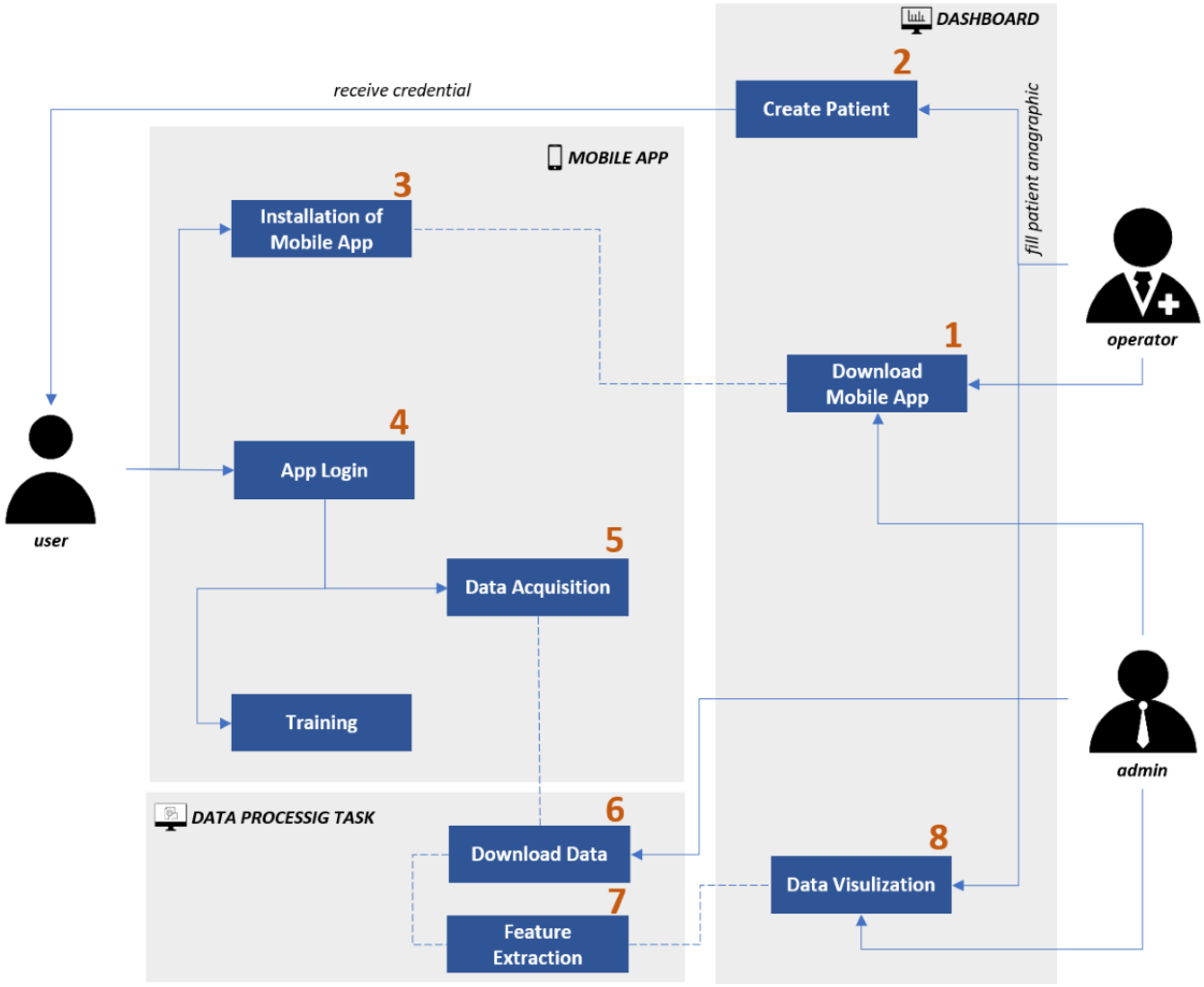

The mobile app is the core element of the sensing platform. During the study, the app was available for Android platforms only as this operating system enables more flexibility in the management and access to the data registries and sensors. The mobile app uses the sensor made available by the Android framework to interact with the inertial measurement unit sensors embedded in the smartphone and with the social and communication registries made available by the operating system. The sensors to be used for collecting data and related sampling frequencies can be set through a parametric configuration table allowing a dynamic fine tuning of the acquisition parameters without the need for updating the app on users' devices.

The following embedded sensors and registries are used as raw data sources by the QMP mobile app:

- Accelerometer sensor
- Gyroscope sensor
- Barometer sensor
- Magnetometer sensor
- GPS sensor
- Exchanged kBs per app registry
- Calls log registry
- Short message service log registry
- Screen brightness registry

The data acquired through the sensors are locally stored on the device as separated raw text files, one for each sensor. The raw files are then sent through an https encrypted communication protocol when a Wi-Fi connection is available in order to reduce the internal memory occupation and user data plan consumption. After the first log-in, the app runs in the background without any intervention from the user.

Data Processing

The features extracted from the raw data are based on the main findings reported in the literature according to a previous review of ours [27]. Table 1 summarizes the features calculated from raw data.

Table 1. Behavioral features extracted by QuantifyMyPerson.

Feature	Description
Calls	
mean_incoming	Average duration of incoming calls (seconds)
mean_outgoing	Average duration of outgoing calls (seconds)
tot_call_length	Total call duration (seconds)
outgoing_call	Number of calls made
Brightness	
mean_time_usage	Average duration of a session of use (from screen switch on to screen switch off)
number_switch_on	Number of times screen is switched on
b_*n* (24)	Seconds of phone's use from hour *n–1* to *n* with hourly granularity over the whole 24 hours
Apps	
tot_kb_social	Kilobytes consumed in social app (Facebook, Instagram, Twitter, LinkedIn)
tot_kb_communication	Kilobytes consumed in communication app (WhatsApp, Messenger, Telegram, Skype, Hangouts)
tot_kb_navigation	Kilobytes consumed in navigation app (Chrome, Firefox, proprietary browser, Google, YouTube, Tripadvisor)
tot_kb	Total kilobytes consumed in a day
GPS	
number_of_clusters	Number of places visited
time_outside	Percentage of time spent outside the home
location_variance	Variability in a participant's location calculated as location_variance = $(\sigma^2_{long} + \sigma^2_{lat})$, where σ^2_{long} and σ^2_{lat} represent the variance of the longitude and latitude, respectively, of the GPS location coordinates
Entropy	Measure of how uniformly a participant spends time at different locations. Let p_i denote the percentage of time that a participant spends in location cluster *i*. The entropy of the participant is calculated as entropy = $-(p_i * log(p_i))$
visited_clusters	Latitude and longitude coordinates of the visited places according to the distance from home
Activity	
m_amp_*n* (24)	Average of the acceleration signal amplitude from hour *n*–1 to *n* with hourly granularity over the whole 24 hours
s_a_*n* (24)	Seconds of high activity from hour *n*–1 to *n* with hourly granularity over the whole 24 hours
s_r_*n* (24)	Seconds of low activity from hour *n*–1 to *n* with hourly granularity over the whole 24 hours
percentage_activity	High activity/(high activity + low activity)

Study Design

A sample of 12 healthy people was recruited for this initial feasibility study for a time span of 7 months. As the aim of this study is to assess how smartphone-based passive sensing platforms cope with heterogeneous and complex environment, any Android user was considered eligible irrespective of the smartphone model, connection availability, or digital literacy. The final goal was to highlight any possible criticality that could occur during normal use under free-living conditions.

The participants' smartphones included 5 different smartphone brands and 11 different models running Android operating system versions from 4.4 to 7. The brand distribution shows a prevalence of Samsung and Huawei devices. The mean age of the selected participants was 39 (SD 5.4) years, the majority were male (8/12, 67%), and the average number of days of use was 62.

All participants were informed of the study aims and modalities when installing and running the app. Data handling was fully compliant with the General Data Protection Regulation. To ensure proper awareness about the acquired and stored data and aim of the study, an in-app communication approach was adopted consisting of an interactive wizard that describes the data sources used and the scope of the study. This approach ensures proper communication about data management and study aims through a clear description that can be understood by everyone regardless of the digital literacy of the enrolled subject.

Each participant's identity was pseudoanonymized with a random user ID, keeping the ID map separated from all other acquired data so that data cannot be traced back to individuals. Participant data were uploaded on a secured server using encrypted SSL protocol to ensure they cannot be intercepted by third parties. When people left the study, their personal data were removed while the raw data acquired during the study and the calculated features remain anonymously stored for scientific research purposes.

Results

Data Acquisition System

The system was first assessed in terms of performance with the 2-fold objective of evaluating the impact of the mobile app on the daily use of the smartphone and quality of the acquired data. As reported in the study description section, the device brand distribution spanned the most relevant Android market players. Samsung devices showed a prevalence of 33% (4/12) within the considered sample followed by Huawei devices with 25% (3/12), Xiaomi (8%), Asus (17%), and Honor (17%). This population distribution is fairly aligned with the brand fragmentation reported in the Android Fragmentation report [28] and the most recent Statista's global smartphone market share [29]. Thus, the sample under analysis mirrors the Android user population making the recruited participants a representative sample.

During the validation phase, no issues concerning normal smartphone functioning were reported, and the everyday use of the smartphone was not hindered by the background activity of the app. The app was installed on the user smartphone without impacting the running of already installed apps. No lags or limits in functionalities were reported during the study period.

The average battery consumption trend of the smartphones, with and without the monitoring app on board, are compared in Figure 3. The battery drain analysis was made comparing performance within the same operational environments (running apps, operative system, connection type). The two trends are comparable with an acceptable increase in power consumption when the app is up and running. This trend confirms the known battery drain issues for smartphone-based passive sensing platforms, but the battery consumption can be well managed by tuning acquisition parameters such as sensors sample rate, data writing frequency, and data sending frequency.

Figure 3. Comparison of the average daily battery consumption trend for the same smartphone with and without QuantifyMyPerson on board and running.

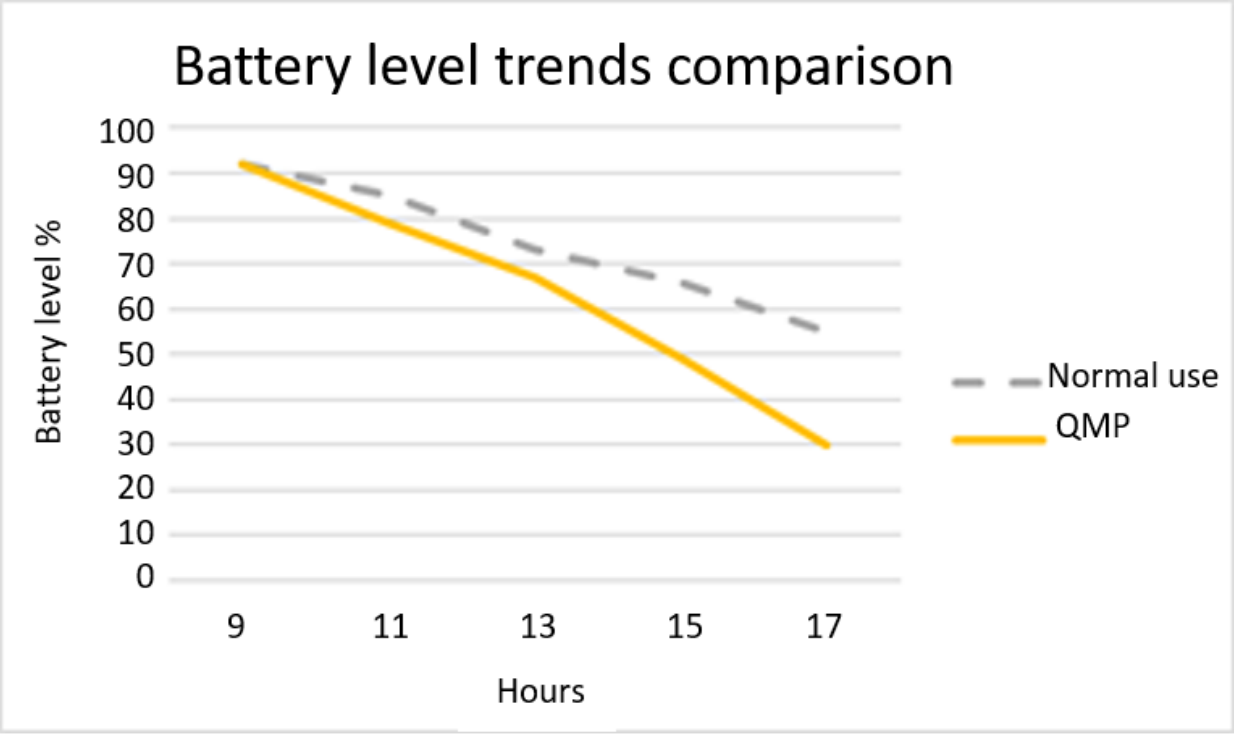

Because of the implementation by some manufacturers of battery consumption management policies, some commercial devices do not allow continuous data acquisition from both the phone's register and embedded sensors. This aspect could negatively influence reproducibility and scalability of smartphone-based monitoring systems especially within the Android ecosystem due to high level of fragmentation (brand, devices, and OS versions) if compared with the iOS systems [28].

By analyzing the up time of each sensor within the selected population of users during the acquisition period, we identified two subgroups based on the behavior of their smartphone: subgroup A consisted of 7 users for whom the specific policies of the phone operating system do not impact on the continuity of data; subgroup B consisted of 5 users with smartphones whose proprietary operating system policies have a strong impact on the continuity of acquisition (Table 2 and Figure 4).

The most widely used battery consumption management policies switch the embedded sensors off when the phone is not used (ie, when the screen is off for some time) and when there are no changes in the GPS signal (when GPS is active). The phone is woken up again when one of the two situations changes.

This behavior makes clear that data from embedded sensors are lost mainly when the phone is still (ie, it is not used, and it is not moved). That means that most of the lost data from sensors might be not associated with periods of activity (assuming that users are carrying the phone on their person). So, the related loss of information should be not relevant, but more focused tests are still needed to validate this first outcome.

Table 2. Classification of user device within subgroup A and B according to the proprietary smartphone management policies.

Subgroup	Device brand and model
A	
	Asus Zenfone 4
	Samsung S4
	Samsung S6
	ASUS Zenfone 2 Laser
	Samsung S5
	Redmi 3S
B	
	Honor 8
	Huawei P10 Lite
	Honor 7
	Huawei P9 Lite
	Huawei P8 Lite

Figure 4. Comparison between the integrity of acquired data between a subgroup A user and a subgroup B user. Grey bars represent the timespan in which the brightness of the display has been detected, blue points identify GPS data collection, and the orange line comprises 5 Hz sampled embedded sensors data.

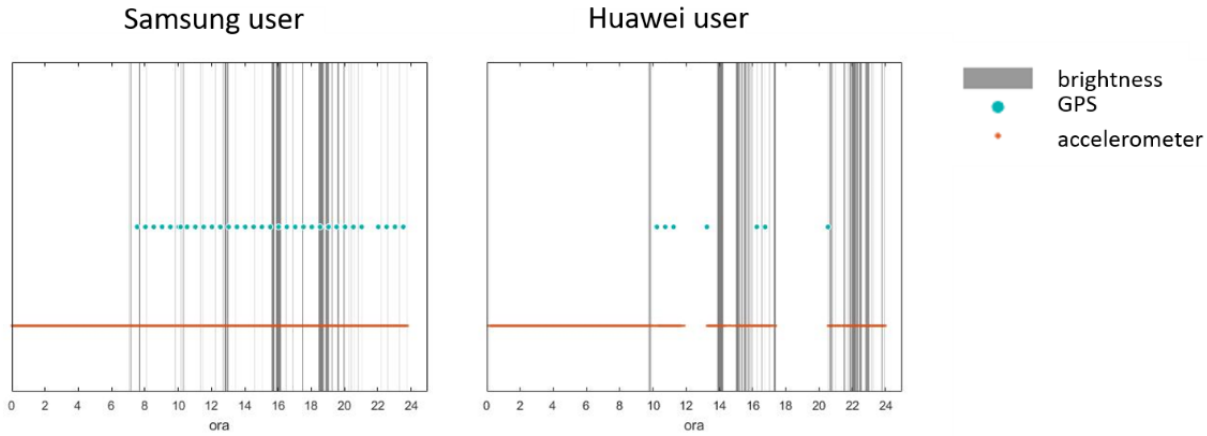

The quality and quantity of data are the main strengths of a continuous monitoring approach. Smartphone sensor issues, memory leaks, poor connection quality, and smartphone use in free-living condition have real impact on the quality of the collected data regardless the specific brand of the smartphone.

To assess these aspects, the data integrity percentage has been calculated using the following formula:

This measure is aimed at quantifying the percentage of data actually acquired while the app runs. The hours of acquired data are considered as the timespan during which the samples are acquired without interruption greater than 1 second. This measure provides an indirect computation of data samples lost during an acquisition session and allows us to spot gaps in the data.

Data integrity is a crucial parameter for the identification of the most appropriate data processing and feature extraction techniques. Datasets with a very low data integrity index should be not considered for frequency-based processing techniques or proper resampling techniques should be implemented.

This parameter might be used as a quality control parameter before mathematically or visually analyzing data. This approach should also be considered to ensure compliance with the medical device regulation (EU) 2017/745 on the risk of data misuse for clinical evidence extraction.

Within this study, the global data integrity percentage is 84% considering the entire sample of users, but a slightly different behavior was observed between the two subgroups of users described in the previous section. In particular, subgroup B is characterized by a lower value of data integrity percentage (60%) compared with subgroup A (96%). The analysis performed on the accelerometer, brightness, and GPS signals reveals that the lower data integrity percentage observed for the subgroup B of users is due to the previously described acquisition holes during which the smartphone kills the acquisition routine according to proprietary power-saving

policies. At this time, no solutions have been found due to the proprietary policies implemented that are business confidential and differ between smartphone models and brands.

Data integrity has not been negatively impacted by poor or absent Wi-Fi connections and in some cases all the data were properly stored and sent even if the smartphone was not connected to Wi-Fi for a few days (up to 3). The data transfer protocol has proved to be efficient and capable of handling unreliable connections.

Thus, the strategy adopted for sending large raw data files based on file chunks periodically sent and attached to the master file stored on the remote repository provides a reliable data exchange protocol. This strategy allows decentralization of the computational power needed and thus reduces the impact on performance of the users' smartphones. This approach is largely used for the management of data collection through a big data approach, and it is at the core of the edge computing paradigm that allows the implementation of sparse technological frameworks.

Data Processing

Even if the focus of this study is not the clinical evaluation of the smartphone-based passive sensing platform, the collected data have been processed with the aim of extracting the features identified in the literature and evaluating their potentialities in identifying behavior trends and shifts for the analyzed users. The processing task was executed daily through an automatic routine.

The computed features were analyzed in order to investigate the information content and assess whether the typology and integrity of the available data could match with the data processing requirements for the analysis of trends and anomalies about human behavior. First, a principal component analysis was performed on the whole pool of features extracted with the aim of detecting the most descriptive set of features. The following features were identified as the most descriptive:

- GPS-related features such as movement index, location variance, and normalized entropy
- Hourly activity features—in particular, in the timespan that goes from 10 AM to 9 PM
- Hourly brightness features—in particular, in the timespan that goes from 11 AM to 10 PM

Thus, the selected features were used to extract information about the variance between each day and detect anomalous days. This approach starts from the evidence reported by Berrouiguet [30] on the analysis of GPS-based features and validates its feasibility with a larger set of features than the ones investigated here. The set of features was analyzed using a k-Nearest Neighbor Global Anomaly Score in order to detect the days that differ from others within the period of use of QMP (Figure 5). This analysis showed a repeatable pattern for each user along the period of acquisition discriminating between the nonworking days and the working days. Public holidays instead were detected as the most relevant outliers showing the ability of the system to easily detect the days that differ most because of nonstandard behavior of the user.

Figure 5. k-Nearest Neighbors Global Anomaly Score graph for a selected user. Points represent the calculated anomaly score for each day with the red points representing days with the highest values of anomaly.

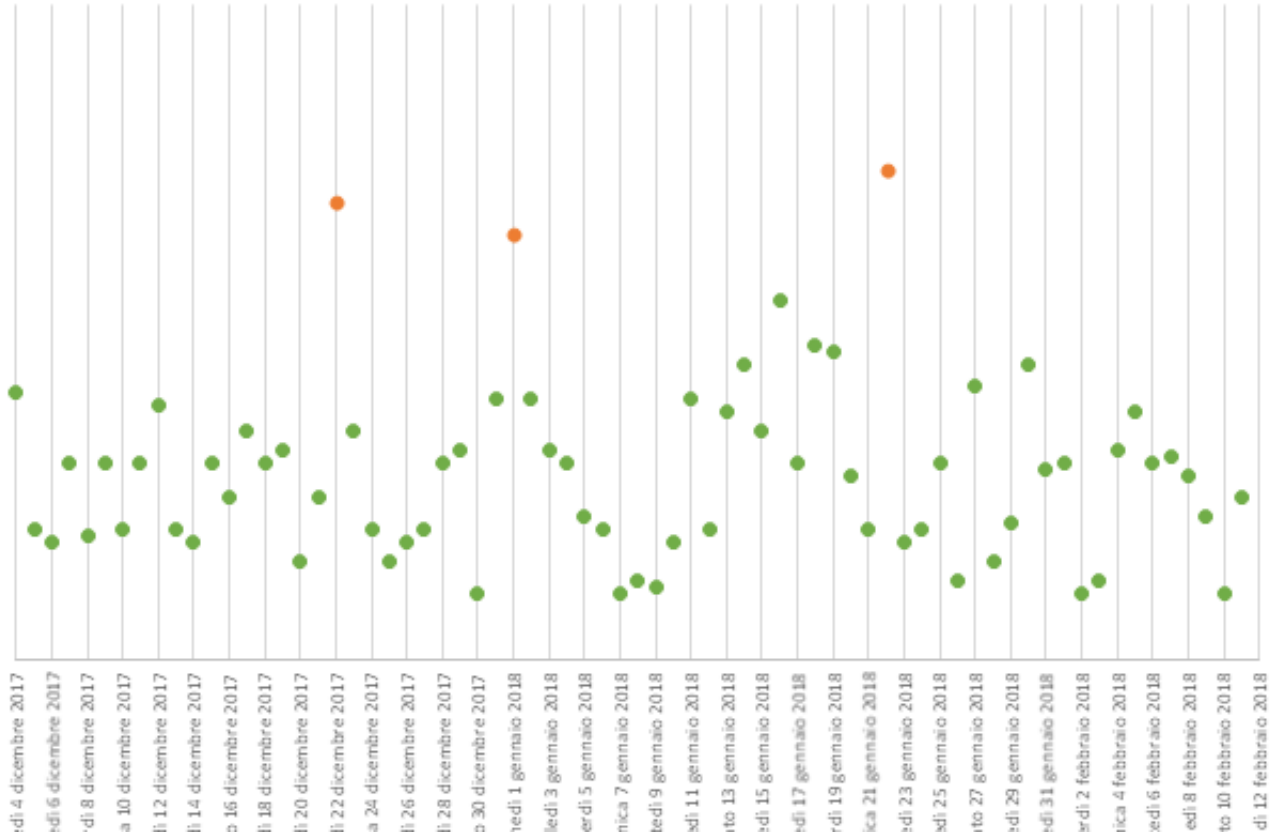

People use their smartphones for different purposes and through different interaction modalities regardless their of demographic data, which has been demonstrated to not have relevant impacts on the smartphone-related behavior [31] Smartphones are strongly integrated in every aspect of people's lives acting as a reliable behavioral mirror [32] enabling the longitudinal monitoring and indirect assessment of cognitive and physical status. Further analyses are ongoing in order to better assess the potentialities of identifying clinically relevant and behavior-related trends through a wider clinical trial. The first data analysis shows promising results for users belonging to both subgroup A and B. However, further investigation is still needed in order to find the best data normalization method that takes advantage of the data integrity parameters for each of the identified subgroups.

Discussion

Principal Findings

In this paper, we presented the results of a validation test aimed to assess the reliability of smartphone-based passive sensor systems and the related integrity of the acquired data. Also, a preliminary assessment of the informative content of these data and their correlation to real user behavior has been presented with the aim of associating the data integrity with the capability to extract valuable insights from data.

All participants used the system consistently and actively for the period of the study without any kind of technological constraint. The proposed approach proved to be able to manage the flow of data correctly without a consistent loss of information and provide a daily update of the calculated features. The method used to acquire data from the embedded sensors through a mobile app was able to work with the heterogenous and complex technical environment ensuring a good level of reliability and maintaining a good level of performance of the users' smartphones without impacting the already installed apps. The system also registered a high level of acceptability due to the good level of integration in the normal use of the smartphone in conjunction with an adequate level of transparency and ubiquitousness that ensured reliable and meaningful results. Two participants (17%) asked to interrupt the study after 1 month due to battery drain effects, but the users continued the study when the battery drain effect was mitigated by activating the GPS sensor only for limited time spans within the day.

The current smartphone evolution is highly focused on the optimization of the battery consumption for the most energy-consuming sensors such as GPS and Bluetooth as many of the most common apps require their continuous running (eg, COVID-19 tracking apps). Thus, the impact on battery drain is also expected to be reduced for passive sensor platforms such as the one used in this study. Besides, the use of monitoring tools in the frame of a structured digital health approach will further justify the power consumption side effect thanks to demonstrated care benefits.

In this study, data acquisition, performed by means of the users' own smartphones without any limitations or technological eligibility criteria, reached a remarkable integrity of the globally acquired data—14,970 hours of collected sample out of 17,845 hours of acquisition (84%)—that surpasses the performances presented in previous publications [33], proving the potentialities of passive sensing platforms. However, different behaviors observed for subgroup A and B have some impacts on the data integrity ratio with 96% and 60%, respectively, when kept separately. Brand-related operating system policies still have the most important impact on data integrity due to the observed fragmentation of the Android services.

The availability of different sensor data allows us to describe each subject in terms of physical activity (accelerometer data), social interaction (calls, communications, and social network data), and georeferenced data. This approach provides an overall description of each user that can be used to continuously monitor both the psychological and physical status, strengthening the added value of this type of system which can provide a comprehensive description of quality of life and well-being. The wide range of data made available by monitoring platforms can also be considered the necessary starting point for data fusion approaches [34].

Preliminary analysis of the obtained results shows that the data fusion between different sensors provides a valuable key to interpret personal behavior. In particular, the demonstrated capability of identifying anomalous days is strongly dependent on the variability in content of the acquired data and can represent a strong starting point for different clinical applications. Furthermore, the habits about smartphone use itself could be used as a valid behavioral descriptors. For example, intrapersonal changes in frequency and duration of smartphone daily usage or the inactivity period of the smartphone due to the fact the user has not carried the smartphone can be used as indirect behavioral descriptors. Thus, the fusion between data acquired from different contexts gives a comprehensive description considering all the aspects that can be impacted by changing physical or psychological condition. Also, the smartphone use parameters (eg, screen time, battery use) can be used to normalize the calculated features, reducing the bias due to different smartphone use that can impact the reliability of the collected data.

Limitations

This study has been conducted on a limited number of subjects with a focus on Android devices. A wider study should be conducted including a wider pool of devices and subjects. Furthermore, assessment of the approach on acute and chronic patients is required to ensure generalizability in the clinical application domain.

The use of mobile apps for health monitoring is still in an early phase. To foster their acceptance at a wider level, making the collected information routinely useful for the health care system, clinical validations are necessary to select the best parameters to investigate each pathological condition. However, analysis of this aspect was outside the scope of this study, which focused on assessment of perceived technical limitations to daily use.

Conclusion

In this paper, we present a study that contributes as an additional step to broad distribution of smartphone-based monitoring

platforms. We described the technical approach used to implement a smartphone-based passive platform, its characteristics, and the potentialities of this type of solution to provide insights to patients and clinicians. The quality of the acquired data and performance of the system are quite dependent on the proprietary policies implemented by each smartphone brand even if the acquisition through smartphone-embedded sensors as presented in this article is able to provide a good level of accuracy within an heterogenous pool of devices. The preliminary analysis performed on the raw data collected provides initial encouraging results that must be better validated through well-structured clinical trials with the aim of substantiating the clinical evidence of monitoring systems and their capability of extracting indexes that could be used as reliable descriptors and predictors of the disease path.

In the future, we will continue this work deepening the technical validation of this type of platform to assess performance and quality of the collected data on a wider study cohort including the most recent Android updates and newest smartphone brands. Furthermore, the research will focus on the assessment of the data fusion potentialities for the extraction of valuable clinical insights according to the characteristics of the collected data. Additionally, as the performance of this type of monitoring system is quite depending on the policies of each smartphone producer, a wider discussion could address guidelines that could match with the needs of mHealth in the near future.

Discussion about the repeatability and reliability of smartphone-based passive sensing platforms should also drive the debate about software as medical device and its applicability in the current regulatory framework. This is still an open issue [35] whose resolution will be necessary to drive the successful use of monitoring systems as scalable and reliable supports for the clinical practice. Also, ethical and security aspects will be investigated to make the system as secure as possible by design. Thus, a quantified technical characterization of the system in terms of reproducibility and robustness of the provided measurements will be necessary, and the proposed article could be considered a good methodologic starting point.

Conflicts of Interest

None declared.

References

1. Lamonaca F, Polimeni G, Barbé K, Grimaldi D. Health parameters monitoring by smartphone for quality of life improvement. Measurement 2015 Sep;73:82-94. [doi: 10.1016/j.measurement.2015.04.017]
2. Trossen D, Pavel D. AIRS: a mobile sensing platform for lifestyle management research and applications. ICST Trans Mobile Comm Appl 2013 Dec 14;1(3):1-15. [doi: 10.4108/mca.1.3.e8]
3. Düking P, Fuss FK, Holmberg H, Sperlich B. Recommendations for assessment of the reliability, sensitivity, and validity of data provided by wearable sensors designed for monitoring physical activity. JMIR Mhealth Uhealth 2018 Apr 30;6(4):e102 [FREE Full text] [doi: 10.2196/mhealth.9341] [Medline: 29712629]
4. Smets E, Rios Velazquez E, Schiavone G, Chakroun I, D'Hondt E, De Raedt W, et al. Large-scale wearable data reveal digital phenotypes for daily-life stress detection. NPJ Digit Med 2018;1:67 [FREE Full text] [doi: 10.1038/s41746-018-0074-9] [Medline: 31304344]
5. Cornet VP, Holden RJ. Systematic review of smartphone-based passive sensing for health and wellbeing. J Biomed Inform 2018 Jan;77:120-132. [doi: 10.1016/j.jbi.2017.12.008] [Medline: 29248628]
6. Bauer AM, Iles-Shih M, Ghomi RH, Rue T, Grover T, Kincler N, et al. Acceptability of mHealth augmentation of collaborative care: a mixed methods pilot study. Gen Hosp Psychiatry 2017 Nov 24;51:22-29. [doi: 10.1016/j.genhosppsych.2017.11.010] [Medline: 29272712]
7. Tambs K, Rønning T, Prescott CA, Kendler KS, Reichborn-Kjennerud T, Torgersen S, et al. The Norwegian Institute of Public Health twin study of mental health: examining recruitment and attrition bias. Twin Res Hum Genet 2009 Apr;12(2):158-168 [FREE Full text] [doi: 10.1375/twin.12.2.158] [Medline: 19335186]
8. Bjerkeset O, Nordahl HM, Larsson S, Dahl AA, Linaker O. A 4-year follow-up study of syndromal and sub-syndromal anxiety and depression symptoms in the general population: the HUNT study. Soc Psychiatry Psychiatr Epidemiol 2008 Mar;43(3):192-199. [doi: 10.1007/s00127-007-0289-6] [Medline: 18064394]
9. Spring B, Pellegrini C, McFadden HG, Pfammatter AF, Stump TK, Siddique J, et al. Multicomponent mHealth intervention for large, sustained change in multiple diet and activity risk behaviors: the Make Better Choices 2 randomized controlled trial. J Med Internet Res 2018 Jun 19;20(6):e10528 [FREE Full text] [doi: 10.2196/10528] [Medline: 29921561]
10. Dogan E, Sander C, Wagner X, Hegerl U, Kohls E. Smartphone-based monitoring of objective and subjective data in affective disorders: where are we and where are we going? Systematic review. J Med Internet Res 2017 Jul 24;19(7):e262 [FREE Full text] [doi: 10.2196/jmir.7006] [Medline: 28739561]
11. Majumder S, Deen MJ. Smartphone sensors for health monitoring and diagnosis. Sensors (Basel) 2019 May 09;19(9):1 [FREE Full text] [doi: 10.3390/s19092164] [Medline: 31075985]
12. Baig MM, GholamHosseini H, Connolly MJ. Mobile healthcare applications: system design review, critical issues and challenges. Australas Phys Eng Sci Med 2015 Mar;38(1):23-38. [doi: 10.1007/s13246-014-0315-4] [Medline: 25476753]
13. Yu Z, Wang Z. Sensor-based behavior recognition. In: Human Behavior Analysis: Sensing and Understanding. Singapore: Springer; 2020.

14. Boonstra TW, Nicholas J, Wong QJ, Shaw F, Townsend S, Christensen H. Using mobile phone sensor technology for mental health research: integrated analysis to identify hidden challenges and potential solutions. J Med Internet Res 2018 Jul 30;20(7):e10131 [FREE Full text] [doi: 10.2196/10131] [Medline: 30061092]
15. Hossain C, Poellabauer C. Challenges in building continuous smartphone sensing applications. 2016 Presented at: 2016 IEEE 12th International Conference on Wireless and Mobile Computing, Networking and Communications (WiMob); 2016; New York. [doi: 10.1109/WiMOB.2016.7763202]
16. Saeb S, Zhang M, Karr CJ, Schueller SM, Corden ME, Kording KP, et al. Mobile phone sensor correlates of depressive symptom severity in daily-life behavior: an exploratory study. J Med Internet Res 2015;17(7):e175 [FREE Full text] [doi: 10.2196/jmir.4273] [Medline: 26180009]
17. Sano, Phillips A, Yu A, McHill A, Taylor S, Jaques N, et al. Recognizing academic performance, sleep quality, stress level, and mental health using personality traits, wearable sensors and mobile phones. Int Conf Wearable Implant Body Sens Netw 2015 Jun:1. [doi: 10.1109/BSN.2015.7299420] [Medline: 28516162]
18. Sano A, Pickard RW. Stress recognition using wearable sensors and mobile phones. 2013 Presented at: Humaine Association Conference on Affective Computing and Intelligent Interaction; 2013; Geneva p. 671-676. [doi: 10.1109/acii.2013.117]
19. Palmius N, Osipov M, Bilderbeck AC. A multi-sensor monitoring system for objective mental health management in resource constrained environments. 2014 Presented at: Appropriate Healthcare Technologies for Low Resource Settings (AHT 2014); 2014; London p. 4. [doi: 10.1049/cp.2014.0764]
20. Farhan AA, Yue C, Morillo R. Behavior vs. introspection: refining prediction of clinical depression via smartphone sensing data. 2016 Presented at: 2016 IEEE Wireless Health (WH); 2016; Bethesda p. 1-8. [doi: 10.1109/wh.2016.7764553]
21. Gruenerbl A, Oleksy P, Bahle G. Towards smart phone based monitoring of bipolar disorder. Proc Second ACM Workshop Mobile Syst Appl Serv Healthc 2012;3:1-6. [doi: 10.1145/2396276.2396280]
22. Wang R, Chen F, Chen Z. StudentLife: assessing mental health, academic performance and behavioral trends of college students using smartphones. Proc 2014 ACM Int Jt Conf Pervasive Ubiquitous Comput 2014:3-14. [doi: 10.1145/2632048.2632054]
23. Farhan AA, Lu J, Bi J. Multi-view bi-clustering to identify smartphone sensing features indicative of depression. 2016 Presented at: 2016 IEEE First International Conference on Connected Health: Applications, Systems and Engineering Technologies (CHASE); 2016; Washington p. 264-273. [doi: 10.1109/chase.2016.27]
24. Jacob C, Sanchez-Vazquez A, Ivory C. Social, organizational, and technological factors impacting clinicians' adoption of mobile health tools: systematic literature review. JMIR Mhealth Uhealth 2020 Feb 20;8(2):e15935 [FREE Full text] [doi: 10.2196/15935] [Medline: 32130167]
25. Gurupur VP, Wan TTH. Challenges in implementing mHealth interventions: a technical perspective. Mhealth 2017;3:32 [FREE Full text] [doi: 10.21037/mhealth.2017.07.05] [Medline: 28894742]
26. Maher NA, Senders JT, Hulsbergen AFC, Lamba N, Parker M, Onnela J, et al. Passive data collection and use in healthcare: a systematic review of ethical issues. Int J Med Inform 2019 Sep;129:242-247. [doi: 10.1016/j.ijmedinf.2019.06.015] [Medline: 31445262]
27. Seppälä J, De Vita I, Jämsä T, Miettunen J, Isohanni M, Rubinstein K, M-RESIST Group, et al. Mobile phone and wearable sensor-based mHealth approaches for psychiatric disorders and symptoms: systematic review. JMIR Ment Health 2019 Feb 20;6(2):e9819 [FREE Full text] [doi: 10.2196/mental.9819] [Medline: 30785404]
28. Kovach S. Android Fragmentation Report. URL: https://www.opensignal.com/sites/opensignal-com/files/data/reports/global/data-2015-08/2015_08_fragmentation_report.pdf [accessed 2020-12-15]
29. Share of smartphone unit sales to end users by vendor from the 1st quarter of 2016 to the 4th quarter of 2020. URL: https://www.statista.com/statistics/266220/global-smartphone-market-share-by-vendor-in-2007-and-2008/ [accessed 2021-04-28]
30. Berrouiguet S, Ramírez D, Barrigón ML, Moreno-Muñoz P, Carmona Camacho R, Baca-García E, et al. Combining continuous smartphone native sensors data capture and unsupervised data mining techniques for behavioral changes detection: a case series of the evidence-based behavior (eB2) study. JMIR Mhealth Uhealth 2018 Dec 10;6(12):e197 [FREE Full text] [doi: 10.2196/mhealth.9472] [Medline: 30530465]
31. Falaki H, Mahanjan R, Kandula S. Diversity in smartphone usage. Proc 8th Int Conf Mobile Syst Appl Serv 2010:179-194. [doi: 10.1145/1814433.1814453]
32. Akeret K, Vasella F, Geisseler O, Dannecker N, Ghosh A, Brugger P, et al. Time to be "smart"—opportunities arising from smartphone-based behavioral analysis in daily patient care. Front Behav Neurosci 2018;12:303 [FREE Full text] [doi: 10.3389/fnbeh.2018.00303] [Medline: 30568582]
33. Rickard N, Arjmand H, Bakker D, Seabrook E. Development of a mobile phone app to support self-monitoring of emotional well-being: a mental health digital innovation. JMIR Ment Health 2016 Nov 23;3(4):e49 [FREE Full text] [doi: 10.2196/mental.6202] [Medline: 27881358]
34. Kelly D, Condell J, Curran K, Caulfield B. A multimodal smartphone sensor system for behaviour measurement and health status inference. Inf Fusion 2020 Jan;53:43-54. [doi: 10.1016/j.inffus.2019.06.008]
35. Benjamens S, Dhunnoo P, Meskó B. The state of artificial intelligence-based FDA-approved medical devices and algorithms: an online database. NPJ Digit Med 2020;3:118 [FREE Full text] [doi: 10.1038/s41746-020-00324-0] [Medline: 32984550]

Abbreviations

CIMON: Crew Interactive MObile CompanioN
mHealth: mobile health
QMP: QuantifyMyPerson

Edited by G Eysenbach; submitted 10.07.19; peer-reviewed by S Albakri, T Silva, X Ding; comments to author 21.08.20; revised version received 15.10.20; accepted 17.04.21; published 11.05.21.

Please cite as:
Tonti S, Marzolini B, Bulgheroni M
Smartphone-Based Passive Sensing for Behavioral and Physical Monitoring in Free-Life Conditions: Technical Usability Study
JMIR Biomed Eng 2021;6(2):e15417
URL: https://biomedeng.jmir.org/2021/2/e15417
doi:10.2196/15417
PMID:

Original Paper

A Transcranial Magnetic Stimulation Trigger System for Suppressing Motor-Evoked Potential Fluctuation Using Electroencephalogram Coherence Analysis: Algorithm Development and Validation Study

Keisuke Sasaki[1*], BA; Yuki Fujishige[2*], BE; Yutaka Kikuchi[3*], MPH; Masato Odagaki[1,2,4*], PhD

[1]Department of Environment and Life Engineering, Graduate School of Maebashi Institute of Technology, Maebashi, Japan

[2]Department of Systems Life Engineering, Maebashi Institute of Technology, Maebashi, Japan

[3]Department of Rehabilitation for Intractable Neurological Disorders, Institute of Brain and Blood Vessels Mihara Memorial Hospital, Isesaki, Japan

[4]Division of Systems Life Engineering, Graduate School of Maebashi Institute of Technology, Maebashi, Japan

[*]all authors contributed equally

Corresponding Author:
Masato Odagaki, PhD
Department of Systems Life Engineering
Maebashi Institute of Technology
460-1 Kamisadorimachi
Maebashi, 371-0816
Japan
Phone: 81 27 265 7337
Email: odagaki@maebashi-it.ac.jp

Abstract

Background: Transcranial magnetic stimulation (TMS), when applied over the primary motor cortex, elicits a motor-evoked potential (MEP) in electromyograms measured from peripheral muscles. MEP amplitude has often been observed to fluctuate trial to trial, even with a constant stimulus. Many factors cause MEP fluctuations in TMS. One of the primary factors is the weak stationarity and instability of cortical activity in the brain, from which we assumed MEP fluctuations originate. We hypothesized that MEP fluctuations are suppressed when TMS is delivered to the primary motor cortex at a time when several electroencephalogram (EEG) channels measured on the scalp are highly similar in the frequency domain.

Objective: We developed a TMS triggering system to suppress MEP fluctuations using EEG coherence analysis, which was performed to detect the EEG signal similarity between the 2 channels in the frequency domain.

Methods: Seven healthy adults participated in the experiment to confirm whether the TMS trigger system works adequately, and the mean amplitude and coefficient of the MEP variation were recorded and compared with the values obtained during the control task. We also determined the experimental time under each condition and verified whether it was within the predicted time.

Results: The coefficient of variation of MEP amplitude decreased in 5 of the 7 participants, and significant differences (P=.02) were confirmed in 2 of the participants according to an F test. The coefficient of variation of the experimental time required for each stimulus after threshold modification was less than that without threshold modification, and a significant difference (P<.001) was confirmed by performing an F test.

Conclusions: We found that MEP could be suppressed using the system developed in this study and that the TMS trigger system could also stabilize the experimental time by changing the triggering threshold automatically.

(JMIR Biomed Eng 2021;6(2):e28902) doi:10.2196/28902

KEYWORDS

motor-evoked potential; transcranial magnetic stimulation; electroencephalogram; coherence; variability; fluctuation; trigger; threshold; coefficient of variation; primary motor cortex

Introduction

Transcranial magnetic stimulation (TMS) is a noninvasive method of stimulating cortical neurons [1]. The stimulus coil placed on the scalp generates induced electric fields in the brain, which then stimulate cortical neurons. TMS over the primary motor cortex (M1) has been used to evaluate corticospinal excitability in perioperative assessment [2]. When TMS is delivered to the M1, the efferent signal passes through the corticospinal tract [3]; consequently, the motor-evoked potential (MEP) can be measured using an electromyogram (EMG) of the peripheral muscle with a latency of approximately 20 ms following TMS. The amplitude of the MEP in TMS is often unstable and fluctuates even under similar conditions [4-8]. There are several possible factors that affect the variability of MEP amplitude, which vary depending on internal and external factors [9,10]. Furthermore, there are many factors involved, such as changes in body temperature, blood pressure, the atmosphere in the laboratory, and the participant's posture. It is thus difficult to identify the factors that affect MEP fluctuations. If the fluctuation of the MEP amplitude can be suppressed, this suppression method could be applied in a wide range of fields.

We assumed that one possible factor of MEP fluctuation in TMS was the change in the state of cortical stationarity. Cortical excitability can be measured using an electroencephalogram (EEG) [11]. The similarity of the measured EEG is calculated using coherence analysis, which is a method for calculating the correlation between 2 EEG signals in the frequency domain. We hypothesized that the fluctuation of MEP amplitude must be suppressed when TMS is delivered to the M1 at a time when the electroencephalograms of 2 channels measured on the scalp are highly similar in the frequency domain. In addition, we surmised that the experimental time should be controlled to maintain the accuracy of the experimental data. In this study, we developed an online TMS trigger system for the suppression of MEP fluctuations using EEG coherence analysis while controlling the experimental time.

Methods

TMS Trigger System

Figure 1 shows an overview of the proposed system. This system is composed of a single-pulse TMS device (Magstim 200^2, Magstim Co, Ltd), an EEG device (Polymate Mini AP108, Miyuki Giken Co, Ltd,), an IW2PAD EMG (frequency characteristics: 5.3-442 Hz, common-mode rejection ratio: 94 dB; Oisaka Electronic Equipment Ltd), a data acquisition device (USB-6210, National Instruments), and a PC. Software for sending the trigger signal to the TMS device under specific EEG conditions was developed. EEG data measured from P3 and C4 of the international 10–20 system were continuously transmitted to a PC via Bluetooth. The EEG was recorded at a sampling rate of 500 Hz and filtered using a fourth-order Butterworth bandpass filter with a cutoff frequency of 1 Hz to 30 Hz. The EMG results were measured using a data acquisition device connected via a USB. An online EEG analysis was performed during the trial. The triggering signal was sent to the TMS device when the preset TMS condition was satisfied; the data acquisition device then began measuring the MEP waveform from the first dorsal interosseous muscle of the right index finger using the EMG device. The EMG was recorded at a sampling rate of 5 kHz.

Coherence analysis was performed to detect the EEG signal similarity between the 2 channels in the frequency domain. The coherence of the 2 EEG signals was calculated using the following equation:

where P_{P3} and P_{C4} are the power spectrum densities of each EEG waveform, and $P_{P3\text{-}C4}$ is the cross-power spectrum density of the 2 EEG waveforms. Therefore, the coherence function indicates the similarity between 2 EEG waveforms in the frequency domain. Coh (β), which is the area of the coherence function between 14 Hz and 30 Hz, is defined as the average value of coherence in the β frequency band (Figure 2).

Figure 1. TMS trigger system using EEG coherence analysis. DAQ: data acquisition device; EEG: electroencephalogram; EMG: electromyogram; FDI: first dorsal interosseous; TMS: transcranial magnetic stimulation.

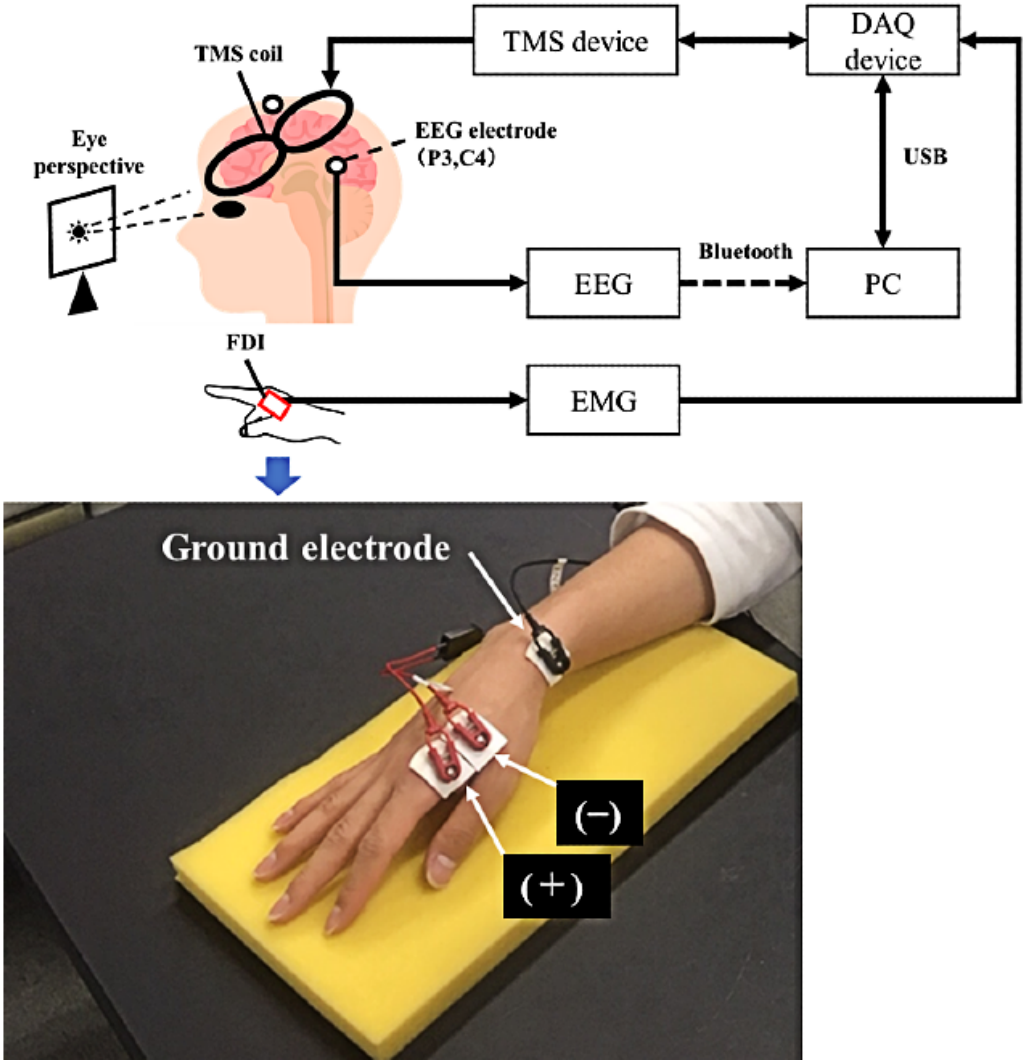

Figure 2. Data processing. The coherence function indicates the frequency spectrum of correlation between 2 EEG channels (P3 and C4). Coh (β) is defined as the average value of coherence between 14 Hz and 30 Hz. The values of Coh (β) are used to determine the transcranial magnetic stimulation trigger timing. EEG: electroencephalogram.

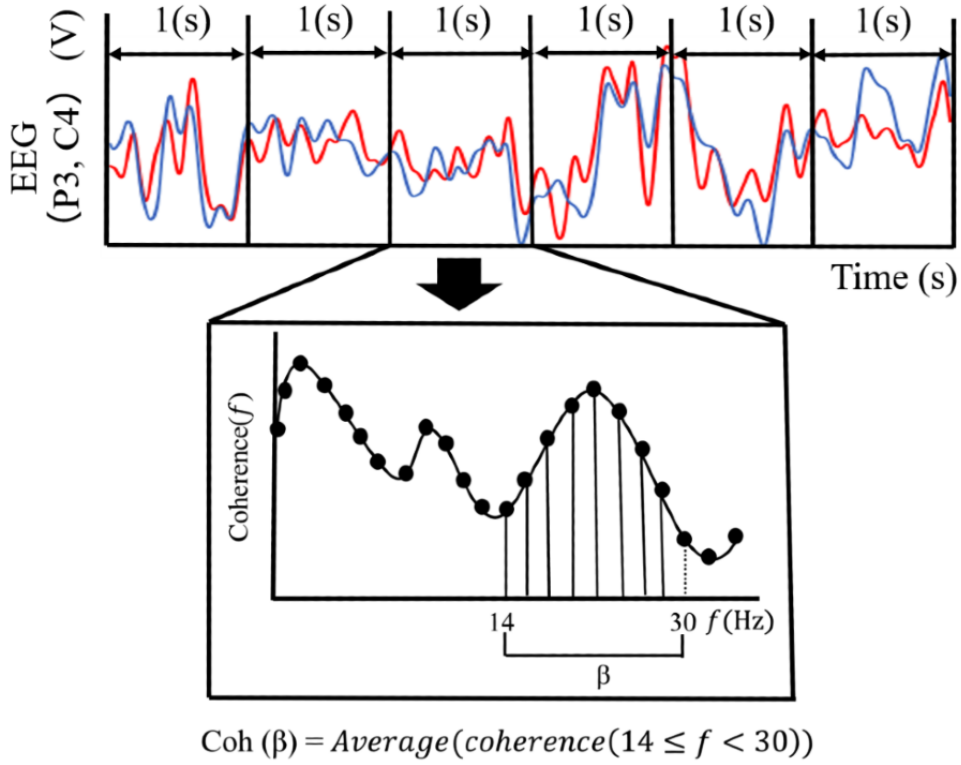

TMS Triggering Threshold

Prior to the experiments, we measured the participants' EEG for 180 seconds, analyzed the 180 data points divided into 1-second fragments, and confirmed the characteristics of Coh (β). The system predicted that the trigger could be performed 6 times in 180 seconds under these thresholds; that is, once every 30 seconds on average (Figure 3). Considering that the maximum standby time was 60 seconds in the TMS device, we assumed that TMS should be output in approximately 30 seconds, which was the median of the maximum standby time.

Figure 4 shows the flowchart of the experimental protocol. In the proposed system, the threshold was automatically modified to be a loose condition if there was no stimulus in 30 seconds. Online coherence analysis was performed on the EEG data once every second during the experiment, and the TMS trigger signal was sent from the data acquisition device to the TMS device at the time when the EEG coherence value of Coh (β) was greater than the threshold value (Coh [β] ≥ threshold), and TMS was applied to the M1 immediately.

The EEG coherence analysis was paused following TMS and then resumed after 10 seconds. Because the maximum standby time was 60 seconds in the TMS device, the capacitor bank in the TMS device was manually charged if there was no TMS over 60 seconds. If 30 seconds passed from the beginning of the experiment, the threshold of Coh (β) was updated with a Δthreshold = –0.05 for every second until the TMS was applied. Once the TMS trigger was output, the threshold value was set to the initial value.

Figure 3. Presetting of the initial threshold. We determined the initial threshold of Coh (β) under which the trigger could be performed 6 times in 180 seconds. EEG: electroencephalogram.

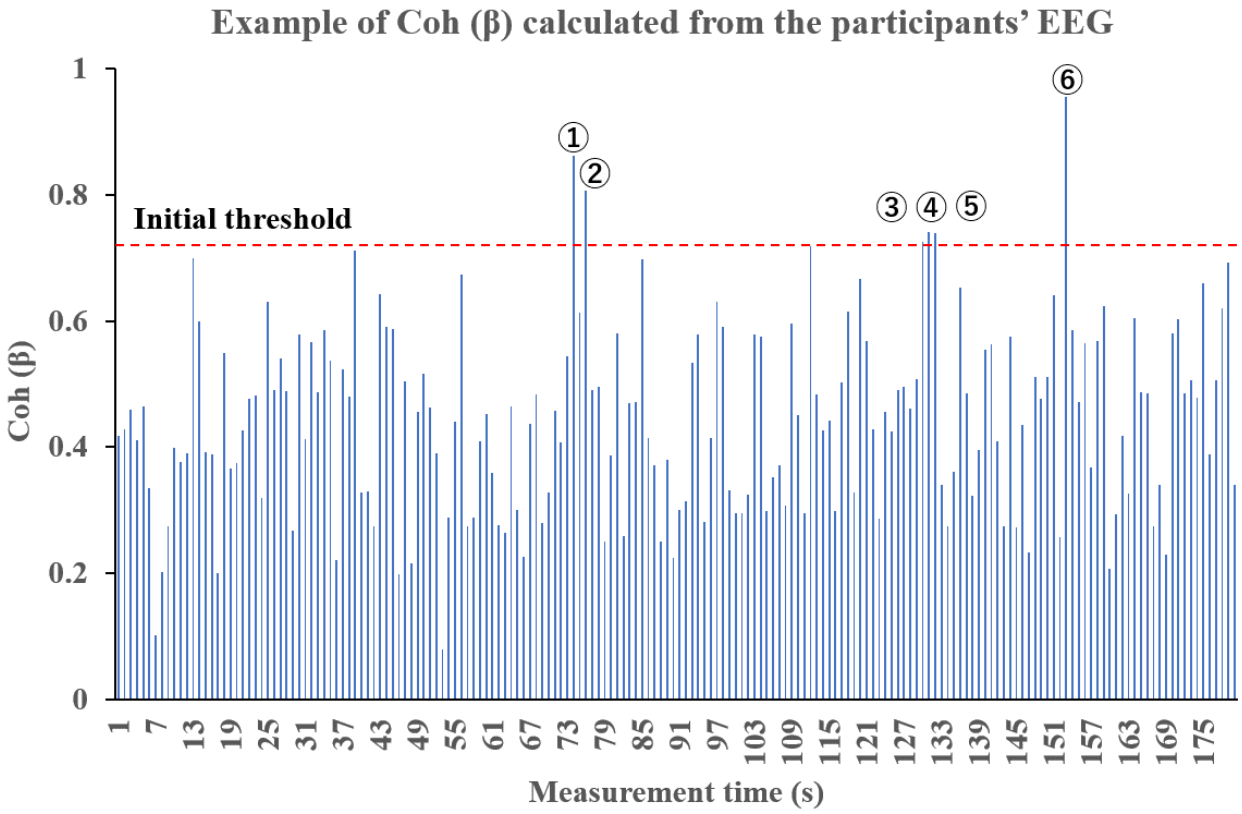

Figure 4. Flowchart of one section of coherence analysis in the TMS trigger system. EEG: electroencephalogram; TMS: transcranial magnetic stimulation.

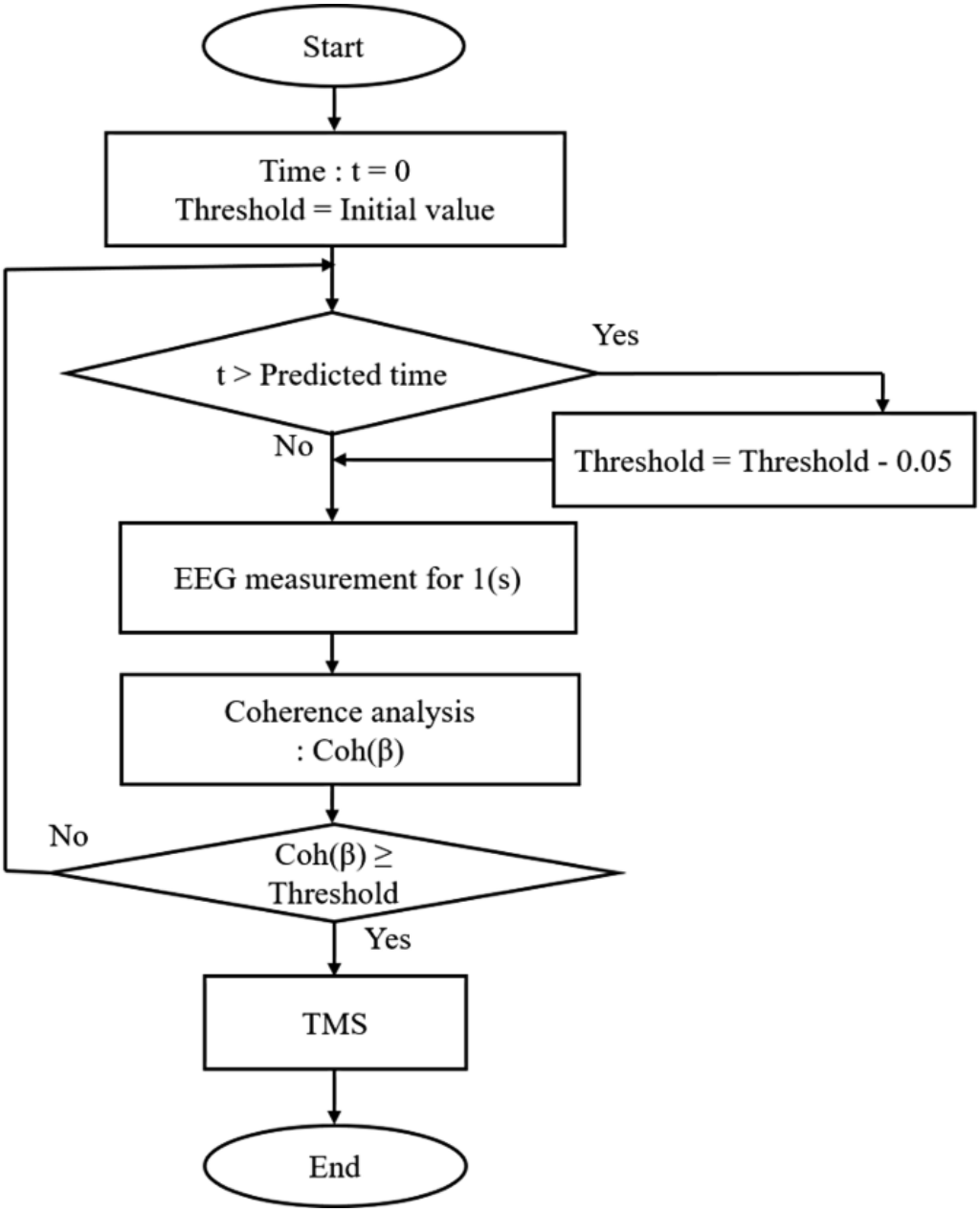

Experimental Evaluation of the TMS Trigger System

We performed an experimental evaluation of the TMS triggering system to suppress MEP fluctuation and TMS trigger timing. The participants for the experiment included 7 healthy adults (6 males and 1 female; mean age 26 years, SD 8.2 years). None of the participants had a history of physical neuropathy or epilepsy. Prior to the experiments, written informed consent based on the Declaration of Helsinki was obtained from all participants for publication. All procedures used in this study were approved by the ethics committee of the Maebashi Institute of Technology.

The participants were asked to gaze at a single point with their eyes open while at rest, TMS over the left M1 was applied, and MEP caused by TMS was measured from the first dorsal interosseous muscle of the right index finger. We applied TMS 10 times in total, and the stimulation intensity was 150% of the resting motor threshold. The trigger condition was set as Coh (β) ≥ threshold, and the MEP was derived using the TMS trigger system. As the control task, TMS was applied at random intervals between 25 and 35 seconds to stimulate M1 and derive MEP without using the TMS trigger system.

To confirm whether the TMS system was effective, the mean amplitude and coefficient of variation of the MEP were recorded and compared with the values in the control task. We also determined the experimental time under each condition and verified whether it was within the predicted time.

Results

Table 1 summarizes the initial trigger thresholds for all 7 participants in the stimulus trigger condition of Coh (β) ≥ threshold. These threshold values were obtained from the EEG data from 180 seconds of testing. In this experiment, we determined the threshold for TMS output in 30 seconds.

Table 1. Summary of initial thresholds of Coh (β) for all participants.

Participant	Sex (M/F)	Age (years)	Coh (β)[a]
Participant 1	M	24	.660
Participant 2	M	25	.770
Participant 3	M	46	.530
Participant 4	F	22	.570
Participant 5	M	22	.695
Participant 6	M	22	.671
Participant 7	M	22	.670

[a]Coh (β): the area of the coherence function between 14 Hz and 30 Hz, defined as the average value of coherence in the β frequency band.

Figure 5 shows the average MEP amplitude measured under trigger conditions and controls for each participant. The vertical axis indicates the average MEP amplitudes in 10 trials, and the error bars represent the SD. As evident in Figure 5, no remarkable changes in the MEPs were observed. Table 2 shows the coefficient of variation (CV) of the MEP amplitude. An *F* test was performed to examine the significant differences. When the trigger condition of Coh (β) ≥ threshold was fulfilled, the CV decreased in 5 out of 7 participants, and a significant difference of 5% was confirmed in 2 of the participants.

Figure 5. The mean of MEP amplitudes. MEP: motor-evoked potential.

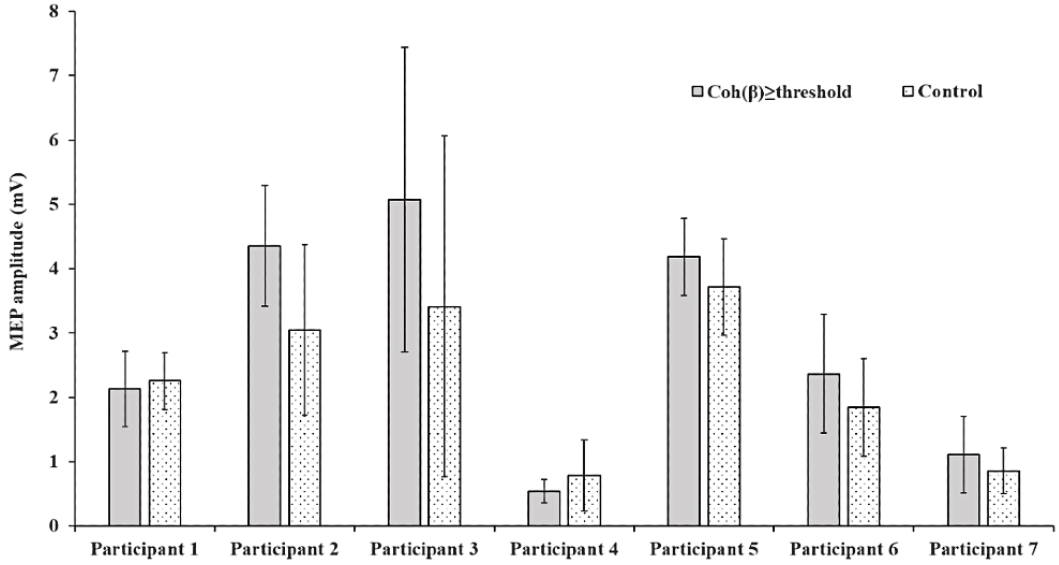

Table 2. Comparison of the coefficients of variation of motor-evoked potential amplitudes (*F* test).

Coefficient of variation value	Participant						
	1	2	3	4	5	6	7
Coh (β)[a] ≥ threshold	0.276	0.215[b]	0.467	0.343[b]	0.143	0.390	0.534
Control	0.196	0.436[b]	0.777	0.699[b]	0.202	0.410	0.419

[a]Coh (β): the area of the coherence function between 14 Hz and 30 Hz, defined as the average value of coherence in the β frequency band.

[b]A significant difference (*P*=.02) was confirmed in this participant.

Table 3 shows the recorded experimental times. It was confirmed that the actual time without threshold modification was longer than the predicted time in 4 out of 7 participants, but the actual time with threshold modification was longer than the predicted time in 1 out of 7 participants.

Table 4 shows the mean, SD, and CV of the experimental time required for each stimulus in all participants. It was confirmed that the CV of the experimental time required for each stimulus with threshold modification was less than that without threshold modification. An *F* test was performed to determine the significant difference, and a significant difference of 1% was observed.

Table 5 shows the transition of Coh (β) at the time of stimulation. The mean value of Coh (β) for the 10 stimuli is shown at the bottom.

Table 3. Comparison of predicted time and actual elapsed time.

Time	Participant						
	1	2	3	4	5	6	7
Predicted time (seconds)	311	310	312	311	311	312	315
Actual time (seconds)							
Without threshold modification	344[a]	141	174	739[a]	356[a]	453[a]	245
With threshold modification	251	215	216	223	159	147	354[b]

[a]The actual time without threshold modification was longer than the predicted time.

[b]The actual time with threshold modification was longer than the predicted time.

Table 4. Mean, SD, and CV[a] of experimental time required for each stimulus in all participants (*F* test).

Value	Without threshold modification	With threshold modification
Mean (seconds)	35.0	22.4
SD (seconds)	41.1	13.8
CV	1.17[b]	0.616[b]

[a]CV: coefficient of variation.

[b]A significant difference ($P<.001$) was confirmed.

Table 5. Transition of Coh (β)[a] at the time of stimulation. The initial triggering threshold, the transition of Coh (β) in 10 stimuli, and the average of Coh (β) are shown for each participant.

Value	Participant (Coh [β])						
	1	2	3	4	5	6	7
Initial triggering threshold	≥.660	≥.770	≥.530	≥.570	≥.695	≥.671	≥.670
1st time	.698	.856	.624	.635	.720	.672	.672
2nd time	*.557*[b]	.777	.632	*.388*	.937	.676	*.341*
3rd time	*.363*	.792	.569	.580	*.612*	*.748*[c]	*.557*
4th time	.718	.786	*.627*[c]	.950	.754	*.724*[c]	*.271*
5th time	.700	*.828*[c]	.551	.600	.962	.762	*.606*
6th time	.661	.781	.571	*.416*	*.657*	.696	*.403*
7th time	.664	.826	.545	*.445*	.719	.702	*.359*
8th time	.684	*.744*	*.620*	.669	.746	.671	*.633*
9th time	*.435*	.817	.559	.648	.955	.685	*.475*
10th time	*.607*	*.579*	*.430*	.684	*.442*	.672	*.322*
Mean	.609	.773	.560	.601	.750	.692	.464

[a]Coh (β): the area of the coherence function between 14 Hz and 30 Hz, defined as the average value of coherence in the β frequency band.

[b]Italics indicate cases where the initial triggering threshold was modified to be set lower.

[c]Coh (β) at the time of stimulation satisfied the initial triggering threshold even when the threshold was modified to be set lower.

Discussion

Principal Findings

The number of cases where the initial triggering threshold was modified to be set lower were 3 or fewer in 10 stimulus incidences in all participants except for participants 1 and 7 (Table 2). We further found that the CV decreased in all participants except for participants 1 and 7 (Table 2). These results indicate that the fluctuation of MEP amplitude decreased when the modification of the initial triggering threshold of TMS did not occur frequently. In addition, the mean values of Coh (β) from all participants except for participants 1 and 7 (Table 5) exceeded the initial triggering threshold. This means that the proposed system worked effectively, and the initial triggering threshold was appropriate in these cases. Although the initial triggering threshold was modified in participants 2, 3, and 6 (Table 5), the Coh (β) at the time of stimulation eventually

exceeded the initial triggering threshold. Thus, it is probable that the change in EEG was transient.

The triggering threshold was modified 4 and 9 times out of the 10 stimuli in participants 1 and 7 (Table 5), respectively. Because the number of modifications in participants 1 and 7 was larger than that of the others, the actual time with threshold modification for these participants was longer than that of the others. In participant 7, it was confirmed that the actual time was longer than the predicted time. The MEP fluctuations in these 2 participants were not suppressed because the mean values of Coh (β) at the stimulation in participants 1 and 7 were smaller than the initial thresholds. This fact paradoxically suggests that MEP fluctuations are suppressed when Coh (β) is high. In participant 7, the system modified the initial threshold in 9 of the 10 stimulus incidences, so it is probable that the participant was in an unsteady state at the time of the experiment.

Comparison With Previous Studies

Ogata et al [12] suggested that M1 excitability can be predicted by EEG oscillations before TMS. The MEP amplitude increased when the α band's power was high, and the power of the β band did not affect the MEP amplitude. In addition, several studies have shown that β oscillations are inhibited when MEP amplitudes increase [12-16]. Generally, the α wave decreases and the β wave increases when the participants do not close their eyes. Considering that the coherence analysis used in this study quantified the similarity of EEG power and the MEP from participants who did not close their eyes, it is probable that the MEP fluctuation was suppressed because the β band's power level was high.

Interpretation of the Findings

It is suggested that the system we developed could suppress the fluctuation of MEP amplitude under the steady state and could also reduce the variation in the experimental time required for each stimulus, as shown in Table 4. We concluded that avoiding an unexpected extension of the experimental time can stabilize the participant's condition and contribute to improving the accuracy of the experimental data.

Strengths and Limitations

The system developed in this study had several limitations. It was difficult to determine the steady state of the participant and the timing at which the MEP amplitude could be efficiently suppressed. Owing to the specifications of the TMS device, we set the initial triggering threshold at the time when it appeared, approximately once every 30 seconds. There is no guarantee that this initial value is determined while the participant is in the steady state. If the initial value is determined while the participant is in the unsteady state, the MEP amplitude may not be adequately suppressed. If the triggering threshold is higher, the MEP amplitude may be suppressed more, but considering the burden on the participant and the accuracy of the experimental data, we prefer to shorten the experimental time. Therefore, we developed a system that modifies the triggering threshold. In this system, if the initial triggering threshold is not satisfied, it is lowered to avoid an extended experimental time. However, if the participant remains in an unsteady state, the triggering threshold may remain low, and eventually, the MEP amplitude may not be suppressed. Therefore, it is difficult to determine how high the initial triggering threshold, Coh (β), should be, and further verification is required.

No other studies that suppressed MEP amplitude fluctuations using EEG coherence analysis exist besides this study. The EEG rhythm comprehensively reflects the biological response to external and physiological factors [17-19]. This system has the advantage that the state of the brain can be stabilized by monitoring the EEG similarity between the left and right hemispheres when TMS is delivered to the M1. In addition, this system enables control of the actual experimental time as well as the suppression of MEP amplitude fluctuations. We are certain that this is an essential element for practical clinical use.

Future Perspectives

In clinical practice, MEP is measured to avoid nerve damage during neurosurgery and orthopedic surgery [20]. Even under similar conditions, the MEP amplitude often fluctuates, and it is difficult to identify the cause immediately [4,5]. If the fluctuation of MEP amplitude that is unrelated to the surgical operation can be suppressed, the incidence of false positives can be reduced, which can contribute to patient safety. During the operation, both rapid procedures and the suppression of MEP amplitude fluctuation are required to avoid placing a burden on the patient.

The current system can only set the triggering threshold lower when the actual time is longer than the predicted time. If the system can set the triggering threshold higher or lower in response to changes in the participant's condition, the actual experimental time will be closer to the predicted time and MEP fluctuation will be significantly suppressed. In addition, if the system can be improved in future studies and determine whether a participant is in a steady state online while measuring the MEP, the triggering threshold can be changed more responsively, and the fluctuation of MEP amplitude that causes false positives can be suppressed. It can also help avoid perioperative complications. Thus, we will continue to improve our system to contribute to clinical applications.

Conclusions

We developed a TMS trigger system to suppress MEP fluctuations using feedback-type EEG coherence analysis. We suggest that the fluctuations in MEP amplitude could be suppressed by applying TMS to the M1 when Coh (β) is high while controlling the experimental time.

Conflicts of Interest

None declared.

References

1. Barker A, Jalinous R, Freeston I. Non-invasive magnetic stimulation of human motor cortex. Lancet 1985 May 11;1(8437):1106-1107. [doi: 10.1016/s0140-6736(85)92413-4] [Medline: 2860322]
2. Nakagawa M, Sasaki R, Tsuiki S, Miyaguchi S, Kojima S, Saito K, et al. Effects of passive finger movement on cortical excitability. Front Hum Neurosci 2017;11:216 [FREE Full text] [doi: 10.3389/fnhum.2017.00216] [Medline: 28515687]
3. Malcolm MP, Triggs WJ, Light KE, Shechtman O, Khandekar G, Gonzalez Rothi LJ. Reliability of motor cortex transcranial magnetic stimulation in four muscle representations. Clin Neurophysiol 2006 May;117(5):1037-1046. [doi: 10.1016/j.clinph.2006.02.005] [Medline: 16564206]
4. Yamashita A, Ishida K, Matsumoto M. Circumstances and problems of motor evoked potential monitoring during descending thoracic and thoracoabdominal aortic surgery. J.J.S.C.A 2014;34(7):868-874. [doi: 10.2199/jjsca.34.868]
5. Takatani T, Shigematsu H, Motoyama Y, Nakase H, Kawaguchi M. The usefulness of intraoperative check-lists and safety management for intraoperative neuro-monitoring. Japanese Journal of Clinical Neurophysiology (in Japanese) 2019;47(3):131-138.
6. Kiers L, Cros D, Chiappa K, Fang J. Variability of motor potentials evoked by transcranial magnetic stimulation. Electroencephalogr Clin Neurophysiol 1993 Dec;89(6):415-423. [doi: 10.1016/0168-5597(93)90115-6] [Medline: 7507428]
7. Ellaway P, Davey N, Maskill D, Rawlinson S, Lewis H, Anissimova N. Variability in the amplitude of skeletal muscle responses to magnetic stimulation of the motor cortex in man. Electroencephalogr Clin Neurophysiol 1998 Apr;109(2):104-113. [doi: 10.1016/s0924-980x(98)00007-1] [Medline: 9741800]
8. Wiethoff S, Hamada M, Rothwell JC. Variability in response to transcranial direct current stimulation of the motor cortex. Brain Stimul 2014;7(3):468-475. [doi: 10.1016/j.brs.2014.02.003] [Medline: 24630848]
9. Truccolo WA, Ding M, Knuth KH, Nakamura R, Bressler SL. Trial-to-trial variability of cortical evoked responses: implications for the analysis of functional connectivity. Clin Neurophysiol 2002 Feb;113(2):206-226. [doi: 10.1016/s1388-2457(01)00739-8] [Medline: 11856626]
10. Mitchell W, Baker M, Baker S. Muscle responses to transcranial stimulation in man depend on background oscillatory activity. J Physiol 2007 Sep 01;583(Pt 2):567-579 [FREE Full text] [doi: 10.1113/jphysiol.2007.134031] [Medline: 17627997]
11. Mizuno K, Abe T, Ushiba J, Kawakami M, Ohwa T, Hagimura K, et al. Evaluating the effectiveness and safety of the electroencephalogram-based brain-machine interface rehabilitation system for patients with severe hemiparetic stroke: protocol for a randomized controlled trial (BEST-BRAIN Trial). JMIR Res Protoc 2018 Dec 06;7(12):e12339 [FREE Full text] [doi: 10.2196/12339] [Medline: 30522993]
12. Ogata K, Nakazono H, Uehara T, Tobimatsu S. Prestimulus cortical EEG oscillations can predict the excitability of the primary motor cortex. Brain Stimul 2019;12(6):1508-1516. [doi: 10.1016/j.brs.2019.06.013] [Medline: 31235367]
13. Zarkowski P, Shin C, Dang T, Russo J, Avery D. EEG and the variance of motor evoked potential amplitude. Clin EEG Neurosci 2006 Jul;37(3):247-251. [doi: 10.1177/155005940603700316] [Medline: 16929713]
14. Sauseng P, Klimesch W, Gerloff C, Hummel F. Spontaneous locally restricted EEG alpha activity determines cortical excitability in the motor cortex. Neuropsychologia 2009 Jan;47(1):284-288. [doi: 10.1016/j.neuropsychologia.2008.07.021] [Medline: 18722393]
15. Mäki H, Ilmoniemi RJ. EEG oscillations and magnetically evoked motor potentials reflect motor system excitability in overlapping neuronal populations. Clin Neurophysiol 2010 Apr;121(4):492-501. [doi: 10.1016/j.clinph.2009.11.078] [Medline: 20093074]
16. Khademi F, Royter V, Gharabaghi A. Distinct beta-band oscillatory circuits underlie corticospinal gain modulation. Cereb Cortex 2018 Apr 01;28(4):1502-1515 [FREE Full text] [doi: 10.1093/cercor/bhy016] [Medline: 29415124]
17. Tobimatsu S. Mechanism of EEG rhythm expression. Japanese Journal of Clinical Neurophysiology. (in Japanese) 2014;42(6):358-364. [doi: 10.11422/jscn.42.358]
18. Steriade M. Corticothalamic resonance, states of vigilance and mentation. Neuroscience 2000;101(2):243-276. [doi: 10.1016/s0306-4522(00)00353-5] [Medline: 11074149]
19. Hobson JA, Pace-Schott EF. The cognitive neuroscience of sleep: neuronal systems, consciousness and learning. Nat Rev Neurosci 2002 Sep;3(9):679-693. [doi: 10.1038/nrn915] [Medline: 12209117]
20. Watanabe K, Watanabe T, Takahashi A, Saito N, Hirato M, Sasaki T. Transcranial electrical stimulation through screw electrodes for intraoperative monitoring of motor evoked potentials. Technical note. J Neurosurg 2004 Jan;100(1):155-160. [doi: 10.3171/jns.2004.100.1.0155] [Medline: 14743930]

Abbreviations

CV: coefficient of variation
EEG: electroencephalogram
EMG: electromyogram
MEP: motor-evoked potential
M1: primary motor cortex
TMS: transcranial magnetic stimulation

Edited by G Eysenbach; submitted 18.03.21; peer-reviewed by L Holanda; comments to author 09.04.21; revised version received 21.04.21; accepted 27.04.21; published 07.06.21.

Please cite as:
Sasaki K, Fujishige Y, Kikuchi Y, Odagaki M
A Transcranial Magnetic Stimulation Trigger System for Suppressing Motor-Evoked Potential Fluctuation Using Electroencephalogram Coherence Analysis: Algorithm Development and Validation Study
JMIR Biomed Eng 2021;6(2):e28902
URL: https://biomedeng.jmir.org/2021/2/e28902
doi:10.2196/28902
PMID:

Viewpoint

Wearable Bioimpedance Monitoring: Viewpoint for Application in Chronic Conditions

Willemijn Groenendaal[1], PhD; Seulki Lee[1], PhD; Chris van Hoof[2,3,4], PhD

[1]Imec the Netherlands / Holst Centre, Eindhoven, Netherlands

[2]Imec, Leuven, Belgium

[3]One Planet Research Center, Wageningen, Netherlands

[4]Department of Engineering Science, KU Leuven, Leuven, Belgium

Corresponding Author:
Willemijn Groenendaal, PhD
Imec the Netherlands / Holst Centre
High Tech Campus 31
Eindhoven, 5656AE
Netherlands
Phone: 31 404020400
Email: willemijn.groenendaal@imec.nl

Abstract

Currently, nearly 6 in 10 US adults are suffering from at least one chronic condition. Wearable technology could help in controlling the health care costs by remote monitoring and early detection of disease worsening. However, in recent years, there have been disappointments in wearable technology with respect to reliability, lack of feedback, or lack of user comfort. One of the promising sensor techniques for wearable monitoring of chronic disease is bioimpedance, which is a noninvasive, versatile sensing method that can be applied in different ways to extract a wide range of health care parameters. Due to the changes in impedance caused by either breathing or blood flow, time-varying signals such as respiration and cardiac output can be obtained with bioimpedance. A second application area is related to body composition and fluid status (eg, pulmonary congestion monitoring in patients with heart failure). Finally, bioimpedance can be used for continuous and real-time imaging (eg, during mechanical ventilation). In this viewpoint, we evaluate the use of wearable bioimpedance monitoring for application in chronic conditions, focusing on the current status, recent improvements, and challenges that still need to be tackled.

(JMIR Biomed Eng 2021;6(2):e22911) doi:10.2196/22911

KEYWORDS

wearable monitoring; bioimpedance; impedance pneumography; impedance cardiography; body composition; imaging

Introduction

Chronic diseases are currently a major challenge for the global health system [1]. Worldwide, over 70% of deaths are attributed to noncommunicable diseases (NCDs) and mental health. In addition, NCDs are a leading cause of morbidity and disability, including cardiovascular disease, chronic respiratory diseases, cancer, and diabetes [2]. Specifically in the United States, approximately half of the overall population is suffering from one or more chronic diseases [3]; 6 in 10 adults have at least one chronic disease and 4 in 10 adults are suffering from two or more chronic diseases [4]. This not only poses a huge burden on the health care system but is also an economic burden, as chronic diseases account for 86% of the total health care costs in the United States [5].

Some of the main aspects attributing to these high health care costs are the emergency room visits and hospitalizations resulting from acute exacerbations in chronic diseases [6]. At present, these diseases are typically managed based on a few office visits per year [7]. Several studies have shown that more frequent monitoring could lead to early detection of exacerbations such as in heart failure [8] and in asthma [6]. This indicates that continuous or frequent monitoring could also play a role in the management of the large number of patients suffering from chronic diseases [9].

Wearable sensor technology, possibly combined with artificial intelligence (AI), is one of the techniques that provides this type of monitoring. Consequently, the wearable technology market has increased rapidly in recent years. Different wearables have been developed, ranging from simple medical alarms (St John) that people can press when needing help to vital sign patches

for monitoring electrocardiogram (ECG) signals (ePatch BioTelemetry Inc and Vista Solution VitalConnect) and cuff-based blood pressure measurements in a watch (HeartGuide Omron Healthcare Inc). At the same time, different AI methods have been developed and applied to physiological data, ranging from supervised techniques for automatic detection of sleep apnea from the ECG [10] to unsupervised heart rate detection with liquid states [11].

A promising sensing method is wearable bioimpedance monitoring. In this paper, we define a wearable bioimpedance monitoring system as an electronic device containing a bioimpedance sensor capturing the bioimpedance of the wearer that is worn close to or on the surface of the skin, and that allows the wearer to move freely during daily living conditions (ie, that is not attached to any main power supply or desktop device). Bioimpedance is a versatile sensing technology that can be used for a wide array of clinical and lifestyle applications, ranging from body fluid monitoring [12] to gesture monitoring [13] and to monitoring of hemodynamic parameters [14]. In addition, bioimpedance is a noninvasive technology and is of relatively low cost. Specifically, in chronic disease management, bioimpedance has, for example, been explored to monitor patients with asthma [15], heart failure [8], and end-stage kidney disease (ESKD) [16]. Table 1 lists some of the commercially available devices and their application areas as of November 2020. There are still several challenges for the full integration of wearable bioimpedance monitoring into the clinical health care system. Some of these challenges are specific to bioimpedance; however, many are general to wearable monitoring. These challenges include data reliability [17,18], patient usage and compliance [19,20], integration into electrical health records [21,22], actionable insights provided to the user, and the still limited number of clinical trials demonstrating a medical benefit [23]. Here, we discuss the versatile application areas for wearable bioimpedance monitoring, along with the current status, remaining challenges, and future outlook.

Table 1. Wearable bioimpedance devices currently available on the market.

Product	Company	Technology	Application	Market
Auraband	Aura devices, Wilmington DE, USA	Wrist band, hand-to-hand BIVA[a]	Body composition	Consumer
Inbodyband	Inbody, Seoul, Korea	Wrist band, hand-to-hand BIA[b]	Body composition	Consumer
CoVa Monitoring system	ToSense (acquired by Baxter International)	Necklace, thoracic bioimpedance	Heart failure	Medical
Shimmer3 Ebio unit	Shimmer, Dublin, Ireland	Module attached with chest strap, thoracic bioimpedance	Respiration	Research
BX100	Koninklijke Philips N.V., Amsterdam, the Netherlands	Patch, thoracic bioimpedance	Respiration	Medical
µCor3	ZOLL Medical Corporation, Chelmsford, MA, USA	Patch, thoracic RF[c] impedance 0.5-2.5 GHz	Heart failure	Medical
Physioflow	Manatec Biomedical, Poissy, France	Chest module, thoracic bioimpedance	ICG[d]	Medical

[a]BIVA: bioelectrical impedance vector analysis.

[b]BIA: bioelectrical impedance analysis.

[c]RF: radiofrequency.

[d]ICG: impedance cardiography.

Basic Principle of Bioimpedance

Overview

Our aim is to address the clinical application areas for wearable bioimpedance. The aim is not to discuss the technology in full detail; a comprehensive description on bioimpedance is provided elsewhere [24,25]. However, to understand the opportunities and challenges for clinical applications, some background on the technology is needed. Therefore, we first provide a brief overview of the principles of bioimpedance measurements.

Bioimpedance is a method to assess the electrical properties of a tissue. Different tissues such as the bone and fat have different electric properties. In 1996, more than a century after the initial work on electrical properties of biological tissues in 1872 [26], Gabriel et al [27] reported the measurement of dielectric properties of different biological tissues over a large frequency range (10-20 GHz). These experiments and observations formed the basis of subsequent bioimpedance research in various applications.

Bioimpedance reflects the extent to which the living tissue impedes the flow of electrical current. The electrical properties of biological tissue are determined by the characteristics of the extracellular fluid (ECF), cell membranes, and intracellular fluid (ICF). To study the electrical properties, an alternating current with a single frequency measurement or range of frequencies is injected into the tissue and the opposition of the tissue to this current flow (ie, the bioimpedance) is measured.

Bioimpedance measurements at any frequency are expressed as a complex number, with the real part referred to as the resistance and the imaginary part referred to as the reactance. The resistance is regarded as a measure of the obstruction to an electrical current, whereas the reactance is related to the storage

of the electrical current. The resistance is attributed to the fluids in the tissues (including the therein dissolved ions) and the capacitance is attributed to the cell membrane. Since the resistance of the cell membrane is very small, it is often neglected (see electrical scheme in Figure 1B). At low frequencies of the injected current, the current does not penetrate the cells, but mainly flows through the ECF; thus, bioimpedance measurements at low frequency can be used to gain insight into the ECF. However, when using high frequencies for the injected current, the current flows through the cells, and thus the measurements provide insights into both the cellular and the extracellular components (Figure 1A).

Figure 1. (A) Low-frequency current travels around the cell, while high frequency current can penetrate cells. (B) Electrical model of the tissue with extracellular resistance (Re), intracellular resistance (Ri), and conductance representing the cell membrane (Cm). (C) Illustration of bioimpedance spectroscopy data visualized in the R-Xc plane. Increasing frequencies of the injected alternating current appear counterclockwise in the plot. (D) Tetrapolar electrode configuration in bioimpedance measurement. ECF: extracellular fluid; ETI: electrode tissue impedance; ICF: intracellular fluid; Iinject: injected current; Vmeasred: measured voltage.

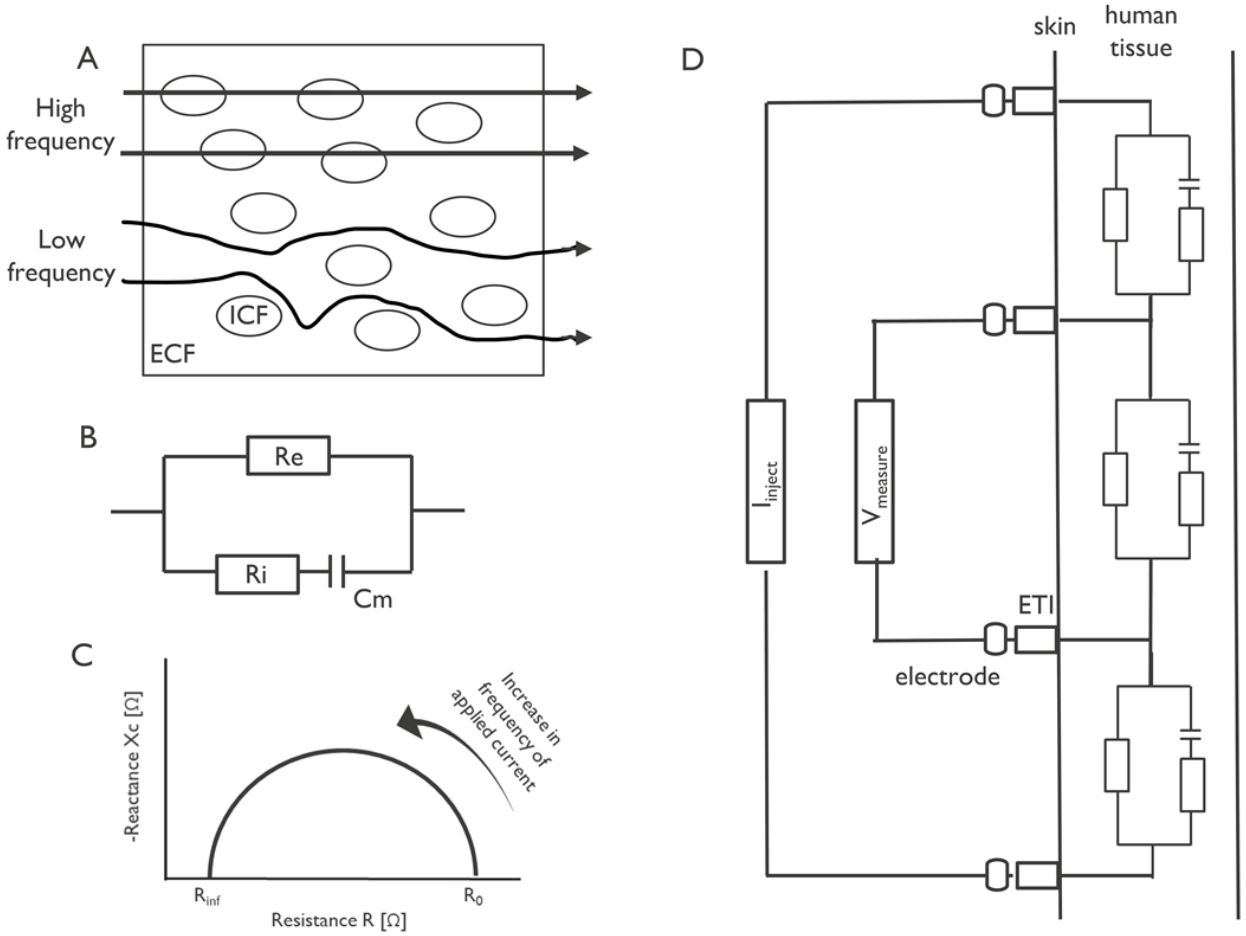

The resistance and reactance can be used to calculate the phase angle and the magnitude. The phase angle is calculated by the arc tangent of the ratio of reactance and resistance at a certain frequency. The phase angle is therefore considered to be a useful metric for cellular health, and is expected to be an indicator of the cellular integrity, cell mass, and extracellular versus intracellular water content. The magnitude is calculated as the square root of the sum of the two vectors.

In general, bioimpedance has been applied to three types of problems: (1) dynamic monitoring, applied mainly in the chest to monitor respiration and hemodynamic parameters; (2) slowly evolving parameters such as body composition monitoring; and (3) electrical impedance tomography (EIT) or imaging. To address these application areas, different types of bioimpedance measurements have been developed. There are several measurement methods with various numbers of electrodes, namely 2, 3, and 4. Here, we only describe the tetrapolar configuration with 4 electrodes since this minimizes the effect of electrode tissue impedance (ETI), which is undesired in real-life bioimpedance measurements. Measurements using a tetrapolar electrode configuration and a single frequency of the injected current are applied to assess either dynamic changes in vital parameters or body composition. The latter measurements are referred to as single-frequency bioimpedance analysis (SF-BIA). A second approach to assess body composition is through multifrequency bioimpedance measurements, either through multifrequency bioimpedance analysis (MF-BIA) or bioimpedance spectroscopy (BIS) [26,28]. Finally, EIT measurements are performed using either single or multiple frequencies of the injected current and an array of at least 8 electrodes.

Single-Frequency Measurements for Dynamic Monitoring

To obtain the bioimpedance of a tissue, an alternating current is applied to the tissue. Electrodes are placed on the surface of the skin to ensure electrical contact with the tissue. As mentioned above, a tetrapolar electrode configuration is often used to circumvent the effect of ETI. In such a configuration, two electrodes are dedicated for the current injection and the other two are used for obtaining the voltage measurement (Figure 1D). The configuration, or positioning, of the electrodes together with the electrical properties of the underlying tissue will determine the current path of the injected current through the body. For example, current injected through electrodes positioned on the thorax will flow through part of the thorax underlying these electrodes. Therefore, electrode positioning is an important step in the design of the bioimpedance measurement.

Longitudinal thoracic bioimpedance measurements can be performed to assess respiration or hemodynamic parameters. The measured thoracic bioimpedance signal contains a baseline component and a dynamic component. The baseline component is a constant bioimpedance value that is determined by the tissues (eg, the adipose tissue) and does not change during the measurement over several minutes. The dynamic component is related to dynamic changes in the tissue during the measurement (Figure 2). During a measurement of several minutes, a subject breathes and the heart pumps blood through the thorax. Airflow moving in and out of the body and pulsatile blood flow modulate the electrical properties and thus the measured bioimpedance signal. The electrode configuration, by affecting the measured tissue volume, and the frequency of the injected current, by affecting the current path, both influence the baseline and dynamic components of the measurements.

Figure 2. (A) Illustration of body composition consisting of solids (eg, bone, dry cell mass) and fluids. The fluids consist of intracellular fluid (ICF) and extracellular fluid (ECF), with the latter comprising interstitial fluid (ISF) and plasma. (B) Electrode configuration example of respiration monitoring with the measured bioimpedance (bioZ) signal. (C) The measured bioZ signal contains a dynamic component (AC) resulting from physiological changes such as breathing and a baseline component (DC) resulting from tissues (eg, bones, fat and/or muscle).

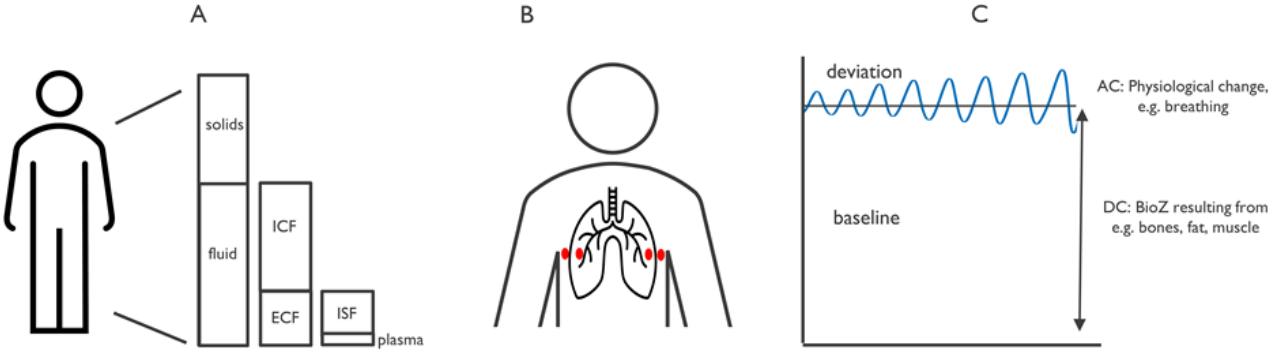

Body Composition Monitoring

The previous section described monitoring of dynamic changes, or the dynamic component of the signal, whereas body composition monitoring is related to the baseline component of the measurement. Body composition parameters obtained through bioimpedance measurements include fat percentage and total body water (TBW) content or the hydration status. TBW is the sum of the extracellular water (ECW) and intracellular water (ICW) content. Reference methods for estimating TBW, ECW, and ICW, such as dilution of radioactive deuterium, bromide, and radioactive potassium, are invasive and expensive. These methods also must be applied under clinical supervision and are not suitable for frequent or ambulatory monitoring.

The simplest method for bioimpedance body composition monitoring is SF-BIA, which is used to estimate TBW, ECW, ICW, and fat free mass (FFM) using statistical analysis. The frequency of the current is set to 50 kHz. SF-BIA is applicable for normal hydrated subjects [29], which uses the inversely proportional relationship between assessed bioimpedance and TBW. SF-BIA first predicts the TBW and FFM using two statistically derived equations [29], and then estimates the ECW and ICW to be 75% and 25% of the TBW, respectively. To improve the body composition estimation, bioimpedance vector analysis (BIVA) was introduced, which also uses single-frequency bioimpedance measurement, mainly at 50 kHz, but the data are normalized to the length of the subject. BIVA provides information about changes in both tissue hydration and soft-tissue mass. However, similar to SF-BIA, BIVA does not provide any quantitative estimate of tissue mass (in kilograms) or fluid volumes (in liters). Therefore, MF-BIA was developed to exploit the frequency dependence of the different tissues. MF-BIA uses a similar approach to SF-BIA, except that it applies a spectrum of frequencies to the body tissue and performs multivariate statistical analysis to estimate TBW, ECW, ICW, and FFM. In contrast, BIS predicts ECW and TBW by determining the resistance at zero frequency (R_0) and infinity frequency (R_{inf}). BIS provides quantitative results on TBW, as well as on ECW and ICW. Typically, a larger number of different frequencies is used in BIS measurements compared to MF-BIA. The measured response at these frequencies is

displayed in the R-Xc plane (plotting resistance vs reactance), as shown in Figure 1C.

Several empirical electrical models have been developed to analyze these measurements. Over the years, different variations of these empirical models have been presented [30,31]. Although these models can describe the data, they are not a true representation of the underlying physiology. One of the earliest models is the Fricke and Morse model [32], which consists of two resistors, ECF resistance and ICF resistance, and a resistor in parallel with a capacitor, which represents the cell membrane. This model has a direct physical interpretation. The most widely used model is the Cole-Cole model [33]. To account for the nonideal capacitive behavior of cell membranes, an additional parameter (α) was added to this model. Although this improved the accuracy of the fit, the interpretability of the model was reduced. The resistance values at infinitely low R_o and high R_{inf} are easily derived from the analysis and relate to ECF and TBW.

EIT Measurements

EIT originates from the 1970s [34] and is an imaging technique with relatively low resolution when compared with traditional imaging techniques such as magnetic resonance imaging (MRI) or computed tomography (CT). However, EIT has the advantage of low costs, low power, no radiation, a high temporal solution, and the potential to be wearable [35].

EIT estimates the conductivity distribution within a given volume. The measurement exploits the fact that different tissues vary in their electrical properties. To assess the conductivity distribution, EIT uses electrical alternating currents injected from the surface area of the volume. Toward this end, electrodes are placed around the surface of the volume of interest (eg, the thorax). Currently, EIT systems often consist of 8 to 16 electrodes per ring of electrodes. The electrodes used for current injection and voltage measuring are continuously changed in specific patterns. The measured voltages are used in the reconstruction of the image, which is an ill-posed nonlinear inverse problem. Two types of images can be derived from EIT measurements: a difference or an absolute image. Difference images are created by measuring the same volume multiple times and then subtracting and dividing by a reference dataset. The reference dataset can be generated with the same measurement setting, but the data are collected at a different moment in time (time-difference EIT) or with a different frequency of the injected current (frequency-difference EIT). The reconstruction will lead to the difference image, which may be relevant during respiration monitoring. The absolute image shows the absolute properties of the area of interest. Several groups have developed solutions for image reconstruction, including the freely available software EIDORS [36,37]. Initially, image reconstruction was performed in a 2D manner using a single ring of electrodes. Subsequent methods have been developed for 2.5D or 3D reconstruction using multiple rings of electrodes covering a volume [38].

Application Areas of Bioimpedance Monitoring for Chronic Conditions

Applications of Focus

Owing to its versatile nature, wearable bioimpedance can be used for a wide range of clinical and lifestyle applications, which include body composition monitoring, monitoring of hemodynamic parameters, respiratory monitoring, and imaging. Here, we focus on the use of wearable bioimpedance monitoring in chronic diseases. This section is divided in three parts: monitoring dynamic parameters, slowly evolving parameters, and imaging.

Dynamic Parameters in the Chest

Overview

Dynamic changes in thoracic impedance consist of two parts: a respiratory and a hemodynamic or cardiac contribution. Impedance pneumography monitors the changes induced by respiration in the impedance of the thorax, whereas impedance cardiography measures the changes due to the cardiac contribution. In measuring either component, the other is typically regarded as a disturbance of the signal.

Impedance Pneumography

Currently, respiratory status is assessed in clinical practice in patients with chronic obstructive pulmonary disease (COPD), asthma, and sleep apnea. In patients with COPD and asthma, a spirometer is used to assess respiratory function. Spirometer tests require a face mask or mouthpiece and trained medical personnel to perform the test well. These prerequisites make the test obtrusive and unsuitable for ambulatory monitoring. Similarly, sleep apnea is diagnosed in a sleep lab using polysomnography with many cables, requiring a complex set up. For these reasons, less invasive methods are being investigated that can provide continuous and ambulatory monitoring in a comfortable and unobtrusive manner. Impedance pneumography is being studied as one such a technology.

During the impedance pneumography measurement, electrodes are placed on the chest to obtain the thoracic bioimpedance (Figure 3). These electrodes can be attached with lead wires to a device or integrated in a patch. The dynamic component of the measured signal relates to the varying electrical properties in the chest, encompassing breathing. In the measurement, an aggregate signal is measured of the underlying tissue. This volume comprises not only the lungs but also other tissues of the thorax, such as the muscles and the fat. To determine the applicability of the signal, it is necessary to understand the different contributions to, or the origin of, the signal. Some studies have investigated the contributions of the underlying tissue to the measured bioimpedance signal using either animal models or computer simulations [39-43]. Animal studies from the 1960s and 1970s focused on the contributions of chest movement and respiratory volume to the bioimpedance signal [42,43]. Subsequent studies in human subjects showed that during normal breathing, the relation between volume and bioimpedance appeared to be linear [44-48]. However, during abnormal breathing, the relation between volume and

bioimpedance appeared nonlinear, indicating the contribution of additional components to the signal. These contributions can be seen during sleep apnea events monitored with bioimpedance [49]. Recently, Blanco-Almazan et al [50] showed that both respiratory volume and chest movement contribute to the bioimpedance signal during normal breathing and during inspiratory loading conditions, with the contribution of chest movement becoming more important when muscle activity was the highest.

Figure 3. Example of a wearable device (imec the Netherlands, Eindhoven, the Netherlands). (B) Example impedance pneumography data. The figure shows the similarity between bioimpedance and spirometer data for an increasing respiratory volume protocol.

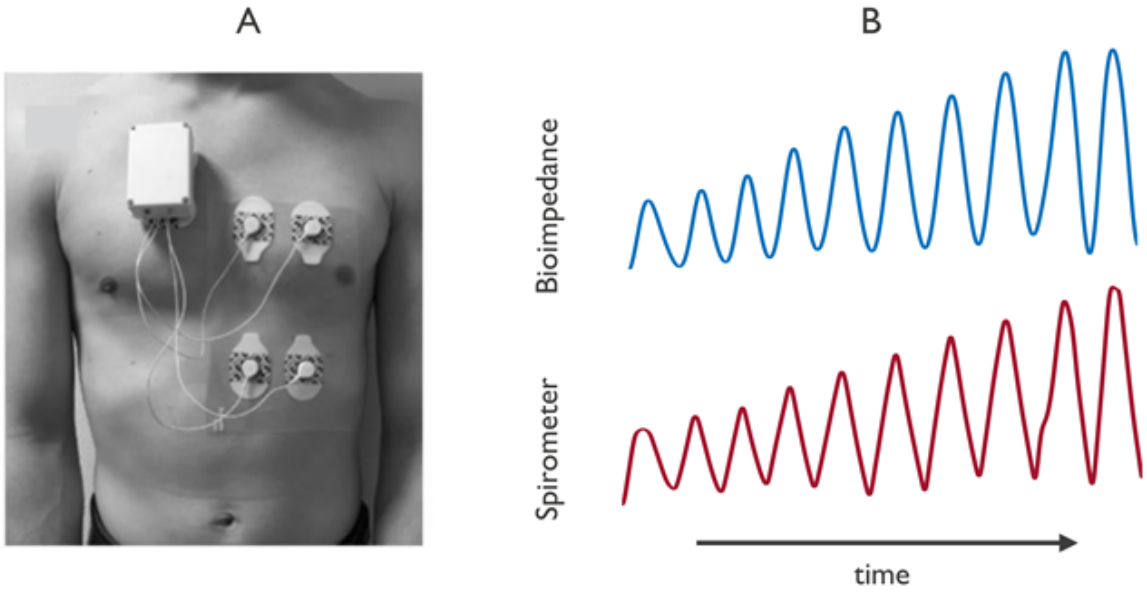

Another topic of research has been the effect of electrode positioning, which has been studied using computational modeling and data collection in volunteers. The electrode positioning influences the volume that is being investigated. Finite element models of (part of) the thorax have been constructed, in which the electrode position was varied to optimize the measurement location for monitoring the lung area [39-41]. Using this approach, positions were compared in terms of sensitivity (percentage contribution of the lung tissue to the measured bioimpedance signal) and specificity (the amplitude of the lung contribution). The simulations showed that the electrode locations around the middle of the thorax reflect impedance changes in the lung region. Data were collected on human volunteers using different electrode configurations and were compared against those obtained using a reference device (eg, a spirometer) [45,46,48,51]. This comparison also showed that the locations around the middle of the thorax were able to accurately capture respiration.

Several studies have assessed the applicability of impedance pneumography for respiration monitoring in chronic conditions. In children, nocturnal impedance pneumography measurements can be used to monitor the increased tidal flow variability as associated with childhood asthma risk [52]. In addition, it was shown that impedance pneumography and direct pneumotachograph measurements had a similar relation with lung function in infants with respiratory symptoms. However, in infants with clinically observed airway obstruction, the measured tidal breathing flow parameters differed between impedance pneumography and direct pneumotachograph [15], which further support that factors other than volume contribute to the bioimpedance measurement.

In adults, impedance pneumography has been applied in patients with COPD and sleep apnea. In patients with COPD, bioimpedance measurements were combined with electromyography and mechanomyography measurements assessing muscle activity [53], showing the applicability of noninvasive multimodal respiratory assessment. Regarding sleep apnea, recent work evaluated a shirt with ECG and bioimpedance for monitoring in healthy volunteers [54]. In addition, in patients with sleep apnea, a wearable bioimpedance device was able to detect apnea events, which opens opportunities for unobtrusive screening, diagnostics, and treatment monitoring in sleep apnea [49]. Finally, in the hospital setting, impedance pneumography is currently available for respiratory monitoring, although typically in a nonwearable form. An example is the ExSpiron Minute Ventilation System (Respiratory Motion Inc), which has been tested in the postanesthesia care unit and the intensive care unit [55,56].

Impedance Cardiography

Cardiac output is related to how much blood the heart delivers to the body, which is measured to assess the status of the heart, relevant in many chronic conditions such as heart failure. Cardiac output can be assessed with several technologies such as Doppler echocardiography and intracardiac catherization. Echocardiography is time-consuming and requires trained medical personnel, whereas catherization is invasive. Impedance cardiography has been proposed as a noninvasive and potentially ambulatory method to assess hemodynamic parameters such as cardiac output. The possibility to measure hemodynamic

parameters noninvasively with impedance has been studied for a long time [14]. In general, 4 electrodes are used for the impedance measurement to assess changes in thoracic bioimpedance related to the cardiac cycle. The ECG signal is collected simultaneously to time the cardiac events. Different electrode configurations have been proposed to measure the impedance cardiography signal. Initially, four band electrodes were used, with two electrodes positioned around the neck and two around the abdomen. These band electrodes were subsequently replaced by round electrodes [57] (see Figure 4). Alternative electrode configurations have been evaluated. For example, one configuration positions one electrode on the forehead, the lowest one above the leading edge of the heart, and the remaining two in between [58]. Desktop devices are typically used for these measurements, but some studies have also investigated wearable devices [59-62].

Figure 4. Left: Electrode configurations for impedance cardiography (ICG) measurement, using either red electrodes or yellow electrodes, with current injection electrodes (I) and voltage electrodes (V). Right: electrocardiogram (ECG) and ICG signals showing characteristic morphology with the B point as an example.

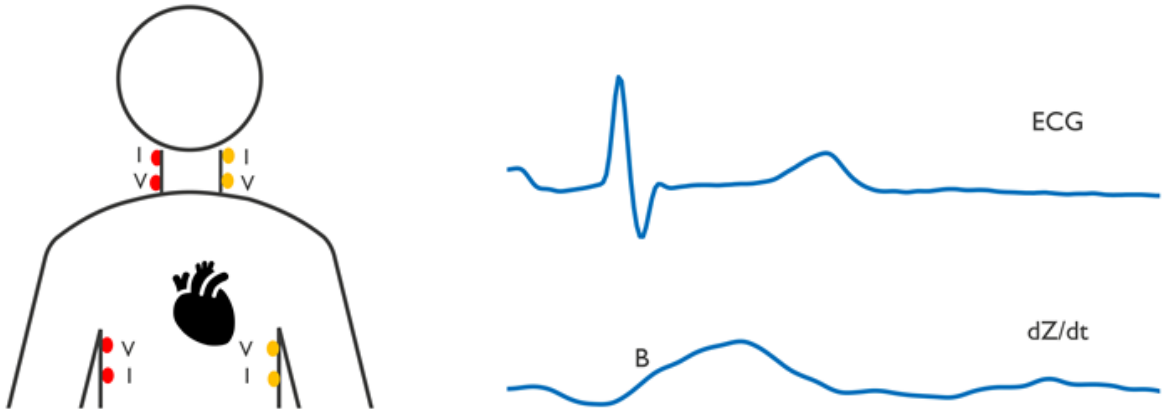

The measured impedance signal (*Z*) varies with the contraction of the heart. In the derivative of the signal (*dZ/dt*), different points have been shown to correspond with different parts of the cardiac cycle, such as the B-point with the opening of the aortic valve. The measured impedance and its derivative are used in formulas for an approximation of stroke volume. The first such model was presented by Kubicek, which was modified in subsequent studies [63]. All models to derive stroke volume use assumptions such as those related to the shape of the thorax (cylinder or truncated cone), current path, blood resistance, and origin of the pulsatile impedance changes. To fully understand the signal and its applicability for clinical monitoring, the origin of the signal needs to first be understood; however, the origin of this signal seems to be complicated and has led to controversy in the field. Recently, de Sitter et al [64] compared different mathematical models that aim to understand the underlying physiological signals that contribute to the change in bioimpedance used in impedance cardiography in a systematic review. This comparison showed no consensus in the origin of the change in the bioimpedance signal, highlighting the complexity and the controversy around this topic.

At the same time, many studies have tried to validate this technique on different clinical use cases. A portion of these studies showed good results in the comparison of impedance cardiography with standard clinical methods such as the invasive thermodilution pulmonary artery catheter [65-67], whereas other studies showed insufficient agreement between the measurements [68-70]. In addition to validation studies, the potential role of impedance cardiography in disease diagnosis and disease management has been evaluated. For disease management, not only absolute values are of interest but also relative changes in stroke volume or cardiac output. For example, in stable heart failure patients, regular impedance cardiography measurements have been shown to have predictive value for near-term recurrent decompensation [71].

Stroke volume and cardiac output monitoring are of substantial interest for many diseases. The use of impedance cardiography to assess these parameters has gained interest because of its advantages of noninvasiveness, relatively low cost, and relative simplicity. However, there is still no consensus on the origin of the signal. In addition, the results for absolute monitoring are inconsistent. Many studies have assessed validation in different use cases and the applicability for different diseases, with mixed results. Therefore, further work is needed to fully understand the signal and its applicability for chronic disease.

Slowly Evolving Parameters

Besides monitoring dynamic parameters, bioimpedance is used for monitoring more slowly evolving parameters such as body composition and fluid status. Measurements related to body composition are reflected by the baseline component of the bioimpedance measurement. These measurements are often performed with benchtop devices measuring total body impedance from the hand to foot, using models (eg, the Cole-Cole model as explained in the Principle of Bioimpedance section above) to convert the impedance values into body composition parameters. In the domain of chronic diseases, these measurements have been used to assess malnutrition or body fluids, such as overhydration, dehydration, or local fluid buildup (eg, pulmonary edema). Early attempts to evaluate pulmonary edema in patients with bioimpedance originate from the 1970s [72]. More recently, wearable bioimpedance has been

used for fluid monitoring such as in patients with congestive heart failure and those with ESKD undergoing hemodialysis treatment [16,73].

Hemodialysis is a life-saving treatment for patients with ESKD. However, in these patients, mortality levels are high and many patients suffer from cardiovascular complications. The nature of hemodialysis treatment (three 4-hour treatments per week) results in large fluid changes in the patient. Fluid builds up during the interdialytic period and is rapidly extracted during the 4-hour hemodialysis treatment. In patients with ESKD, fluid overload in the interdialytic period is associated with a higher cardiovascular risk, disease progression, and a rise in cardiovascular morbidity and overall mortality [74-76]. Maintaining optimal fluid balance in the body of a patient with ESKD is still a challenge. In current clinical practice, treatment is based on the dry weight of a patient, but objective dry weight assessment is currently lacking in clinical routine practice. Bioimpedance monitoring could play a role in maintaining fluid balance in patients with ESKD and has been associated with improvement of cardiovascular parameters [12,77,78] in studies using benchtop devices. Being able to unobtrusively and continuously monitor the fluid status could provide even larger value. Studies have shown that local wearable thoracic bioimpedance measurements can be used to accurately track fluid and weight loss during hemodialysis [16,79], but future work is needed, including exploring the potential for monitoring at home.

At the same time, studies have focused on wearable bioimpedance fluid monitoring in patients with congestive heart failure. In these patients, the pumping capability of the heart is reduced, and fluid can build up in the lungs or the extremities. Bioimpedance monitoring has also been used to assess pulmonary congestion. Several studies have shown the benefit of daily and continuous monitoring in patients with congestive heart failure in the form of portable benchtop devices [80,81], wearables [73,82-84], or even implantables [85,86]. Wearable bioimpedance monitoring predicted decompensation and hospitalizations [8,87]. Moreover, wearable bioimpedance monitoring was shown to be a useful marker for 30-day mortality and rehospitalization after diuretic treatment during hospitalization in patients with congestive heart failure treated with diuretic therapy [84].

Bioimpedance measurements, in combination with empirical models, have also been frequently used to study body composition in terms of muscle mass and body fat content, and are available in clinical settings through devices such as Maltron BodyScan 920-II (Maltron International Ltd) and Fresenius Body Composition Monitor (Fresenius Medical Care Pte Ltd). These measurements have also been used to assess malnutrition [88]. However, since slowly evolving processes underly these applications, they have mainly been studied with benchtop devices.

Imaging Using EIT

Medical imaging enables gaining a view of the inside of the body. There are many imaging modalities currently available, such as MRI, radiography, ultrasound, and functional near-infrared spectroscopy. Some of these modalities use radiation (such as radiography), expensive equipment (such as MRI), or trained personnel. Therefore, some of these techniques only allow for obtaining a snapshot of the status of the patient. Imaging using EIT has the advantage of being continuous, low cost, low power, and with wearable potential, but the spatial resolution of the image of this modality is relatively low in comparison with that of other imaging modalities such as CT and MRI. Currently, the main use of EIT is during mechanical ventilation, which is used to monitor the ventilation of both lungs to protect the patient from lung damage caused by the ventilator. With respect to chronic conditions, the use of EIT in other application areas shows potential but requires more research. In patients with pulmonary conditions such as COPD, EIT could provide the spatial distribution of the pulmonary function to enable tracking regional lung function over time or after an intervention such as respiratory muscle training or the use of a bronchodilator [89]. It was suggested that monitoring spatial differences could improve patient phenotyping, monitoring disease and treatment effects, and predicting clinical outcomes [37,89]. EIT could also bring value to other chronic diseases such as epileptic monitoring and stroke. Being able to continuously monitor brain activity could help in locating the regions of the brain involved in epileptic seizures [90]. Hand gesture recognition could aid in physical disabilities such as those present after stroke [13].

One of the potential benefits of EIT is that it could be wearable. Currently, there are no wearable EIT systems on the market, but several research prototypes have been developed [13,91-94]. These wearable systems have been shown to capture respiration [92,93]. Another system combines EIT with multilead ECG in a vest, thereby opening up the possibility to measure respiration and impedance changes from the cardiac region [91]. In a very different application area, Zhang et al [13] used EIT for hand gesture monitoring.

To date, besides during mechanical ventilation, EIT has mainly been applied in controlled laboratory settings. Before wearable EIT can be applied for the monitoring of chronic conditions, further steps in development and validation need to be taken, such as in handling the imaging during daily living conditions. Finally, the added clinical value needs to be demonstrated for the different application areas before the technology will be widely adopted.

Challenges and Outlook

Hurdles for Broad Application

Electrical principles have long been used in the medical field, and bioimpedance measurements have been explored for many decades. Initially, these measurements were performed with large benchtop devices, but more recently have been assessed in wearable form with consideration of many different applications, ranging from respiratory volume to cardiac output and from body composition monitoring to imaging. The relatively low cost of the system and its noninvasiveness make bioimpedance an interesting sensor technology for wearable monitoring of chronic conditions. However, there are still several hurdles to be overcome before bioimpedance will be widely adopted in clinical practice. Some of these hurdles apply

to wearable bioimpedance, while others do not solely apply to bioimpedance monitoring but should be considered in the broader context of all wearable monitoring techniques. Here, we will discuss both aspects.

Challenges and Limitations of Wearable Bioimpedance

As indicated in the preceding sections, wearable bioimpedance is a promising technique owing to its advantages of low cost, wearability potential, and noninvasiveness. However, like all technologies, wearable bioimpedance has some disadvantages. First, bioimpedance measurements, as is the case for many wearable measurements, are prone to motion artifacts. Collecting data in a real-world environment is prone to activities leading to these artifacts. Corrupted data can lead to misinterpretation of the state of a patient; therefore, solutions to either prevent or remove these artifacts are crucial. To prevent motion artifacts, one might ask the subject to sit still during a measurement to capture slowly evolving parameters, which may be performed once a day for approximately 1 minute, such as for measuring body composition. Alternatively, measurements could be triggered or filtered at certain postures or activity levels [95,96]. However, this is not suitable for ambulatory monitoring of dynamic parameters such as respiration monitoring, when one is interested in respiration throughout the day. The two main strategies to handle corrupted data in impedance pneumography are so-called “quality indicators” that exclude corrupted data or to try to salvage corrupted data by using motion artifact reduction techniques. Motion artifact reduction is often applied to ECG and photoplethysmography signals [97-100], but to a lesser extend to impedance pneumography signals. For example, Ansari et al [101] compared different methods for different types of movement. Regarding the so-called quality indicators, Charlton et al [102] reviewed the methods of obtaining quality indicators for respiratory signals and concluded that further research is needed to design powerful quality indicator algorithms for different applications [102]. Recently, they also published a quality assessment method for impedance pneumography signals [103]. Similar to impedance pneumography, artifact handling is relevant for impedance cardiography measurements, including both absolute and relative measures. Artifacts in the impedance cardiography signal make it more difficult to detect the fiducials such as the B-point in the signal, resulting in less accurate estimates of stroke volume and cardiac output. Three approaches for artifact handling have been used in the analysis of impedance cardiography signals: artifact detection [104], artifact reduction [105-107], and posthoc outlier removal from estimated parameters [108].

As mentioned above, the electrode positioning influences the measured volume. As such, changing the electrode position slightly will lead to a change in the measured volume and thus changes the measured impedance value. This is relevant when looking at small changes over measurements that require exact electrode repositioning, but is not important when looking at derived metrics that are not related to the signal amplitude such as the respiratory rate. To circumvent the effect of electrode positioning on the absolute measured value, algorithmic solutions should be developed to correct for these differences or electrode position, and independent metrics should be developed.

In addition, measurements that do not require device or electrode reattachment are subject to change. The condition of the skin can change over time as can the adhesive capability of the electrodes. Adhesive materials for electrodes are optimized for their maximal comfort and endurance.

Finally, bioimpedance is affected by body composition. Depending on the body composition, the current path through the body will differ. In the case of obesity, the current would need to penetrate a larger layer of fat before reaching the underlying tissues, which will affect the measured impedance values. Since there are many different body shapes, personalization of the measurements could circumvent this issue.

General Challenges for Wearables and Wearable Bioimpedance-Based Devices

Although there are some wearable devices on the market for clinical use, such as Holter devices and cardiac rhythm monitoring patches, most wearables have not yet been approved for medical use. Their use has mainly been studied in the research domain thus far [17]. Tests in a controlled or laboratory environment may not represent use in the real world, and validation in resting conditions may not represent (daily life) motion situations [18]. Therefore, there is a need to collect real-word evidence. There is also variability between devices [17], indicating the need for standardization of evaluation of wearables in the assessment of reliability, sensitivity, and validity of the data [18], further signaling the necessity to collect real-word evidence.

Dinh-Le et al [22] reviewed the integration of wearable technology from electronic health records. One associated challenge with this approach is related to the large streams of data that must comply with all privacy and security standards. In addition, patients fear misuse of their data, potentially leading to discrimination and changes in coverage by insurance companies. Therefore, patients should be well informed on the data collection and handling procedures. In addition, proprietary and closed systems pose difficulties with regard to system interoperability and connectivity.

The data streams generated by wearable devices that are often worn 24/7 present another challenge. The current health systems are not prepared for handling such high volumes of rapidly accumulating data [109]. Besides data storage, the vast amount of data is another major challenge, as the data also need to be analyzed. Clinical decision support systems have been implemented that generate false alarms in some cases such as drug interactions or elevated blood pressure. Reliability of these alarms is crucial, since health care providers could experience alarm fatigue due to the large number of false alarms [110,111]. AI is believed to have great potential in the field of clinical data analytics [112]. Regarding bioimpedance monitoring, AI has been shown to be able to detect sleep apnea events [49] and to estimate dry weight in pediatric patients on chronic hemodialysis [113]. However, these algorithms should not stop at classification but should further lead to actionable insights for the health care provider or the patient. Integration of these algorithms on the devices could help in achieving the ultimate goal of developing closed-loop care-providing wearables [112].

As indicated above, the use of many wearables for clinical applications is currently limited to the research domain. It is widely acknowledged that for further acceptance and integration into clinical practice, the proof of medical benefit of wearables through dedicated medical trials is needed [9,18,22,23,112]. Additionally, health care cost should be evaluated for the long and the short term. Wearables are often proposed as a solution against rising health care costs [9,114]. However, there are also examples that show an increase of health care resource utilization with wearables [20].

Interestingly, the view of patients has been less well studied from these aspects. Tran et al [19] explored the perspectives of patients on wearable devices and AI in health care in France. Their study showed that half of the patients felt that digital technology and AI techniques are an important opportunity. However, the study also showed that the patients are not ready for fully automated care. One out of three patients refused one of the devices or AI systems, and patients highlighted the risks regarding privacy and data misusage, the absence of a human interaction and relations, and uncertainty of reliability.

The role of the patient has also been highlighted in studies using technology showing low compliance and large dropouts [115,116]. Nevertheless, other studies have shown good compliance [117]. Interestingly, studies have indicated that patients can experience monitoring as obtrusive and undesired, and that it can even lead to higher depression scores [118]. Several studies have focused on increasing the comfort level and decreasing the obtrusiveness of wearables to circumvent these problems, looking at the possibility to integrate bioimpedance measurements in clothing [54], the use of flexible and stretchable materials [119], and to increase battery life [82]. In some use cases, “nearables” could be used as an alternative to wearables, leading to invisible and effortless methods. One such example is the integration of bioimpedance measurements in chairs or beds via capacitively coupled bioimpedance [120].

Summary and Prospects

Although bioimpedance monitoring is not a new concept, wearable bioimpedance monitoring for chronic conditions is a relatively new field. In this viewpoint, we have shown the potential of bioimpedance monitoring in application areas such as respiration, cardiac, body composition, and fluid monitoring, as well as the remaining challenges that need to be addressed before it can be widely adopted in the medical field. Nevertheless, wearable bioimpedance monitoring has large potential to change monitoring and disease management for patients suffering from chronic diseases such as respiratory, cardiac, or kidney disease by enabling low-cost and low-power home-monitoring solutions. These developments can further have an impact on health care costs and quality of life of patients with chronic diseases.

Conflicts of Interest

None declared.

References

1. Yach D, Hawkes C, Gould CL, Hofman KJ. The global burden of chronic diseases: overcoming impediments to prevention and control. JAMA 2004 Jun 02;291(21):2616-2622. [doi: 10.1001/jama.291.21.2616] [Medline: 15173153]
2. Third UN high-level meeting on noncommunicable diseases. 2018 Sep 27. URL: https://www.un.org/pga/73/event/prevention-of-non-communicable-diseases/ [accessed 2020-01-03]
3. Milani RV, Lavie CJ. Health care 2020: reengineering health care delivery to combat chronic disease. Am J Med 2015 Apr;128(4):337-343. [doi: 10.1016/j.amjmed.2014.10.047] [Medline: 25460529]
4. About chronic diseases. Centers for Disease Control and Prevention. URL: https://www.cdc.gov/chronicdisease/about/index.htm [accessed 2020-07-21]
5. Multiple Chronic Conditions Chartbook. Agency for Healthcare Research and Quality. URL: https://www.ahrq.gov/sites/default/files/wysiwyg/professionals/prevention-chronic-care/decision/mcc/mccchartbook.pdf [accessed 2020-01-03]
6. Finkelstein J, Jeong IC. Machine learning approaches to personalize early prediction of asthma exacerbations. Ann N Y Acad Sci 2017 Jan;1387(1):153-165 [FREE Full text] [doi: 10.1111/nyas.13218] [Medline: 27627195]
7. Milani RV, Bober RM, Lavie CJ. The role of technology in chronic disease care. Prog Cardiovasc Dis 2016;58(6):579-583. [doi: 10.1016/j.pcad.2016.01.001] [Medline: 26772623]
8. Cuba Gyllensten I, Bonomi AG, Goode KM, Reiter H, Habetha J, Amft O, et al. Early indication of decompensated heart failure in patients on home-telemonitoring: a comparison of prediction algorithms based on daily weight and noninvasive transthoracic bio-impedance. JMIR Med Inform 2016 Feb 18;4(1):e3 [FREE Full text] [doi: 10.2196/medinform.4842] [Medline: 26892844]
9. Joshi M, Ashrafian H, Aufegger L, Khan S, Arora S, Cooke G, et al. Wearable sensors to improve detection of patient deterioration. Expert Rev Med Devices 2019 Feb;16(2):145-154. [doi: 10.1080/17434440.2019.1563480] [Medline: 30580650]
10. Varon C, Caicedo A, Testelmans D, Buyse B, Van Huffel S. A novel algorithm for the automatic detection of sleep apnea from single-lead ECG. IEEE Trans Biomed Eng 2015 Sep;62(9):2269-2278. [doi: 10.1109/TBME.2015.2422378] [Medline: 25879836]

11. Das A, Pradhapan P, Groenendaal W, Adiraju P, Rajan RT, Catthoor F, et al. Unsupervised heart-rate estimation in wearables with Liquid states and a probabilistic readout. Neural Netw 2018 Mar;99:134-147. [doi: 10.1016/j.neunet.2017.12.015] [Medline: 29414535]
12. Hur E, Usta M, Toz H, Asci G, Wabel P, Kahvecioglu S, et al. Effect of fluid management guided by bioimpedance spectroscopy on cardiovascular parameters in hemodialysis patients: a randomized controlled trial. Am J Kidney Dis 2013 Jun;61(6):957-965. [doi: 10.1053/j.ajkd.2012.12.017] [Medline: 23415416]
13. Zhang Y, Harrison C. Tomo: wearable, low-cost electrical impedance tomography for hand gesture recognition. 2015 Presented at: UIST 2015. 28th Annual ACM Symposium on User Interface Software & Technology; November 2015; Charlotte, NC URL: https://dl.acm.org/doi/abs/10.1145/2807442.2807480 [doi: 10.1145/2815585]
14. Kubicek WG, Patterson RP, Witsoe DA. Impedance cardiography as a noninvasive method of monitoring cardiac function and other parameters of the cardiovascular system. Ann NY Acad Sci 1970 Jul;170(2 International):724-732. [doi: 10.1111/j.1749-6632.1970.tb17735.x]
15. Malmberg LP, Seppä VP, Kotaniemi-Syrjänen A, Malmström K, Kajosaari M, Pelkonen AS, et al. Measurement of tidal breathing flows in infants using impedance pneumography. Eur Respir J 2017 Feb 19;49(2):1600926 [FREE Full text] [doi: 10.1183/13993003.00926-2016] [Medline: 28182566]
16. Anand I, Doan A, Ma K, Toth J, Geyen K, Otterness S, et al. Monitoring changes in fluid status with a wireless multisensor monitor: results from the Fluid Removal During Adherent Renal Monitoring (FARM) study. Congest Heart Fail 2012;18(1):32-36. [doi: 10.1111/j.1751-7133.2011.00271.x] [Medline: 22277175]
17. Piwek L, Ellis DA, Andrews S, Joinson A. The rise of consumer health wearables: promises and barriers. PLoS Med 2016 Feb;13(2):e1001953 [FREE Full text] [doi: 10.1371/journal.pmed.1001953] [Medline: 26836780]
18. Düking P, Fuss FK, Holmberg H, Sperlich B. Recommendations for assessment of the reliability, sensitivity, and validity of data provided by wearable sensors designed for monitoring physical activity. JMIR Mhealth Uhealth 2018 Apr 30;6(4):e102 [FREE Full text] [doi: 10.2196/mhealth.9341] [Medline: 29712629]
19. Tran V, Riveros C, Ravaud P. Patients' views of wearable devices and AI in healthcare: findings from the ComPaRe e-cohort. NPJ Digit Med 2019 Jun 14;2(1):53. [doi: 10.1038/s41746-019-0132-y] [Medline: 31304399]
20. Steinhubl SR, Waalen J, Edwards AM, Ariniello LM, Mehta RR, Ebner GS, et al. Effect of a home-based wearable continuous ECG monitoring patch on detection of undiagnosed atrial fibrillation: The mSToPS randomized clinical trial. JAMA 2018 Jul 10;320(2):146-155 [FREE Full text] [doi: 10.1001/jama.2018.8102] [Medline: 29998336]
21. Phillips SM, Cadmus-Bertram L, Rosenberg D, Buman MP, Lynch BM. Wearable technology and physical activity in chronic disease: opportunities and challenges. Am J Prev Med 2018 Jan;54(1):144-150 [FREE Full text] [doi: 10.1016/j.amepre.2017.08.015] [Medline: 29122356]
22. Dinh-Le C, Chuang R, Chokshi S, Mann D. Wearable health technology and electronic health record integration: scoping review and future directions. JMIR Mhealth Uhealth 2019 Sep 11;7(9):e12861 [FREE Full text] [doi: 10.2196/12861] [Medline: 31512582]
23. Bianchi MT. Sleep devices: wearables and nearables, informational and interventional, consumer and clinical. Metabolism 2018 Jul;84:99-108. [doi: 10.1016/j.metabol.2017.10.008] [Medline: 29080814]
24. Lukaski HC. Evolution of bioimpedance: a circuitous journey from estimation of physiological function to assessment of body composition and a return to clinical research. Eur J Clin Nutr 2013 Jan 9;67(Suppl 1):S2-S9. [doi: 10.1038/ejcn.2012.149] [Medline: 23299867]
25. Grimnes S, Martinsen O. Bioimpedance and Bioelectricity Basics - 2nd Edition. Cambridge, MA: Academic Press; Mar 03, 2008.
26. Kyle UG, Bosaeus I, De Lorenzo AD, Deurenberg P, Elia M, Gómez JM, Composition of the ESPEN Working Group. Bioelectrical impedance analysis--part I: review of principles and methods. Clin Nutr 2004 Oct;23(5):1226-1243. [doi: 10.1016/j.clnu.2004.06.004] [Medline: 15380917]
27. Gabriel S, Lau RW, Gabriel C. The dielectric properties of biological tissues: II. Measurements in the frequency range 10 Hz to 20 GHz. Phys Med Biol 1996 Nov 01;41(11):2251-2269. [doi: 10.1088/0031-9155/41/11/002] [Medline: 8938025]
28. Piccoli A, Rossi B, Pillon L, Bucciante G. A new method for monitoring body fluid variation by bioimpedance analysis: the RXc graph. Kidney Int 1994 Aug;46(2):534-539 [FREE Full text] [doi: 10.1038/ki.1994.305] [Medline: 7967368]
29. Khalil S, Mohktar M, Ibrahim F. The theory and fundamentals of bioimpedance analysis in clinical status monitoring and diagnosis of diseases. Sensors (Basel) 2014 Jun 19;14(6):10895-10928 [FREE Full text] [doi: 10.3390/s140610895] [Medline: 24949644]
30. Pethig R. Dielectric properties of body tissues. Clin Phys Physiol Meas 1987 Feb 14;8(Suppl 4A):5-12. [doi: 10.1088/0143-0815/8/4a/002] [Medline: 3568571]
31. Jonscher AK. Dielectric relaxation in solids. J Phys D Appl Phys 1999 Jan 01;32(14):R57-R70. [doi: 10.1088/0022-3727/32/14/201]
32. Fricke H, Morse S. The electric resistance and capacity of blood for frequencies between 800 and 4(1/2) million cycles. J Gen Physiol 1925 Nov 20;9(2):153-167 [FREE Full text] [doi: 10.1085/jgp.9.2.153] [Medline: 19872239]
33. Cole KS, Cole RH. Dispersion and absorption in dielectrics I. Alternating current characteristics. J Chem Physics 1941 Apr;9(4):341-351. [doi: 10.1063/1.1750906]

34. Henderson RP, Webster JG. An impedance camera for spatially specific measurements of the thorax. IEEE Trans Biomed Eng 1978 May;BME-25(3):250-254. [doi: 10.1109/tbme.1978.326329]
35. Adler A, Boyle A. Electrical impedance tomography: tissue properties to image measures. IEEE Trans Biomed Eng 2017 Nov;64(11):2494-2504. [doi: 10.1109/TBME.2017.2728323] [Medline: 28715324]
36. Adler A, Lionheart WRB. Uses and abuses of EIDORS: an extensible software base for EIT. Physiol Meas 2006 May;27(5):S25-S42. [doi: 10.1088/0967-3334/27/5/S03] [Medline: 16636416]
37. Frerichs I, Amato MBP, van Kaam AH, Tingay DG, Zhao Z, Grychtol B, TREND study group. Chest electrical impedance tomography examination, data analysis, terminology, clinical use and recommendations: consensus statement of the TRanslational EIT developmeNt stuDy group. Thorax 2017 Jan 05;72(1):83-93 [FREE Full text] [doi: 10.1136/thoraxjnl-2016-208357] [Medline: 27596161]
38. Metherall P, Barber DC, Smallwood RH, Brown BH. Three-dimensional electrical impedance tomography. Nature 1996 Apr 11;380(6574):509-512. [doi: 10.1038/380509a0] [Medline: 8606768]
39. Yang F, Patterson RP. A simulation study on the effect of thoracic conductivity inhomogeneities on sensitivity distributions. Ann Biomed Eng 2008 May 26;36(5):762-768. [doi: 10.1007/s10439-008-9469-0] [Medline: 18299989]
40. Yang F, Patterson RP. The contribution of the lungs to thoracic impedance measurements: a simulation study based on a high resolution finite difference model. Physiol Meas 2007 Jul;28(7):S153-S161. [doi: 10.1088/0967-3334/28/7/S12] [Medline: 17664633]
41. Beckmann L, van Riesen RD, Leonhardt S. Optimal electrode placement and frequency range selection for the detection of lung water using Bioimpedance Spectroscopy. 2007 Presented at: 29th Annual International Conference of the IEEE Engineering in Medicine and Biology Society; 2007; Lyon, France p. 2685-2688. [doi: 10.1109/iembs.2007.4352882]
42. Baker LE, Geddes LA, Hoff HE, Chaput CJ. Physiological factors underlying transthoracic impedance variations in respiration. J Appl Physiol 1966 Sep;21(5):1491-1499. [doi: 10.1152/jappl.1966.21.5.1491] [Medline: 5332246]
43. Kawakami K, Watanabe A, Ikeda K, Kanno R, Kira S. An analysis of the relationship between transthoracic impedance variations and thoracic diameter changes. Med Biol Eng 1974 Jul;12(4):446-453. [doi: 10.1007/BF02478600] [Medline: 4465560]
44. Grenvik A, Ballou S, McGinley E, Millen JE, Cooley WL, Safar P. Impedance pneumography. Comparison between chest impedance changes and respiratory volumines in 11 healthy volunteers. Chest 1972 Oct;62(4):439-443. [doi: 10.1378/chest.62.4.439] [Medline: 5077999]
45. Seppä V, Viik J, Naveed A, Väisänen J, Hyttinen J. Signal waveform agreement between spirometerimpedance pneumography of six chest band electrode configurations. Berlin Heidelberg: Springer; 2009 Presented at: World Congress on Medical Physics and Biomedical Engineering; September 7-12, 2009; Munich, Germany p. 689-692. [doi: 10.1007/978-3-642-03885-3_191]
46. Seppa V, Viik J, Hyttinen J. Assessment of pulmonary flow using impedance pneumography. IEEE Trans Biomed Eng 2010 Sep;57(9):2277-2285. [doi: 10.1109/tbme.2010.2051668]
47. Koivumäki T, Vauhkonen M, Kuikka JT, Hakulinen MA. Bioimpedance-based measurement method for simultaneous acquisition of respiratory and cardiac gating signals. Physiol Meas 2012 Aug 20;33(8):1323-1334. [doi: 10.1088/0967-3334/33/8/1323] [Medline: 22813948]
48. Blanco-Almazan D, Groenendaal W, Catthoor F, Jane R. Wearable bioimpedance measurement for respiratory monitoring during inspiratory loading. IEEE Access 2019;7:89487-89496. [doi: 10.1109/access.2019.2926841]
49. Van Steenkiste T, Groenendaal W, Dreesen P, Lee S, Klerkx S, de Francisco R, et al. Portable detection of apnea and hypopnea events using bio-impedance of the chest and deep learning. IEEE J Biomed Health Inform 2020 Sep;24(9):2589-2598. [doi: 10.1109/jbhi.2020.2967872]
50. Blanco-Almazán D, Groenendaal W, Catthoor F, Jané R. Chest movement and respiratory volume both contribute to thoracic bioimpedance during loaded breathing. Sci Rep 2019 Dec 27;9(1):20232. [doi: 10.1038/s41598-019-56588-4] [Medline: 31882841]
51. Seppä VP, Hyttinen J, Uitto M, Chrapek W, Viik J. Novel electrode configuration for highly linear impedance pneumography. Biomed Tech (Berl) 2013 Feb;58(1):35-38. [doi: 10.1515/bmt-2012-0068] [Medline: 23348215]
52. Seppä VP, Pelkonen AS, Kotaniemi-Syrjänen A, Viik J, Mäkelä MJ, Malmberg LP. Tidal flow variability measured by impedance pneumography relates to childhood asthma risk. Eur Respir J 2016 Jun;47(6):1687-1696 [FREE Full text] [doi: 10.1183/13993003.00989-2015] [Medline: 26989106]
53. Blanco-Almazan D, Groenendaal W, Lozano-Garcia M, Estrada-Petrocelli L, Lijnen L, Smeets C, et al. Combining bioimpedance and myographic signals for the assessment of COPD during loaded breathing. IEEE Trans Biomed Eng 2021 Jan;68(1):298-307. [doi: 10.1109/tbme.2020.2998009]
54. Mirmohamadsadeghi L, Fallet S, Buttu A, Saugy J, Rupp T, Heinzer R, et al. Sleep apnea detection using features from the respiration and the ecg recorded with smart-shirts. 2014 Presented at: IEEE Biomedical Circuits and Systems Conference (BioCAS); 2014; Lausanne, Switzerland p. 61-64. [doi: 10.1109/biocas.2014.6981645]
55. Galvagno SM, Brayanov J, Corneille MG, Voscopoulos CJ, Sordo S, Ladd D, et al. Non-invasive respiratory volume monitoring in patients with traumatic thoracic injuries. Trauma 2014 Oct 29;17(3):219-223. [doi: 10.1177/1460408614551977]

56. Voscopoulos C, MacNabb C, Freeman J, Galvagno S, Ladd D, George E. Continuous noninvasive respiratory volume monitoring for the identification of patients at risk for opioid-induced respiratory depression and obstructive breathing patterns. J Trauma Acute Care Surg 2014 Sep;77(3 Suppl 2):S208-S215. [doi: 10.1097/TA.0000000000000400] [Medline: 25159358]
57. Woltjer HH, Bogaard HJ, de Vries PMJM. The technique of impedance cardiography. Eur Heart J 1997 Sep 01;18(9):1396-1403. [doi: 10.1093/oxfordjournals.eurheartj.a015464] [Medline: 9458444]
58. Meijer J, Elbertse E, Boesveldt S, Berendse H, Verdaasdonk R. Using the initial systolic time interval to assess cardiac autonomic nervous function in Parkinson's disease. J Electr Bioimpedance 2011;2(1):98-101. [doi: 10.5617/jeb.216]
59. Panfili G, Piccini L, Maggi L, Parini S, Andreoni G. A wearable device for continuous monitoring of heart mechanical function based on Impedance CardioGraphy. 2006 Presented at: International Conference the IEEE Engineering Medical and Biology Society (EMBC); August 31-September 3, 2006; New York City, NY p. 5968-5971. [doi: 10.1109/iembs.2006.260250]
60. Marquez J, Rempfler M, Seoane F, Lindecrantz K. Textrode-enabled transthoracic electrical bioimpedance measurements towards wearable applications of impedance cardiography. J Electr Bioimpedance 2013;4(1):45-50. [doi: 10.5617/jeb.542]
61. Murali S, Rincon F, Atienza D. A wearable device for physical and emotional health monitoring. : IEEE; 2015 Presented at: Computing in Cardiology Conference (CinC); 2015; Nice, France. [doi: 10.1109/cic.2015.7408601]
62. Yazdanian H, Mahnam A, Edrisi M, Esfahani M. Design and implementation of a portable impedance cardiography system for noninvasive stroke volume monitoring. J Med Signals Sens 2016;6(1):47-56. [doi: 10.4103/2228-7477.175871]
63. Bernstein DP, Lemmens HJM. Stroke volume equation for impedance cardiography. Med Biol Eng Comput 2005 Aug;43(4):443-450. [doi: 10.1007/bf02344724]
64. de Sitter A, Verdaasdonk RM, Faes TJC. Do mathematical model studies settle the controversy on the origin of cardiac synchronous trans-thoracic electrical impedance variations? A systematic review. Physiol Meas 2016 Aug 17;37(9):R88-R108. [doi: 10.1088/0967-3334/37/9/r88]
65. Louvaris Z, Spetsioti S, Andrianopoulos V, Chynkiamis N, Habazettl H, Wagner H, et al. Cardiac output measurement during exercise in COPD: A comparison of dye dilution and impedance cardiography. Clin Respir J 2019 Apr;13(4):222-231. [doi: 10.1111/crj.13002] [Medline: 30724023]
66. Scherhag A, Kaden JJ, Kentschke E, Sueselbeck T, Borggrefe M. Comparison of impedance cardiography and thermodilution-derived measurements of stroke volume and cardiac output at rest and during exercise testing. Cardiovasc Drugs Ther 2005 Mar;19(2):141-147. [doi: 10.1007/s10557-005-1048-0] [Medline: 16025233]
67. Cotter G, Moshkovitz Y, Kaluski E, Cohen AJ, Miller H, Goor D, et al. Accurate, noninvasive continuous monitoring of cardiac output by whole-body electrical bioimpedance. Chest 2004 Apr;125(4):1431-1440. [doi: 10.1378/chest.125.4.1431] [Medline: 15078756]
68. McIntyre JP, Ellyett KM, Mitchell EA, Quill GM, Thompson JM, Stewart AW, Maternal Sleep in Pregnancy Study Group. Validation of thoracic impedance cardiography by echocardiography in healthy late pregnancy. BMC Pregnancy Childbirth 2015 Mar 28;15(1):70 [FREE Full text] [doi: 10.1186/s12884-015-0504-5] [Medline: 25886289]
69. Panagiotou M, Vogiatzis I, Jayasekera G, Louvaris Z, Mackenzie A, Mcglinchey N, et al. Validation of impedance cardiography in pulmonary arterial hypertension. Clin Physiol Funct Imaging 2018 Mar 06;38(2):254-260. [doi: 10.1111/cpf.12408] [Medline: 28168802]
70. Engoren M, Barbee D. Comparison of cardiac output determined by bioimpedance, thermodilution, and the Fick method. Am J Crit Care 2005 Jan;14(1):40-45. [Medline: 15608107]
71. Packer M, Abraham WT, Mehra MR, Yancy CW, Lawless CE, Mitchell JE, Prospective EvaluationIdentification of Cardiac Decompensation by ICG Test (PREDICT) Study InvestigatorsCoordinators. Utility of impedance cardiography for the identification of short-term risk of clinical decompensation in stable patients with chronic heart failure. J Am Coll Cardiol 2006 Jun 06;47(11):2245-2252 [FREE Full text] [doi: 10.1016/j.jacc.2005.12.071] [Medline: 16750691]
72. Fein A, Grossman RF, Jones JG, Goodman PC, Murray JF. Evaluation of transthoracic electrical impedance in the diagnosis of pulmonary edema. Circulation 1979 Nov;60(5):1156-1160. [doi: 10.1161/01.cir.60.5.1156] [Medline: 487548]
73. Cuba-Gyllensten I, Gastelurrutia P, Riistama J, Aarts R, Nuñez J, Lupon J, et al. A novel wearable vest for tracking pulmonary congestion in acutely decompensated heart failure. Int J Cardiol 2014 Nov 15;177(1):199-201. [doi: 10.1016/j.ijcard.2014.09.041] [Medline: 25499378]
74. Hung S, Kuo K, Peng C, Wu C, Lien Y, Wang Y, et al. Volume overload correlates with cardiovascular risk factors in patients with chronic kidney disease. Kidney Int 2014 Mar;85(3):703-709 [FREE Full text] [doi: 10.1038/ki.2013.336] [Medline: 24025647]
75. Chazot C, Wabel P, Chamney P, Moissl U, Wieskotten S, Wizemann V. Importance of normohydration for the long-term survival of haemodialysis patients. Nephrol Dial Transplant 2012 Jun 17;27(6):2404-2410. [doi: 10.1093/ndt/gfr678] [Medline: 22253067]
76. Tsai Y, Tsai J, Chen S, Chiu Y, Hwang S, Hung C, et al. Association of fluid overload with kidney disease progression in advanced CKD: a prospective cohort study. Am J Kidney Dis 2014 Jan;63(1):68-75. [doi: 10.1053/j.ajkd.2013.06.011] [Medline: 23896483]

77. Onofriescu M, Mardare NG, Segall L, Voroneanu L, Cuşai C, Hogaş S, et al. Randomized trial of bioelectrical impedance analysis versus clinical criteria for guiding ultrafiltration in hemodialysis patients: effects on blood pressure, hydration status, and arterial stiffness. Int Urol Nephrol 2012 Apr 19;44(2):583-591. [doi: 10.1007/s11255-011-0022-y] [Medline: 21688195]
78. Moissl U, Arias-Guillén M, Wabel P, Fontseré N, Carrera M, Campistol JM, et al. Bioimpedance-guided fluid management in hemodialysis patients. Clin J Am Soc Nephrol 2013 Sep;8(9):1575-1582 [FREE Full text] [doi: 10.2215/CJN.12411212] [Medline: 23949235]
79. Schoutteten MK, Vranken J, Lee S, Smeets CJP, De Cannière H, Van Hoof C, et al. Towards personalized fluid monitoring in haemodialysis patients: thoracic bioimpedance signal shows strong correlation with fluid changes, a cohort study. BMC Nephrol 2020 Jul 11;21(1):264 [FREE Full text] [doi: 10.1186/s12882-020-01922-6] [Medline: 32652949]
80. Shochat M, Charach G, Meyler S, Meisel S, Weintraub M, Mengeritsky G, et al. Prediction of cardiogenic pulmonary edema onset by monitoring right lung impedance. Intensive Care Med 2006 Aug;32(8):1214-1221. [doi: 10.1007/s00134-006-0237-z] [Medline: 16775717]
81. Shochat MK, Shotan A, Blondheim DS, Kazatsker M, Dahan I, Asif A, et al. Non-invasive lung impedence-guided preemptive treatment in chronic heart failure patients: a randomized controlled trial (IMPEDANCE-HF Trial). J Card Fail 2016 Sep;22(9):713-722. [doi: 10.1016/j.cardfail.2016.03.015] [Medline: 27058408]
82. Lee S, Polito S, Agell C, Mitra S, Firat Yazicioglu R, Riistama J, et al. A low-power and compact-sized wearable bio-impedance monitor with wireless connectivity. In: Journal of Physics: Conference Series. 2013 Apr 18 Presented at: International Conference on Electrical Bio-Impedence (ICBEI) and XIV Conference on Electrical Impedence Tomography (EIT); April 22-25, 2013; Heilbad Heiligenstadst, Germany p. 012013. [doi: 10.1088/1742-6596/434/1/012013]
83. Gastelurrutia P, Cuba-Gyllensten I, Lupon J, Zamora E, Llibre C, Caballero, et al. Wearable vest for pulmonary congestion tracking and prognosis in heart failure: A pilot study. Int J Cardiol 2016 Jul 15;215:77-79. [doi: 10.1016/j.ijcard.2016.04.024] [Medline: 27111163]
84. Smeets CJP, Lee S, Groenendaal W, Squillace G, Vranken J, De Cannière H, et al. The added value of in-hospital tracking of the efficacy of decongestion therapy and prognostic value of a wearable thoracic impedance sensor in acutely decompensated heart failure with volume overload: prospective cohort study. JMIR Cardio 2020 Mar 18;4(1):e12141 [FREE Full text] [doi: 10.2196/12141] [Medline: 32186520]
85. Yu C, Wang L, Chau E, Chan RH, Kong S, Tang M, et al. Intrathoracic impedance monitoring in patients with heart failure: correlation with fluid status and feasibility of early warning preceding hospitalization. Circulation 2005 Aug 09;112(6):841-848. [doi: 10.1161/CIRCULATIONAHA.104.492207] [Medline: 16061743]
86. van Veldhuisen DJ, Braunschweig F, Conraads V, Ford I, Cowie MR, Jondeau G, DOT-HF Investigators. Intrathoracic impedance monitoring, audible patient alerts, and outcome in patients with heart failure. Circulation 2011 Oct 18;124(16):1719-1726. [doi: 10.1161/CIRCULATIONAHA.111.043042] [Medline: 21931078]
87. Khandwalla RM, Birkeland K, Zimmer R, Banet M, Pede S, Kedan I. Predicting heart failure events with home monitoring: use of a novel, wearable necklace to measure stroke volume, cardiac output and thoracic impedance. J Am Coll Cardiol 2016 Apr;67(13):1296. [doi: 10.1016/s0735-1097(16)31297-9]
88. Trtovac D, Lee J. The use of technology in identifying hospital malnutrition: scoping review. JMIR Med Inform 2018 Jan 19;6(1):e4 [FREE Full text] [doi: 10.2196/medinform.7601] [Medline: 29351894]
89. Vogt B, Zhao Z, Zabel P, Weiler N, Frerichs I. Regional lung response to bronchodilator reversibility testing determined by electrical impedance tomography in chronic obstructive pulmonary disease. Am J Physiol Lung Cell Mol Physiol 2016 Jul 01;311(1):L8-L19 [FREE Full text] [doi: 10.1152/ajplung.00463.2015] [Medline: 27190067]
90. Witkowska-Wrobel A, Aristovich K, Faulkner M, Avery J, Holder D. Feasibility of imaging epileptic seizure onset with EIT and depth electrodes. Neuroimage 2018 Jun;173:311-321 [FREE Full text] [doi: 10.1016/j.neuroimage.2018.02.056] [Medline: 29499314]
91. Rapin M, Braun F, Adler A, Wacker J, Frerichs I, Vogt B, et al. Wearable sensors for frequency-multiplexed EIT and multilead ECG data acquisition. IEEE Trans Biomed Eng 2019 Mar;66(3):810-820. [doi: 10.1109/tbme.2018.2857199]
92. Hong S, Lee J, Bae J, Yoo H. A 10.4 mW electrical impedance tomography SoC for portable real-time lung ventilation monitoring system. IEEE J Solid-State Circuits 2015 Nov;50(11):2501-2512. [doi: 10.1109/jssc.2015.2464705]
93. Kim M, Jang J, Kim H, Lee J, Lee J, Lee J, et al. A 1.4-m Ω-sensitivity 94-dB dynamic-range electrical impedance tomography SoC and 48-channel Hub-SoC for 3-D lung ventilation monitoring system. IEEE J Solid-State Circuits 2017 Nov;52(11):2829-2842. [doi: 10.1109/jssc.2017.2753234]
94. Huang J, Hung Y, Wang J, Lin B. Design of wearable and wireless electrical impedance tomography system. Measurement 2016 Jan;78:9-17. [doi: 10.1016/j.measurement.2015.09.031]
95. Lee S, Squillace G, Smeets C, Vandecasteele M, Grieten L, de Francisco R, et al. Congestive heart failure patient monitoring using wearable bio-impedance sensor technology. : IEEE; 2015 Presented at: 37th Annual International Conference of the IEEE Engineering in Medicine and Biology Society (EMBC); 2015; Milan, Italy. [doi: 10.1109/embc.2015.7318393]
96. Demura S, Yamaji S, Goshi F, Nagasawa Y. The influence of posture change on measurements of relative body fat in the bioimpedance analysis method. J Physiol Anthropol Appl Human Sci 2001 Jan;20(1):29-35 [FREE Full text] [doi: 10.2114/jpa.20.29] [Medline: 11320777]

97. Van Helleputte N, Konijnenburg M, Pettine J, Jee D, Kim H, Morgado A, et al. A 345 µW multi-sensor biomedical SoC with bio-impedance, 3-channel ECG, motion artifact reduction, and integrated DSP. IEEE J Solid-State Circuits 2015 Jan;50(1):230-244. [doi: 10.1109/jssc.2014.2359962]
98. Zhang Y, Song S, Vullings R, Biswas D, Simões-Capela N, van Helleputte N, et al. Motion artifact reduction for wrist-worn photoplethysmograph sensors based on different wavelengths. Sensors (Basel) 2019 Feb 07;19(3):673 [FREE Full text] [doi: 10.3390/s19030673] [Medline: 30736395]
99. Zhang Z, Pi Z, Liu B. TROIKA: a general framework for heart rate monitoring using wrist-type photoplethysmographic signals during intensive physical exercise. IEEE Trans Biomed Eng 2015 Feb;62(2):522-531. [doi: 10.1109/TBME.2014.2359372] [Medline: 25252274]
100. Lee H, Chung H, Lee J. Motion artifact cancellation in wearable photoplethysmography using gyroscope. IEEE Sensors J 2019 Feb 1;19(3):1166-1175. [doi: 10.1109/jsen.2018.2879970]
101. Ansari S, Ward KR, Najarian K. Motion artifact suppression in impedance pneumography signal for portable monitoring of respiration: an adaptive approach. IEEE J Biomed Health Inform 2017 Mar;21(2):387-398. [doi: 10.1109/jbhi.2016.2524646]
102. Charlton PH, Birrenkott DA, Bonnici T, Pimentel MAF, Johnson AEW, Alastruey J, et al. Breathing rate estimation from the electrocardiogram and photoplethysmogram: a review. IEEE Rev Biomed Eng 2018;11:2-20. [doi: 10.1109/rbme.2017.2763681]
103. Charlton PH, Bonnici T, Tarassenko L, Clifton DA, Beale R, Watkinson PJ, et al. An impedance pneumography signal quality index: Design, assessment and application to respiratory rate monitoring. Biomed Signal Proces 2021 Mar;65:102339. [doi: 10.1016/j.bspc.2020.102339]
104. Forouzanfar M, Baker F, Colrain I, de ZM. Automatic artifact detection in impedance cardiogram using pulse similarity index. : IEEE; 2019 Presented at: 41st Annual International Conference of the IEEE Engineering in Medicine and Biology Society (EMBC); 2019; Berlin, Germany. [doi: 10.1109/embc.2019.8856542]
105. Riese H, Groot PFC, van den Berg M, Kupper NHM, Magnee EHB, Rohaan EJ, et al. Large-scale ensemble averaging of ambulatory impedance cardiograms. Behav Res Methods Instrum Comput 2003 Aug;35(3):467-477. [doi: 10.3758/bf03195525] [Medline: 14587556]
106. Pandey V, Pandey P. Cancellation of respiratory artifact in impedance cardiography. : IEEE; 2005 Presented at: 27th Annual Conference of the IEEE Engineering in Medicine and Biology Society (EMBC); 2005; Shanghai, China. [doi: 10.1109/iembs.2005.1615729]
107. Cieslak M, Ryan WS, Babenko V, Erro H, Rathbun ZM, Meiring W, et al. Quantifying rapid changes in cardiovascular state with a moving ensemble average. Psychophysiology 2018 Apr 03;55(4):e13018. [doi: 10.1111/psyp.13018] [Medline: 28972674]
108. Forouzanfar M, Baker FC, de Zambotti M, McCall C, Giovangrandi L, Kovacs GTA. Toward a better noninvasive assessment of preejection period: A novel automatic algorithm for B-point detection and correction on thoracic impedance cardiogram. Psychophysiology 2018 Aug;55(8):e13072 [FREE Full text] [doi: 10.1111/psyp.13072] [Medline: 29512163]
109. Kalid N, Zaidan AA, Zaidan BB, Salman OH, Hashim M, Muzammil H. Based real time remote health monitoring systems: a review on patients prioritization and related "big data" using body sensors information and communication technology. J Med Syst 2017 Dec 29;42(2):30. [doi: 10.1007/s10916-017-0883-4] [Medline: 29288419]
110. Ramirez M, Maranon R, Fu J, Chon J, Chen K, Mangione C, et al. Primary care provider adherence to an alert for intensification of diabetes blood pressure medications before and after the addition of a "chart closure" hard stop. J Am Med Inform Assoc 2018 Sep 01;25(9):1167-1174 [FREE Full text] [doi: 10.1093/jamia/ocy073] [Medline: 30060013]
111. Kesselheim AS, Cresswell K, Phansalkar S, Bates DW, Sheikh A. Clinical decision support systems could be modified to reduce 'alert fatigue' while still minimizing the risk of litigation. Health Aff (Millwood) 2011 Dec;30(12):2310-2317. [doi: 10.1377/hlthaff.2010.1111] [Medline: 22147858]
112. Dunn J, Runge R, Snyder M. Wearables and the medical revolution. Per Med 2018 Sep;15(5):429-448 [FREE Full text] [doi: 10.2217/pme-2018-0044] [Medline: 30259801]
113. Niel O, Bastard P, Boussard C, Hogan J, Kwon T, Deschênes G. Artificial intelligence outperforms experienced nephrologists to assess dry weight in pediatric patients on chronic hemodialysis. Pediatr Nephrol 2018 Oct 9;33(10):1799-1803. [doi: 10.1007/s00467-018-4015-2] [Medline: 29987454]
114. Koydemir HC, Ozcan A. Wearable and implantable sensors for biomedical applications. Annu Rev Anal Chem 2018 Jun 12;11(1):127-146. [doi: 10.1146/annurev-anchem-061417-125956] [Medline: 29490190]
115. Radin J, Steinhubl S, Su A, Bhargava H, Greenberg B, Bot B, et al. The healthy pregnancy research program: transforming pregnancy research through a ResearchKit app. NPJ Digit Med 2018;1:45. [doi: 10.1038/s41746-018-0052-2] [Medline: 31304325]
116. McConnell MV, Shcherbina A, Pavlovic A, Homburger JR, Goldfeder RL, Waggot D, et al. Feasibility of obtaining measures of lifestyle from a smartphone app: the MyHeart Counts Cardiovascular Health Study. JAMA Cardiol 2017 Jan 01;2(1):67-76. [doi: 10.1001/jamacardio.2016.4395] [Medline: 27973671]

117. Evans J, Papadopoulos A, Silvers CT, Charness N, Boot WR, Schlachta-Fairchild L, et al. Remote health monitoring for older adults and those with heart failure: adherence and system usability. Telemed J E Health 2016 Jun;22(6):480-488 [FREE Full text] [doi: 10.1089/tmj.2015.0140] [Medline: 26540369]
118. O'Kane MJ, Bunting B, Copeland M, Coates VE, ESMON study group. Efficacy of self monitoring of blood glucose in patients with newly diagnosed type 2 diabetes (ESMON study): randomised controlled trial. BMJ 2008 May 24;336(7654):1174-1177 [FREE Full text] [doi: 10.1136/bmj.39534.571644.BE] [Medline: 18420662]
119. van den Brand J, de Kok M, Sridhar A, Cauwe M, Verplancke R, Bossuyt F, et al. Flexible and stretchable electronics for wearable healthcare. : IEEE; 2014 Presented at: 44th European Solid State Device Research Conference (ESSDERC); 2014; Venice Lido, Italy p. 206-209. [doi: 10.1109/essderc.2014.6948796]
120. Castro I, Patel A, Torfs T, Puers R, Van Hoof C. Capacitive multi-electrode array with real-time electrode selection for unobtrusive ECG BIOZ monitoring. 2019 Presented at: 41st Annual International Conference of the IEEE Engineering and Medical Biology Society (EMBC); 2019; Berlin, Germany p. 5621-5624. [doi: 10.1109/embc.2019.8857150]

Abbreviations

AI: artificial intelligence
BIS: bioimpedance spectroscopy
BIVA: bioelectrical impedance vector analysis
COPD: chronic obstructive pulmonary disease
CT: computed tomography
ECF: extracellular fluid
ECG: electrocardiogram
ECW: extracellular water
EIT: electrical impedance tomography
ESKD: end-stage kidney disease
ETI: electrode tissue impedance
FFM: fat free mass
ICF: intracellular fluid
ICW: intracellular water
MF-BIA: multifrequency bioimpedance analysis
MRI: magnetic resonance imaging
NCD: noncommunicable disease
SF-BIA: single-frequency bioimpedance analysis
TBW: total body water

Edited by G Eysenbach; submitted 27.07.20; peer-reviewed by IC Jeong, H Zhang; comments to author 01.11.20; revised version received 01.03.21; accepted 06.04.21; published 11.05.21.

Please cite as:
Groenendaal W, Lee S, van Hoof C
Wearable Bioimpedance Monitoring: Viewpoint for Application in Chronic Conditions
JMIR Biomed Eng 2021;6(2):e22911
URL: https://biomedeng.jmir.org/2021/2/e22911
doi:10.2196/22911
PMID:

Short Paper

Neural Network Pattern Recognition of Ultrasound Image Gray Scale Intensity Histograms of Breast Lesions to Differentiate Between Benign and Malignant Lesions: Analytical Study

Arivan Ramachandran[1*], MBBS; Shivabalan Kathavarayan Ramu[2,3*], MBBS, MD

[1]Postgraduate Institute of Medical Education and Research, Chandigarh, India

[2]Mahatma Gandhi Medical College and Research Institute, Puducherry, India

[3]All India Institute of Medical Sciences, New Delhi, India

[*]all authors contributed equally

Corresponding Author:
Shivabalan Kathavarayan Ramu, MBBS, MD
Mahatma Gandhi Medical College and Research Institute
Medical College Road, Pillayarkuppam
Puducherry, 607402
India
Phone: 91 9999850584
Email: shivfrcs@gmail.com

Abstract

Background: Ultrasound-based radiomic features to differentiate between benign and malignant breast lesions with the help of machine learning is currently being researched. The mean echogenicity ratio has been used for the diagnosis of malignant breast lesions. However, gray scale intensity histogram values as a single radiomic feature for the detection of malignant breast lesions using machine learning algorithms have not been explored yet.

Objective: This study aims to assess the utility of a simple convolutional neural network in classifying benign and malignant breast lesions using gray scale intensity values of the lesion.

Methods: An open-access online data set of 200 ultrasonogram breast lesions were collected, and regions of interest were drawn over the lesions. The gray scale intensity values of the lesions were extracted. An input file containing the values and an output file consisting of the breast lesions' diagnoses were created. The convolutional neural network was trained using the files and tested on the whole data set.

Results: The trained convolutional neural network had an accuracy of 94.5% and a precision of 94%. The sensitivity and specificity were 94.9% and 94.1%, respectively.

Conclusions: Simple neural networks, which are cheap and easy to use, can be applied to diagnose malignant breast lesions with gray scale intensity values obtained from ultrasonogram images in low-resource settings with minimal personnel.

(JMIR Biomed Eng 2021;6(2):e23808) doi:10.2196/23808

KEYWORDS

radiology; imaging; neural network; images

Introduction

Breast cancer is the most common cancer in Indian women with a prevalence of 25.8 per 100,000. Lack of adequate breast cancer screening, diagnosis at a later stage, and unavailability of resources are quoted as the main reasons for the increase in mortality in patients with breast cancer in India [1]. The breast cancer mortality in South Asia increased from 6.12 to 9.14 per 100,000 according to a 25-year study [2]. Multiple imaging modalities like ultrasonogram, x-ray mammography, computed tomography, positron emission tomography, and magnetic resonance imaging are being used to screen, diagnose, and evaluate breast cancer.

Ultrasound is one of the basic radiological imaging modalities available in hospitals and it is the imaging modality of choice in suspicious breast lesions in young women and pregnant women. Ultrasound has higher accuracy and sensitivity in the detection of malignant lesions compared to x-ray mammography

[3]. Even with higher accuracy of ultrasonograms, the presence of significant interobserver variability is a notable disadvantage of ultrasonograms. This problem can be solved using radiomics-based diagnostic methods since it standardizes the substantial amount of data available for diagnosis [4].

Application of artificial intelligence for image recognition and classification is an upcoming method and can be implemented in areas with resource and personnel limitations, as it is suggested that neural network–based differentiation of breast lesions has the capacity to substantially reduce unnecessary biopsies and can perform equivalent to trained human radiologists [5,6]. In this study, we are evaluating the efficiency of convolutional neural networks (CNNs) in classifying malignant and benign breast ultrasonogram images downloaded from an online data set based on their gray scale intensity histograms.

Methods

This study is a machine learning–based retrospective diagnostic classification. Ultrasound images of 100 malignant and 100 benign breast lesions were downloaded from an open-access repository [7]. The images were in bitmap format, and the size ranged from 7 to 33 kB (Figure 1).

The images were then loaded in ImageJ software (Wayne Rasband). The image despeckling was done to improve the contrast resolution of the images because ultrasonogram images are known to have speckle noise [8].

The region of interest (ROI) was drawn over the breast lesions in all 200 images by a board-certified radiologist, and the gray scale intensity histogram values were extracted (Figure 2).

The values were entered in a data sheet and were imported to the MATLAB R2020b software (MathWorks).

A total of 200 histograms values were divided by automated randomization available in the software into a training set containing 70% (n=140) of the total images, a validation set containing 15% (n=30) of the total images, and a test set containing 15% (n=30) of the total images.

The in-built application of MATLAB R2020b named neural net pattern recognition was used. It is a two-layer feed-forward network with sigmoid hidden and softmax output neurons. The network was trained with scaled conjugate backpropagation available in the software. In our study, we used 30 hidden neurons (Figure 3) [9]. An input file containing the gray scale intensity histogram values (256 values) was fed to the neural network, and a target file containing the output as either malignant or benign was loaded. Supervised training was initiated, and the results were obtained. The flowchart of the methodology is given in Figure 4.

Figure 1. Ultrasound image (bitmap format) showing hypoechoic malignant breast lesion.

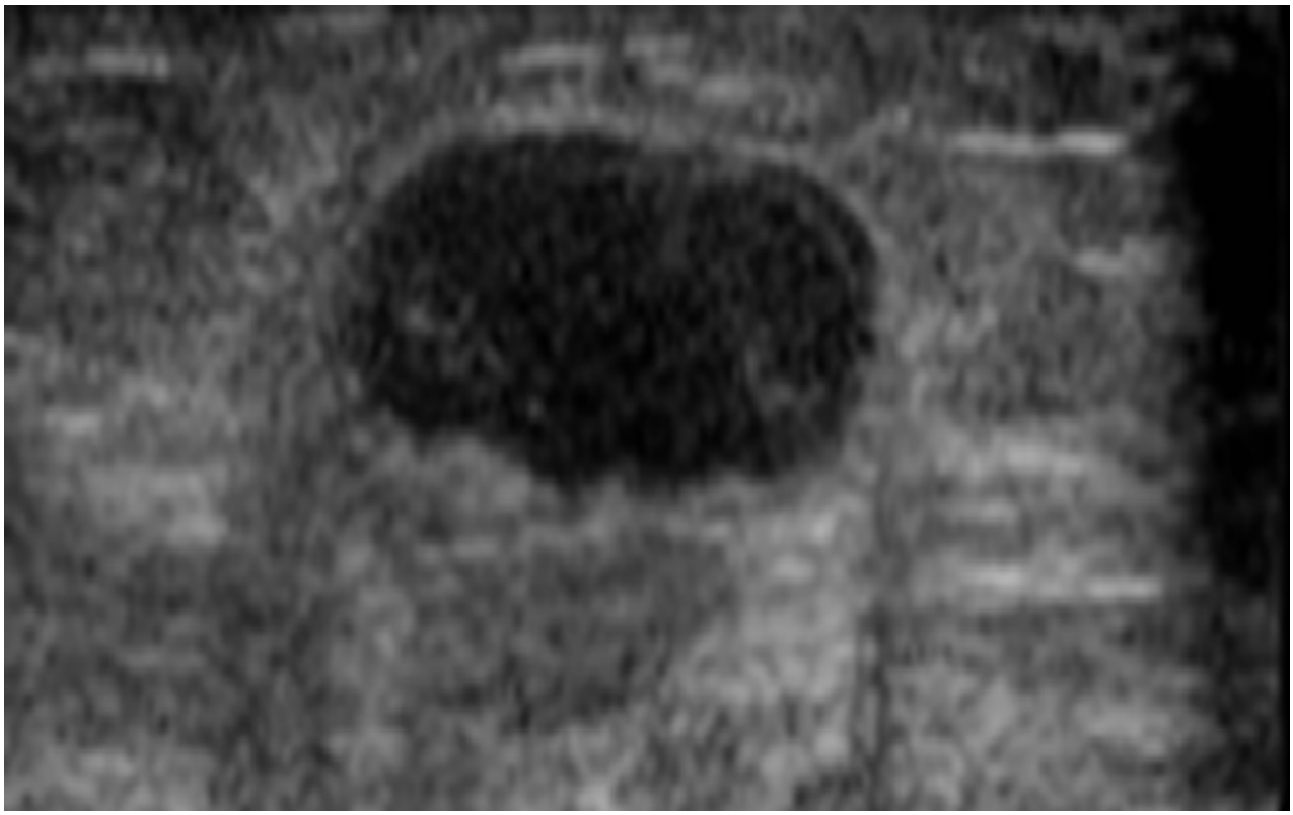

Figure 2. Despeckled ultrasound image of a hypoechoic malignant breast lesion. The image shows the freehand region of interest drawn over the lesion using ImageJ software. Gray scale intensity histogram (red arrow) of the lesion showing the mean, median, and SD values.

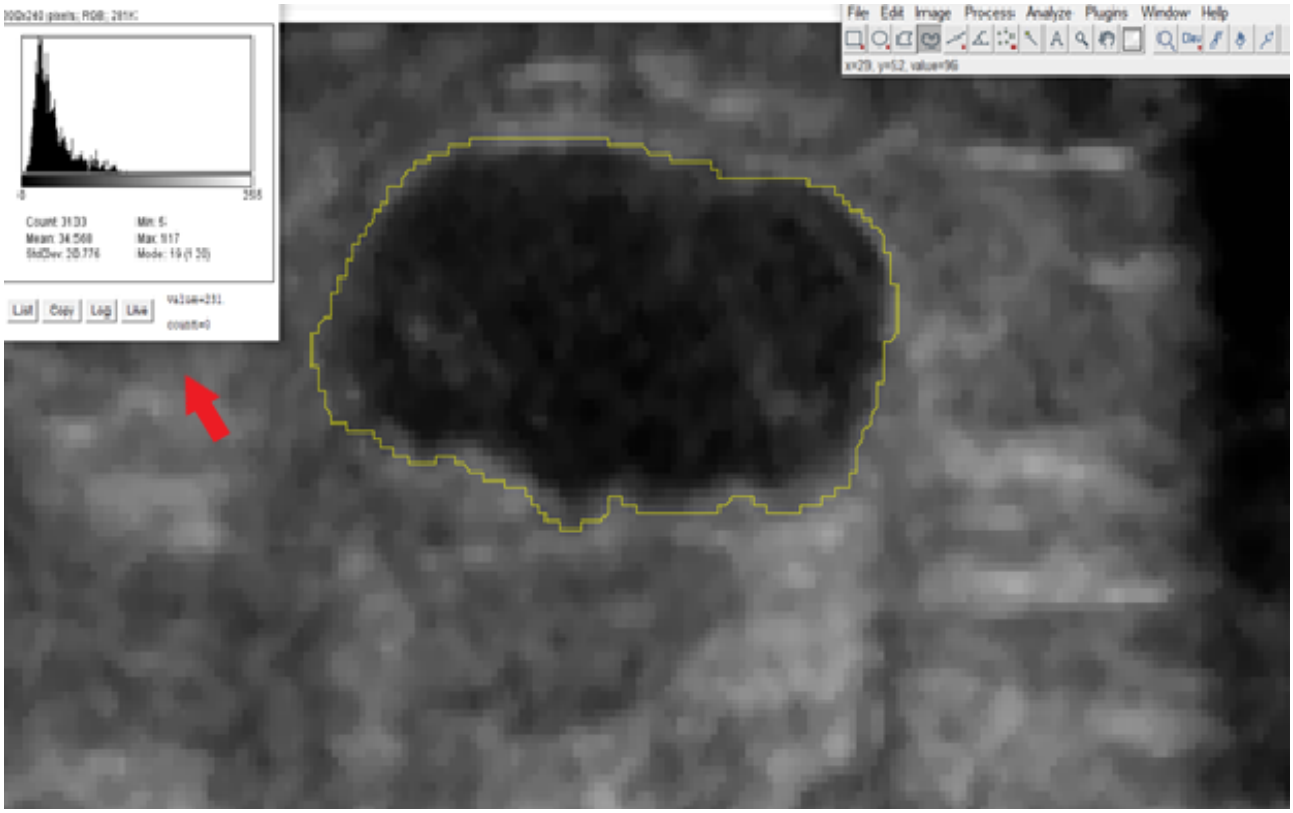

Figure 3. Graphical diagram of the neural network in MATLAB 2020b used for the study with algorithms used for training and performance.

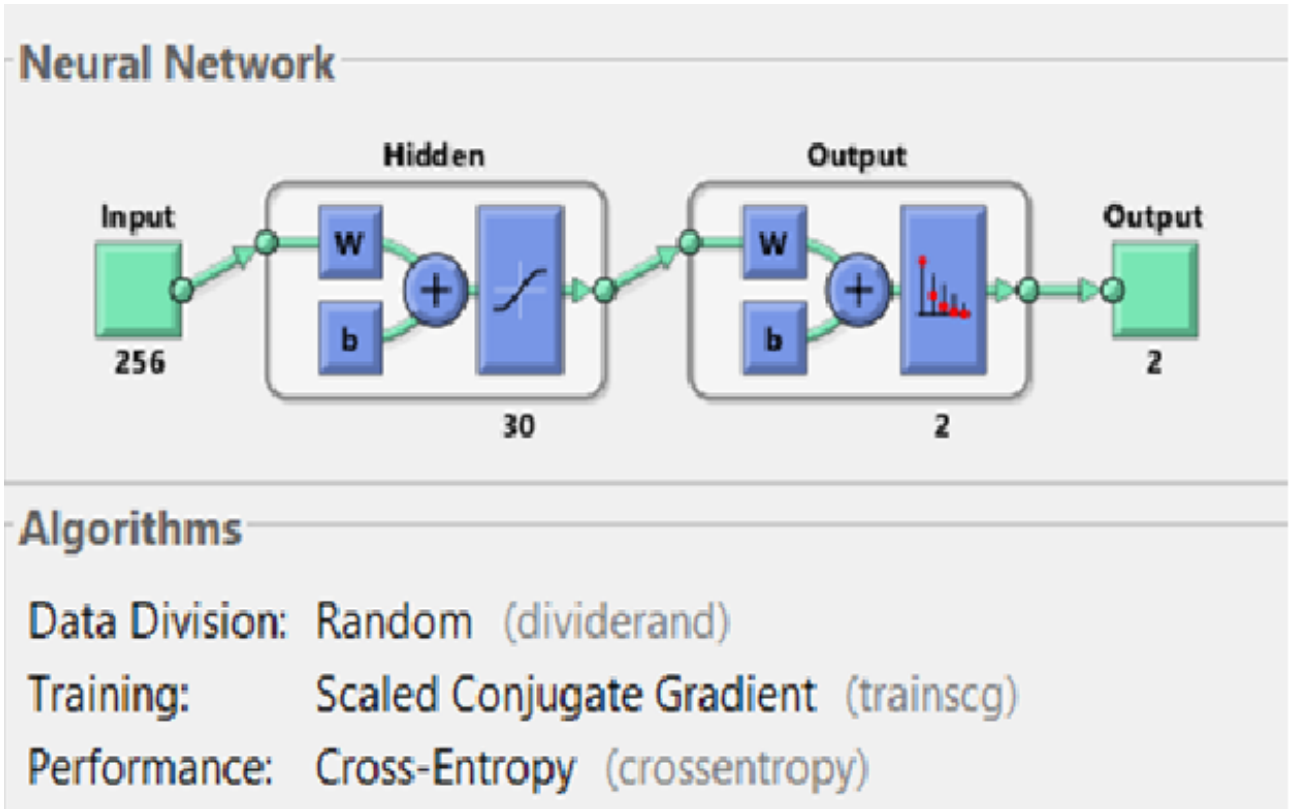

Figure 4. Flowchart describing the workflow of the CNN training and testing performed in the study. CNN: convolutional neural network; ROI: region of interest.

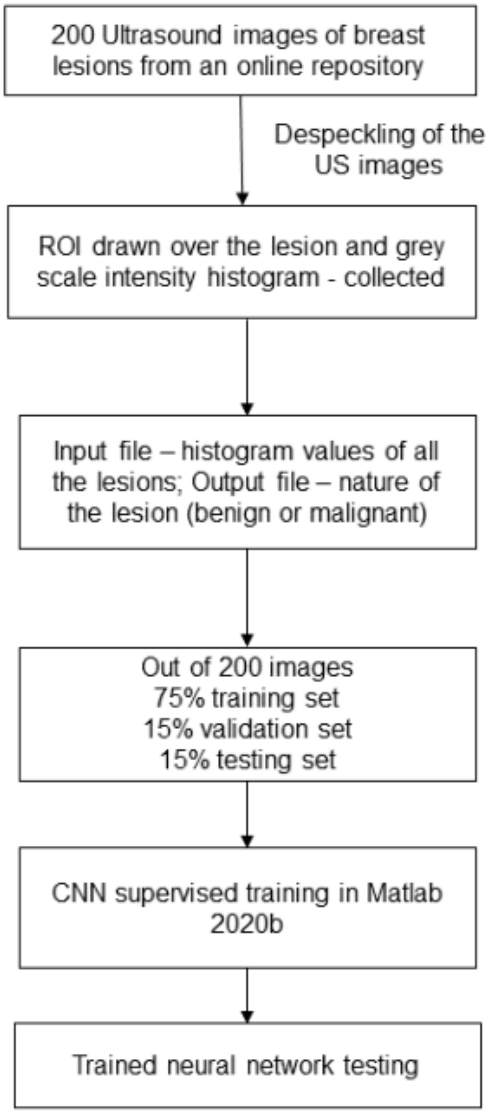

Results

The supervised training was completed in ~1 second. The training of the CNN took 20 iterations (1 iteration=1 epoch in our study) with 6 validation checks.

The performance of the CNN was measured using cross entropy as a parameter, and the best validation performance was 0.073783, achieved at the 14th epoch (Figure 5).

The error histogram exhibiting the number of errors committed by the CNN during the training in each set was acquired (Figure 6).

The results of the training were derived, and the trained neural network was tested using the same data set. The confusion matrix and ROC of the results achieved by the trained neural network was plotted.

The following describes the values useful for the clinicians in making the diagnostic decision. During training, the CNN on the testing data set showed a sensitivity of 80.0% and a specificity of 93.3%. The accuracy and precision were 86.7% and 92.3%, respectively. The trained neural network, which was tested on the whole data set, showed good results. The sensitivity was 94.9% and the specificity was 94.1%. The negative predictive value and precision of the trained CNN were 95% and 94%, respectively, with an accuracy of 94.5% (Figure 7). The receiver operating curves of the CNN on various data sets during training and the trained CNN, with class 1 as benign breast lesion and class 2 as malignant breast lesion, plotted in the x-axis as the false-positive rate and y-axis as true-positive rate are shown (Figure 8).

Figure 5. Performance graph of the convolutional neural network training (x-axis: epoch; y-axis: cross-entropy). The best validation performance achieved was 0.0737829 at the 14th epoch. The mean performance was 0.1381, and the median was 0.08445. The red graph shows the performance of the test data set (70% of the data).

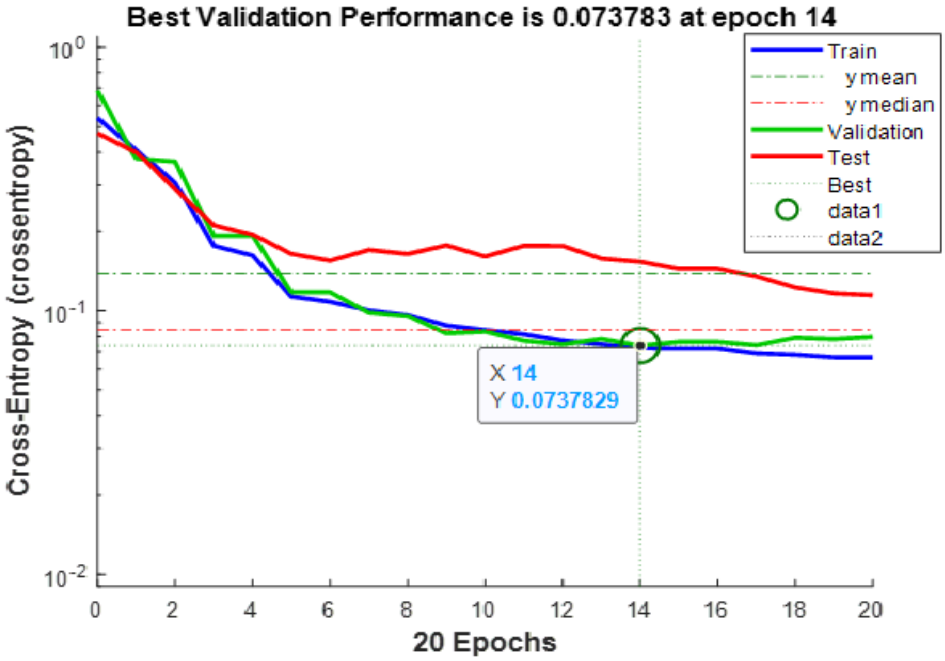

Figure 6. Error histogram with 20 bins (x-axis: error values; y-axis: instances). The histogram shows that zero error lies between the two bins with center error values –0.04756 and 0.04756. The bins with center error values –0.04756 and 0.04756 show the majority of the data fed to the convolutional neural network having error values in that range followed by bins with center error values –0.1427 and 0.1427.

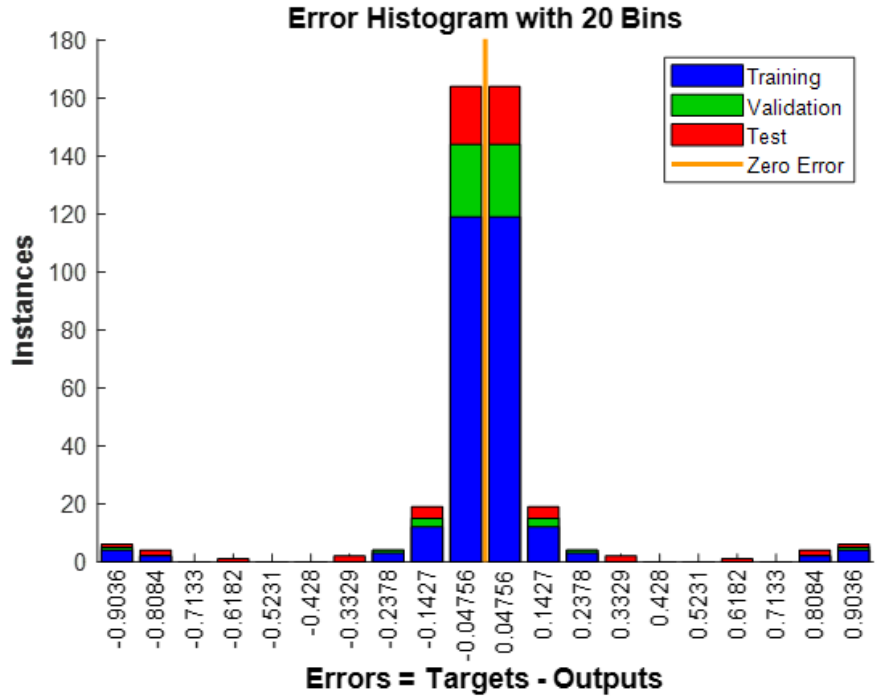

Figure 7. A) Confusion matrices obtained by training the convolutional neural network (CNN) of the training data, validation data, test data, and all the data sets combined. B) Confusion matrix of the trained CNN exhibiting an accuracy of 94.5% and precision of 94%.

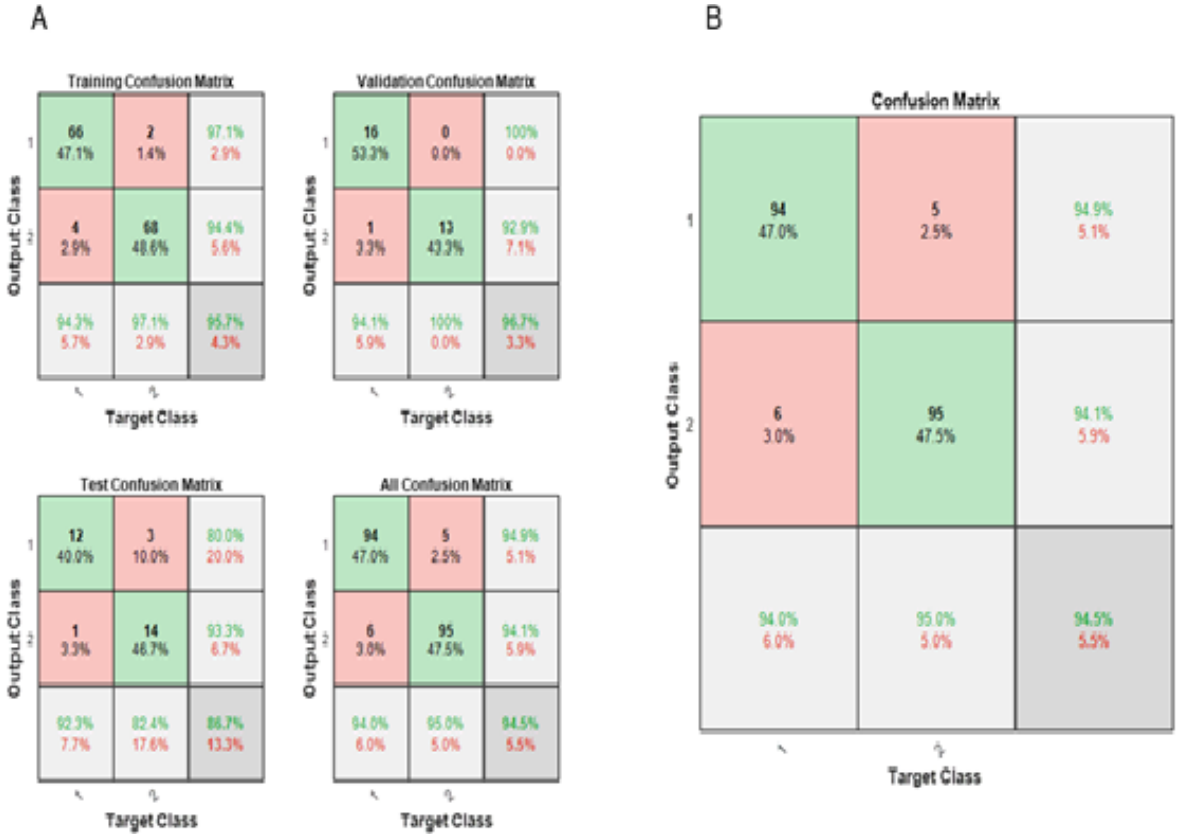

Figure 8. A) ROCs of the training set, validation set, test set, and all sets combined (Class 1: benign; Class 2: malignant). B) ROC of the trained convolutional neural network showing excellent performance with detection rate. ROC: receiver operating curve.

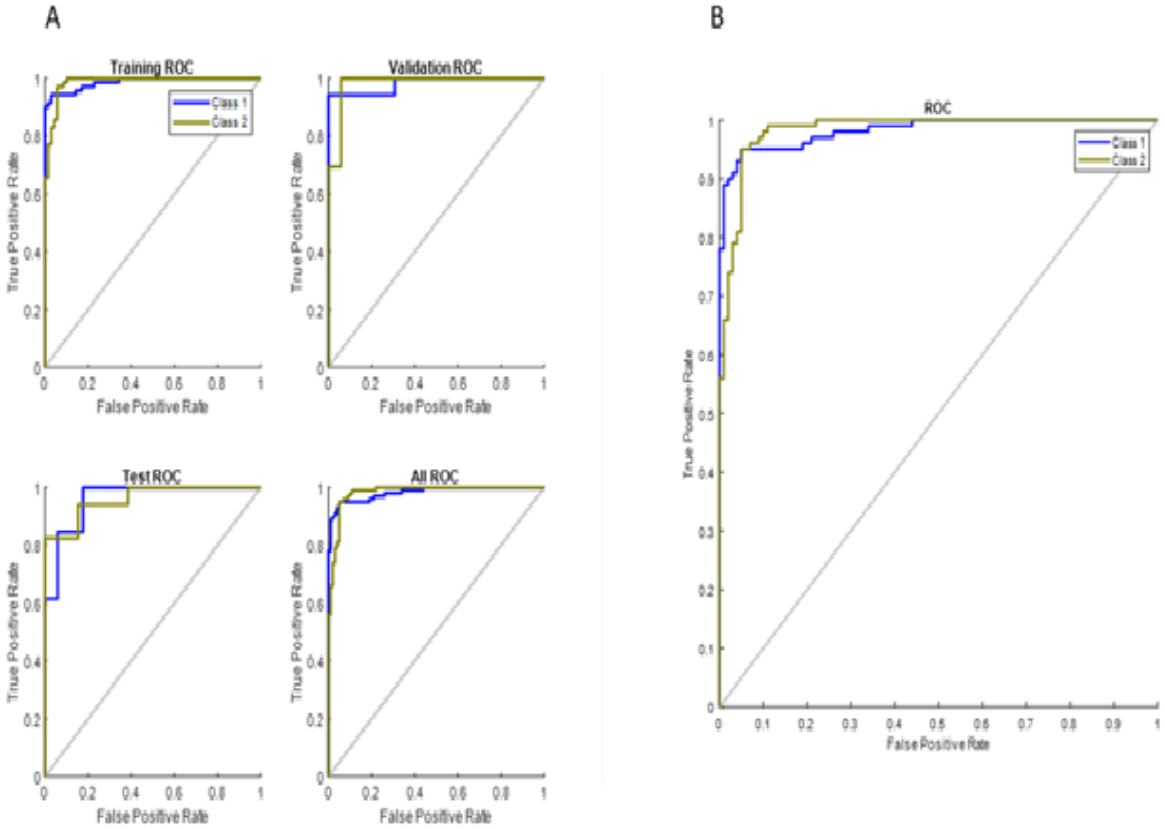

Discussion

Ultrasonograms can be used to define the morphological features of a lesion, and the lesion is reported with details of shape, margin, echo pattern, location, and posterior acoustic characteristics [10]. Terms used for reporting echo findings are subjective and qualitative. In a study conducted by Rahbar et al [11], malignancy was detected in 67% of the lesions with spiculated margins. Of all the lesions, 71% of the hypoechoic lesions and 100% of the hyperechoic lesions turned out to be benign. The US Breast Imaging Reporting and Data System was created to standardize breast US reporting and thereby categorizing breast lesions based on their risk of being a malignancy [12]. Positive predictive values of US features—spiculated margin and irregular shape—were 86% and 62%, respectively, in a study conducted with 403 patients, among which 35% had malignancy. Hyperechoic patterns were not present in any of the malignant lesions in this study [13]. Histogram analysis of gray scale intensity is a quantitative measure of the echo pattern in a lesion, hence can provide objective assessment of the lesion. Erol et al [14] used lesion echogenicity ratios to differentiate between malignant and benign lesions. The mean lesion echogenicity ratio values for benign lesions was 1.63 (SD 0.41) and for malignant lesions was 3.1 (SD 0.87), and the study showed statistically significant difference between malignant and benign lesions.

Machine learning algorithms to diagnose malignant lesions is a highly pursued research topic. A study using a fuzzy support vector machine analyzed eight textural features, three fractal dimensions, and two histogram-based features in identifying a malignant breast lesion in 87 cases reported an accuracy, sensitivity, specificity, precision predictive value, and negative predictive value of 94.25%, 91.67%, 96.08%, 94.29%, and 94.23%, respectively [15]. They analyzed mean, variance, skewness, kurtosis, energy, and entropy of the histogram values using stepwise regression and found out that variance and entropy were the two histogram-based optimal variables that will be useful in diagnosing malignancy. A study by Wang et al [16] used a multi-view CNN and had a sensitivity of 88.6% and specificity of 87.6% in detecting malignancy in ultrasonogram images of 316 breast lesions in two views.

Gray scale intensity values as a sole predictor of malignancy with the help of neural networks was explored in this study. Our study showed an extraordinary performance with an accuracy of 94.5% and precision of 94%, which is slightly higher than in the study by Shi et al [15]. The advantages of our study were that only gray scale histogram values were used to diagnose malignancy, which is easy and convenient to collect, making it easier to reproduce, and that a simple neural network was used with a training duration of ~1 second, making it a viable option in low-resource settings with limited professionals.

The limitations of this study were that US acquisition parameters were not mentioned in the data set, which makes it difficult to standardize the protocol to the general population since US imaging parameters might vary from place to place, and ROIs drawn by different people can vary, which can affect the histogram values, but the effect will be minimal since CNN analyzes the skewness, entropy, variance, kurtosis, and energy of the gray scale intensity values.

Conflicts of Interest

None declared.

References

1. Malvia S, Bagadi SA, Dubey US, Saxena S. Epidemiology of breast cancer in Indian women. Asia Pac J Clin Oncol 2017 Aug;13(4):289-295. [doi: 10.1111/ajco.12661] [Medline: 28181405]
2. Azamjah N, Soltan-Zadeh Y, Zayeri F. Global trend of breast cancer mortality rate: a 25-year study. Asian Pac J Cancer Prev 2019 Jul 01;20(7):2015-2020 [FREE Full text] [doi: 10.31557/APJCP.2019.20.7.2015] [Medline: 31350959]
3. Devolli-Disha E, Manxhuka-Kërliu S, Ymeri H, Kutllovci A. Comparative accuracy of mammography and ultrasound in women with breast symptoms according to age and breast density. Bosn J Basic Med Sci 2009 May;9(2):131-136. [doi: 10.17305/bjbms.2009.2832] [Medline: 19485945]
4. Kim J, Kim HJ, Kim C, Kim WH. Artificial intelligence in breast ultrasonography. Ultrasonography 2021 Apr;40(2):183-190. [doi: 10.14366/usg.20117] [Medline: 33430577]
5. Goldberg V, Manduca A, Ewert DL, Gisvold JJ, Greenleaf JF. Improvement in specificity of ultrasonography for diagnosis of breast tumors by means of artificial intelligence. Med Phys 1992;19(6):1475-1481. [doi: 10.1118/1.596804] [Medline: 1461212]
6. Dumane V, Shankar PM, Piccoli CW, Reid JM, Forsberg F, Goldberg BB. Computer aided classification of masses in ultrasonic mammography. Med Phys 2002 Sep;29(9):1968-1973. [doi: 10.1118/1.1500401] [Medline: 12349916]
7. Rodrigues PS. Breast ultrasound image. Mendeley Data. 2017 Dec 31. URL: https://data.mendeley.com/datasets/wmy84gzngw/1 [accessed 2019-12-01]
8. Joel T, Sivakumar R. An extensive review on despeckling of medical ultrasound images using various transformation techniques. Appl Acoustics 2018 Sep;138:18-27. [doi: 10.1016/j.apacoust.2018.03.023]
9. MATLAB. MathWorks. 2020 Aug 26. URL: https://www.mathworks.com/products/matlab.html [accessed 2020-12-01]

10. Blaichman J, Marcus JC, Alsaadi T, El-Khoury M, Meterissian S, Mesurolle B. Sonographic appearance of invasive ductal carcinoma of the breast according to histologic grade. AJR Am J Roentgenol 2012 Sep;199(3):W402-W408. [doi: 10.2214/AJR.11.7374] [Medline: 22915433]
11. Rahbar G, Sie AC, Hansen GC, Prince JS, Melany ML, Reynolds HE, et al. Benign versus malignant solid breast masses: US differentiation. Radiology 1999 Dec;213(3):889-894. [doi: 10.1148/radiology.213.3.r99dc20889] [Medline: 10580971]
12. Magny SJ, Shikhman R, Keppke AL. Breast imaging reporting and data system. StatPearls. 2021. URL: https://pubmed.ncbi.nlm.nih.gov/29083600/ [accessed 2021-04-28]
13. Hong AS, Rosen EL, Soo MS, Baker JA. BI-RADS for sonography: positive and negative predictive values of sonographic features. AJR Am J Roentgenol 2005 Apr;184(4):1260-1265. [doi: 10.2214/ajr.184.4.01841260] [Medline: 15788607]
14. Erol B, Kara T, Gürses C, Karakoyun R, Köroğlu M, Süren D, et al. Gray scale histogram analysis of solid breast lesions with ultrasonography: can lesion echogenicity ratio be used to differentiate the malignancy? Clin Imaging 2013;37(5):871-875. [doi: 10.1016/j.clinimag.2013.04.007] [Medline: 23830704]
15. Shi X, Cheng HD, Hu L. Mass detection and classification in breast ultrasound images using fuzzy SVM. In: Proceedings of the 9th Joint International Conference on Information Sciences. 2006 Presented at: JCIS-06; October 8-11, 2006; Taiwan. [doi: 10.2991/jcis.2006.257]
16. Wang Y, Choi EJ, Choi Y, Zhang H, Jin GY, Ko SB. Breast cancer classification in automated breast ultrasound using multiview convolutional neural network with transfer learning. Ultrasound Med Biol 2020 May;46(5):1119-1132. [doi: 10.1016/j.ultrasmedbio.2020.01.001] [Medline: 32059918]

Abbreviations

CNN: convolutional neural network
ROI: region of interest

Edited by G Eysenbach; submitted 24.08.20; peer-reviewed by P Lei, MI Saripan; comments to author 09.11.20; revised version received 04.03.21; accepted 04.04.21; published 02.06.21.

Please cite as:
Ramachandran A, Kathavarayan Ramu S
Neural Network Pattern Recognition of Ultrasound Image Gray Scale Intensity Histograms of Breast Lesions to Differentiate Between Benign and Malignant Lesions: Analytical Study
JMIR Biomed Eng 2021;6(2):e23808
URL: https://biomedeng.jmir.org/2021/2/e23808
doi:10.2196/23808
PMID:

Original Paper

Integrating Physiological Data Artifacts Detection With Clinical Decision Support Systems: Observational Study

Shermeen Nizami[1*], PhD; Carolyn McGregor AM[2*], PhD; James Robert Green[1*], PhD

[1]Systems and Computer Engineering, Carleton University, Ottawa, ON, Canada

[2]University of Oshawa Institute of Technology, Oshawa, ON, Canada

[*]all authors contributed equally

Corresponding Author:
James Robert Green, PhD
Systems and Computer Engineering
Carleton University
1125 Colonel By Drive
Ottawa, ON, K1S 5B6
Canada
Phone: 1 613 520 2600 ext 1463
Email: jrgreen@sce.carleton.ca

Abstract

Background: Clinical decision support systems (CDSS) have the potential to lower the patient mortality and morbidity rates. However, signal artifacts present in physiological data affect the reliability and accuracy of the CDSS. Moreover, patient monitors and other medical devices generate false alarms while processing physiological data, further leading to alarm fatigue because of increased noise levels, staff disruption, and staff desensitization in busy critical care environments. This adversely affects the quality of care at the patient bedside. Hence, artifact detection (AD) algorithms play a crucial role in assessing the quality of physiological data and mitigating the impact of these artifacts.

Objective: The aim of this study is to evaluate a novel AD framework for integrating AD algorithms with CDSS. We designed the framework with features that support real-time implementation within critical care. In this study, we evaluated the framework and its features in a false alarm reduction study. We developed static framework component models, followed by dynamic framework compositions to formulate four CDSS. We evaluated these formulations using neonatal patient data and validated the six framework features: flexibility, reusability, signal quality indicator standardization, scalability, customizability, and real-time implementation support.

Methods: We developed four exemplar static AD components with standardized requirements and provisions interfaces that facilitate the interoperability of framework components. These AD components were mixed and matched into four different AD compositions to mitigate the artifacts' effects. We developed a novel static clinical event detection component that is integrated with each AD composition to formulate and evaluate a dynamic CDSS for peripheral oxygen saturation (SpO_2) alarm generation. This study collected data from 11 patients with diverse pathologies in the neonatal intensive care unit. Collected data streams and corresponding alarms include pulse rate and SpO_2 measured from a pulse oximeter (Masimo SET SmartPod) integrated with an Infinity Delta monitor and the heart rate derived from electrocardiography leads attached to a second Infinity Delta monitor.

Results: A total of 119 SpO_2 alarms were evaluated. The lowest achievable SpO_2 false alarm rate was 39%, with a sensitivity of 80%. This demonstrates the framework's utility in identifying the best possible dynamic composition to serve the clinical need for false SpO_2 alarm reduction and subsequent alarm fatigue, given the limitations of a small sample size.

Conclusions: The framework features, including reusability, signal quality indicator standardization, scalability, and customizability, allow the evaluation and comparison of novel CDSS formulations. The optimal solution for a CDSS can then be hard-coded and integrated within clinical workflows for real-time implementation. The flexibility to serve different clinical needs and standardized component interoperability of the framework supports the potential for a real-time clinical implementation of AD.

(JMIR Biomed Eng 2021;6(2):e23495) doi:10.2196/23495

KEYWORDS

patient monitoring; clinical decision support; systems architecture; biomedical data analytics; alarm fatigue; physiological data artifacts

Introduction

Clinical Decision Support Systems

Clinical decision support systems (CDSS) are computerized health care analytic systems that have the functionality to integrate patient data for their analyses and detect clinically significant patient events. CDSS has the potential to lower patient mortality and morbidity rates when integrated into critical care workflows [1-5]. Clinical event detection (CED) algorithms that identify clinically significant events and early onset indicators of various pathophysiological diseases may be integrated into the CDSS to further exploit this potential [6-10]. Similarly, parameter derivation algorithms that extract clinically useful low-frequency parameters from high-frequency input data are also essential for clinical decision making [11-14]. However, the inherent presence of signal artifacts in physiological data impacts the reliability and accuracy of the analytical results produced by such algorithms [15]. Moreover, commercial physiologic patient monitors used in clinical settings are built using relatively simplistic proprietary algorithms for preprocessing artifacts [16-18]. This results in an unacceptably high rate of false alarms generated by these patient monitors [19]. Such alarms, termed as nuisance or false alarms, result in increased noise levels, staff disruption, and staff desensitization in busy critical care environments [20-22]. False alarms need to be typically silenced or overridden by staff, which leads to alarm fatigue, causing an even bigger hazard of missed alarms and compromising the quality of care at the patient bedside [21,23,24]. The Emergency Care Research Institute, a Pennsylvania-based patient safety organization, issued an annual report of the top 10 health technology hazards. Leading up to and including 2019, the Emergency Care Research Institute has reported medical device alarms to be among the top 10 hazards. The literature has reported false alarm rates (FAR) greater than 70% [25]. The integrity and quality of data are crucial to the success of any analytic system. Therefore, it is important to design and implement CDSS for assessing the quality of data and issue relevant alarms with a high specificity and low FARs. A recent study suggested behavioral methods to reduce false alarms and alarm fatigue in the neonatal intensive care unit (NICU) [26]. The study was conducted in an NICU in a low-income country (India) [26], whereas our study was conducted in a high-income country (Canada) where the recommended behavioral changes have already been implemented [27].

Artifact Detection

Research groups have published several artifact detection (AD) algorithms to assess the quality of physiologic data and minimize the impact of artifacts before analyzing these data for CED. However, a methodological literature review by the authors conveys common limitations in the application of a vast majority of AD algorithms [28]. In this review, we synthesized more than 80 state-of-the-art AD algorithms and discovered the following six shortcomings: most AD algorithms (1) are designed for one specific type of critical care patient population, (2) are validated on data harvested from a single monitor model, (3) generate signal quality indicators (SQIs) that are not yet standardized for useful integration in clinical workflows, (4) operate either in standalone mode or are tightly coupled with other CDSS applications, (5) are rarely evaluated in the real time, and (6) are not implemented in clinical practice [28]. A more recent review on the initiatives to manage and improve alarm systems taken by means of human, organizational, and technical factors for an improved quality of health care also supports our findings [20]. The review reveals gaps between alarm-related standards and how those standards are translated into practice, especially in a clinical environment that uses multiple alarming medical devices from different manufacturers [20]. This suggests standardization across devices from the same and different manufacturers and the use of machine learning to improve the alarm safety [20].

AD Framework

To address the six shortcomings (1)-(6) that are listed above, we designed and developed a novel, multivariate, component-based, standardized AD framework [29]. For the reader's convenience, the *Methods* section provides the background on framework development, including the design of its components and interfaces by developing a common reference model (CRM). The objective is to facilitate the integration of AD and CED algorithms within the CDSS in a standardized manner. To achieve this, we leveraged six framework features *f1 to f6*, which are listed in then Methods section. We designed the AD framework as a test bed to formulate and evaluate multiple combinations of independently developed AD and CED components. Once a combination of AD and CED is affirmed to satisfy clinical needs through offline testing, then that combination can be evaluated in a real-time environment using the middleware technology. In this way, the transition to real-time clinical implementation and validation can be facilitated by using this framework.

For the reader's convenience, this section summarizes the development of the AD framework, as in a previous study [29]. This section comprises the development of the components and interfaces that provide the framework's end-to-end functionality, a CRM for the standardized communication between components across their interfaces and the framework's features.

Components and Interfaces

A framework comprises components that interact with each other and with the system through one or more interfaces to realize the system goals. An *interface* is defined as a means of communicating with or accessing a component [30]. Clearly defined uniform interfaces enable components to make their own functional requirements explicit as well as to enable specifications of other collaborating components. Interfaces stipulate prerequisites, provisions, and constraints of component operations. A component can have one or more interfaces,

selectively instantiated at the runtime depending on the component's role in a particular composition. As described in a previous study [31], an interface can be categorized as (1) requirement, (2) provision, and (3) configuration. Each component has its own operational requirements, specified by its requirement interface, which defines what the system or other components in the system must provide for the component to function [30]. The provision interface makes explicit what a component can provide either to another component or as a contribution to the system output. The configuration interface incorporates a user-defined functionality, further allowing the user to define the runtime parameters for a particular application. A configuration interface can be part of the user interface designed for a clinician to interact with the system settings.

The AD framework comprises the following components: (1) patient data acquisition (PDA), (2) AD, and (3) CED. Each component is composed of low-level code and the following three interfaces: (1) requirement, (2) provision, and (3) configuration. Framework components can interface as either standalone algorithms or in cascade with the same or different types of components.

Common Reference Model

The standardization of interfaces is key for achieving the system goals. This involves defining unambiguous formalisms with semantics that are commonly understood by all components within the framework. A novel CRM was developed to standardize the definitions for these interfaces to facilitate component interoperability within the AD framework [29]. Multiple medical ontologies are in existence to address the measurement of medical parameters such as LOINC (Logical Observation Identifiers Names and Codes), which is a database and universal standard for identifying medical laboratory observations; Systematized Nomenclature of Human Medicine (SNOMED), which is a multiaxial nomenclature for indexing medical records; and the Fast Healthcare Interoperability Resources which is an interoperability standard created by the standards development organization Health Level 7 to enable health data, including clinical and administrative data, to be quickly and efficiently exchanged across medical devices. The CRM interfaces designed as a part of our framework are easily customizable to match any of these standards. CRM comprises metadata that are intended to establish a common understanding of the meaning or semantics of the data exchanged between component interfaces. This allows all framework components to communicate, regardless of their underlying low-level logic. For example, CRM facilitates interfacing a variety of AD algorithms for different types, frequencies, and quality of physiologic data that are commonly processed by CDSS. In particular, the standardization of SQIs is a novel contribution to the development of CRM. The CRM metadata comprise the following layered schema: PatientData (*PatientID*, *DeviceID*, *Data* (*Type*, *TimeStamp*, *Value*, *SQI (SQType* and *SQValue*))). PatientData represents the patient data exchanged between the components. Its schema consists of three properties, as shown in Figure 1 (*PatientID*, *DeviceID*, and *Data*). *PatientID* identifies the patients with whom the data are associated. It can be any type of patient identifier, such as the patient's admission reference number. *DeviceID* represents the hospital or original equipment manufacturer (OEM) identifier for the patient monitor or other devices from which the data are being acquired. The more complex *Data* property has the following four attributes: *Type*, *TimeStamp*, *Value*, and *SQI*. *Type* is a string variable from a controlled schema, naming the physiological data stream. *TimeStamp* is the time at which each datum is logged. A component may have specific data exchange and processing rates, which require data at specific frequencies. Therefore, *TimeStamp* can be used to (1) derive the frequency of data, (2) align multiple data streams for fusion, and (3) annotate events in real time. *Value* contains the numeric or string value of each datum. An *SQI* may also be associated with each datum. This measure of signal quality is provided by the monitor (via a PDA component) or derived by one or more AD algorithms. The *SQI* for each datum is further described by two attributes: *SQType* and *SQValue*. *SQType* is a string variable from a controlled schema, for example, "binary," "rank," "categorical," or "null." New strings can be introduced in this set in the future. "Null" implies there is no SQI available for that particular data type. *SQValue* depends on *SQType*. For example, if *SQType* is "binary," then *SQValue* belongs to a set of 0 or 1. This schema is extensible when needed for newer CDSS formulations. Our preliminary research demonstrates the instantiation of CRM using XML [32].

At runtime, the PDA component inputs patient data and conforms them to the CRM, which are then consumed by the AD and CED components that comprise the CDSS. AD and CED algorithms, published in the past or future, whether standalone or tightly coupled, may be used in CDSS formulations with modifications as needed. The framework is a unique test bed with features of reusability and scalability. These features allow for the creation of new AD configurations by mixing and matching independently developed or decoupled AD components and integrating those components with CED components to serve varying clinical needs. The AD configuration most suited to a clinical need can then be hard-coded and integrated into the clinical workflow for real-time implementation. For example, some recently developed AD algorithms leverage sensor fusion for motion artifact removal while deriving the heart rate (HR) [33-37]. The implementation of these AD and CED algorithms within the framework simply requires modifying their interfaces to comply with the CRM. This would allow for these algorithms to be tested, compared, or combined with extant or newer algorithms to advance research in the field of signal quality and physiologic monitoring.

Figure 1. Common reference model schema consisting of the patient data metadata used by each component's requirement and provision interfaces at input and output. SQ: signal quality; SQI: signal quality indicator.

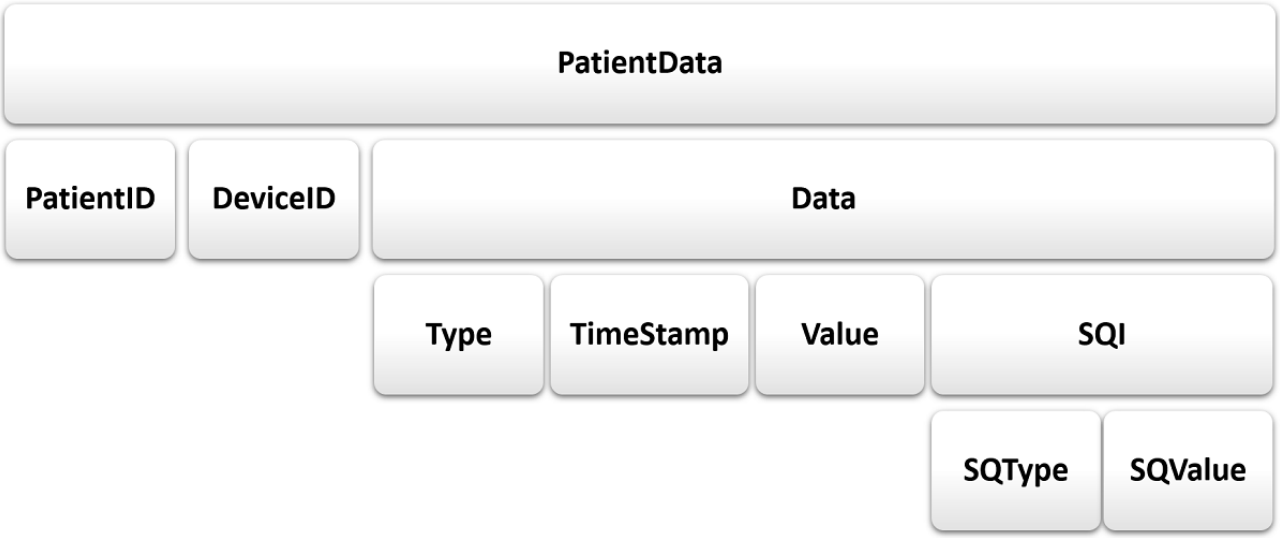

Framework Features

To address the six shortcomings (1)-(6) identified in state-of-the-art AD algorithms in a previous study [28], we developed an AD framework with the following six features *f1* to *f6* The framework design supports: (*f1*) flexibility to serve the needs of patient populations from different types of critical care units through generalization and customizability, (*f2*) reusability across multiple types of physiological data harvested by different OEM monitors, (*f3*) standardized definitions of SQI that promote interoperability and comparison between independently developed components, (*f4*) reusability and scalability by mixing and matching several AD and CED components in various combinations, (*f5*) customizability to evaluate and compare the performance of multiple combinations of independently developed components on offline and potentially real-time patient data when integrated with clinical workflow, and (*f6*) standardized component interfaces that can potentially support real-time clinical implementation of AD. This study validates the six framework features *f1* to *f6*.

Research Contribution

The main contribution of this paper is the dynamic evaluation of the AD framework as a test bed, given the clinical context of false alarm reduction in medical devices. In this study, we first developed a catalog of several exemplar AD components and a single CED component. The interfaces of all these components comply with the CRM, such that they can be integrated within the AD framework. Given the motivation for false alarm reduction, we designed a novel CED component that can generate peripheral oxygen saturation (SpO_2) alarms. We then created four unique CDSS configurations by mixing and matching different AD components from the catalog with the same SpO_2 alarm generation CED component. The *Methods* section describes the research methodology, including the development of the framework component catalog and the four CDSS formulations used for evaluating the framework and its features. This section demonstrates how the framework leverages existing AD algorithms by incorporating them with the SpO_2 alarm–generating CED component. The four configurations are designed and evaluated based on the results and recommendations in the state-of-the-art research linked to the reduction of false alarms generated by OEM monitors. Although CRM has been developed after an extensive review of the literature that summarizes the requirements, provisions, and configurations for many existing AD algorithms, it is expected that the CRM will continue to evolve because a wide variety of new AD and CED algorithms with differing data needs are implemented as components within this framework. For example, a new OEM alarm management system, Philips Care Event, was evaluated along with the optimization of the clinical workflow in the NICU [25]. The OEM system delay time for saturation-related alarms was increased from 10 to 20 seconds, and the averaging time was decreased from 10 to 4 seconds without changing the standard alarm settings. This strategy led to a reduction in the number of $SpO_2 \leq 80\%$ alarms and an increase in nurses' response to alarms [25]. This is an exemplar state-of-the-art CED strategy that can be easily accommodated and evaluated in combination with various AD techniques using our framework to further reduce false alarms and subsequent alarm fatigue. In this way, the framework can facilitate the discovery of optimal CDSS formulations through the mixing and matching of new AD and CED components supported by an evolving CRM.

Methods section describes the framework evaluation methodology comprising the data collection method and performance evaluation metrics of sensitivity (Sn) and FAR. For framework validation, we used real patient data collected from 11 neonates during a clinical study at the NICU of the Children's Hospital of Eastern Ontario (CHEO), Ottawa, Ontario, Canada. Harvested data streams include HR, pulse rate (PR), SpO_2, and their corresponding alarms from physiologic patient monitors. Several conditions, such as hypothermia (peripheral vasoconstriction), edema (increased thickness and, therefore, diffusion distance for oxygen), increased skin pigmentation, and shock, are known to decrease the clinical reliability of SpO_2. None of the patients in this study had any such condition.

Results section provides the performance evaluation results in terms of Sn and FAR of the SpO_2 alarms generated by each of the four CDSS formulations. Once a CDSS formulation is affirmed to satisfy clinical needs through offline testing by applying this methodology, the optimal combination can be evaluated in a real-time environment using the middleware technology. This will facilitate the real-time implementation of the optimal CDSS formulation through hard-coded integration within clinical workflows.

It should be noted that all four CDSS formulations deploy the same CED component for SpO_2 alarm generation. Hence, the sensitivity of the CED component to the error profiles and the impact of errors remain controlled or constant across all experiments. Therefore, the reported Sn and FAR values reflect the performance of the four different AD configurations, regardless of the performance of the CED component. In other words, the framework evaluation reported here remains independent of the performance of the CED component. This validates the use of the framework as a test bed to discover the optimal combination of AD components with a CED component that is designed for a specific clinical problem. In the future, the framework can be similarly deployed with another CED component for different clinical problems.

Discussion section discusses the research contributions and provides a detailed discussion on the validation of the six framework features (*f1*) to (*f6*). Section 7 concludes the paper and suggests directions for future work.

Methods

Overview

According to Larsen [30], beyond designing and building a component-based framework, its evaluation requires static models that illustrate component structures as well as dynamic models that illustrate component collaboration. This paper first develops a catalog of static PDA, AD, and CED components. Subsequently, four dynamic compositions of these components were formulated and evaluated using real patient data. Each of the AD components processes physiological data streams in the form of numeric or string values, and the CED component generates alarms on the SpO_2 data stream. The requirements and provision interfaces of all components comply with the CRM, such that they can be integrated within the AD framework. Each configuration is integrated with PDA and CED components to formulate a CDSS that generates SpO_2 alarms at its output.

The following subsections expand upon this research methodology: *Components Catalog* develops a catalog of framework components; *CDSS Formulations* mixes and matches these components to build and evaluate four different CDSS formulations; and the *Evaluation* subsection uses real patient data to evaluate the performance of each CDSS formulation, thereby validating the use of the framework as a test bed; and determining the optimal CDSS formulation for SpO_2 alarm generation. Once a combination is affirmed to satisfy clinical needs through offline testing by applying this method, the optimal combination can be evaluated in a real-time environment using the middleware technology. This will facilitate the real-time implementation of the optimal CDSS formulation through hard-coded integration within clinical workflows.

Components Catalog

In this subsection, we develop a catalog of framework components comprising an original PDA component, four AD components, and one novel CED component. The catalog represents a model instantiation of the framework comprising the original PDA and CED components designed in collaboration with our clinical partners. The catalog is not meant to represent an exhaustive or particularly novel set of AD components; rather, it tailors the interfaces of existing AD algorithms to comply with the CRM.

PDA Component

As defined in our earlier research, the PDA component inputs patient data from sources that include, but are not limited to, OEM patient monitors, clinical data entry, lab results, physician's order, and patient demographics from electronic health records [29]. In this research, the PDA inputs the physiological data and alarm streams from the OEM monitors and translates these data to the schema defined by the CRM. It then feeds these data to one or more AD components, as shown in the CDSS flowcharts in Figure 2. In these workflows, the hardware and software requirements are factored in the PDA component. The hardware comprises the Digi International Edgeport4 (Digi International), which consists of the Eltima Port Monitor Professional Edition Software v4.x (Eltima Software) for data logging with additional customized software written in JAVA to conform the OEM-generated data streams to the CRM. Specifically, the *Data.Type* (SpO_2, HR, PR, and alarm status) and corresponding *Data.Values* were extracted from each interleaved OEM data packet. Each packet was produced by the monitor at 0.5 Hz. The low-level code of the PDA component interpolated and synchronized the data streams at 1 Hz. As the OEM monitors fail to provide an explicit SQI stream for any of the data types, a default SQI stream with a *SQType*="binary" and *SQValue*=1 is generated by the PDA component for each data type using MATLAB (MathWorks).

Figure 2. Low-level component code for clinical event detection and generation of peripheral oxygen saturation alarms. SpO2: peripheral oxygen saturation; SQI: signal quality indicator.

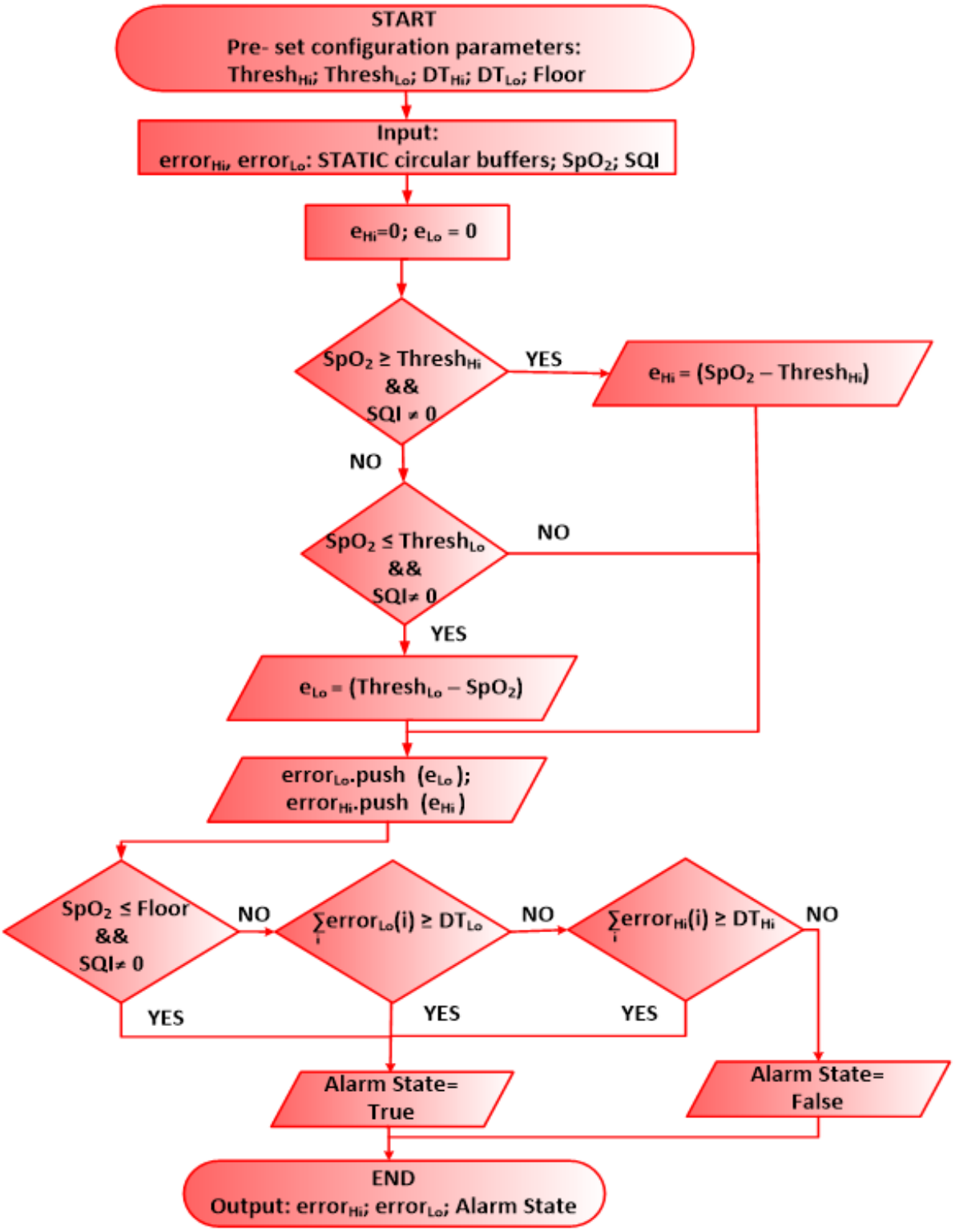

AD Components

We surveyed a wide variety of techniques used by AD algorithms to detect, mitigate, and suppress physiological artifacts that are found in clinical settings [28]. To demonstrate the framework composition, we developed four AD components exemplifying the following diverse AD functionalities: (1) data and SQI deinterlacing, (2) SQI fusion, (3) data fusion, and (4) data smoothing. Although each exemplar component differs in its low-level code, all components conform to the CRM. The low-level code and configuration interfaces for each functional group of the components are described as follows.

ADDIL DeInterlace Component

Some monitors produce a single output stream, which is, in fact, interlaced with the data and SQI. The AD_{DIL} component is

designed to deinterlace (*DIL*) these two information streams by allowing the user to define a set of symbols (*artSyms*) to be associated with the corresponding SQI values. Typically, *artSyms* is a list of artifact indicators specified by the manufacturer, which could be either numeric or string values that replace the value of the datum. For example, for Infinity monitors (Dräger Medical Systems), the set of *artSyms* would include {NaN,^^,5}, where Not-a-number (NaN) is substituted for any missing datum, ^^ is an artifact indicator, and 5 is an alarm state (ie, part of the alarms stream) indicating a lead disconnection. Therefore, a data segment interlaced with artifacts is logged with the corresponding *artSyms* value. In a different example, Philips Intellivue MP70 monitors (Philips) generate a value of "2" in the alarms data stream in case of leads disconnection. However, with the alarm data stream connected to the input of the AD_{DIL} component, the value "2" can be identified by the component as an *artSyms*. In such a way, the component can deinterlace the alarms stream and generate a corresponding binary SQI stream, where the value "2" would be replaced by a 0. The low-level code for AD_{DIL} is given by equation (1).

if (Data.Value(i) artSyms); $SQI_{out}(i)=SQI_{Match}$(Data.Value(i)); end **(1)**

The configuration interface of the AD_{DIL} component specifies the Data.Type to be examined, *artSyms*, and the corresponding set of *SQValue* (SQI_{Match}). This AD component produces a "rank" *SQType*, with "binary" being a special case of "rank," where SQI_{Match}=0. Multiple instances of this component were cascaded in the AD framework in this validation study.

ADFuseSQI Fuse SQI Component

The $AD_{FuseSQI}$ component accepts more than one data stream at its requirements interface, along with the respective SQI of each stream. This component combines *N* incoming SQI inputs to generate a single fused SQI (*FuseSQI*). The fused SQI value is equal to the operator, that is, the minimum, maximum, or average SQI value from all the input SQI data at any given instant. This requires all the input *SQTypes* to be the same. The low-level code for $AD_{FuseSQI}$ is shown in equation (2).

$SQI_{out}(i)$=operator (SQI_1, SQI_2,..., SQI_N) **(2)**

The configuration interface of the $AD_{FuseSQI}$ component defines *N*, the required input *SQType* (same as output), and the operator (min, max, and avg) to be applied to all input SQI values. In addition, the configuration interface can specify which data types to forward at the provision interface, as only a subset of the input streams may be required beyond this component. Equation (2) is a relatively simple depiction of data fusion. Data can be fused at different levels of abstraction, requiring a more complex combination of operators and weighting [38].

ADDiff Differential Component

The AD_{Diff} component calculates an absolute differential error function between two input data streams, $Data_1$ and $Data_2$. This error value was then compared with a configured threshold. The input "binary" SQI streams are examined such that if either stream has a poor signal quality, then the output *SQValue*=0. This component can be used in the case where two independent measurements of the same physiological parameter are provided; then, this component will derive an SQI by exploiting data fusion. The configuration interface specifies the *output SQType* to be produced; the *Data.Type* of $Data_1$ and $Data_2$; the number of SQI thresholds, n_{Thresh}, to be applied to the difference; the ordered set of thresholds ($SQThresh_j;j=1:n_{Thresh}$); and the set of n_{Thresh}+1 *SQValues* (SQI_j) corresponding to each threshold with the additional *SQValue* for the default case ($SQI_{default}$). The configuration interface can specify which data types to forward at the provision interface. The low-level code for this component is illustrated in equation (3), as follows:

$SQI_{out}(i)=SQI_{default}$;
if ($Data_1$.SQI.SQValue(i)==0) || ($Data_2$.SQI.SQValue(i)==0);
return; diff=|$Data_1$.Value(i)−$Data_2$.Value(i)|;
for j=1: n_{Thresh}
{if (diff ≤ $SQThresh_j$){$SQI_{out}(i)=SQI_j$;break;}}end
(3)

The AD_{Diff} component can derive a "rank" *SQType* stream from HR and PR streams by configuring the component to have *output SQType* set to "rank"; the *Data.Type* of $Data_1$=HR and $Data_2$=PR; n_{Thresh}=3; *SQThresh*={6,12,18}; and SQI_j={3,2,1,0}, where the $SQI_{default}$=0. This configuration of the AD_{Diff} component was used in the validation study.

For example, consider the work on wearable devices and systems published by He et al [39]. Their study synchronously collected the data of ballistocardiogram, electrocardiography (ECG), and photoplethysmography. Their study suggests checking if all three physiological signals measure the same values for HR so that this information can be used to ensure that the acquired data are not corrupted. However, their study did not demonstrate whether and how it checks for data quality. Such a system would benefit from using the AD_{Diff} component.

ADMedFilt Median Filter Component

The $AD_{MedFilt}$ component implements a median filter (*MedFilt*). It is used for smoothing a stream of data to mediate abrupt transient artifacts. The configuration interface defines the size of the sliding window Med_{WW} for use while computing the median value. Its requirement interface inputs a single data type and its corresponding SQI stream. Each datum in the output data stream was equal to the median of the past Med_{WW} input data samples. Only a subset of these Med_{WW} may actually be used in computing the median because the $AD_{MedFilt}$ component only includes the data within the sliding window for which the input SQI is acceptable. The SQI stream passed through this component and remained unchanged. By comparing the filtered and unfiltered data using an AD_{Diff} component, one can compute an SQI proportional to the degree of smoothing applied to each point. The $AD_{MedFilt}$ component was used in CDSS formulations in this study.

CED Component

In this subsection, we develop a novel CED component that generates SpO_2 alarms. By discussing and reaching consensus with our clinical collaborators at CHEO, we translated clinical rules into low-level logic to create a CED component with a requirements interface that conforms to the CRM. Alarm generation studies suggest these two approaches to reduce the FAR: (1) modifying or adjusting the alarm thresholds and (2) introducing alarm annunciation delays, that is, a delay between when an alarm threshold is crossed and when the alert is sounded or displayed [25,40-43]. These studies test alarm annunciation delays anywhere from 5 to 120 seconds for a variety of physiological data types. However, none of these studies quantify the trade-off between Sn and FAR resulting from their suggested alarm generation algorithms. In our study, the CED component incorporates both approaches described above to reduce FAR. Its low-level code allows for adjusting the alarm thresholds by reduction in the lower SpO_2 alarm threshold and increment in the upper SpO_2 alarm threshold. During evaluation, both limits were adjusted by 3%, which corresponds to the manufacturer-specified margin of error in the accuracy of the pulse oximeter reading. Therefore, the low alarm threshold, $Thresh_{Lo}$, is breached if the SpO_2 value is lower than the alarm threshold of the OEM monitor by at least 3%, and the upper alarm threshold $Thresh_{Hi}$ is breached if the SpO_2 value is higher than the alarm threshold of the OEM monitor by at least 3%. Incorporating the second approach, the low-level code of the CED allows for tuning the alarm annunciation delays (CED_{DT}) between 5 and 60 seconds.

Figure 2 shows a flowchart of the low-level source code of the CED component. In this case, the user is an expert who composes the CDSS in collaboration with the clinician. The user can set tunable parameters at the configuration interface, including values for $Thresh_{Lo}$, $Thresh_{Hi}$, DT_{LO}, DT_{HI}, and Floor. Floor is an absolute minimum SpO_2 value determined by clinicians, typically in the range of 50%-75%. We set a Floor value below because SpO_2 sensors are unable to calibrate at such low values; hence, the true state of the patient can no longer be determined, and the CED must alarm to alert the clinician to come and check the patient. The CED continuously compares the SpO_2 value with the lower and upper limits, $Thresh_{Lo}$ and $Thresh_{Hi}$, respectively. A history of threshold breaches gets stored in circular buffers, $error_{Lo}$ and $error_{Hi}$. These breaches are summed over a sliding window such that the total error is a function of both the magnitude and duration of the threshold breaches. The integrated error is continuously compared with the tunable lower and upper decision thresholds, DT_{LO} and $DT_{HI.}$ These decision thresholds are set proportional to the CED_{DT} value, which is set at the configuration interface of the CED component. Specifically, DT_{LO} is set equal to CED_{DT}, and DT_{HI} is set to twice the CED_{DT} because high SpO_2 alarms are not clinically deemed to be as dangerous as low SpO_2 alarms. Therefore, the CED waits twice as long to generate a high SpO_2 alarm as compared with a low SpO_2 alarm. The decision to generate an alarm is based on three conditions, as shown in Figure 2. The CED generates an alarm if the incoming SpO_2 value is less than or equal to the set value of Floor and the incoming SQI is not zero, or if the integrated errors, namely $error_{Lo}$ or $error_{Hi}$, exceed DT_{LO} or DT_{HI}, respectively. Here, we configured parameters suitable for the neonatal population. Users may tune the parameters specific to other patient populations.

CDSS Formulations

This section describes the dynamic framework compositions of the four CDSS formulations. MATLAB was used for the dynamic framework modeling. Table 1 lists the requirements, provisions, and configuration interfaces for each AD component deployed in the four CDSS formulations.

Table 1. Artifact detection component interfaces used in clinical decision support systems formulations.

AD[a] component	Interface		
	Requirements	Provisions	Configuration
CDSS[b] #1 and CDSS #2			
AD_{Dil}	[SpO_2[c] Alarms, SQI[d]]	[SpO_2Alarms, SQI]	*artSyms*[e]{NaN[f],^^,5}
AD_{Dil}	[SpO_2, SQI]	[SpO_2, SQI]	*artSyms*{NaN,^^,5}
$AD_{FuseSQI}$	[SpO_2 Alarms, SQI]; [SpO_2, SQI]	[SpO_2, SQI]	N=2; operator (min); *SQType*[g]="binary"
CDSS #2 (additional component)			
$AD_{MedFilt}$	[SpO_2, SQI]	[SpO_{2Med}, SQI]	Med_{WW}[h] *={5,10,20,25,30,35,60}*
CDSS # 3 and CDSS #4			
AD_{Dil}	[HR[i], SQI]	[HR, SQI]	*artSyms*{NaN,^^,5}
AD_{Dil}	[PR[j], SQI]	[PR, SQI]	*artSyms*{NaN,^^,5}
AD_{Dil}	[SpO_2, SQI]	[SpO_2, SQI]	*artSyms*{NaN,^^,5}
AD_{Dil}	[SpO_2Alarms, SQI]	[SpO_2 Alarms, SQI]	*artSyms*{NaN,^^,5}
$AD_{FuseSQI}$	[SpO_2Alarms, SQI]; [SpO_2, SQI]	[SpO_2, SQI]	*N*=2;operator(min); *SQType*="binary"
AD_{Diff}	[HR, SQI]; [PR, SQI]	[PR, SQI]	*Data1.Type="HR";Data2.Type="PR";SQType*="binary"; *SQThresh*={6,12,18};$SQI_{default}$=*0*
$AD_{FuseSQI}$	[SpO_2, SQI]; [PR, SQI]	[SpO_2, SQI];	N=2; operator(min); *SQType*="binary"
CDSS # 4 (additional component)			
$AD_{MedFilt}$	[SpO_2, SQI]	[SpO_{2Med}, SQI]	Med_{WW} *={5,10,20,25,30,35,60}*

[a]AD: artifact detection.

[b]CDSS: clinical decision support systems.

[c]SpO_2: peripheral oxygen saturation.

[d]SQI: signal quality indicator.

[e]*artSyms*: a list of artifact indicators with corresponding values of SQI specified by the manufacturer.

[f]NaN: Not-a-number.

[g]SQType: a string variable from a controlled schema with corresponding types of SQI.

[h]Med_{WW}: size of the sliding window of the median filter.

[i]HR: heart rate.

[j]PR: pulse rate.

CDSS #1

CDSS #1 constitutes the simplest of the four compositions designed for this study. A flowchart for CDSS #1 is shown in Figure 3. This flowchart has three functional horizontal swim lanes, depicting the PDA, AD, and CED components of the integrated CDSS. Each data stream is represented by a tuple with both data and SQI information. The input data stream is sourced only by the SpO_2 sensor comprising two data types, namely, SpO_2 and SpO_2 alarm status (*SpO_2Alarm*). The low-level logic of the PDA component maps the incoming values to its respective data type (*SpO_2 or SpO_2Alarm*) and assigns a default *SQValue* of 1 to each datum of each *Data.Type* because an SQI value is not provided by the OEM monitor in this case.

The AD composition pipeline in CDSS #1 consists of two ADDILs and one $AD_{FuseSQI}$ component. The AD_{DIL} component deinterlaces the OEM-generated artifacts, whereas the $AD_{FuseSQI}$ component combines the SQI streams from the two AD_{DIL} components. The PDA provides *SpO_2* and its associated *SQI* stream to one instantiation of AD_{DIL} while providing *SpO_2Alarm* and its *SQI* stream to the second instantiation of AD_{DIL}. The low-level code of the AD_{DIL} component deinterlaces the OEM-specified artifact values. Here, the user-set configuration interface includes *artSyms*={NaN,^^,5} and SQI_{Match}=0. The "NaN" string implies missing data, and the "^^" symbol represents OEM-specified artifact values in the *SpO_2* stream, whereas "5" is interlaced within the *SpO_2Alarm* to imply that the SpO_2 sensor is off. Hence, the use of the two AD_{DIL} components would provide the original data streams of

Data.TypeSpO$_2$ and *SpO$_2$Alarm*, along with their respective *SQI* streams, with *SQValue*=0 wherever the *Data.Value* is equal to any one of the *artSyms*. These 2 data streams and their associated *SQI* streams are then input to the requirements interface of an AD$_{FuseSQI}$ component. The low-level code of the AD$_{FuseSQI}$ component fuses two or more incoming *SQI* inputs to generate a single fused *SQI* value. In this formulation, the operator is set to *min*; hence, it provides an output *SQValue* that is the minimum of the 2 input *SQValue* for which *SQType*="binary." As shown in Figure 3, this output SQI stream is associated with the original SpO$_2$ stream that is required by the CED component.

Figure 3. Flowchart showing the patient data acquisition, artifact detection, and clinical event detection components in clinical decision support systems CDSS # 1 and 2 formulations. CDSS: clinical decision support systems; ECG: electrocardiography; HR: heart rate; PDA: patient data acquisition; PPG: photoplethysmography; PR: pulse rate; SpO2: peripheral oxygen saturation; SQI: signal quality indicator.

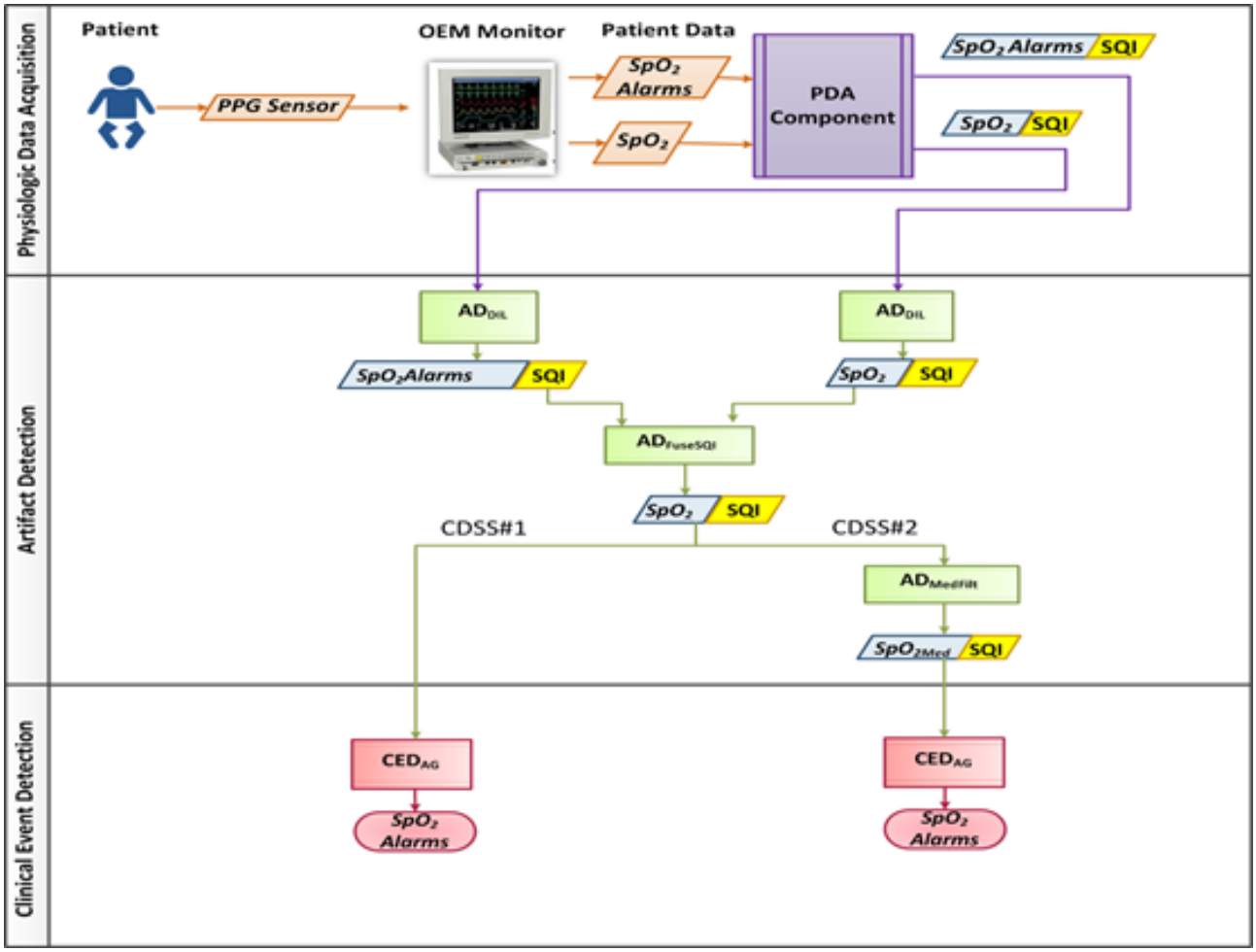

CDSS #2

CDSS #2 extends the CDSS #1 formulation by adding an AD$_{MedFilt}$ component to process the *SpO$_2$* data stream through a median filter for reducing transient artifacts. This extension is labeled CDSS #2 in Figure 3. The low-level code of the AD$_{MedFilt}$ configuration interface comprises a tunable parameter *Med$_{WW=}${5,10,20,25,30,35,60}*, and the component produces a median filtered *SpO$_{2Med}$* data stream and its associated SQI stream, which are then passed to the requirements interface of the CED component.

CDSS #3

CDSS #3 leverages data fusion to derive an estimate of the signal quality for *SpO$_2$*. Here, an AD$_{Diff}$ component computes the difference between the PR and HR. Physiologically, PR and HR are equal, representing the mechanical and electrical pumping rates of the heart, respectively. Therefore, any difference between PR and HR serves as a proxy for signal quality measurements. In this study, HR is considered as the gold standard. Therefore, a large difference between the instantaneous PR and HR values indicates that the PR has deviated and is not reliable. In this case, a low SQI is assigned to both PR and SpO$_2$ because both are sourced from the same sensor. Figure 4 shows the PDA, AD, and CED components in the flowchart for CDSS #3. The low-level code of the AD$_{Diff}$ component computes the difference between the instantaneous HR and PR values. By comparing that difference to a threshold, a "binary" *SQType* is generated, which is then passed to the requirements interface of the CED component. The configuration interface was set with a single threshold to produce a "binary" *SQType*. The SQI threshold (*SQThresh*) is varied in the range {6,12,18} to examine its effect, and the results are reported separately for each.

Figure 4. Flowchart showing the patient data acquisition, artifact detection, and clinical event detection components in clinical decision support systems CDSS # 3and 4 formulations. CDSS: clinical decision support systems; ECG: electrocardiography; HR: heart rate; PDA: patient data acquisition; PPG: photoplethysmography; PR: pulse rate; SpO2: peripheral oxygen saturation; SQI: signal quality indicator.

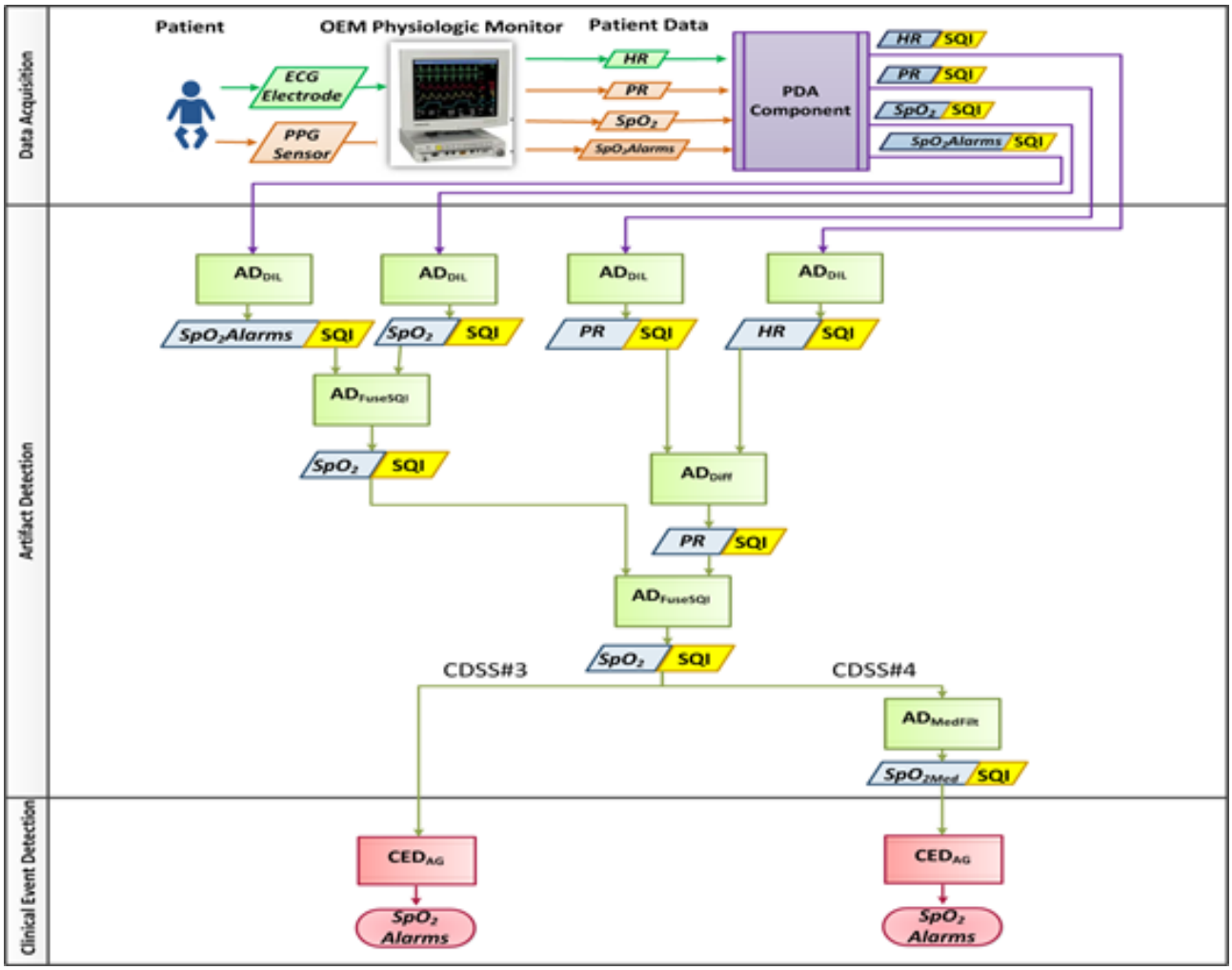

CDSS #4

CDSS #4 builds on the composition of CDSS #3, as depicted in Figure 4. Here, an $AD_{MedFilt}$ component is added such that the SpO_2 data stream can be median filtered to produce SpO_{2Med} data and SQI streams, which are then fed to the requirements interface of the CED component. The tuned values of Med_{WW} include {5,10,20,25,30,35,60}.

Evaluation

Clinical Data Collection

Data were collected during a clinical study conducted in the CHEO NICU. The study was approved by the hospital's Research Ethics Board. In total, 11 neonatal patients with diverse pathologies were enrolled in this study. The following time-stamped data streams and corresponding alarms were collected simultaneously from each infant at a frequency of one reading every 2 seconds (0.5 Hz): PR and SpO_2 from a pulse oximeter (Masimo SET SmartPod Model # MS16356, Masimo Corp) integrated with an Infinity Delta monitor (Dräger Medical Systems) as well as HR derived from ECG leads attached to a second Infinity Delta monitor. HR and PR are parameters that estimate the rate at which the heart beats per min (bpm). Although HR and PR are acquired independent of each other, they essentially represent the exact same functionality of the heart, albeit in electrical and mechanical contexts, respectively. HR is acquired through ECG leads, which are electrical sensors, and PR is acquired using optical sensors attached to the pulse oximeter. Moreover, the pulse oximeter derives SpO_2 using the same optical sensor data. This implies that the quality of the PR data stream reflects the quality of the SpO_2 data stream. Therefore, to evaluate the framework as a CDSS that generates SpO_2 alarms, we selected the HR as the gold standard for comparison with the quality of the PR data stream. The reason for selecting the HR patient data acquired from the Infinity Delta monitor as the gold standard is that these monitors are used for continuous patient monitoring at the research site (CHEO); therefore, clinicians depend on the vital sign data displayed by these monitors to routinely assess the patients. Second, we evaluated the SpO_2 alarm generation performance of the framework as compared with the Masimo SET SmartPod pulse oximeter. Again, this pulse oximeter was selected for comparison because it is routinely used for continuous patient monitoring at the CHEO. RS232 serial ports on both Infinity Delta monitors were connected through Digi International Edgeport4 (Digi International) hardware to a USB port on a computer. Eltima Port Monitor Professional Edition Software

v4.x (Eltima Software) was installed on the same computer to read and log data transmitted by each monitor in real time. Thus, a total of 79,200 data points from each physiologic data type were used for analysis. To synchronize data collected from the 2 OEM monitors, these samples were interpolated to obtain one sample every second, resulting in 158,400 data points from each data type. Information regarding patient demographics, inclusion and exclusion criteria, and the detailed methods of data acquisition and data annotation can be found in the author's earlier research on this data set [44]. A previous study manually counted and categorized patient monitoring alarms [44]. Clinicians, including bedside nurses and neonatologists, validated and categorized the alarms generated by patient monitors. However, manual counting introduces the likelihood of human error. To minimize this likelihood, the process of counting and categorizing the alarms was automated by running the data through a computerized script. This resulted in the identification and categorization of 119 alarms generated by the Masimo pulse oximeter across all 11 patients. These alarms were validated against the clinicians' original validation and categorization criteria from [44]. The Sn and FAR of the Masimo pulse oximeter were found to be 85% and 46%, respectively.

Evaluation Metrics

Data from all 11 patients were used as an input to evaluate each of the four integrated formulations, CDSS #1-4. Leave-one-out cross-validation was used to compute two performance metrics, Sn and FAR. Data from a set of 10 patients were used to tune the components and from the remaining patients to generate alarms. This was repeated 11 times, each time changing the patient for whom the data were left out as a test case.

We then compared the alarm generation performance of each CDSS composition with that of the OEM monitor. Using the OEM monitor's Sn of 85% and FAR of 46%, we formulated equations (4) and (5) to measure the difference between the Sn and FAR values of the CDSS formulations and the OEM monitor and report that as a percent change. Negative values of percentage change indicate reduction, and positive values indicate increments in Sn and/or FAR. These are reported as (% change in Sn) and (% change in FAR) by equations 4 and 5, respectively.

Results

Overview

This section presents the performance evaluation results for all four formulations CDSS #1-4 in terms of Sn and FAR, which are averaged across all 11 cross-validation trials. Tables 2 and 3 summarize the pooled results for achieved Sn values of >75% and >80%, respectively. These Sn thresholds were chosen arbitrarily, and other threshold values may be chosen depending on the clinical needs. These tables show the best achievable results expressed as (Sn [% change in Sn], FAR [% change in FAR]) in all four CDSS formulations. The formulations were tabulated based on the inclusion of the $AD_{MedFilt}$ and AD_{Diff} components. Figure 5 shows the graphical results from all four CDSS formulations as linear plots of Sn (%) and corresponding FAR (%) achieved by tuning the parameters Med_{WW}, CED_{DT}, and *SQThresh*, where applicable to a CDSS. As the configuration parameters of the AD and CED components are varied (tuned), the total number of alarms that are generated also varies. By reporting the performance metrics of Sn and FAR in terms of percentages, we can compare the results across the four CDSS formulations. Here, we compare the best results achieved and tabulated in Tables 2 and 3.

Table 2. The best possible (Sn [% change in Sn], FAR ([% change in FAR]) achieved in clinical decision support systems #1-4, where sensitivity≥75%. Tunable parameters are specified for each case.

$AD_{MedFilt}$[a]	AD_{Diff}[b]	
Yes	• CDSS[c] #4 • Med_{WW}[d]=10, CED_{DT}[e]=15, • SQThresh[f]=18: (76 [−10.5%], 36 [−21.7%])	• CDSS #2 • Med_{WW}=15, CED_{DT}=12: (75 [−11.7%], 32 [−30.4%])
No	• CDSS #3 • CED_{DT}=20, SQThreshf=18: (78 [−8.2%], 47 [21.7%])	• CDSS #1 • CED_{DT}=15: (76 [−10.5%], 40 [−15%])

[a]$AD_{MedFilt}$: AD median filter component.

[b]AD_{Diff}: AD differential filter component.

[c]CDSS: clinical decision support systems.

[d]Med_{WW}: size of the sliding window of the median filter.

[e]CED_{DT}: alarm annunciation delay.

[f]SQThresh: the ordered set of thresholds.

Table 3. The best possible (Sn [% change in Sn], FAR [% change in FAR]) achieved in clinical decision support systems #1-4, where sensitivity ≥80%. Tunable parameters are specified for each case.

$AD_{MedFilt}$	AD_{Diff}	
	Yes	No
Yes	• CDSS[a] #4 • Med_{WW}[b]=10, CED_{DT}[c]=5, SQThresh[d]=18: (80 [−5.8%], 44 [−4.3%])	• CDSS #2 • Med_{WW}=10, CED_{DT}=10: (80 [−5.8%], 39 [−15.2%])
No	• CDSS #3 • CED_{DT}=12, SQThresh=12: (82 [−3.5%], 50 [8.6%])	• CDSS #1 • CED_{DT}=12: (80 [−5.8%], 41 [−10.8%])

[a]CDSS: clinical decision support systems.

[b]Med_{WW}: size of the sliding window of the median filter.

[c]CED_{DT}: alarm annunciation delay.

[d]SQThresh: the ordered set of thresholds.

Figure 5. Results of sensitivity (%) and false alarm rate (%) plotted against the relevant tunable parameters CED_{DT} and Med_{WW} for (a) clinical decision support system CDSS #1, (b) clinical decision support system CDSS #2, (c) clinical decision support system CDSS #3 with SQThresh=18, and (d) clinical decision support system CDSS #4 with SQThresh=18. FAR: false alarm rate.

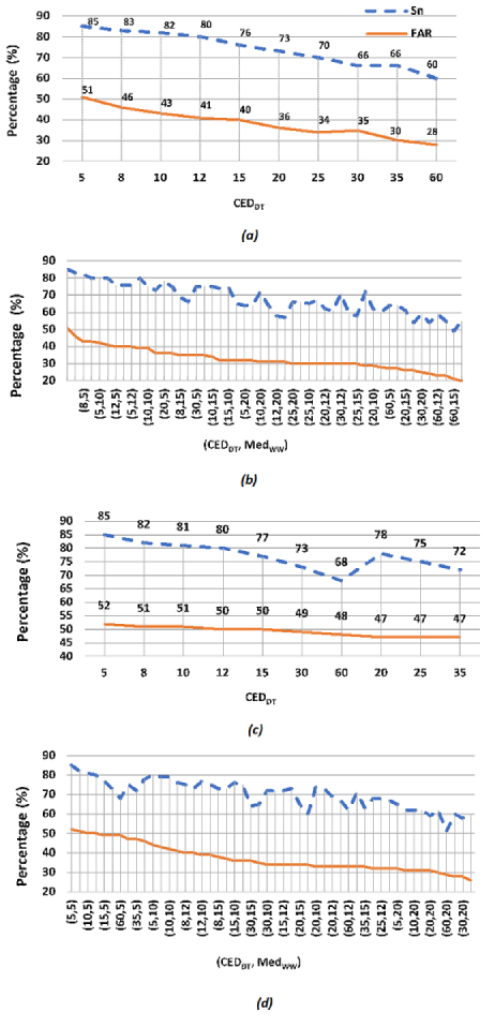

CDSS #1

The best achievable result for CDSS #1 is (Sn, FAR)=(80, 41) and is obtained when CED_{DT}=12, where Sn≥80%. If Sn is only required to be ≥75%, then the best achievable performance becomes (Sn, FAR)=(76, 40) when CED_{DT}=15. The FAR (40%) was 15% less than that of the OEM's FAR (46%). This is achieved at the cost of decreasing Sn (76%) by 10.5% than the Sn of the OEM (85%).

CDSS #2

Table 2 shows that the best achievable result for CDSS #2 is (Sn, FAR)=(80, 39) when Med_{WW}=10 and CED_{DT}=10, where Sn≥80%. In this formulation, Sn≥80% was achievable only when Med_{WW}≤10. If Sn is allowed to be ≥75%, then the best achievable performance becomes (Sn, FAR)=(75, 32) when Med_{WW}=15 and CED_{DT}=12.

CDSS #3

In CDSS #3, with the AD_{Diff} component configured with *SQThresh*=6, the best achievable result for (Sn, FAR)=(86, 52) with CED_{DT}=5. The CDSS performance was worse for all other CED_{DT} thresholds at *SQThresh*=6. Although this CDSS performs with an improved Sn (86%) as compared with the OEM's Sn (85%), the cost is an increase of 13% in the FAR (52%) as compared with the OEM's FAR (46%).

With the AD_{Diff} component configured with *SQThresh*=12, the best achievable (Sn, FAR) is (82, 50) when CED_{DT}=12 for both values of the required Sn≥80% and Sn≥75%. The CDSS performance was worse for all other CED_{DT} thresholds at *SQThresh*=12. When the AD_{Diff} component is configured with *SQThresh*=18, the best achievable result for (Sn, FAR)=(80, 50), with CED_{DT}=12 with a threshold of Sn≥80%, and the best achievable result for (Sn, FAR) is (78, 47), with CED_{DT}=20 while maintaining Sn≥75%. Thus, CDSS #3 was not able to beat the OEM monitor's FAR (46%) at any of the parameter settings that were tested.

CDSS #4

When the AD_{Diff} component of CDSS #4 is configured with *SQThresh*=6 and the sensitivity requirement is ≥80%, the best achievable result for (Sn, FAR)=(84, 52) when Med_{WW}=5 and CED_{DT}=5. When Sn≥75%, the best achievable (Sn, FAR)=(75, 40) when Med_{WW}=10 and CED_{DT}=12. Med_{WW}>10 resulted in lower (Sn, FAR) values, where Sn<75. If the AD_{Diff} component is configured with *SQThresh*=12 and Sn≥80%, then the best achievable result for (Sn, FAR)=(82, 49) with Med_{WW}=5 and CED_{DT}=12. When Sn≥75%, the best achievable (Sn, FAR)=(75, 37) is obtained when Med_{WW}=12 and CED_{DT}=12. Med_{WW}>12 resulted in lower (Sn, FAR) values, where Sn<75. Table 3 shows the results from CDSS #4, where the AD_{Diff} component is configured with *SQThresh*=18 and Sn≥80%, and the best achievable result (Sn, FAR)=(80, 44) is obtained when Med_{WW}=10 and CED_{DT}=5. When Sn≥75%, the best achievable result (Sn, FAR)=(76, 36) is obtained when Med_{WW}=10 and CED_{DT}=15. Med_{WW}>12 resulted in lower (Sn, FAR) values, where Sn<75.

Discussion

Principal Findings

The overarching contribution of this study is the illustration of dynamic framework models and their evaluation using clinical data. In this section, we also discuss how this evaluation leads to the validation of the six framework features (*f1*) to (*f6*).

Framework Evaluation

As described in the *Evaluation* section, the data set used in this evaluation contained 119 alarms across all 11 patients in this study. This data set represents a unique and valuable resource because it includes the detailed annotations of artifacts, alarms, clinical events, clinical interventions, and observations. The patients in our study represented a neonatal population with varying disease severity, weight, and gestational age. Although such a wide range of patients provides for the development of widely applicable rules, as discussed above, many decision thresholds are required to be patient centric. For example, one patient was far more ill than the other 10 patients, with 32% of the associated clinical events. Other limitations of the data set include a possible ambiguity in categorizing alarms as true versus false, especially in cases where the SpO_2 reading hovers around the OEM monitor's alarm threshold setting. In this study, such indeterminate alarms were categorized as false alarms. The study sample size was limited because of hospital logistics and resources. In the future, a larger sample size could facilitate subgroup analyses with division based on clinical characteristics, weight, and gestational and chronological age of infants.

From the evaluation results presented in Table 2 under the criterion that Sn≥75%, we infer that CDSS #2 results in the best achievable performance of (Sn, FAR)=(75,32) when Med_{WW}=15 and CED_{DT}=12. Although a considerable reduction in Sn was observed (11.7%), this parameter combination resulted in a significant reduction in FAR (30.4%). From Table 3, we conclude that CDSS #2 also gives the best possible performance of Sn=80% and FAR=39%, representing percentage reductions of 5.8% and 15.2% for Sn and FAR, respectively. Therefore, CDSS #2 is considered the optimal formulation out of all four CDSS because of the largest reduction in FAR while maintaining Sn≥80%. The optimal parameters for this formulation were Med_{WW}=10 and CED_{DT}=10.

The results of CDSS #1 illustrate the effects of varying the CED decision threshold (CED_{DT}) on the performance of CDSS. By adjusting this threshold, the system could be made more conservative or permissive, leading to an explicit trade-off between Sn and FAR. This CED_{DT} is patient-centered and may be adjusted depending on the severity of disease and clinical resources available, for example, the nurse-to-patient ratio may differ in the NICU versus that in the general ward. A comparison of the results from CDSS #1 and #2 indicates that the use of $AD_{MedFilt}$ significantly improved both the Sn and FAR of the CDSS. As expected, increasing the median filter width reduced both Sn and FAR because the median filter smoothed out transient SpO_2 values. The range of median filter widths was evaluated in combination with a range of CED_{DT} values seeking the combination that provided the greatest decrease in FAR while maintaining a Sn≥80% or ≥75%. Although these Sn thresholds were somewhat arbitrary, they reflect the need to detect the majority of true clinical events.

CDSS #3 and #4 leveraged data fusion via an AD_{Diff} component to identify periods of low signal quality. Clifford et al [45] recommended that an SQI be generated for each datum when a known error rate is available for calibration. Following this,

we hypothesized that by computing the error rate from the combined information from two different sensor modalities, PR from SpO_2 and HR from ECG, an SQI signal could be generated and increased performance would be achievable. The results for three different AD_{Diff} threshold values failed to demonstrate an improved performance. In fact, the frequency of all three types of alarms, namely, true, missed, and false, increased with the use of AD_{Diff}. A close inspection of the generated alarms revealed the fragmentation of previously contiguous alarms into more alarms of shorter duration. This was due to the instantaneous masking of individual SpO_2 values because of transient disparities between HR and PR, which are not necessarily associated with prolonged periods of low signal quality. We observe that an incremental trend in *SQThresh* values, that is, from 6 to 12 to 18, demonstrates a decreasing trend in Sn and FAR percentages in both CDSS #3 and #4. In future work, the CED algorithm may be modified to process the SQI in a variety of ways that may lead to improved performance. Suggestions for future exploration include either retaining the previous alarm state during periods of low signal quality or appraising cumulative SQI values instead of instantaneous ones.

In summary, dynamic framework modeling showed that the lowest achievable FAR was 39% at a sensitivity of 80%, when compared across all four CDSS formulations.

Framework Features

The four dynamic CDSS formulations serve to validate the 6 framework features (*f1*) to (*f6*) as follows:

(f1) Flexible in serving the differing needs of patient populations from different types of critical care units through generalization and customizability. The CRM includes several fields to generalize and customize each component, for example, Data.Type and Data.SQType. Although the data in this validation study were collected at the NICU, the inherent flexibility of the framework can accommodate various types of data streams acquired from other types of critical care units. Similarly, the component-based nature of this framework allows for the creation of CED components relevant to different clinical domains and for their integration with the most appropriate available AD components. As a result, the components catalog, dynamic framework models, and analyses are not restricted in application to the NICU. This could be demonstrated using future experiments based on data from other units, whether gathered specifically for this research or taken from repositories such as Physio Net [46].

(*f2*) Reusable across multiple types of physiological data harvested by different OEM monitors: The configuration interface of each component permits the setting of OEM-specific and Data.Type-specific values such that the same component may be applied to various physiological data types arising from different OEM monitors. For example, the artSyms configuration parameter allows the AD_{DIL} component to identify artifacts flagged by different OEM monitors. AD components selected from the catalog were used to process different physiological streams acquired by different OEM monitors in various experiments. For example, the AD_{DIL} component is used to process the HR from the Dräger OEM monitor and SpO_2 and PR from the Masimo OEM pulse oximeter. This validates the reusability of the framework and its components across multiple types of physiological data harvested by different OEM monitors.

(*f3*) Standardized definitions of SQI that promote interoperability between independently developed components: The CRM defines standardized types of SQI, such as, “continuous,” “rank,” and “binary.” These experiments used multiple components to generate the SQI. These components were developed based on the current algorithms identified in the literature review. For example, the AD_{Diff} component is derived from the work of Yu et al [47] and applied to the HR and PR streams in experiments 3 and 4, whereas the CED component leverages the ideas of threshold modification and alarm annunciation delays that were introduced in previous studies [40-43]. These experiments demonstrate the integration of components that were developed independently and whose interoperability is facilitated through the use of standardized SQI, as defined in the framework’s CRM.

(*f4*) Reusability and scalability by cascading, mixing, and matching several AD and CED components in various combinations: By requiring all component interfaces to conform to the standardized CRM, interoperability is promoted, allowing for component reuse and the creation of highly complex pipelines leveraging simple and well-tested components. Each of the four models represented a different component composition. The analyses in each composition vary in scale through the reuse and cascading of components. This mixing and matching are made possible by the adherence of each component to the CRM. Comparing the flowcharts in Figures 3 and 4, there is an increase in the number of instantiations of the AD_{DIL} component from 2 to 4 between CDSS #1 and #3. This demonstrates that the framework supports reusability and scalability by cascading, mixing, and matching several components.

(*f5*) Customizability to evaluate and compare the performance of multiple combinations of independently developed components on offline and potentially real-time patient data when integrated with clinical workflows: A literature review reveals that AD algorithms are typically developed and validated in offline environments [28]. This study illustrates the dynamic framework evaluation using real patient data offline. This validates the use of the framework as a test bed for multiple combinations of independently developed components. Once a combination is affirmed to satisfy clinical needs through offline testing, that combination can then be evaluated in a real-time environment using the middleware technology. In this way, the transition to real-time clinical implementation and validation is facilitated. A number of studies have suggested the introduction of delays in alarm annunciation to reduce FARs. This strategy is expected to reduce the FAR. However, there is a lack of quantitative evaluation in terms of the impact of such a strategy on Sn and FAR. The framework developed here promotes and enables such a quantitative study design, as demonstrated by the experiments developed here. In fact, it was found that such strategies failed to suppress false alarms while

maintaining a sufficiently high Sn. This shows that the customizability of the framework allows for performance evaluation and comparison of multiple combinations of independently developed components on offline and potentially real-time patient data when integrated with clinical workflows.

(*f6*) Standardized component interfaces that can potentially support real-time clinical implementation of AD: If independent research and OEM groups choose to implement their algorithms within the context of the framework, that is, adhering to the CRM, then it is more likely that these algorithms will reach clinical implementation because the CRM supports interoperability between all components. Furthermore, the framework simplifies information technology (IT) requirements for hospitals because it provides a unified functional environment in which all AD and CED components required by multiple critical care units can be supported and executed. Finally, the framework facilitates the testing and validation of new algorithms across different clinical settings, populations, critical care units, and pathologies. This will make the system more robust and therefore more likely to be adopted [48]. There is a paucity of CDSS for real-time clinical implementation. One hurdle to their clinical adoption is the requirement to transform complex algorithms for real-time implementation. By implementing the required algorithms within the framework, the algorithms will be made suitable for execution in real time. The four experiments were implicitly designed to run the framework components in a real-time streaming environment. The composition of the analysis in each experiment was evaluated using a simulated real-time environment. As a result, with negligible reformulation, the optimal framework composition resulting from this evaluation can be integrated within clinical workflows. Therefore, we conclude that *the standardized component interface design warranted by the CRM supports real-time clinical implementation of AD within CDSS*.

Conclusions

This research evaluated a novel AD framework that standardizes the interoperability of AD and CED algorithms for integration within the CDSS. The framework provides a unique test bed with the ability to create and integrate new AD compositions by mixing and matching independently developed or decoupled AD components with CED components that are designed to deliver specific clinical outcomes. This study validates the use of the AD framework in a clinical study using real patient data from the NICU. Several combinations of AD and CED components were evaluated, thereby illustrating the validity of the six framework features, namely, *f1-f6*, including flexibility, reusability, standardization of SQI, scalability, customizability, and support for real-time implementation.

Future work will include the implementation of a wide range of AD and CED components to further leverage the interoperability provided by the CRM. Although the CRM has been developed following an extensive review of the literature that summarizes the requirements, provisions, and configurations for many existing AD algorithms, it is expected that the CRM will continue to evolve as a wide variety of new AD and CED algorithms with differing data needs are implemented as components within this framework. Further validation of the framework can be conducted by independent research groups. The clinical benefits of this research will be broadly realized through the integration of the framework in real-time CDSS to enhance the quality of data analytics. In this way, framework implementation within clinical workflows offers the potential to improve the quality of care for patients and clinicians in critical care.

Acknowledgments

SN thanks the research collaborators at CHEO, Kim Greenwood, Dr JoAnn Harrold, and Dr Nick Barrowman, for facilitating the clinical study and dedicating many hours to discuss the engineering, clinical, and statistical aspects. SN thanks fellow scientists and engineers, Amna Basharat, Maryam Kaka, Aly Khedr, and Mohamed Hozayen, for computing and illustration support. Natural Sciences and Engineering Research Council of Canada funded this research.

Authors' Contributions

SN completed her postdoctoral research fellowship at the IBM Centre for Advanced Studies, Ottawa. She conducted her postdoctoral research project at CHEO, Ottawa, for which she received the Best Project Outcomes award at IBM, CASCON, Markham, Ontario, Canada 2017. She received the Best Women in Engineering Paper Award at IEEE Intl. The Symposium on Medical Measurements and Applications was held at the Mayo Clinic in Rochester, Minnesota, United States, in 2017. She received a patent for a patient monitoring system invention (US patent #10,297,143 issued in May 2019) with IBM as an assignee. CMAM is a Professor and Canada Research Chair (Alumni) in the Faculty of Business and IT, University of Ontario Institute of Technology, and a professor in the School of Software, Faculty of Engineering and IT, University of Technology Sydney. CMAM has led pioneering research in big data analytics, real-time stream processing, artificial intelligence, temporal data mining, patient journey modeling, and cloud computing. She now progresses this research within the context of critical care medicine, mental health, astronaut health, and military and civilian tactical training. She has received many awards for her research, including, most recently, the Best Paper at the 2017 IEEE Life Science Conference, Sydney, Australia. JRG is a professor at the Department of Systems and Computer Engineering, Carleton University, Ottawa, Canada. His current research interests include pattern classification challenges within biomedical informatics, patient monitoring, computational acceleration of scientific computing, and the design of novel assistive devices.

Conflicts of Interest

None declared.

References

1. Stehlik P, Bahmanpour A, Sekercioglu YA, Darzin P, Marriott JL. Fundamental elements identified for success of disease state management clinical decision support systems. Electron J Heal Informatics 2015;9(1):e6 [FREE Full text]
2. Minutolo A, Esposito M, de Pietro G. A pattern-based approach for representing condition-action clinical rules into DSSs. In: Elleithy K, Sobh T, editors. Innovations and Advanced Techniques in Systems, Computing Sciences and Software Engineering. New York, USA: Springer; 2013:777-789.
3. Pryor M, White D, Potter B, Traill R. Evaluating online diagnostic decision support tools for the clinical setting. Stud Health Technol Inform 2012;178:180-185. [Medline: 22797039]
4. Horsky J, Schiff GD, Johnston D, Mercincavage L, Bell D, Middleton B. Interface design principles for usable decision support: a targeted review of best practices for clinical prescribing interventions. J Biomed Inform 2012 Dec;45(6):1202-1216 [FREE Full text] [doi: 10.1016/j.jbi.2012.09.002] [Medline: 22995208]
5. Drummond WH. Neonatal informatics--dream of a paperless NICU: part four: integrating caregiving, automated process management, and clinical decision support. NeoReviews 2010 Apr 01;11(4):174-183. [doi: 10.1542/neo.11-4-e174]
6. Ruminski CM, Clark MT, Lake DE, Kitzmiller RR, Keim-Malpass J, Robertson MP, et al. Impact of predictive analytics based on continuous cardiorespiratory monitoring in a surgical and trauma intensive care unit. J Clin Monit Comput 2019 Aug 18;33(4):703-711. [doi: 10.1007/s10877-018-0194-4] [Medline: 30121744]
7. Fairchild KD, Nagraj VP, Sullivan BA, Moorman JR, Lake DE. Oxygen desaturations in the early neonatal period predict development of bronchopulmonary dysplasia. Pediatr Res 2019 Jun 29;85(7):987-993 [FREE Full text] [doi: 10.1038/s41390-018-0223-5] [Medline: 30374050]
8. Percival J, McGregor C, Percival N, James A. Enabling the integration of clinical event and physiological data for real-time and retrospective analysis. Inf Syst E-Bus Manage 2014 Jan 20;13(4):693-711. [doi: 10.1007/s10257-014-0232-9]
9. Thommandram A, Pugh JE, Eklund JM, McGregor C, James AG. Classifying neonatal spells using real-time temporal analysis of physiological data streams: algorithm development. Point-of-Care Healthcare Technologies (PHT) IEEE 2013:240-243. [doi: 10.1109/pht.2013.6461329]
10. Nizami S, Green JR, Eklund M, McGregor C. Heart disease classification through HRV analysis using parallel cascade identification and fast orthogonal search. In: Proceedings of the IEEE International Workshop on Medical Measurements and Applications. 2010 Presented at: IEEE International Workshop on Medical Measurements and Applications; April 30-May 1, 2010; Ottawa, Ontario, Canada p. 134-139. [doi: 10.1109/memea.2010.5480217]
11. Lázaro J, Gil E, Bailón R, Mincholé A, Laguna P. Deriving respiration from photoplethysmographic pulse width. Med Biol Eng Comput 2013 Feb 21;51(1-2):233-242. [doi: 10.1007/s11517-012-0954-0] [Medline: 22996834]
12. Mestek M, Addison P, Neitenbach A, Bergese S, Kelley S. Accuracy of continuous noninvasive respiratory rate derived from pulse oximetry in congestive heart failure patients. Chest 2012 Oct;142(4):113A. [doi: 10.1378/chest.1390275]
13. Addison PS, Watson JN, Mestek ML, Mecca RS. Developing an algorithm for pulse oximetry derived respiratory rate (RR(oxi)): a healthy volunteer study. J Clin Monit Comput 2012 Feb 10;26(1):45-51 [FREE Full text] [doi: 10.1007/s10877-011-9332-y] [Medline: 22231359]
14. Li Q, Mark RG, Clifford GD. Artificial arterial blood pressure artifact models and an evaluation of a robust blood pressure and heart rate estimator. BioMed Eng OnLine 2009;8(1):13. [doi: 10.1186/1475-925x-8-13]
15. McShea M, Holl R, Badawi O, Riker R, Silfen E. The eICU Research Institute - a collaboration between industry, health-care providers, and academia. IEEE Eng Med Biol Mag 2010 Mar;29(2):18-25. [doi: 10.1109/memb.2009.935720]
16. Raymer KE, Bergström J, Nyce JM. Anaesthesia monitor alarms: a theory-driven approach. Ergonomics 2012 Sep 25;55(12):1487-1501. [doi: 10.1080/00140139.2012.722695] [Medline: 23009678]
17. Schmid F, Goepfert MS, Kuhnt D, Eichhorn V, Diedrichs S, Reichenspurner H, et al. The wolf is crying in the operating room. Anesth Analg 2011;112(1):78-83. [doi: 10.1213/ane.0b013e3181fcc504]
18. Takla G, Petre JH, Doyle DJ, Horibe M, Gopakumaran B. The problem of artifacts in patient monitor data during surgery: a clinical and methodological review. Anesth Analg 2006 Nov;103(5):1196-1204. [doi: 10.1213/01.ane.0000247964.47706.5d] [Medline: 17056954]
19. Li D, Jeyaprakash V, Foreman S, Groves AM. Comparing oxygen targeting in preterm infants between the Masimo and Philips pulse oximeters. Arch Dis Child Fetal Neonatal Ed 2012 Jul 13;97(4):311-312. [doi: 10.1136/fetalneonatal-2011-301395] [Medline: 22415392]
20. Bach TA, Berglund L, Turk E. Managing alarm systems for quality and safety in the hospital setting. BMJ Open Qual 2018 Jul 25;7(3):e000202 [FREE Full text] [doi: 10.1136/bmjoq-2017-000202] [Medline: 30094341]
21. Garber MD. Monitor alarm fatigue. AAP Grand Rounds 2015 Sep 01;34(3):27. [doi: 10.1542/gr.34-3-27]
22. Solet JM, Barach PR. Managing alarm fatigue in cardiac care. Prog Pediatr Cardiol 2012 Jan;33(1):85-90. [doi: 10.1016/j.ppedcard.2011.12.014]

23. Chopra V, McMahon LF. Redesigning hospital alarms for patient safety: alarmed and potentially dangerous. J Am Med Assoc 2014 Mar 26;311(12):1199-1200. [doi: 10.1001/jama.2014.710] [Medline: 24590296]
24. Berner ES. Clinical decision support systems: state of the art. Agency for Healthcare Research and Quality U.S. Department of Health and Human Services. 2009. URL: https://digital.ahrq.gov/sites/default/files/docs/page/09-0069-EF_1.pdf [accessed 2021-05-20]
25. Varisco G, van de Mortel H, Cabrera-Quiros L, Atallah L, Hueske-Kraus D, Long X, et al. Optimisation of clinical workflow and monitor settings safely reduces alarms in the NICU. Acta Paediatr 2021 Apr;110(4):1141-1150 [FREE Full text] [doi: 10.1111/apa.15615] [Medline: 33048364]
26. Sahoo T, Joshi M, Madathil S, Verma A, Sankar M, Thukral A. Quality improvement initiative for reduction of false alarms from multiparameter monitors in neonatal intensive care unit. J Educ Health Promot 2019;8:203 [FREE Full text] [doi: 10.4103/jehp.jehp_226_19] [Medline: 31807593]
27. Armbruster J, Schmidt B, Poets CF, Bassler D. Nurses' compliance with alarm limits for pulse oximetry: qualitative study. J Perinatol 2010 Aug;30(8):531-534 [FREE Full text] [doi: 10.1038/jp.2009.189] [Medline: 20010614]
28. Nizami S, Green JR, McGregor C. Implementation of artifact detection in critical care: a methodological review. IEEE Rev Biomed Eng 2013;6:127-142. [doi: 10.1109/rbme.2013.2243724]
29. Nizami S, Green JR, McGregor C. An artifact detection framework for clinical decision support systems. In: Proceedings of the World Congress on Medical Physics and Biomedical Engineering. 2015 Presented at: World Congress on Medical Physics and Biomedical Engineering; June 7-12, 2015; Toronto, ON, Canada p. 1393-1396. [doi: 10.1007/978-3-319-19387-8_339]
30. Larsen G. Component-based enterprise frameworks. Commun ACM 2000 Oct;43(10):24-26. [doi: 10.1145/352183.352196]
31. De Cesare S, Lycett M, Macredie R. The Development of Component-based Information Systems. Armonk, NY: M. E. Sharpe; 2006:1-240.
32. Nizami S, Green JR, McGregor C. Service oriented architecture to support real-time implementation of artifact detection in critical care monitoring. In: Proceedings of the Annual International Conference of the IEEE Engineering in Medicine and Biology Society. 2011 Presented at: Annual International Conference of the IEEE Engineering in Medicine and Biology Society; Aug. 30 - Sept. 3, 2011; Boston, MA, USA. [doi: 10.1109/iembs.2011.6091221]
33. Jarchi D, Casson AJ. Towards photoplethysmography-based estimation of instantaneous heart rate during physical activity. IEEE Trans Biomed Eng 2017 Sep;64(9):2042-2053. [doi: 10.1109/tbme.2017.2668763]
34. Khan E, Hossain FA, Uddin SZ, Alam SK, Hasan MK. A robust heart rate monitoring scheme using photoplethysmographic signals corrupted by intense motion artifacts. IEEE Trans Biomed Eng 2016 Mar;63(3):550-562. [doi: 10.1109/tbme.2015.2466075]
35. Dao D, Salehizadeh SM, Noh Y, Chong JW, Cho CH, McManus D, et al. A robust motion artifact detection algorithm for accurate detection of heart rates from photoplethysmographic signals using time–frequency spectral features. IEEE J Biomed Health Inform 2017 Sep;21(5):1242-1253. [doi: 10.1109/jbhi.2016.2612059]
36. Pu L, Chacon PJ, Wu H, Choi J. Novel tailoring algorithm for abrupt motion artifact removal in photoplethysmogram signals. Biomed Eng Lett 2017 Nov 9;7(4):299-304 [FREE Full text] [doi: 10.1007/s13534-017-0037-0] [Medline: 30603179]
37. Borges G, Brusamarello V. Sensor fusion methods for reducing false alarms in heart rate monitoring. J Clin Monit Comput 2016 Dec 6;30(6):859-867. [doi: 10.1007/s10877-015-9786-4] [Medline: 26439831]
38. Chan A, Englehart K, Hudgins B, Lovely D. Multiexpert automatic speech recognition using acoustic and myoelectric signals. IEEE Trans Biomed Eng 2006 Apr;53(4):676-685. [doi: 10.1109/tbme.2006.870224]
39. He DD, Winokur ES, Sodini CG. An ear-worn vital signs monitor. IEEE Trans Biomed Eng 2015 Nov;62(11):2547-2552. [doi: 10.1109/tbme.2015.2459061]
40. Burgess LP, Herdman TH, Berg BW, Feaster WW, Hebsur S. Alarm limit settings for early warning systems to identify at-risk patients. J Adv Nurs 2009 Sep;65(9):1844-1852. [doi: 10.1111/j.1365-2648.2009.05048.x] [Medline: 19694847]
41. Taenzer AH, Pyke JB, McGrath SP, Blike GT. Impact of pulse oximetry surveillance on rescue events and intensive care unit transfers. Anesthesiology 2010 Feb;112(2):282-287. [doi: 10.1097/aln.0b013e3181ca7a9b]
42. Welch J. An evidence-based approach to reduce nuisance alarms and alarm fatigue. Biomed Instrum Technol 2011;Suppl:46-52. [doi: 10.2345/0899-8205-45.s1.46] [Medline: 21599481]
43. Welch J, Kanter B, Skora B, McCombie S, Henry I, McCombie D, et al. Multi-parameter vital sign database to assist in alarm optimization for general care units. J Clin Monit Comput 2016 Dec 6;30(6):895-900 [FREE Full text] [doi: 10.1007/s10877-015-9790-8] [Medline: 26439830]
44. Nizami S, Greenwood K, Barrowman N, Harrold J. Performance evaluation of new-generation pulse oximeters in the NICU: observational study. Cardiovasc Eng Technol 2015 Sep 9;6(3):383-391. [doi: 10.1007/s13239-015-0229-7] [Medline: 26577369]
45. Clifford G, Long W, Moody G, Szolovits P. Robust parameter extraction for decision support using multimodal intensive care data. Philos Trans A Math Phys Eng Sci 2009 Jan 28;367(1887):411-429 [FREE Full text] [doi: 10.1098/rsta.2008.0157] [Medline: 18936019]

46. Goldberger AL, Amaral LA, Glass L, Hausdorff JM, Ivanov PC, Mark RG, et al. PhysioBank, PhysioToolkit, and PhysioNet: components of a new research resource for complex physiologic signals. Circulation 2000 Jun 13;101(23):215-220. [doi: 10.1161/01.cir.101.23.e215] [Medline: 10851218]
47. Yu C, Liu Z, McKenna T, Reisner AT, Reifman J. A method for automatic identification of reliable heart rates calculated from ECG and PPG waveforms. J Am Med Informatics Assoc 2006 May 01;13(3):309-320. [doi: 10.1197/jamia.m1925]
48. Crnkovic I, Larsson M. Building Reliable Component-Based Software Systems. Boston, MA: Artech House; 2002:1-454.

Abbreviations

AD: artifact detection
CDSS: clinical decision support systems
CED: clinical event detection
CHEO: Children's Hospital of Eastern Ontario
CRM: common reference model
DIL: designed to deinterlace
ECG: electrocardiography
FAR: false alarm rate
HR: heart rate
IT: information technology
NaN: Not-a-number
NICU: neonatal intensive care unit
OEM: original equipment manufacturer
PDA: patient data acquisition
PR: pulse rate
SpO2: peripheral oxygen saturation
SQI: signal quality indicator

Edited by G Eysenbach; submitted 13.08.20; peer-reviewed by T Sagi, A James; comments to author 16.11.20; revised version received 23.02.21; accepted 04.04.21; published 27.05.21.

Please cite as:
Nizami S, McGregor AM C, Green JR
Integrating Physiological Data Artifacts Detection With Clinical Decision Support Systems: Observational Study
JMIR Biomed Eng 2021;6(2):e23495
URL: https://biomedeng.jmir.org/2021/2/e23495
doi:10.2196/23495
PMID:

Publisher:
JMIR Publications
130 Queens Quay East.
Toronto, ON, M5A 3Y5
Phone: (+1) 416-583-2040
Email: support@jmir.org